

**Computational Strategies for Dynamic Analysis of Reinforced Concrete
Structures Subjected to Blast Loading**

By
Seyed Hamid Changiz Rezaei
B.Sc.

Faculty of Engineering
Department of Civil Engineering

A Thesis Submitted to the School of Graduate Studies
in Partial Fulfillment of the Requirements
for the Degree

Master of Applied Science

McMaster University
Hamilton, Ontario, Canada
August 2008

© Copyright by Seyed Hamid Changiz Rezaei, 2008

**Computational Strategies for Dynamic Analysis of Reinforced Concrete
Structures Subjected to Blast Loading**

Master of Applied Science (2008)
(Civil Engineering)

McMaster University
Hamilton, Ontario

TITLE: **Computational Strategies for Dynamic Analysis of Reinforced Concrete Structures Subjected to Blast Loading**

AUTHOR: **Seyed Hamid Changiz Rezaei, B.Sc.**

SUPERVISOR: **Dr. Wael W. El-Dakhakhni**

Number of Pages: **254 pages (i-ix, 1-245)**

Abstract

There has always been a challenge for designing structures against extreme dynamic loads. Blast loading falls under these loads category and blast resistant design has been gaining more interest during the past decade. Among different types of structures, Reinforced Concrete (RC) structures are usually recommended to be used for blast resistant design. However, the nonlinearities associated with these structures make their accurate analysis complicated. Therefore, simplified techniques have been introduced for nonlinear dynamic analysis of these structures. This study focuses on developing simplified computational strategies for the dynamic analysis of blast loaded RC elements including beams, panels/slabs and columns. For RC beams, the basis for commonly used Single-Degree-of-Freedom (SDOF) models has been outlined. A Multi-Degrees-of-Freedom (MDOF) model which takes into account the concrete nonlinear properties has been developed and the effect of varying the number of degrees-of-freedom (DOF) on response has been studied. Results showed that increasing the number of DOF affects the pressure-impulse ($P-I$) diagrams, especially in the impulsive regime, as the extent of damage increased. In addition, the model was compared with the experimental data and showed good agreement. For RC panels, a SDOF technique, based on the US Army Technical Manual TM5-1300 instructions, was constructed and results were compared with the ones obtained from explicit Finite Element (FE) analysis. Compared to the FE results, SDOF model yielded conservative predictions for deflection but it usually underestimated the dynamic reactions. A modification for reaction calculation was proposed which resulted in significantly better prediction of the reaction for the impulsive range of loading. Finally, considering the important role of columns in providing the overall stability of the structure, a MDOF model was developed for RC columns and the load carrying capacity of the columns was investigated for different levels of axial load, strain rate and damage. Increasing the strain rate enhanced the column's cross section properties whereas increasing the levels of axial load reduced the cross section curvature and the column deflection capacities. Results also showed that good detailing at the supports can significantly improve the load carrying capacity of RC columns.

Acknowledgements

First and foremost, I would like to express my deepest gratitude to Dr. W. El-Dakhakhni for his role as my mentor and thesis advisor. His extensive knowledge in the field of structural engineering has been of great value for my research. He is not only an outstanding mentor, but also a good friend. His understanding, encouragement and continuous personal guidance and support for his students are definitely exceptional. I would also like to extend my appreciation to Dr. W. Mekky and Dr. G. Razaqpur for their suggestions and help during this work. In addition, I appreciate the interest and guidance of my defense committee members, Dr. M. Tait and Dr. P. Guo, who both provided very helpful and thorough reviews of my thesis.

I would also like to thank my advisor and the Department of Civil Engineering for their financial supports. My research support provided by McMaster's Centre for Effective Design of Structures funded through Ontario Research and Development Challenge Fund is gratefully acknowledged.

I would like to thank my friends, Majid Maleki, Alireza Azami, Mohsen Chitsaz, Kian Karimi and Hanif Mahmoodzadeh, for all of their encouragement and help during my graduate studies. Finally, as always, I am deeply indebted to my parents, Fatemeh and Mohsen, and my siblings, Saeed and Setareh, for their love and support throughout my studies and my life.

Co-Authorship

This thesis has been prepared in accordance with the regulations for a sandwich thesis format or as a compilation of research papers stipulated by the Faculty of Graduate Studies at McMaster University and has been co-authored.

Chapter 2: Response Sensitivity of Blast Loaded Reinforced Concrete Beams to the Number of Degrees of Freedom (*Submitted for publication, the Canadian Journal of Civil Engineering*)

By: S.H. Changiz Rezaei, W.W. El-Dakhakhni, W.F. Mekky and A.G. Razaqpur

SDOF and MDOF analysis were performed by S.H. Changiz Rezaei in consultation with Dr. El-Dakhakhni and Dr. W.F. Mekky. Chapter 2 was written by S.H. Changiz Rezaei. It was edited by Dr. W.W. El-Dakhakhni.

Chapter 3: Response of Two-Way Reinforced Concrete Panels to Blast (*to be Submitted*)

By: S.H. Changiz Rezaei, W.W. El-Dakhakhni and W.F. Mekky

Instructions on using LS-DYNA and FE modeling were given by Dr. W.F. Mekky. SDOF and FE analysis were conducted by S.H. Changiz Rezaei in consultation with Dr. W.W. El-Dakhakhni. Chapter 3 was written by S.H. Changiz Rezaei and edited by Dr. W.W. El-Dakhakhni.

Chapter 4: Capacity Assessment of Reinforced Concrete Columns Subjected to Blast (*to be Submitted*)

By: S.H. Changiz Rezaei, W.W. El-Dakhakhni and W.F. Mekky

MDOF modeling and analysis were carried out by S.H. Changiz Rezaei in consultation with Dr. El-Dakhakhni and Dr. W.F. Mekky. Chapter 4 was written by S.H. Changiz Rezaei and edited by Dr. W.W. El-Dakhakhni.

Contents

Abstract	iii
Acknowledgements	iv
Co-Authorship	v
Chapter 1 Thesis Summary	1
1.0 Introduction	1
1.1 Background and Research Objective	1
1.2 Explosion and Blast Loading	4
1.3 Dynamic Analysis	5
1.4 Strain Rate Effect	7
1.4.1 Dynamic Increase Factor (<i>DIF</i>)	8
1.4.1.1 Concrete	9
1.4.1.2 Steel	10
1.5 Numerical Time Integration	11
1.6 Summary of the Research Papers and Conclusions	13
1.7 Suggestions for Future Work	17
1.8 References	18
Chapter 2 Response Sensitivity of Blast Loaded Reinforced Concrete Beams to the Number of Degrees of Freedom	25
2.0 Introduction	26
2.1 Model Development	29
2.1.1 SDOF Model	29

2.1.2 MDOF Model	33
2.1.2.1 Numerical Integration Scheme	35
2.1.2.2 Material Stress-Strain Relationship	36
2.1.2.2.1 Concrete	36
2.1.2.2.2 Steel	38
2.1.2.3 Strain Rate Effects	39
2.1.2.3.1 Concrete	39
2.1.2.3.2 Steel	41
2.1.2.4 Strain Rate Estimation	42
2.2 Numerical Results and Discussion	44
2.2.1 Overall Procedure	44
2.2.2 Partially Damaged Cases	47
2.2.2.1 Comparison with Different SDOF Models	48
2.2.2.2 Dynamic Shear Comparison with Closed Form Solutions	50
2.2.3 Comparison with Experimental Results	52
2.2.4 Totally Damaged Cases	53
2.2.4.1 Required Number of DOF for Different P_0 and T_L	54
2.2.5 Effect of Number of DOF on the Pressure-Impulse Diagrams	55
2.3 Conclusions	56
Chapter 3 Response of Two-Way Reinforced Concrete Panels to Blast	95
3.0 Introduction	96
3.1 Model Development	99

3.1.1 SDOF Model	99
3.1.2 SDOF Model in TM5-1300	103
3.1.2.1 Load-Mass Factors	104
3.1.2.2 Resistance Force Function	107
3.1.2.3 Support Reaction	112
3.1.3 Strain Rate Effects	112
3.1.3.1 Concrete compressive strength	113
3.1.3.2 Steel yield stress	114
3.1.3.3 <i>DIF</i> estimation	115
3.2 Numerical Results and Discussion	118
3.2.1 Overall Procedure	118
3.2.2 FE Models	119
3.2.3 SDOF Models with Different Flexural Rigidities	122
3.2.4 Pressure-impulse diagrams	125
3.2.4.1 <i>P-I</i> diagrams for simply supported panels	126
3.2.4.2 <i>P-I</i> diagrams for clamped panels	130
3.2.5 Support Reactions	133
3.2.5.1 Implementing the Effect of Applied Load in TM5-1300's Method	134
3.2.5.2 Results for Different Methods	135
3.3 Conclusions	137
Chapter 4 Capacity Assessment of Reinforced Concrete Columns	191
 Subjected to Blast	

4.0 Introduction	192
4.1 Model development	195
4.1.1 MDOF Model for a RC Column	195
4.1.2 Material Stress-Strain Relationship	197
4.1.2.1 Concrete	197
4.1.2.2 Steel	199
4.1.3 Strain Rate Effects	200
4.1.3.1 Concrete	200
4.1.3.2 Steel	203
4.1.4 Strain Rate Estimation	204
4.2 Numerical Results and Discussion	206
4.2.1 Overall Procedure	206
4.2.2 Section Properties	207
4.2.2.1 Moment-Curvature Diagrams	207
4.2.2.2 Axial Force-Moment Interaction Diagrams	209
4.2.3 Damage Assessment	210
4.2.3.1 $P-I$ Diagrams	211
4.2.3.2 Effect of Axial Load on $P-I$ Diagrams	212
4.2.3.3 Effect of Good Detailing on Load Carrying Capacity	213
4.2.3.4 Rotational Capacity at the Fully Damaged State	214
4.2.3.5 Damage Screening	214
4.3 Conclusions	215

Chapter 1 Thesis Summary

1.0 Introduction

This chapter summarizes the thesis, starting with the background and the research objectives. This will be followed by the basic methodology and the main points to be considered for the analysis of structures subjected to blast. This chapter is concluded by a summary of the research papers, main conclusions, and recommendations for future research.

1.1 Background and Research Objectives

During the past few decades, there has been a growing interest in the designing of structures against blast loads. Among different construction materials, reinforced concrete (RC) is usually recommended for blast resistant construction. Although steel structures provide greater ductile response compared to RC structures, several concerns related to their connections render their use limited. In fact, blast events usually result in catastrophic failures and therefore, the importance of good connection details become more significant. As a matter of fact, failure of a steel connection may result in an overall progressive collapse of the structure even if individual steel members are capable of resisting blast loads. In addition, RC structures provide good fire and inertial resistance compared to steel structures.

To analyze a blast loaded RC elements to evaluate their maximum response quantities (e.g. displacements, moments and shear forces), nonlinear dynamic analysis is required to evaluate these quantities. However, the exact analysis of these structural elements is

difficult due to their inherent nonlinearity. Therefore, simplified computational strategies based on single degree of freedom (SDOF) or multi degrees of freedom (MDOF) models have been introduced.

There are a number of investigations in which SDOF or MDOF techniques have been employed to study the response of structural members under blast or impact loading. Krauthammer et al. (1990) used the moment-curvature relationship for a RC beam and evaluated the deflected shape corresponding to different static load increments. Subsequently, they considered the deflected shape as the vibration mode shape in their SDOF model. Agreement between numerical and experimental results was obtained when uncertainties associated with the loading were accounted for in the SDOF model. Louca and Harding (1997) considered the first mode of vibration and used the Lagrange equation to study the dynamic response of steel plates with or without imperfections. They found good correlation between their models and finite element models for plates with low aspect ratios. Pan and Watson (1998) derived the equation of motion by obtaining the strain energy and kinetic energy expressions for an assumed parametric mode shape and studied the response of plates in different loading range for elastic and elasto-plastic material. Their model overestimated the deflections for plates subjected to high impulsive load which was attributed to the lack of tensile membrane resistance in their model. Schleyer and Hsu (2000) considered a beam with arbitrary support conditions and divided the beam into two elastic segments. A number of elastic-perfectly plastic translational and torsional springs were used in order to connect these two segments to each other and also to model support conditions. They considered a

combination of the mode shapes of the clamped beam, simply supported beam and a triangular mode shape in the model and found their numerical results to be consistent with those of finite element models. Boutros (2000) considered three generalized coordinates (midspan deflection, plastic kink angle at midspan, plastic axial deformation) and used virtual work to find the dynamic equation of motion of simply supported beams subjected to blast. The comparison of numerical results with test data suggested that consistent results may be obtained by considering 5% damping in the model and assuming 5% of the beam length for the midspan plastic hinge length. Low and Hao (2002) used SDOF systems, originally suggested by Biggs (1964) and Krauthammer et al. (1986), in order to investigate different failure modes for one way RC members. They concluded that impulsive blast loads tend to cause direct shear failure while blast loads with lower amplitude and longer duration have a higher tendency to bring about flexural failure.

The current study focuses on using simplified techniques such as SDOF and MDOF modeling for performing nonlinear dynamic analysis of RC components (i.e. beams, panels and columns) under blast load. The basics of commonly used SDOF models have been explained and a MDOF model which takes the nonlinear properties of concrete into account was developed for RC beams and RC columns. SDOF model for RC panels, based on the US army technical manual TM5-1300 (1990) instructions, have been employed and results obtained from this model was compared with results. The following

sections will highlight the main issues involved in the analysis of structural elements subjected to blast.

1.2 Explosion and Blast Loading

During an explosion, a chemical reaction is initiated. This leads to a sudden rise of temperature within the surrounding air. Consequently, a layer of compressed air, forming the blast wave or the “shock front”, is generated which contains most of the energy released by the blast. When the shock wave reaches an obstacle (structure), the pressure increases to its maximum value (side-on overpressure). Then, this pressure decays exponentially within a short time (positive phase duration), and finally, as the air cools down, the pressure drops a little below the ambient pressure for a longer duration (negative phase duration). During this duration, a partial vacuum exists resulting in a suction condition. A typical time history of a blast load is shown in Fig. 1.1(a). In practice, the negative phase is neglected because of its smaller intensity and the positive phase blast load is approximated with a triangular load as shown in the Fig. 1.1(b) (Beshara 1994).

The side-on overpressure and impulse, which is the area under pressure-time history, are usually given as a function of the scaled distance, Z , in the form of charts or figures (Bangash, M.Y.H and Bangash, T. 2005). The scaled distance is expressed as:

$$Z = \frac{R}{W^{1/3}} \quad (1.1)$$

Where R is the distance from the center of explosion in meters and W is the charge mass expressed in kilograms of TNT. The TNT is taken as a reference explosive and the actual mass of the charge from sources other than TNT should be converted to a TNT equivalent mass. This is usually done by obtaining conversion factor based on the explosive's specific energy and that of TNT.

It should also be noted that when the blast wave strikes an obstacle, depending on the direction of its propagation, it can be reflected and the overpressure can be amplified by as much as 20 folds. Therefore, the effect of reflection should also be taken into account for estimating a blast load. Figures like Fig. 1.2 are available in references such as Baker (1983) and Bangash (2005) in order to evaluate the side-on pressure, P_s , impulse, i_s , and their corresponding reflected values (i.e. reflected pressure, P_r , reflected impulse, i_r).

1.3 Dynamic Analysis

In order to design a structural element against extreme dynamic loads such as blast, the maximum response quantities such as displacement and shear are needed. Therefore, nonlinear dynamic analysis should be carried out to evaluate these quantities. It should also be noted that damping is neglected during dynamic analysis since the maximum response usually occurs at the first cycle and effect of damping on response is negligible. For dynamic analysis, there are usually two groups of methods: analytical (macro) models and finite element (FE) models.

Macro models are usually based of SDOF analysis. This nonlinear analysis method considers the primary mode of vibration to represent the dynamic behavior of the structural element. Assuming a shape function for the first mode, the structural element is idealized by a SDOF model. Deflection obtained from this equivalent system should represent the actual deflection of the actual system at a certain location (e.g. element mid span). To satisfy this constraint, the external work, kinetic energy and strain energy of the two systems are equated for the different levels of deformation (e.g. elastic, elastic-plastic, or fully plastic conditions) and consequently, a transformation factor, K_{LM} , which is called load-mass factor, is found for each stage of deformation. Therefore, the dynamic equation of motion can be expressed as:

$$K_{LM} m\ddot{x} + R(x) = F(t) \quad (1.2)$$

Where m is the element mass, x and \ddot{x} are the displacement and acceleration of a certain point (e.g. midspan). $R(x)$ is the resistance force as a function of displacement and $F(t)$ is the applied blast load as a function of time. It should also be noted that a resistance-displacement function must be evaluated for the structural element which can be established either experimentally or by using plastic analysis. In addition, the load-mass factors have been tabulated in references such as Biggs (1964); TM5-1300 (1990); Mays and Smith (1995).

Finite element analysis (FEA) considers the whole continuous system. It divides the structural model into a large number of small elements and solves the equation of motion

for each node. With the development of nonlinear FEA, it is possible to carry out more advanced analysis. In recent years, different material models were developed and advancement in high speed computers and numerical solution techniques resulted in a significant reduction of computational time associated with nonlinear dynamic analysis. These efforts lead to development computer software such as LS-DYNA, ANSYS, ABAQUS, ADINA, AUTODYN in order to model and analyze complicated systems in an efficient way.

Although nonlinear FEA is a great tool for blast loaded structure, there are some considerations which make this technique not widely adopted for general use. FEA requires a large number of input data and careful assessment of the validity of the results and thorough knowledge of the method. Moreover, even by using computers with fast processors, FEA can still be extremely time consuming.

In contrast to FEA, macro models require limited input data. They are widely applicable to predict blast effects and relatively easy to use and calibrate. Thus, all design codes are based on the SDOF method and even in the case of complex structures, SDOF methods are usually used for preliminary design.

1.4 Strain Rate Effects

It has been shown by numerous experimental and numerical research programs that concrete and steel exhibit greater strength at high strain rate of loading. This material characteristic becomes more significant for the case of blast loading since the duration of

loading is very small compared to the duration of other dynamic loads such as earthquakes for example. Therefore, the material properties should be modified and the resistance should be enhanced appropriately in order to consider the effect of strain rates.

In order to study the effect of strain rate on material properties, the Split Hopkinson Pressure Bar (SHPB) is usually employed. Kolsky (1949) first used this method to investigate steel properties under dynamic loading. Then, the application of this method spread later to different materials such as metals, ceramics, concrete, soil, foams, plastic and composite (Ross et. al.(1995)). SHPB can produce strain rates as high as 10^4s^{-1} . In this technique, a specimen is placed between two long metallic bars and load transmitted to the specimen through impacting one of the bars. Then, stresses and strains are calculated using one-dimensional elastic stress-wave theory. In order to maintain the validity of the theory and apply a uniform stress, the impact velocity should be limited and proper length-to-diameter ratio should be selected for the specimen. These requirements make the typical size of test specimen very small. Therefore, this method seems to be more appropriate for homogeneous material like steel. It should also be mentioned that testing larger specimen was made possible by employing another technique called plate impact test. Fig. 1.3 shows the schematic views of these tests.

1.4.1 Dynamic Increase Factor (*DIF*)

Dynamic increase factor (*DIF*) basically is the ratio of material dynamic strength to static strength and is reported as a function of strain rate. A number of researchers have

investigated the dynamic behavior of concrete and mortar in order to come up with expressions for the *DIF* at different strain rates.

1.4.1.1 Concrete

One of the main references for the effect of strain rate on the compressive strength of concrete is Bischof and Perry (1991). They discussed several factors that affect the concrete strength at high strain rates such as the concrete static compressive strength, aggregate type, curing, moisture and age. They concluded that the concrete compressive strength is the most predominant factor. In addition, there were no consensus among different researchers on the effect of strain rate on the strain at the peak compressive stress and different variations have been reported.

To obtain the *DIF* of concrete, expressions were proposed by Soroushian et al. (1986); Comité Euro-International du Béton (CEB) (1988); Tedesco et al. (1997); Malvar and Ross (1998). All these formulas differentiate between low to intermediate strain rates and intermediate to high strain rates, and suggest separate relationships for the range of strain rates under consideration. It was also shown that the concrete tensile strength exhibited higher increase than the compressive strength.

CEB (1988) differentiates between low to intermediate strain rate and intermediate to high strain rate, and suggests the following formulas:

$$f_c / f_{cs} = \left(\frac{\dot{\epsilon}}{\dot{\epsilon}_s} \right)^{1.026\alpha_s} \quad \text{for } \dot{\epsilon} \leq 30 \text{ s}^{-1} \quad (1.3-a)$$

$$= \gamma_s \left(\frac{\dot{\epsilon}}{\dot{\epsilon}_s} \right)^{1/3} \quad \text{for } \dot{\epsilon} > 30 \text{ s}^{-1} \quad (1.3-b)$$

Where f_c and f_{cs} are the dynamic and static compressive strength, $\dot{\epsilon}$ is the strain rate, $\dot{\epsilon}_s = 30 \times 10^{-6} \text{ s}^{-1}$ (static strain rate), $\log \gamma_s = 6.156\alpha_s - 2$, $\alpha_s = 1/(5+9(f_{cs}/f_{co}))$, $f_{co} = 10 \text{ MPa} = 1450 \text{ psi}$.

$$f_t / f_{ts} = \left(\frac{\dot{\epsilon}}{\dot{\epsilon}_s} \right)^{1.016\delta} \quad \text{for } \dot{\epsilon} \leq 30 \text{ s}^{-1} \quad (1.4-a)$$

$$= \beta \left(\frac{\dot{\epsilon}}{\dot{\epsilon}_s} \right)^{1/3} \quad \text{for } \dot{\epsilon} > 30 \text{ s}^{-1} \quad (1.4-b)$$

Where f_t and f_{ts} are the dynamic and static tensile strength, $\dot{\epsilon}$ is the strain rate, $\dot{\epsilon}_s = 30 \times 10^{-6} \text{ s}^{-1}$ (static strain rate), $\log \beta = 7.11\delta - 2.33$, $\delta = 1/(10+6(f_{cs}/f_{co}))$, $f_{co} = 10 \text{ MPa} = 1450 \text{ psi}$.

1.4.1.2 Steel

The variation of steel properties with increasing strain rate has been studied by Soroushian and Choi (1987); CEB (1988); Malvar (1998). It has been observed that strain rate mainly enhanced the yield and ultimate stress of steel and it does not have significant effect on steel modulus of elasticity. One of the well known formulas for evaluating the *DIF* of steel has been proposed by Malvar (1998) as follow:

$$DIF = \left(\frac{\dot{\varepsilon}}{10^{-4}} \right)^{\alpha} \quad (1.5-a)$$

where:

$$\alpha = 0.074 - 0.040 \frac{f_y}{414} \quad \text{for yield stress, or} \quad (1.5-b)$$

$$\alpha = 0.019 - 0.009 \frac{f_u}{414} \quad \text{for ultimate stress} \quad (1.5-c)$$

$\dot{\varepsilon}$ is the strain rate. f_y and f_u are the bar yield stress and ultimate stress in MPa.

1.5 Numerical Time Integration

To perform the dynamic analysis, the equation of motion should be solved for each time increment, which usually involves numerical integration of the differential equation of motion. A review of different methods for numerical integration is available in Dokainish and Subbaraj (1989), and Subbaraj and Dokainish (1989).

In general, the numerical technique to solve the differential equation of motion will fall under either an explicit or an implicit method. Each of these methods has its own advantages and disadvantages for each specific problem.

Explicit methods such as the Central Difference and Runge-Kutta Methods use the known quantities (e.g. displacement, velocity, acceleration) at time t (or at some time in the past) and solved the differential equation for their unknown values at time $t + \Delta t$. On the other hand, implicit methods such as the Newmark- β and the Wilson- θ methods solve

for the unknown values at time $t + \Delta t$ using the differential equation at time $t + \Delta t$ which means that the unknown values are implicitly embedded in the equation. As a result, implicit methods involve the simultaneous solution of a set of equations leading to iterative procedures for nonlinear systems. Therefore, with respect to the computational cost per time step, explicit algorithms are much more efficient than implicit ones.

Numerical methods are also assessed based on their accuracy and stability. Accuracy indicates how close the numerical solution is to the exact solution when the time step approaches zero. In other words, truncation error should converge to zero as smaller time steps are used.

Stability can be conditional or unconditional. The numerical scheme is conditionally stable if the numerical solution diverges for time steps beyond a critical time step and it is unconditionally stable if the numerical error is not affected by the time step size, as long as the time step satisfies the accuracy requirements.

Many implicit methods are unconditionally stable while explicit methods are conditionally stable. This means that greater time steps can be selected in implicit algorithms and the time increment is determined regarding accuracy considerations. This is why implicit methods are more beneficial for structural dynamics problem in which the response is governed by the first few modes. Hence, they can usually be applied to earthquake problems since selecting larger time step is permitted. On the other hand, explicit algorithms are usually more appropriate for wave propagation problems in which

the contribution of higher modes to the response can be more significant. Thus, the use of these methods in blast and impact loading (which are high in amplitude and short load duration) is preferable since their solution requires very small time increments.

1.6 Summary of the Research Papers and Conclusions

Paper I: Response Sensitivity of Blast Loaded Reinforced Concrete Beams to the Number of Degrees of Freedom

Contribution of higher modes to the maximum response quantities can be more significant in rapid dynamic loads such as blast and impact. In this study, a MDOF model with varying number of degrees-of-freedom (DOF) was developed for RC beams. Changing the number of DOF, nonlinear dynamic analyses were carried out for MDOF models subjected to series of pressure and impulse pairs and differences in maximum response quantities were compared. Moreover, the model was compared with available experimental data.

Results showed that few DOF are needed to capture the response of partially damaged beams. Results were also compared with several SDOF model results and it was observed that the use of these models may yield comparable results to those found from MDOF analysis if the appropriate flexural rigidity is used. Peak shear obtained from models with elastic response was also compared with closed form solution with a maximum difference of about 20% in the impulsive regime.

A larger number of DOF was needed to capture the flexural failure of RC beams and it was observed that the required number increased with increasing the stiffness. Comparison of Pressure-Impulse ($P-I$) diagrams obtained by using different DOF also indicated that the required number is dependent on the damage and, moreover, large number of DOF affected the $P-I$ diagrams significantly in the impulsive regime for stiff beams. This was attributed to the fact that high impulsive loads can excite modes within a specific frequency range. In addition, by increasing damage, the frequency of vibration decreases and consequently, more modes can possibly fall in that frequency range.

Paper II: Response of Two-Way Reinforced Concrete Panels to Blast

Most of the available studies are limited to evaluating the response of one-way elements under blast loading. In this paper, the basic methodology of SDOF models for two-way RC panels has been outlined, using TM5-1300 code instructions, and a SDOF model was developed for two-way RC panels with different reinforcement and aspect ratios. FE models of these panels were also constructed. Using SDOF models with different flexural rigidity, $P-I$ diagrams were generated and their predictions were compared with data obtained from FEA. In addition, modification was proposed for calculating dynamic reaction and results obtained from different methods were compared.

Comparison between $P-I$ diagram predictions and the FEA results showed that the use of SDOF models with the average of the cracked and the gross flexural rigidity resulted in a better correlation between the SDOF analysis and FEA, especially in the impulsive

regime. Compared to FEA results, the SDOF model gave conservative results for all loading types and significantly overestimated the deflections for pressures with low amplitude and long duration. The observed overestimation was mainly related to the deficiencies in the resistance function for the SDOF models of two-way panels.

Comparison between the dynamic reactions obtained from different techniques and FEA, showed that the proposed modification in TM5-1300 reaction calculation improved the SDOF reaction prediction in the impulsive regime and, unlike the TM5-1300 method which underestimates the reaction, the modified technique yield significantly better predictions for the impulsive realm of loading. In general, there was no significant difference between the different techniques and the modified TM5-1300 method with all methods underestimating the dynamic reaction compared to FEA results in the pressure regime. Therefore, it is recommended to use the proposed modification for the impulsive regime.

Paper III: Capacity Assessment of Reinforced Concrete Columns Subjected to Blast

Considering the inherent nonlinearity of RC, simplified techniques were introduced for analysis of these elements under blast loading. However, many of the available studies considered elements like beams which are not subjected to axial loads. Considering the important role of columns in providing the overall stability of structures, a MDOF model for RC columns was developed which takes into account of axial load effects, strain rate effects and variation of rigidity. Column section properties have been studied under

different levels of axial loads and strain rates. Moreover, $P-I$ diagrams were developed for two types of column details and the load carrying capacity of the columns were evaluated.

Through construction of moment-curvature diagrams for the column's cross section for different levels of axial load, it was shown that the ultimate curvature capacity decreased significantly by increasing the axial load. Moreover, enhancement in material properties with increasing the strain rate resulted in significant amplification of the larger axial force-bending moment interaction diagrams. In addition, it was shown that scaling the material properties by a factor of 1.25 (as proposed by many researchers) cannot capture the axial force and moment capacity enhancement for high values of strain rates in the arrange of 100 s^{-1} to 500 s^{-1} which is very common during blast.

Comparison of the $P-I$ diagrams developed with different axial loads shows that effect of high axial load is more pronounced for the impulsive regime and the maximum difference of 40% can be reached by increasing the axial load level to 70% of column axial load capacity. In addition, presence of axial load reduces the deflection at each damage level significantly. Calculating the RC column end rotation at the fully damaged state also showed that this parameter is not a constant value, as suggested by the TMS-1300, and it was observed that it decreases by increasing level axial load and the column stiffness.

Finally, comparison of the $P-I$ curves for the fully damaged level with ones for the partially damaged level indicates that good detailing at supports can enhanced the load carrying capacity of the columns significantly. In average, the deflection, the impulse asymptote and the pressure asymptote at the partially damaged state were amplified by the factors of 3.6, 2.4 and 1.5, respectively.

1.7 Suggestions for Future Work

The following points are proposed as an extension of this work:

- Studying the effect of support vibration on the overall response of the blast loaded element. Or, in other words, investigation of the possibility of providing isolators in order to reduce the blast load effect on the structural elements.
- Developing simplified numerical techniques to investigate the torsional response of blast loaded structural components.
- Using FEA and experimental results to develop a more comprehensive resistance function for two-way RC elements in order to be used in SDOF analysis.
- Quantifying the resistance function for retrofitted RC elements by FRP sheet in order to be used in SDOF analysis. Or modifying the MDOF model in order to consider the effect of such retrofit scheme in the analysis.
- Using FEA to develop SDOF transformation factors of structural elements which are subjected to non-uniform blast load and calibrate the approximate loading function with the different scaled distances.

- Using FEA to find approximate shape functions and transformation factors for SDOF models of panels with openings.

1.8 References

Baker, W.E. et al. 1933. Explosion hazards and evaluation. Elsevier Scientific Publishing Company, Oxford, UK.

Bangash, M.Y.H and Bangash, T. 2005. Explosion-resistant buildings: design, analysis, and case studies. Springer, Berlin, Heidelberg.

Beshara, F. B. A. 1994. Modeling of blast loading on aboveground structures - I. General phenomenology and external blast. *Computers and Structures*, 51(5): 597-606.

Biggs, J.M. 1964. Introduction to structural dynamics. McGraw-Hill Book Company, New York. .

Bischoff, P. H, and Perry, S. H. 1991. Compressive behavior of concrete at high strain rates. *Materials and Structures*. 24, 425–450.

Boutros, M. K. 2000. Elastic-plastic model of pinned beams subjected to impulsive loading. *J. Eng. Mech.*, 126(9):920-927.

CEB, Comité Euro-International du Béton, 1988. Concrete structures under impact and impulsive loading. CEB Bulletin 187, Lausanne, Switzerland.

Dokainish, M. A., Subbaraj K. 1989. A survey of direct time-integration methods in computational structural dynamics, I-explicit methods. Computers and Structures, 32(6):1371-1386.

Grote, D. L., Park, S. W. and Zhou, M. 2001. Dynamic behavior of concrete at high strain rates and pressures: I. experimental characterization. Int. J. Impact Eng., 25: 869-886.

Kolsky, H. 1949. An investigation of the mechanical properties of materials at very high rates of loading. Proceedings, Physical Society of London, Section B, 62: 676-704.

Krauthammer, T., Bazeos, N., Holmquist, T.J. 1986. Modified SDOF analysis of RC box-type structures. J. Struct. Eng. ,112(4) :726-744.

Krauthammer, T., Shahriar, S. and Shanaa, H. M. 1990. Response of reinforced concrete elements to severe impulsive loads. J. Struct. Eng., 116(4): 1061-1079.

Louca, L. A. and Harding, J. E. 1997. Non-linear analysis of imperfect plates under transient lateral pressure loading. Computers and Structures, 63(1): 27-37.

Low, H. Y., and Hao, H. 2002. Reliability analysis of direct shear and flexural failure modes of RC slabs under explosive loading. *Engineering Structures*, 24, 189–198.

Malvar, L. J. 1998. Review of static and dynamic properties of steel reinforcing bars. *ACI J.*, 95(5): 609-616.

Malvar, L. J., and Ross C. A. 1998. Review of strain rate effects for concrete in tension. *ACI J.*, 95(6): 735-739

Mays, G. C., and Smith, P. D. 1995. Blast effects on buildings: design of buildings to optimize resistance to blast loading. Thomas Telford, New York, NY.

Pan, Y., and Watson, A. 1998. Effect of panel stiffness on resistance of cladding panels to blast loading. *J. Eng. Mech.*, 124(4): 414–421.

Ross, C. A., Tedesco, J. W. and Kuenen, S. T. 1995. Effects of strain rate on concrete strength. *ACI J.*, 92(1): 37–47.

Schleyer, G. K., and Hsu, S. S. 2000. A modelling scheme for predicting the response of elastic plastic structures to pulse pressure loading. *Int. J. Impact Eng.*, 24, 759-777.

Soroushian, P. , and Choi, K. 1987. Steel mechanical properties at different strain rates. J. Struct. Eng., 113(4): 863-872.

Soroushian, P., Choi, K., and Alhamad, A. 1986. Dynamic constitutive behavior of concrete. ACI J., 83(2): 251-258.

Subbaraj, K. and Dokainish, M.A. 1989. A survey of direct time-integration methods in computational structural dynamics-II. Implicit methods. Computers and Structures, 32(6): 1387-1401.

Tedesco, J. W., Ross, C. A., Powell, J. C., and Hughes, M. L. 1997. A strain rate dependent concrete material model for ADINA. Computers and Structures, 64(5), 1053-1067.

TM5-1300, US Department of Army Technical Manual, 1990. Design of structures to resist the effects of accidental explosions. Washington, DC.

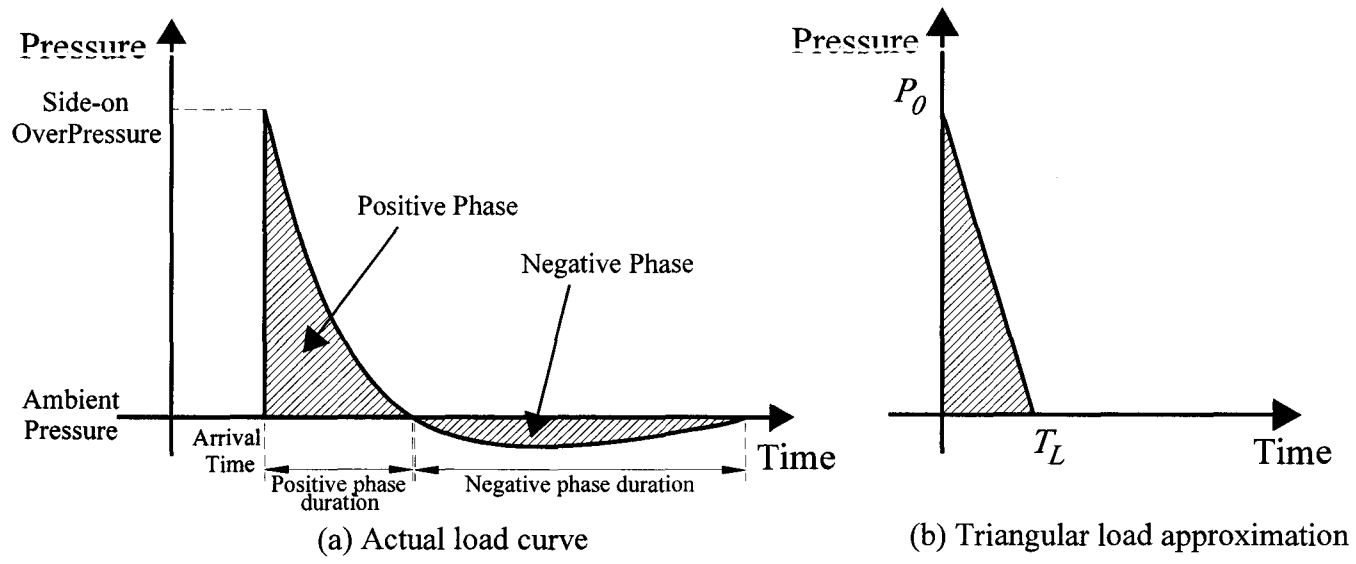


Fig. 1.1: Blast loading time history

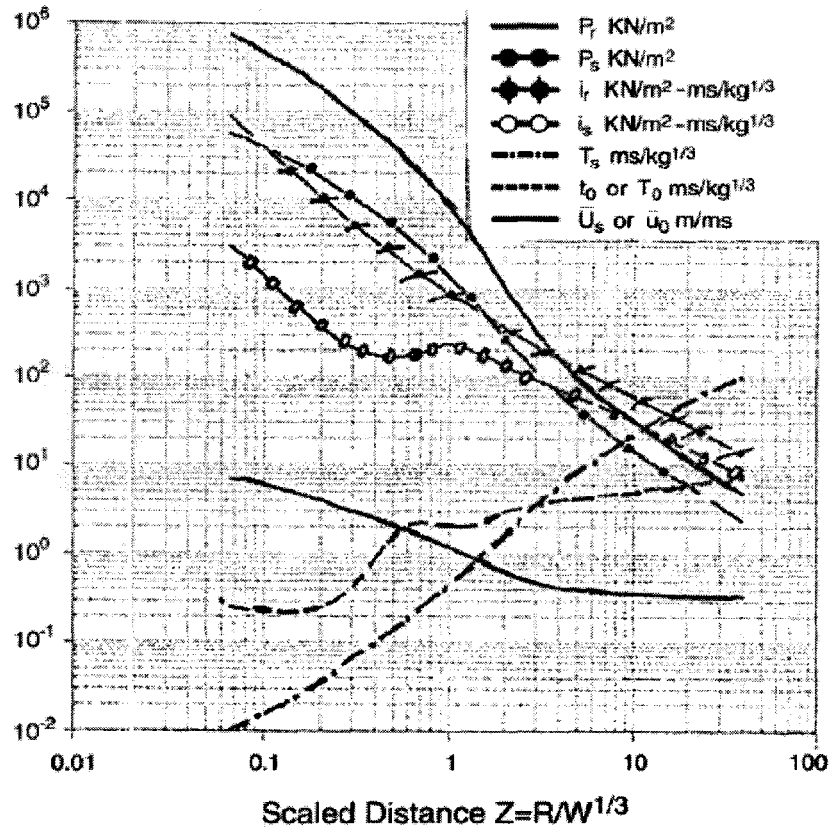
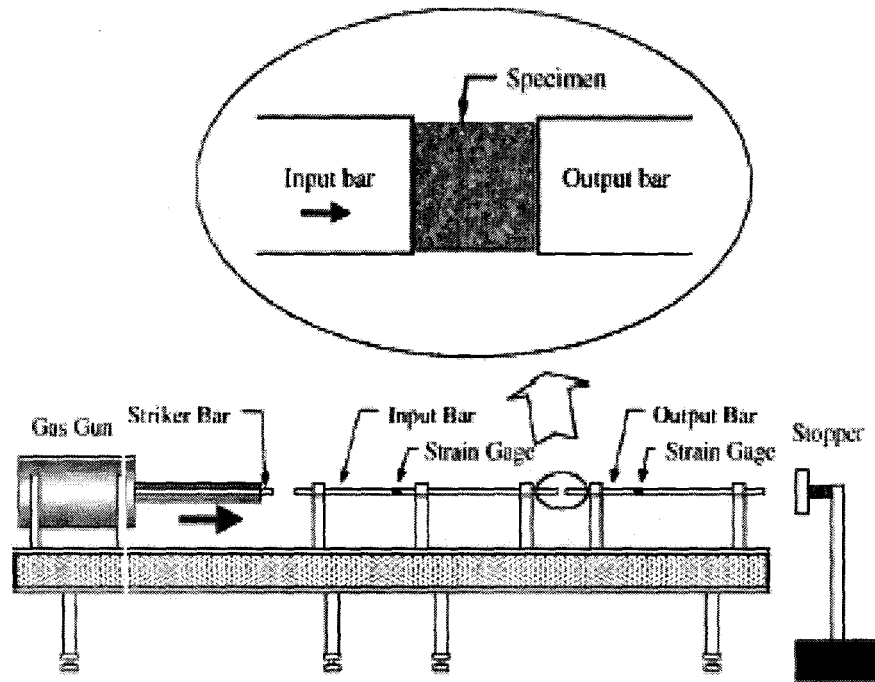


Fig. 1.2: Blast loading parameters as a function of scaled distance (Bangash, M.Y.H and Bangash, T. 2005)

(a)



(b)

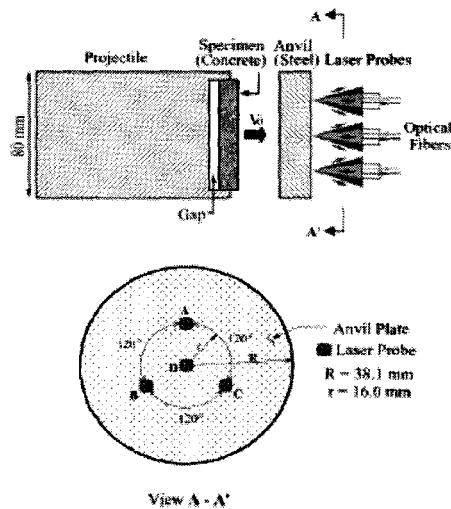


Fig. 1.3: Schematic views of tests for investigating strain rate effect: (a) SHPB test, (b) Plate impact test (Grote et al. 2001)

Chapter 2: Response Sensitivity of Blast Loaded Reinforced Concrete Beams to the Number of Degrees of Freedom

Abstract: Accurate analysis of Reinforced Concrete (RC) structures under blast loading is very complicated due to the nonlinear behavior of concrete and reinforcement and the various failure modes to be considered. Although blast loads can excite large number of modes due to their high frequency content, practical computational tools are usually limited to single degree of freedom (SDOF) models. In addition to oversimplification, SDOF models are known to give inaccurate prediction for shear forces. This is because accurate shear force prediction typically requires more modes than the fundamental mode. In this study, a multi-degree-of-freedom (MDOF) model is developed that takes into account the nonlinear behavior of RC structures and the material strength and deformation dependency on the strain rate. Using this model, a series of dynamic analyses were carried out for two typical structural members, with different combination of blast pressure and impulse. The effect of varying the number of degrees-of-freedom (DOF) was investigated through increasing the number of nodes used to discretize each structural member. Results indicated that a large number of DOF is required to accurately model such structures and that the numbers of DOF is proportional to the extent of damage. Changing the number of DOF also affected the Pressure-Impulse ($P-I$) diagrams for the structural member significantly, especially in the impulsive regime. The model was also compared to available experimental results and showed good agreement.

Keywords: Blast loads; concrete structures; degrees of freedom; dynamic analysis; models; nonlinear analysis.

2.0 Introduction

In order to design a structure to resist a certain level of blast loading, local and global failure should be taken into consideration. When the local response of RC members such as beams and columns is considered, the design philosophy should aim at preventing specific failure modes and/or they should be proportioned to withstand a specific level of damage. On the other hand, when the possibility of global or overall failure is investigated, the design strategy should aim at preventing progressive collapse, providing alternative load paths and increasing the structural redundancy.

Because of the nature of blast loading and the nonlinearity associated with RC structures, nonlinear dynamic analysis must be used to assess the full structural response. The different techniques used for nonlinear dynamic analysis usually fall under two categories: analytical (macro) models and finite element models. Macro models typically employ a Single Degree of Freedom (SDOF) or a Multi Degree of Freedom (MDOF) approach. These models use the fundamental (first) mode of vibration or the first few modes to predict the structure response to blast loading. Analytical models are usually simple and require limited number of input data. On the other hand, nonlinear dynamic analysis using a finite element model usually requires a large number of input parameters and significant experience and knowledge for obtaining reliable and realistic results. However, in early design or analysis stages, it is not feasible to use complex time consuming finite element analyses, therefore, there is a need for relatively simple, yet reasonably accurate methods such as the one described here. This method can also be used to check the overall accuracy of finite element analyses.

Generally, the exact blast loading information including the peak over pressure value and pressure time history may not be available as a result of many uncertainties associated with such loading. However, as can be seen in Fig. 2.1(a), for a typical blast loading, the blast pressure (side-on over pressure) decays in an exponential form during a very short time (positive phase) and finally falls below ambient pressure, stays there for a longer time (negative phase) and has lower pressure intensity (Baker et al. 1983). In practice, the negative phase (suction) can be neglected and the exponential decay loading can be approximated by a triangle which has the same peak pressure but different duration, T_L .

As can be seen in Fig. 2.1(b), the duration is determined based on the time to reach the maximum response. If the maximum structural response occurs after the pressure has decayed to ambient pressure, the equivalent duration is obtained by equating the area under the actual pressure-time curve in the positive phase (the *impulse*) to the area of the idealized triangle load. On the other hand, if the time to reach the maximum response is less than the positive phase duration, the equivalent duration is found by equating the slope of tangent line (at arrival time) on the actual loading curve with the slope of triangle load (Beshara 1994). This idealization is shown in Fig. 2.1(c).

There are a number of investigations in which SDOF or MDOF techniques have been employed to study the response of structural members under blast or impact loading [Biggs (1964); Krauthammer et al. (1986); Krauthammer et al. (1990); Louca and Harding (1997); Pan and Watson (1998); Schleyer and Hsu (2000); Boutros (2000); Low and Hao (2002)]. However, most available research programs, including the ones listed

above, have focused on considering the real first mode or a combination of different assumed mode shapes for the first vibration mode to govern the dynamic response of structural members. Nevertheless, it is well known that higher modes significantly affect the structural response in wave propagation problems such as blast and impact (Ebeling et al. 1997; Subbaraj and Dokainish 1989). This means that models with more degrees of freedom (DOF) may be required to account for the effect of higher modes on the structural response. Moreover, recently published experimental results of RC members tested under blast loading (Razaqpur et al. 2007; Magnusson 2007) showed that shear failure, which can be predicted more accurately by including higher mode effects, was the governing failure mode in many of the tested RC members.

In this paper, a numerical method based on the lumped mass approach is employed to study the significance of using MDOF model with a large number of DOF on the response of RC beams subjected to blast. The strain rate effects are also incorporated in the analysis in order to consider the effect of the rapid rate of loading on member response. A series of blast loading with different pressure and impulse combinations are generated to produce different frequency content and the effect of the large number of DOF on maximum response quantities is considered by increasing the number of nodes used in discretizing these structural members. The following sections outline the model development, including material properties and solution technique, as well as the results of the various analyses.

2.1 Model Development

2.1.1 SDOF Model

Available SDOF analysis techniques applied to individual structural members consider the fundamental vibration response mode of the member and utilize a nonlinear dynamic analysis procedure to evaluate the member response to a certain level of blast loading. In these techniques, the dynamic response of a structural member is approximated by the first mode shape and the dynamic equation of motion is evaluated for an equivalent SDOF system (Figs. 2.2(a) and 2.2(b)). Deflection obtained by solving this equivalent system represents the actual deflection of the structural member at a certain key location (e.g. member midspan). To establish the equivalent SDOF, one needs to evaluate the mass factor, K_M , the resistance factor, K_R and the load factor, K_L , which relate the equivalent mass, the equivalent resistance, and the equivalent load, respectively, in the SDOF system to the actual quantities in the structural system. In general, by equating the external work, kinetic energy and strain energy of the two systems, these factors can be found easily. It is worth mentioning that the load factor is approximately equal to the resistance factor (Mays and Smith 1995). These factors can be evaluated (Biggs 1964) as follows:

$$K_R = K_L = \frac{\int_0^L p\phi(x)dx}{\int_0^L p dx} \quad (2.1)$$

$$K_M = \frac{\int_0^L \rho_m \phi^2(x) dx}{\int_0^L \rho_m dx} \quad (2.2)$$

In the above equations, K_L , K_R , K_M are the load factor, the resistance factor and the mass factor respectively; ρ_m and p are the mass and load per unit length; L is the member length and $\phi(x)$ is the assumed mode shape.

For a nonlinear system, a different shape function is usually considered for each stage of response (e.g. elastic, elastic-plastic, or fully plastic conditions). Consequently, as the shape function changes, new transformation factors are computed for each deflection stage. Using these factors, the dynamic equation of motion for the SDOF model can be written as:

$$K_M m \ddot{y} + K_R R(y) = K_L F(t) \quad (2.3)$$

In this equation, m is the member mass which can be given as: $m = \rho_m \times L$; y and \ddot{y} are the displacement and the acceleration; $R(y)$ is the resistance force as a function of displacement and $F(t)$ is the blast load as a function of time.

It should be noted that, as can be observed from Eq. 2.3, damping is usually not considered in impulsive loading problems such as blast and impact since the maximum response, which is generally the quantity of interest, usually occurs during the first vibration cycle when damping has minimum contribution to the dynamic response.

In order to express the equation of motion in terms of one factor, K_L is divided by K_M and the factor K_{LM} (*Load-Mass factor*) is introduced. The values of the load-mass factors are tabulated and can be found in references such as Biggs (1964); TM5-1300 (1990) and Mays and Smith (1995). Hence, the equation of motion for the equivalent SDOF can be written as:

$$K_{LM} m \ddot{y} + R(y) = F(t) \quad (2.4)$$

In the previous equation, the static load-deflection relationship of the structural member should be constructed in order to use it as the resistance-displacement function, $R(y)$. These resistance-displacement relationships can be found either experimentally, using appropriate code equations, or using plastic analysis. If plastic analysis is used, then the force, R_u , which initiates a plastic hinge within the structural member is calculated, the

corresponding static deflection, Δ_y , is found and the resistance-deformation relationship is simplified as shown in Fig. 2.2(c).

In the case of RC member, an effective flexural rigidity, EI_{eff} , is needed to compute the deflection obtained for the corresponding applied static load. Biggs (1964) suggested using the average of the cracked section rigidity, EI_{cr} , and the gross rigidity, EI_g , for deflection calculation. It should be noted that other international RC design codes [ACI 318-05 (2005); CSA A23.3-04 (2005); EuroCode 2 (1992); NZS 3101:1995 (1995)] employ different expressions for EI_{eff} .

Figure 2.3 shows the forces exerted on a simply supported beam subjected to a blast pressure. As can be seen in this figure, both the inertial force and the applied blast load should be considered in order to find the correct dynamic reaction, V_d , at the supports. Considering the primary response mode, Biggs (1964) used the equilibrium conditions for the forces shown in Fig. 2.3 to derive the following equation for the dynamic reaction:

$$V_d(t) = \beta_R \times R(t) + \beta_F \times F(t) \quad (2.5)$$

This equation expresses the dynamic reaction, $V_d(t)$, at a time t as the summation of fractions of the resistance force, $R(t)$, and the applied force, $F(t)$, at time t , with β_R and β_F being constants, which are modified for each stage of displacement (e.g. elastic, elastic-plastic, or fully plastic).

2.1.2 MDOF Model

As mentioned earlier, in nonlinear analysis of RC members subjected to dynamic loading the material stiffness should be adjusted for each loading increment or with increased displacement. The members must also be discretized to account for the stiffness variation across the member length. As a result, for this type of analysis, finite element models, which require special experience and significant modeling and solution time, are usually employed.

To reduce the difficulties associated with nonlinear dynamic analysis of continuous systems, MDOF models based on the lumped mass approach can be employed. In these techniques, the structural member is replaced by a series of discrete connected nodes and the material properties are concentrated at these nodes. Using a finite difference method, the dynamic analysis of an RC member subjected to blast can be performed as explained below.

Figure 2.4 shows a simple beam divided into $(n+1)$ segments. The lumped mass and load at the i^{th} node are, respectively, $LM_i = \rho_m (\Delta x)$ and $F_i = p(\Delta x)$, in which Δx is the segment length.

The dynamic equilibrium equation for the i^{th} node will be:

$$LM_i \ddot{y}_i + V_{i-1,i} - V_{i,i+1} + C_i \dot{y}_i = F_i(t) \quad (2.6)$$

where:

$y_i, \dot{y}_i, \ddot{y}_i$ = i^{th} node displacement, velocity and acceleration, respectively.

LM_i = Lumped mass at the i^{th} node

C_i = Damping for the i^{th} node

$F_i(t)$ = Lumped blast load at the i^{th} node

$V_{i-1,i}, V_{i,i+1}$ = Shear force values between the $(i-1)^{th}$ and the i^{th} node, and shear between the i^{th} and the $(i+1)^{th}$ node, respectively.

By considering the free body diagram of a typical nodal mass (Fig. 2.4), the preceding shear forces can be written as:

$$V_{i-1,i} = \frac{M_i - M_{i-1}}{\Delta x} \quad (2.7)$$

$$V_{i,i+1} = \frac{M_{i+1} - M_i}{\Delta x} \quad (2.8)$$

where:

M_{i-1}, M_i, M_{i+1} = Moment at the $(i-1)^{th}$, the i^{th} and the $(i+1)^{th}$ node, respectively.

Δx = Segment length

and employing Eqs. 2.7 and 2.8, Eq. 2.6 can be rewritten as:

$$LM_i \ddot{y}_i - \frac{M_{i-1} - 2M_i + M_{i+1}}{\Delta x} + C_i \dot{y}_i = F_i(t) \quad (2.9)$$

The curvature, ϕ , can be obtained at each node using the following finite difference approximation:

$$\phi \cong -\frac{d^2 y}{dx^2} \cong \frac{-1}{\Delta x^2} (y_{i+1} - 2y_i + y_{i-1}) \quad (2.10)$$

Hence, the corresponding moment at each node can be found from the moment-curvature diagram evaluated for the beam cross section. Equation 2.9 is then solved numerically for each time increment. Adopting this technique, the nonlinear behaviour of RC members can be analyzed and the post damage state can be modeled easily using the MDOF approach. As noted earlier, damping is not considered in the MDOF model since the maximum response, which is generally of interest, usually occurs during the first vibration cycle when damping has minimum contribution to the dynamic response.

2.1.2.1 Numerical Integration Scheme

In this study, the Central Difference Method, which is an explicit method, is used and the following formulation, which is employed by Krauthammer et al. (1993), is considered for estimating the critical time step, t_{cr} :

$$t_{cr} = \Delta x / C_L \quad (2.11)$$

where the wave velocity, C_L , is given by:

$$C_L = \left[\frac{E(1-\nu)}{(1+\nu)(1-2\nu)\rho} \right]^{1/2} \quad (2.12)$$

In the above expressions, Δx is the node spacing, E is the elastic modulus, ν is Poisson's ratio and ρ is the mass density of reinforced concrete.

A time step size of $0.05 t_{cr}$ obtained from the previous equation was compared to even smaller values and the least value was selected in the analysis. These smaller values were 1×10^{-6} second for $n \leq 40$ and 1×10^{-7} seconds for $n > 40$, n being the number of nodes in the MDOF model. Since the order of time step is very small, it is important to note that enough numerical precision should be considered during the analysis in order to prevent truncation errors created by the computer itself. Therefore, all calculations in this study were carried out by employing double precision.

2.1.2.2 Material Stress-Strain Relationship

2.1.2.2.1 Concrete

Numerous stress-strain relationships for concrete and reinforcing steel are available in the literature. For concrete in compression, different relationships expressed in terms of the

compressive strength, the strain at this compressive strength, and the concrete modulus of elasticity have been proposed (Scott et al. 1982; Dilger et al. 1984; Soroushian et al. 1986; Mander et al. 1988). In this study, the following relationship proposed by Popovics (1973) is adopted:

$$\sigma_c = f'_c \frac{q(\varepsilon / \varepsilon_c)}{q - 1 + (\varepsilon / \varepsilon_c)^{qk}} \quad (2.13)$$

where:

ε, σ_c = Strain and corresponding compressive stress

f'_c, ε_c = Maximum compressive stress and corresponding strain

q, k = Curve fitting parameters which are given by $0.8 + f'_c / 17$ and $0.67 + f'_c / 62$, respectively, where f'_c is in MPa.

Equation 2.13 is easy to use and was shown to be capable of modeling initial tangent stiffness and the post-peak behavior by Bentz (2000).

For tension stiffening, different equations have been proposed by Vecchio and Collins (1982), Collins and Mitchell (1987), Tamai et al. (1987), and Bentz (2005). These relationships may be appropriate for a specific section since tension stiffening is dependent on the bond characteristics which vary from section to section. In this study, the Vecchio and Collins (1982) relationship, given by:

$$\sigma_t = \frac{f_t'}{1 + \sqrt{200\varepsilon_t}} \quad (2.14)$$

was used, in which, ε_t, σ_t are the tensile strain and corresponding tensile stress, and f_t' is the tensile strength taken as 10% of the compressive strength.

2.1.2.2.2 Steel

A number of formulations were proposed for the reinforcing steel stress-strain relationship and all of them consist of three zones: elastic, yield plateau and strain hardening. In this study, Hoehler and Stanton (2006) model was used. According to their formulation, the strain-stress relationship for steel is expressed as:

$$\sigma = E \times \varepsilon \quad \text{for } \varepsilon \leq \varepsilon_y \quad (2.15-a)$$

$$\sigma = \sigma_y + (\varepsilon - \varepsilon_y) \times E_y \quad \text{for } \varepsilon_y \leq \varepsilon \leq \varepsilon_{sh} \quad (2.15-b)$$

$$\sigma = \sigma_u - (\sigma_u - \sigma_{sh}) \times \left(\frac{\varepsilon_u - \varepsilon}{\varepsilon_u - \varepsilon_{sh}} \right)^{C_1} \quad \text{for } \varepsilon_{sh} \leq \varepsilon \leq \varepsilon_u \quad (2.15-c)$$

where:

ε, σ = Strain and corresponding stress in the reinforcing steel, respectively.

σ_y, ε_y = Stress and strain at steel yield, respectively.

$\sigma_{sh}, \varepsilon_{sh}$ = Stress and strain at the onset of strain hardening, respectively.

σ_u, ε_u = Ultimate (peak) stress and strain, respectively.

E = Elastic modulus

E_y = Slope of yield plateau

C_1 = Parameter that defines the curvature of the strain hardening curve.

2.1.2.3 Strain Rate Effects

It has been shown by a number of experimental and numerical studies that concrete and steel exhibit significant strength increase under high strain rate of loading. Although it was suggested that inertial effects change the uniaxial stress to uniaxial strain during high strain rate of loading, and this leads to enhancement in material strength (Bischoff and Perry 1991), this characteristic is not well understood due to lack of experimental stress-strain relationships at high strain rate. Most of the experimental results are limited to low strain rates or have been performed on small specimens which may give correct results for isotropic materials such as steel but not for heterogeneous materials such as RC.

As a simplification, the ratio of material dynamic strength to static strength, usually referred to Dynamic Increase Factor (*DIF*), is given as a function of strain rate either graphically (TM5-1300, 1990) or presented in the form of formulas.

2.1.2.3.1 Concrete

For concrete under compression, it has been shown that the increase in compressive strength is more significant than the enhancement of its other properties such as ultimate strain and the elastic modulus. For strength enhancement, expressions were proposed by Comité Euro-International du Béton (CEB) (1988), Tedesco et al. (1997), and Malvar and Ross (1998). All these expressions differentiate between low to intermediate strain rates

and intermediate to high strain rates, and suggest separate relationships for different ranges (Fig. 2.5(a)). It has also been shown that the concrete tensile strength exhibits higher increase than the compressive strength (Fig. 2.5(b)). There is no consensus among different researchers on the effect of strain rate on the strain at the peak compressive stress and different variations have been reported (Bischoff and Perry 1991).

Tedesco et al. (1997) used their experimental results obtained from a number of Split-Hopkinson Pressure Bar (SHPB) tests for concrete with different strength and moisture, and employed some regression equations in their concrete model. Malvar and Ross (1998) considered a large number of test results and modified CEB (1988) formula for concrete under tension. Since Tedesco's experiment cover strain rates up to $1 \times 10^3 \text{ s}^{-1}$ and Malvar's equation has been obtained by considering large number of data, Tedesco's relations for concrete under compression and Malvar's formula for concrete under tension are adopted in this study. Tedesco et al. (1997) considered these equations for concrete under compression:

$$f_{cd} / f_{cs} = 0.758 \log \dot{\epsilon} + 1.058 \geq 1.0 \text{ for } \dot{\epsilon} \leq 63.1 \text{ s}^{-1} \quad (2.16\text{-a})$$

$$f_{cd} / f_{cs} = 0.758 \log \dot{\epsilon} - 0.289 \leq 2.5 \text{ for } \dot{\epsilon} \geq 63.1 \text{ s}^{-1} \quad (2.16\text{-b})$$

$$\epsilon_{cd} / \epsilon_{cs} = 1.08 + 0.112 \log \dot{\epsilon} + 0.0193 (\log \dot{\epsilon})^2 \quad (2.16\text{-c})$$

where f_{cd} and ϵ_{cd} are concrete dynamic compressive strength and corresponding dynamic strain, and f_{cs} and ϵ_{cs} are their static values, $\dot{\epsilon}$ is the strain rate in s^{-1} .

Malvar's equations for concrete under tensions are:

$$f_{td} / f_{ts} = \left(\frac{\dot{\epsilon}}{\dot{\epsilon}_s} \right)^\delta \text{ for } \dot{\epsilon} \leq 1.0 \text{ s}^{-1} \quad (2.17-a)$$

$$f_{td} / f_{ts} = \beta \left(\frac{\dot{\epsilon}}{\dot{\epsilon}_s} \right)^{1/3} \text{ for } \dot{\epsilon} \geq 1.0 \text{ s}^{-1} \quad (2.17-b)$$

Where f_{td} and f_{ts} are the dynamic and static tensile strength, $\dot{\epsilon}$ is the strain rate. The static strain rate, $\dot{\epsilon}_s$, is taken as $30 \times 10^{-6} \text{ s}^{-1}$ for compression, and, $\dot{\epsilon}_s = 1 \times 10^{-6} \text{ s}^{-1}$ for tension, $\beta = 10^{(6\delta-2)}$, and $\delta = 1 / (1 + 8 f_{cs} / f_{co})$, where $f_{co} = 10 \text{ MPa}$.

2.1.2.3.2 Steel

For steel, it has been observed that yield and ultimate stress increase with increasing strain rate but the modulus of elasticity is not affected by the rate of loading. Similar to concrete, relationships are given for reinforcing steel by Soroushian and Choi (1987); CEB (1988); Malvar (1998). Malvar's formulations were used in the present analyses because of the large number of test results at different strain rates that were used to verify his expressions:

$$DIF = \left(\frac{\dot{\epsilon}}{10^{-4}} \right)^\alpha \quad (2.18-a)$$

where:

$$\alpha = 0.074 - 0.040 \frac{f_y}{414} \quad \text{for yield stress, or} \quad (2.18-b)$$

$$\alpha = 0.019 - 0.009 \frac{f_u}{414} \quad \text{for ultimate stress} \quad (2.18-c)$$

$\dot{\epsilon}$ is the strain rate f_y and f_u are the bar yield stress and ultimate stress in MPa.

As can be seen in Fig. 2.5(c) and Fig. 2.5(d), the stress-strain curves will be scaled corresponding to the specific strain rate. For concrete, the maximum compressive stress and the corresponding strain are scaled by the *DIF* values given in Eq. 2.16 while the maximum tensile stress is scaled by the *DIF* value given in Eq. 2.17. For steel, the yield and ultimate stress are amplified by the *DIF* values given in Eq. 2.18.

2.1.2.4 Strain Rate Estimation

In order to use the appropriate *DIF*, a procedure to find the strain rate corresponding to a specific blast load would need to be established. Different methods such as finding maximum curvature rate (Kulkarni and Shah 1998) or deriving an approximate strain rate equation (Krauthammer et al. 1994) have been proposed. These methods estimate the order, rather than the exact value of the strain since the latter is too complicated to be modeled using simple tools. Nevertheless, because the method described by Krauthammer et al (1994), is simple and accurate enough, it was adopted in this study. To obtain the *DIF*, the load-strain relation at extreme fibers for a section resulting from a uniform load should be evaluated. Considering the simply supported beam shown in Fig. 2.6, the strains at the tensile and compressive fiber at the midspan of this beam are given by:

$$\varepsilon_c = \left(\frac{pl^2}{8}\right)\left(\frac{h_c}{EI_{cr}}\right) \quad (2.19-a)$$

$$\varepsilon_t = \left(\frac{pl^2}{8}\right)\left(\frac{h_t}{EI_{cr}}\right) \quad (2.19-b)$$

where ε_c and ε_t are strains at the extreme compressive and tensile fiber, respectively; p is the uniform blast load; h_c and h_t are the compression depth and the tension depth of the cross section, respectively; EI_{cr} is the cracked flexural rigidity and L is the beam span. If the moment-curvature relationship at a certain strain rate is approximated as elastic-perfectly-plastic, then $EI_{cr} = M_y / \phi_y$, where M_y and ϕ_y are the yield moment and curvature at yield, respectively.

Consequently, the strain rate at the extreme fibers can be obtained by evaluating the derivative of Eqs. 2.19-a and 2.19-b with respect to time as follows:

$$\frac{\partial \varepsilon_c}{\partial t} = \frac{\partial p}{\partial t} \left(\frac{l^2}{8}\right) \left(\frac{h_c}{EI_{cr}}\right) \quad (2.20-a)$$

$$\frac{\partial \varepsilon_t}{\partial t} = \frac{\partial p}{\partial t} \left(\frac{l^2}{8}\right) \left(\frac{h_t}{EI_{cr}}\right) \quad (2.20-b)$$

As an approximation, a strain rate value, $\dot{\varepsilon}$, can be assigned for the whole cross section by taking the average of strain rates obtained from Eqs. 2.20-a and 2.20-b:

$$\dot{\varepsilon} = \frac{\partial p}{\partial t} \left(\frac{l^2}{16} \right) \left(\frac{h_c + h_t}{EI_{cr}} \right) \quad (2.21-a)$$

or

$$\dot{\varepsilon} = \frac{\partial p}{\partial t} \left(\frac{l^2}{16} \right) \left(\frac{h}{EI_{cr}} \right) \quad (2.21-b)$$

where h is the beam height.

For a triangular load idealization (Fig. 2.1(b)), Eq. 2.21-b can be simplified to:

$$\dot{\varepsilon} = \frac{p_0}{T_L} \left(\frac{l^2 h}{16} \right) \left(\frac{\phi_y}{M_y} \right) \quad (2.22)$$

where p_0 and T_L are peak blast load per unit length and loading duration, respectively.

A similar procedure can be used for RC beams with different loading and support condition, where the strain rate for each beam section can be evaluated through similar approximation. In this way, the proposed model would be capable of considering the distribution of strain rate variation along the beam length.

2.2 Numerical Results and Discussion

2.2.1 Overall Procedure

In order to investigate the effect of varying number of DOF, a clamped-clamped and a simply supported RC beam with identical material and cross sectional properties are analyzed. The clamped beam is used to study the effect of higher stiffness (compared to

the simply supported beam) on the response. The beam has equal amount of positive and negative steel with the reinforcement ratio of 1% each. The beam has a of 600 mm deep, and a 400 mm wide cross section and span length of 4.0 m. A 30 MPa concrete is used and the yield and ultimate strengths of the steel reinforcement were 400 MPa and 600 MPa, respectively.

Using the triangular load approximation of the actual blast loading as explained earlier, the beams are subjected to a series of pressure and impulse combinations. This means that for a specific peak pressure, the duration of the load is changed and consequently new values of impulse are generated. For each combination of pressure and load duration, the number of nodes (DOF) is increased from 2 to 30 for the simply supported beam and from 2 to 40 for the clamped beam.

Following the method explained earlier, the strain rate is obtained for each node and the material properties are adjusted accordingly. As discussed earlier the concrete tensile strength is known to be more sensitive to the strain rate than the compressive strength. Moreover, the *DIF* for concrete under tension is significant for strain rates higher than $1s^{-1}$. Therefore, for load cases in which the maximum strain rate is greater than $1s^{-1}$, separate strain rates and moment curvature relationships are evaluated for each node. For other load cases (i.e. cases with strain rate less than $1s^{-1}$), the maximum strain rate value and the corresponding moment-curvature relationship is used for all the beam nodes. The ultimate curvature is defined as the point on the moment-curvature curve at which half of the beam height is crushed in compression. The analysis would stop when the number of

failed nodes (nodes having curvature greater than ultimate curvature) reaches three for the clamped beam (at both supports and at the midspan) and one (at the midspan) for the simply supported beam. The numerical procedure is summarized in the flow chart shown in Fig. 2.7.

A total of 27 and 25 load cases were analyzed for the simply supported beam and the clamped beam, respectively. The blast loads included six peak pressure values ($P_0=100, 500, 750, 1,000, 2,500$ and $5,000$ kPa) and five load durations ($T_L= 0.003, 0.005, 0.01, 0.1$ and 1.0 s).

Among these combinations, the simply supported beam survived 15 load scenarios (S-1 to S-15 in Table 2.1(a)) and the clamped beam survived 17 load scenarios (C-1 to C-17 in Table 2.1(b)). The rest of the beams (12 simply supported beams and 8 clamped beams) failed totally under the particular combination of blast and impulse acting on them. Therefore, the results for the two sets of beams will be discussed separately.

It should be noted that more studies would be needed to cover a wider range of span/depth and reinforcement ratios, different support conditions and different ranges of pressure and impulse. However, the different load parameters and support conditions considered in this study can be considered adequate to give an overall understanding and demonstrate the effects of considering different MDOF systems in the analysis of RC beams subjected to blast.

2.2.2 Partially Damaged Cases

The variation of maximum displacement, curvature and shear for the simply supported beam are depicted versus the number of nodes for two pressure values (1,000 kPa, 2,500 kPa) in Fig. 2.8. It can be seen that the variations in maximum displacement, curvature and shear decrease significantly with increasing node number and, typically, a minimum of three nodes, five nodes and ten nodes are needed to predict the displacement, curvature and shear, respectively, within the specified convergence limit (defined as 5% response difference between successive MDOF models).

As expected, a larger number of nodes (DOF) is needed to estimate the shear (Clough and Penzien 1993). Table 2.1(a) shows the difference between the predicted displacement, curvature and shear values obtained using three, five and ten nodes, to the corresponding predicted values using thirty nodes for all the partially damaged cases, expressed as a percentage of the latter. As the results show, the maximum difference between the results obtained for all of the response parameters using thirty nodes and those obtained using fewer nodes is approximately 11% (Beam S-1).

Similar results are given in Fig. 2.9 for the clamped beam. This figure shows the variations of maximum response quantities with increasing number of nodes for the two previous peak pressure values (i.e. 1,000 kPa, 2,500 kPa). Compared to the simply supported case, the dynamic shear is higher and the displacement is lower for the clamped beam as a result of its higher stiffness. It can also be noted that the required number of nodes for the displacement and the curvature values to converge is significantly greater than that for the simply supported beam case. This can be attributed

to the higher vibration frequency of the clamped beam compared to the simple beam, which, combined with the high frequency content in blast loads, leads to significant higher mode contributions to the response. Thus, more nodes (DOF) would be needed to model the C-Beam responses. As observed from Fig. 2.9, a minimum of ten nodes for both displacement and curvature, while a minimum of twelve nodes is required for shear to obtain results that are accurate enough to satisfy the 5% convergence limit.

Table 2.1(b) shows the difference between the predicted maximum displacement, curvature and shear values obtained using ten, ten and twelve nodes, respectively, and the corresponding values obtained using forty nodes for partially damaged clamped beams, expressed as a percentage of the more accurate values. As the results show, the maximum difference between the response values obtained using forty nodes and those obtained using fewer nodes occurs in predicting shear and it is 13.9% of the more accurate value (Beam C-8).

2.2.2.1 Comparison with Different SDOF Models

The maximum response quantities for displacement and shear obtained from a MDOF model, which is used with the minimum numbers proposed earlier, are compared with the results obtained from different SDOF models. Four SDOF models with different commonly used flexural rigidity, EI , are considered. These SDOF models are based on the cracked section, EI_{cr} , gross section, EI_g , average of the cracked and the gross section rigidities, EI_{ave} , and the rigidity expression recommended by the CSA A23.3-04, (2005) Standards for computing RC beams deflection, EI_{CSA} .

It should be noted that the EI_{CSA} is a function of the maximum moment in the beam and as a result it is a function of the resistance. Therefore, the use of EI_{CSA} results in a nonlinear resistance. The resulting problem is solved for each time increment using the Newton-Raphson method. In the solution of SDOF system the maximum strain rate obtained from the proposed MDOF model is used. One additional SDOF system considered is a 1 node MDOF system, which is the same as the MDOF system described earlier but using only a single node at the beam midspan.

The percentage difference between the displacements and shears obtained from five different SDOF systems and the MDOF system are given in Tables 2.2(a) and 2.2(b) with the calculated absolute maximum differences obtained for each model shown in bold. Considerable scatter exists in the results obtained from several different commonly used SDOF models which emphasizes the high dependency of the SDOF models on EI . The SDOF (EI_{cr}) model overestimates the displacement by 23.7% (Beam S-14) to 132.6% (Beam C-4). In contrast, the SDOF (EI_g) model underestimates the displacement by 41.1% (beam S-7). Both the SDOF (EI_{cr}) and the SDOF (EI_g) models also underestimate the value of shear by 46.9% (beam S-1) and 19.1% (beam S-1), respectively. The SDOF (EI_{ave}) and SDOF (EI_{CSA}) models give better prediction with a maximum difference of around 31% (Beams S-1 and S-13) for the two response quantities. It should also be noted that the SDOF (EI_{CSA}) model yields better prediction of the response than the SDOF (EI_{ave}) model for clamped beam since it considers the combination of the supports

and midspan rigidities in the analysis (70% of midspan rigidity and 15% of each support rigidity) to obtain the overall rigidity (CSA A23.3-04 2005).

As can be observed from Table 2.2, use of a single node in the MDOF model [MDOF (*1 node*)] leads to highly inaccurate prediction of the displacement which is overestimated by 210% (Beam C-14). This is because the curvature is approximated inaccurate and the variation along the beams is not modeled correctly. The results are better for simply supported beams because of the lack of such variation. It can also be seen that MDOF (*1 node*) model underestimates the shear by about 60% on average in both the S- and C Beams as a result of lumping of the mass and load at one point only.

Overall, good results can be obtained for both the displacement and the shear using SDOF if an appropriate value is used for correct EI . The comparison shows that for some values of beam and load parameters the use of EI_{ave} and EI_{CSA} can yield results that are close to those obtained from a MDOF model.

2.2.2.2 Dynamic Shear Comparison with Closed Form Solutions

For elastic behaviour, Biggs' (1964) closed form solution (Eq. 2.5) can be used to estimate the maximum shear based on the first mode of vibration compared to the maximum shear obtained from the proposed MDOF model. Biggs' expressions for simply supported and the clamped-clamped beams are given as follow:

$$V_d = 0.39R(t) + 0.11F(t) \quad \text{for simply supported beams} \quad (2.23-a)$$

$$V_d = 0.36R(t) + 0.14F(t) \quad \text{for clamped beams} \quad (2.23-b)$$

Where V_d is the dynamic shear at support and $F(t)$ and $R(t)$ are the applied load and the elastic resistance as a function of time, respectively. The time of maximum shear can be found from the MDOF model and consequently, $F(t)$ and $R(t)$ can be calculated. It should be noted that $R(t)$ can be obtained as a function of moment, $M(t)$, at support and midspan for the simply supported and the clamped-clamped beam, respectively; (i.e. $8M(t)/4$ and $12M(t)/4$)

Table 2.3 gives the shear obtained from the MDOF model (using ten nodes for the S-Beams and twelve nodes for the C-Beams) for the beams that remained elastic under the indicated blast load. Knowing the time, t , to reach the maximum shear, the applied load, $P(t)$, and moment, $M(t)$, can be specified. The corresponding shear, obtained from Eq. (2.23-a) (for simply supported beams) and Eq. (2.23-b) (for clamped beams), are also given in the same table along with the difference between the two sets of values expressed as a percentage of the MDOF values. As can be seen from the same table, for a certain peak pressure, the difference decreases with increasing load duration and the maximum value occurs for short duration of loading. This can be justified based on the fact that the frequency content of the load is higher for such small values of T_L and more modes are needed to accurately predict the shear.

Table 2.3 also shows that there is relatively small difference between the shear force values predicted using the MDOF model with ten or twelve DOF and those obtained using Eqs. 2.23-a and 2.23-b, with the maximum difference being around 20%.

Therefore, it can be concluded that, in the *elastic* range, the dynamic shear can be adequately predicted using Biggs' closed form solution except for the case of very short duration (*impulsive*) blast loads.

2.2.3 Comparison with Experimental Results

There are a limited number of experimental results available in literature for blast loaded RC beams with complete loading time history and design details because of security and classification requirements. Moreover, the uncertainties in pressure and time measurements and support conditions create additional difficulties facing numerical model validations by experimental results.

A simply supported RC beam (Beam B100(12)D2) tested by Magnusson (2007) was used to validate the MDCF modeling technique adopted in this study. This beam was subjected to a blast load that resulted from an explosive charge located at a distance of 10.0 m in a shock tube. The approximate peak pressure and loading duration for this explosion were 845 kPa and 0.012 s, respectively. The concrete compressive strength and yield stress of reinforced bars were 100 MPa and 500 MPa, respectively. The length of the beam was 1.5 m and its cross section was 300 mm wide and 160 mm deep, with 2.2% tensile reinforcement. More details can be found in Magnusson (2007).

Figure 2.10 gives the normalized displacement for the air blast test as predicted by the different models, including the MDOF (with three nodes), the SDOF (EI_{CSA}) and the

SDOF (EI_{ave}). The displacement results have been normalized with respect to the maximum beam displacement (22.8 mm) obtained during the air blast test [Magnusson (2007)]. As the figure shows, the MDOF model gives the best prediction for maximum displacement, with an error of about 9%. It can also be observed that the use of SDOF (EI_{CSA}) model and SDOF (EI_{ave}) model leads to 49% and 34% overestimations of maximum deflection, respectively.

2.2.4 Totally Damaged Cases

For the totally damaged beams, larger number of nodes was needed to capture the failure state. This number varied, depending on the loading and member stiffness. Sample of the results are presented in Figs. 2.11 and 2.12. Figure 2.11 gives the variation of predicted maximum curvature and support shear for a simply supported beam subjected to a peak pressure and positive phase duration of 2,500 kPa and 0.005 s, respectively whereas Fig. 2.12 gives the variation of predicted maximum curvature and support shear for a clamped beam with a peak pressure and positive phase duration of 2,500 kPa and 0.006 s, respectively.

As can be seen in both Figs. 2.11-a and 2.12-a, the curvature varies significantly with increasing number of nodes until the failure criterion is reached. As mentioned earlier, *Failure* in Fig. 2.12-a indicates that half of the beam height is crushed in compression at the supports and at the midspan. In the same figure, *Partial Failure* indicates that half of the beam height is crushed in compression at the supports only.

It should also be noted that the large predicted increase in shear for the clamped beam (Fig. 2.12-b) compared to the simply supported beam (Fig. 2.11-b) is due to the high value of moment near the support. In fact, when flexural failure occurs at support, the node located near the failed node still resists a large moment, Eq. 2.7, and consequently, produces a higher shear.

2.2.4.1 Required Number of DOF for Different P_0 and T_L

Figure 2.13 shows the relationship between the required number of nodes (to capture failure) for different combination of peak pressure, P_0 , and loading duration, T_L , for the simply supported and the clamped beams. As expected, for a specific pressure, the number of nodes increased significantly as the duration decreased. This is attributed, as explained earlier, to the fact that such highly impulsive loads with higher frequency content would excite more modes. It can also be observed that the increase in the required number of nodes with a decrease in pressure duration is even higher for the clamped beams (compared to the simply supported beams) due to their higher stiffness (a maximum of 90 DOF were required as shown in Fig. 2.13).

The high number of DOF required to capture failure suggests that more nodes may be needed to predict increased level of damage. To verify this, *Pressure-Impulse Diagrams* for beams with different level of damage will be constructed and discussed in the following section.

2.2.5 Effect of Number of DOF on the Pressure-Impulse Diagrams

Pressure-Impulse ($P-I$) diagrams usually consist of several contours corresponding to different damage levels (Baker et al. 1983). As illustrated in Fig. 2.14, each contour represents the different combinations of pressure and impulse that will result in the same maximum deflection, maximum curvature, ductility level or same level of damage in the member. Pressure and impulse combinations to the right and/or above each curve produce damage greater than that represented by this curve while the ones to the left and/or below the curve would result in lower damage than indicated by the curve. Each curve in this diagram can be divided into three segments: impulsive loading realm, dynamic loading realm and quasi-static loading realm. The $P-I$ diagram approach is considered a simplified tool to assess the performance of the structural members under specific level of blast load (Baker et al. 1983).

Figures 2.15 and 2.16 show the $P-I$ diagrams for different levels of curvature ductility at midspan and at the supports for the simply supported and the clamped beam, respectively. These curves are obtained using 10 or 30 nodes for the simply supported beam, and 15 or 45 nodes for the clamped beam. As predicted by the MDOF model, the difference between curves increase with increased curvature ductility and the difference is much less in the impulsive loading realm compared to the quasi-static regime. The variation is more significant for the clamped beam due to its higher stiffness and it reaches a maximum of 60% for the clamped beam with a curvature ductility of 5. Similar to the simply supported beam, the change in the impulsive regime is greater because of the higher frequency of the load which excites more modes.

2.3 Conclusions

In this paper, a numerical technique based on the lumped mass approach was employed to perform nonlinear dynamic analysis of RC beams subjected to blast. The model takes into account the concrete and steel nonlinearity and the dependency of the material properties on strain rate. The study aimed at evaluating the effect of modeling RC beams using a large number of DOFs on their dynamic response using the developed MDOF model.

Typical RC beams with clamped and simple support were selected for the study and a series of blast loading with different pressure and impulse combinations was selected to generate different frequency content. The corresponding strain rate for each load was calculated and appropriate dynamic increase factors were used to scale the steel and the concrete properties.

The effect of the number of DOF on maximum response quantities was considered by increasing the number of nodes used to discretize each beam. The results were compared with simple SDOF models and showed significant difference.

Results for partially damaged beams showed that only a few nodes were enough to capture the complete response of the beams. The MDOF results were also compared with different SDOF systems and it was observed that SDOF models may give results that are comparable to those obtained from a MDOF model if an appropriate effective flexural rigidity was selected. For elastic response the peak shear was also compared with an

available closed-form solution for shear and the maximum difference was found to be around 20%.

More nodes were needed to capture flexural failure of the totally damaged beams and the required number increased significantly with increased beam stiffness. Data obtained from failed cases indicated that with increased damage to the beam more nodes were needed in the analysis. This is attributed to the fact that blast load excites a number of modes in a specific frequency range. As the damage increases in the beam, the frequency of vibration will decrease and as a result, more modes fall within that frequency range.

Acknowledgements

This study forms a part of an ongoing research program in McMaster University Centre for Effective Design of Structures (*CEDS*) funded through the Ontario Research and Development Challenge Fund (*ORDCF*). This research falls under *CEDS Focus Area II: Earthquake Engineering and Extreme Dynamic Loading*. The financial support of the Centre is greatly appreciated.

Notation

C_i = damping coefficient for i^{th} node

C_1 = parameter that defines the curvature of the strain hardening curve in reinforcing steel

C_L = wave velocity

DIF = dynamic increase factor

- E = elastic modulus of reinforcing steel
- EI = flexural rigidity
- F = total applied load
- F_i = lumped load at i^{th} node
- f'_c = concrete maximum compressive stress
- f_{cd} = concrete dynamic compressive strength
- f_{co} = parameter of Malvar's equation for concrete
- f_{cs} = concrete static compressive strength
- f'_t = concrete maximum tensile stress
- f_{td} = concrete dynamic tensile strength
- f_{ts} = concrete static tensile strength
- f = reinforced bar stress
- h = beam height
- h_c = compression depth
- h_t = tension depth
- k = curve fitting parameter in the concrete model
- K_L = load factor
- K_R = resistance factor
- K_M = mass factor
- K_{LM} = load-mass factor
- l = beam length

- LM_i = lumped mass at i^{th} node
- m = member mass
- M_{i-1} = moment at $(i-1)^{th}$ node
- M_i = moment at i^{th} node
- M_{i+1} = moment at $(i+1)^{th}$ node
- M_y = yield moment
- n = number of nodes
- p = blast load per unit length
- p_0 = peak blast load per unit length
- P_0 = peak pressure
- q = curve fitting parameter in concrete model
- $R(t)$ = resistance force as a function of time
- t_{cr} = critical time step
- T_L = loading duration
- $V_{i-1,i}$ = shear between $(i-1)^{th}$ and i^{th} node
- $V_{i,i+1}$ = shear between i^{th} and $(i+1)^{th}$ node
- V_d = dynamic reaction
- y = displacement at a specific point (usually, member midspan)
- \ddot{y} = acceleration at a specific point (usually, member midspan)
- y_i = i^{th} node displacement

\dot{y}_i = i^{th} node velocity

\ddot{y}_i = i^{th} node acceleration

α = parameter of Malvar's equation for reinforcing steel

α_{f_y} = parameter of reinforced bar yield stress in Malvar's equation

α_{f_u} = parameter of reinforced bar ultimate stress in Malvar's equation

β = parameter of Malvar's equation for concrete

β_R = resistance force coefficient in Biggs' equation for reaction

β_F = applied load coefficient Biggs' equation for reaction

δ = parameter of Malvar's equation for concrete

Δx = segment length

Δ_y = deflection at the onset of yielding

ε = strain

ε_c = concrete strain at maximum compressive stress

ε_{cd} = concrete dynamic strain at peak compressive stress

ε_{cs} = concrete static strain at peak compressive stress

ε_{sh} = strain at the onset of strain hardening in reinforcing steel

ε_y = strain at steel yield point

ε_u = ultimate (peak) strain in reinforcing steel

$\dot{\varepsilon}$ = strain rate

$\dot{\varepsilon}_s$ = concrete static strain rate

ϕ = curvature

ϕ_y = yield curvature

$\phi(x)$ = assumed mode shape

σ = stress in the reinforcing steel

σ_c = compressive stress in concrete

σ_{sh} = stress at the onset of strain hardening in reinforcing steel

σ_t = tensile stress in concrete

σ_u = ultimate (peak) stress in reinforcing steel

σ_y = stress at steel yield point

ρ = mass density of reinforced concrete

ρ_m = mass per unit length

ν = Poisson's ratio

Subscripts and Superscripts

ave = average

cr = cracked

CSA = Canadian Standards Association

g = gross

y = yield

u = ultimate

References

ACI Committee 318-05. 2005. Building code requirements for structural concrete (ACI 318-05) and commentary (318R-05). American Concrete Institute, Farmington Hills, Mich., USA.

Baker, W.E. et al. 1983. Explosion hazards and evaluation. Elsevier Scientific Publishing Company, Oxford, UK.

Bentz, E. C. 2000. Sectional analysis of reinforced concrete members. PhD Thesis, Department of Civil Engineering, University of Toronto.

Bentz, E. C. 2005. Explaining the riddle of tension stiffening models for shear panel experiments. *J. Struct. Eng.*, 131(9): 1422-1425.

Beshara, F. B. A. 1994. Modeling of blast loading on aboveground structures - I. General phenomenology and external blast. *Computers and Structures*, 51(5): 597-606.

Biggs, J.M. 1964. Introduction to structural dynamics. McGraw-Hill Book Company, New York. .

Bischoff, P. H, and Perry, S. H. 1991. Compressive behavior of concrete at high strain rates. *Materials and Structures*. 24, 425–450.

Boutros, M. K. 2000. Elastic-plastic model of pinned beams subjected to impulsive loading. *J. Eng. Mech.*, 126(9):920-927.

Clough, R., and Penzien, J. 1993. *Dynamics of structures*. McGraw-Hill, Inc., New York.

Collins, M. P., and Mitchell, D. 1987. *Prestressed concrete basics*. Canadian Prestressed Concrete Institute, Ottawa.

CEB, Comité Euro-International du Béton, 1988. *Concrete structures under impact and impulsive loading*. CEB Bulletin 187, Lausanne, Switzerland.

CSA A23.3-04. 2005. *Design of concrete structures*. Canadian Standards Association, Mississauga, Ontario, Canada.

Dilger, W. H, Koch, R., and Kowalczyk R. 1984. Ductility of plain and confined concrete under different strain rates. *ACI J.*, 81(1):73-81.

Dokainish, M. A., Subbaraj K. 1989. A survey of direct time-integration methods in computational structural dynamics, I-explicit methods. *Computers and Structures*, 32(6):1371-1386.

Ebeling, R. M., Green, R. A., and French, S. E. 1997. Accuracy of response of single-degree-of-freedom systems to ground motion. Technical Report ITL-97-7, U.S. Army Engineer Waterways Experiment Station, Vicksburg, MS.

Eurocode 2, European Committee for Standardization (CEN), 1992. Design of concrete structures, part 1-6: General rules and rules for buildings. Brussels.

Hoehler, M. S., and Stanton, J. F. 2006. Simple phenomenological model for reinforcing steel under arbitrary load."J. Struct. Engrg., 132(7): 1061-1069.

Krauthammer, T., Assadi-Lamouki, A., and Shanaa, H. M. 1993. Analysis of impulsively loaded RC structural elements, part 1-theory. Computers and Structures, 48(5):851-860.

Krauthammer, T., Bazeos, N., Holmquist, T.J. 1986. Modified SDOF analysis of RC box-type structures. J. Struct. Eng. ,112(4) :726–744.

Krauthammer, T., Shahrar, S. and Shanaa, H. M. 1990. Response of reinforced concrete elements to severe impulsive loads. J. Struct. Eng., 116(4): 1061-1079.

Krauthammer, T., Shanaa, H.M. and Assadi-Lamouki, A. 1994. Response of reinforced concrete structural elements to severe impulsive loads. Computers and Structures, 53(1): 119-130.

Kulkarni, S.M., and Shah, S.P. 1998. Response of reinforced concrete beams at high strain rates. *ACI J.*, 95(6): 705-715.

Louca, L. A. and Harding, J. E. 1997. Non-linear analysis of imperfect plates under transient lateral pressure loading. *Computers and Structures*, 63(1): 27–37.

Low, H. Y., and Hao, H. 2002. Reliability analysis of direct shear and flexural failure modes of RC slabs under explosive loading. *Engineering Structures*, 24, 189–198.

Magnusson, J. 2007. Structural concrete elements subjected to air blast loading. Licentiate thesis, KTH, Department of Civil and Architectural Engineering, Stockholm, Sweden.

Malvar, L. J. 1998. Review of static and dynamic properties of steel reinforcing bars. *ACI J.*, 95(5): 609-615.

Malvar, L. J., and Ross C. A. 1998. Review of strain rate effects for concrete in tension. *ACI J.*, 95(6): 735-739

Mays, G. C., and Smith, P. D. 1995. Blast effects on buildings: design of buildings to optimize resistance to blast loading. Thomas Telford, New York, NY.

Mander, J. B., Priestley, M. J. N., and Park, R. 1988. Theoretical stress-strain model for confined concrete. *J. Struct. Eng.*, 114(8): 1804-1826.

NZS 3101:1995, (1995). NZS 3101:1995. Part1: The design of concrete structures. Concrete Structures Standard, Wellington, Standards New Zealand.

Pan, Y., and Watson, A. 1998. Effect of panel stiffness on resistance of cladding panels to blast loading. *J. Eng. Mech.*, 124(4): 414–421.

Priestly, M. J. N., Seible, F., and Calvi, G. M. 1996. Seismic design and retrofit of bridges. Wiley, New York.

Popovics, S. 1973. A numerical approach to the complete stress-strain curve of concrete. *Cement and Concrete Research*, 3(5): 583-599.

Razaqpur, A. G., Mekky, W.F., Tolba, A.F., El-Dakhkhni, W.W., Foad, S. and Contestabile, E. 2007. Behavior of reinforced concrete slabs subjected to blast loading: field testing and finite element modeling. Submitted for publication, *ASCE Journal of Structural Engineering*.

Schleyer, G. K., and Hsu, S. S. 2000. A modelling scheme for predicting the response of elastic plastic structures to pulse pressure loading. *Int. J. Impact Eng.*, 24, 759-777.

TM5-1300, US Department of Army Technical Manual, 1990. Design of structures to resist the effects of accidental explosions. Washington, DC.

Vecchio, F. J., and Collins, M. P. 1982. Response of reinforced concrete to in-plane shear and normal stresses. Publ. No. 82-03, Dept. of Civil Engineering, Univ. of Toronto.

Table 2.1: Effect of number of DOFs on the maximum response quantities

(a) Simply supported beam

Beam	T_L (s)	Disp. ¹ (%)	Shear ² (%)	Curvature ³ (%)
$P_\theta=100$ kPa				
ξ -1	0.003	1.0	11.1	2.6
ξ -2	0.010	2.5	6.1	0.2
ξ -3	0.100	4.9	4.5	0.2
ξ -4	1.000	4.9	4.6	0.9
$P_\theta=500$ kPa				
ξ -5	0.003	0.5	5.7	4.2
ξ -6	0.010	1.7	2.7	0.3
ξ -7	0.100	5.5	4.7	1.0
ξ -8	0.200	5.7	1.8	0.8
$P_\theta=750$ kPa				
ξ -9	0.003	0.6	2.5	0.0
S-10	0.010	1.9	2.0	0.9
S-11	0.015	2.8	4.4	2.6
S-12	0.020	3.2	3.2	11.0
$P_\theta=1,000$ kPa				
S-13	0.003	0.3	3.6	1.1
S-14	0.010	2.1	3.7	1.5
$P_\theta=2,500$ kPa				
S-15	0.003	1.8	3.2	4.3

Table 2.1(continued):

(b) Clamped beam

Beam	T_L (s)	Disp. ⁴ (%)	Shear ⁵ (%)	Curvature ⁶ (%)
$P_0=100$ kPa				
C-1	0.003	2.1	3.7	1.5
C-2	0.010	4.7	4.9	1.5
C-3	0.100	4.0	4.2	0.2
C-4	1.000	3.6	4.0	0.4
$P_0=500$ kPa				
C-5	0.003	2.0	2.2	3.0
C-6	0.005	5.4	7.0	11.6
C-7	0.010	6.2	5.2	3.9
C-8	0.100	6.3	13.9	0.8
C-9	1.000	6.5	2.4	0.5
$P_0=750$ kPa				
C-10	0.003	2.4	0.2	4.0
C-11	0.005	5.6	0.0	8.4
C-12	0.010	5.6	3.1	3.2
C-13	0.100	6.7	0.9	2.4
C-14	1.000	7.1	1.0	1.3
$P_0=1,000$ kPa				
C-15	0.003	2.0	0.0	5.3
C-16	0.010	5.1	0.4	1.5
$P_0=2,500$ kPa				
C-17	0.003	2.4	7.7	1.4

¹ Displacement was obtained by using 3 nodes and compared to the same for 30 nodes

² Shear was obtained by using 10 nodes and compared to the same for 30 nodes

³ Curvature was obtained by using 5 nodes and compared to the same for 30 nodes

⁴ Displacement was obtained by using 10 nodes and compared to the same for 40 nodes

⁵ Shear was obtained by using 12 nodes and compared to the same for 40 nodes

⁶ Curvature was obtained by using 10 nodes and compared to the same for 40 nodes

Table 2.2: Difference between the MDOF results and the results of SDOF systems:

(a) Simply supported beam

Beam	T_r (s)	SDOF(EI_c)		SDOF(EI_p)		SDOF(EI_{avg})		SDOF(EI_{CS})		MDOF(1 node)	
		Disp.(%)	Shear(%)	Disp.(%)	Shear(%)	Disp.(%)	Shear(%)	Disp.(%)	Shear(%)	Disp.(%)	Shear(%)
$P_F=100$ kPa											
S-1	0.003	+ 57.7	- 46.9	- 0.3	- 19.1	+ 19.0	- 31.3	- 0.3	- 19.1	- 3.2	- 57.5
S-2	0.010	+ 85.6	- 30.8	- 1.4	- 6.5	+ 28.0	- 15.6	- 1.4	- 6.5	+ 5.2	- 49.3
S-3	0.100	+ 120.7	+ 2.3	- 6.2	+ 5.1	+ 31.5	+ 4.1	- 3.2	- 5.9	+ 14.1	- 45.1
S-4	1.000	+ 122.3	+ 6.5	- 7.6	+ 6.7	+ 30.4	+ 6.5	+ 0.5	- 8.9	+ 15.9	- 45.0
$P_F=500$ kPa											
S-5	0.003	+ 56.6	- 43.3	- 2.1	- 13.0	+ 17.9	- 26.3	+ 1.0	- 28.1	- 2.5	- 56.6
S-6	0.010	+ 50.4	- 7.3	- 20.1	+ 25.4	+ 3.7	+ 13.2	+ 19.8	- 17.5	+ 3.3	- 49.2
S-7	0.100	+ 36.3	- 5.3	- 41.1	- 4.8	- 17.9	- 5.0	+ 22.6	- 5.6	+ 17.9	- 43.8
S-8	0.200	+ 38.6	- 9.8	- 40.9	- 9.4	- 17.3	- 9.6	+ 14.1	- 9.7	+ 18.9	- 43.3
$P_F=750$ kPa											
S-9	0.003	+ 54.8	- 37.6	- 4.6	- 2.9	+ 15.4	- 18.0	+ 5.1	- 30.4	- 5.7	- 54.4
S-10	0.010	+ 34.3	- 3.2	- 28.7	+ 13.8	- 8.1	+ 10.3	+ 18.5	- 11.8	+ 2.6	- 49.9
S-11	0.015	+ 28.9	- 5.1	- 32.2	- 0.3	- 12.6	- 1.8	+ 16.9	- 6.1	+ 7.0	- 47.2
S-12	0.020	+ 30.5	- 10.5	- 31.4	- 7.5	- 11.6	- 8.5	+ 18.3	- 11.0	+ 9.5	- 45.5
$P_F=1,000$ kPa											
S-13	0.003	+ 54.5	- 33.8	- 5.7	+ 3.8	+ 14.4	- 12.5	+ 10.3	- 31.4	- 5.5	- 53.9
S-14	0.010	+ 23.7	- 11.0	- 25.9	- 2.8	- 9.7	- 5.4	+ 13.5	- 12.1	+ 1.7	- 48.8
$P_F=2,500$ kPa											
S-15	0.003	+ 41.8	- 16.2	- 12.8	- 9.2	+ 2.6	- 15.0	+ 19.6	- 22.1	- 4.3	- 51.9
Average(ABS)		55.8	18.0	18.5	10.6	16.0	12.2	11.0	15.1	7.8	49.4
C.O.V		0.5	0.9	0.8	0.7	0.5	0.6	0.7	0.6	0.7	0.1

Table 2.2:(Continued) :

(b) Clamped beam

Beam	$T_r(s)$	SDOF(EI_{cp})		SDOF(EI_p)		SDOF(EI_{mp})		SDOF(EI_{CSA})		MDOF(1 node)	
		Disp.(%)	Shear(%)	Disp.(%)	Shear(%)	Disp.(%)	Shear(%)	Disp.(%)	Shear(%)	Disp.(%)	Shear(%)
$P_f=100 \text{ kPa}$											
C-1	0.003	+ 64.8	- 41.4	- 3.9	- 15.6	+ 20.1	- 27.2	- 3.9	- 15.6	+ 64.5	- 66.9
C-2	0.010	+ 108.2	- 16.4	- 3.6	- 4.6	+ 31.2	- 8.8	- 3.6	- 4.6	+ 135.6	- 52.5
C-3	0.100	+ 130.5	- 4.9	- 3.3	- 3.7	+ 36.2	- 4.1	- 3.3	- 3.7	+ 180.8	- 44.9
C-4	1.000	+ 132.6	- 3.5	- 3.9	- 3.8	+ 36.5	- 3.4	- 3.9	- 3.8	+ 185.5	- 43.9
$P_f=500 \text{ kPa}$											
C-5	0.003	+ 62.5	- 36.9	- 5.3	- 9.2	+ 18.4	- 21.6	- 5.2	- 9.4	+ 62.6	- 65.3
C-6	0.005	+ 74.7	- 18.3	- 9.6	+ 8.2	+ 18.4	- 1.6	- 5.7	- 7.9	+ 86.5	- 56.1
C-7	0.010	+ 84.1	- 3.3	- 14.8	+ 10.4	+ 16.1	+ 5.6	- 0.6	- 12.5	+ 127.1	- 53.2
C-8	0.100	+ 80.4	+ 11.7	- 24.4	+ 13.1	+ 6.5	+ 12.7	+ 12.3	- 8.2	+ 197.0	- 46.3
C-9	1.000	+ 73.5	+ 12.9	- 28.3	+ 12.5	+ 1.8	+ 13.0	+ 16.7	- 6.6	+ 208.6	- 45.2
$P_f=750 \text{ kPa}$											
C-10	0.003	+ 56.2	- 33.3	- 10.1	- 3.2	+ 12.9	- 16.8	- 5.2	- 21.3	+ 58.8	- 64.3
C-11	0.005	+ 61.5	- 14.6	- 16.5	+ 13.0	+ 9.5	+ 2.8	+ 0.9	- 17.8	+ 78.6	- 59.0
C-12	0.010	+ 64.4	- 3.0	- 23.6	+ 11.3	+ 3.7	+ 9.6	+ 11.1	- 17.3	+ 125.1	- 56.9
C-13	0.100	+ 64.8	- 3.7	- 30.4	- 3.0	- 2.2	- 3.3	+ 21.3	- 4.8	+ 200.7	- 46.6
C-14	1.000	+ 69.6	- 6.5	- 29.8	- 6.5	- 0.4	- 6.4	+ 25.3	- 5.7	+ 210.4	- 44.4
$P_f=1,000 \text{ kPa}$											
C-15	0.003	+ 51.1	- 30.2	- 14.3	+ 2.2	+ 8.1	- 12.5	- 4.1	- 25.1	+ 53.7	- 64.6
C-16	0.010	+ 54.0	- 9.0	- 25.0	- 3.0	0.0	- 5.2	+ 15.6	- 10.8	+ 122.8	- 57.0
$P_f=2,500 \text{ kPa}$											
C-17	0.003	+ 37.9	- 23.2	- 12.6	- 7.6	+ 4.3	- 13.8	+ 3.4	- 16.9	+ 43.3	- 61.7
Average(ABS)		74.8	16.0	15.3	7.7	13.3	9.9	8.4	11.3	126.0	54.6
C.O.V		0.3	0.8	0.6	0.5	0.9	0.7	0.9	0.6	0.5	0.2

Table 2.3: Difference between MDOF shear and closed form solution
(a) Simply supported beam

Beam	$T_L(s)$	$t(s)$	$P(t)$ (kPa)	$M(t)$ (kN.m)	MDOF Shear(kN)	Closed- form Shear(kN)	Difference (%)
$P_0=100$ kPa							
S-1	0.003	0.0052	0.0	40.3	40.6	31.5	22.5
S-2	0.010	0.0071	28.9	101.2	91.0	84.1	7.6
S-3	0.100	0.0095	90.5	140.6	129.0	125.6	2.6
S-4	1.000	0.0096	99.0	144.4	132.7	130.1	2.0
$P_0=500$ kPa							
S-5	0.003	0.0053	0.0	193.0	189.7	150.5	20.7
S-6	0.010	0.0082	88.0	395.2	339.6	323.7	4.7
S-7	0.100	0.0122	438.8	634.3	560.4	572.0	2.1
$P_0=750$ kPa							
S-9	0.003	0.0054	0.0	270.7	261.5	211.1	19.3
S-10	0.010	0.0087	99.0	561.4	487.9	455.3	6.7
$P_0=1,000$ kPa							
S-13	0.003	0.0054	0.0	339.6	329.8	264.9	19.7

(b) Clamped beam

Beam	$T_L(s)$	$t(s)$	$P(t)$ (kPa)	$M(t)$ (kN.m)	MDOF Shear(kN)	Closed- form Shear(kN)	Difference (%)
$P_0=100$ kPa							
C-1	0.003	0.0024	20.0	50.3	72.3	58.8	18.7
C-2	0.010	0.0040	61.5	85.0	114.5	105.6	7.8
C-3	0.100	0.0040	96.1	102.4	139.7	132.2	5.4
C-4	1.000	0.0041	99.6	103.8	142.0	134.4	5.3
$P_0=500$ kPa							
C-5	0.003	0.0024	98.3	229.7	335.9	270.1	19.6
C-6	0.005	0.0040	103.5	287.7	396.1	333.9	15.7
C-7	0.010	0.0041	297.0	353.7	494.7	448.6	9.3
C-8	0.100	0.0045	477.7	421.6	594.6	562.3	5.4
C-9	1.000	0.0045	497.8	427.8	607.2	573.5	5.5
$P_0=750$ kPa							
C-10	0.003	0.0024	143.8	318.5	478.2	376.2	21.3
C-11	0.005	0.0025	375.0	369.4	568.9	482.9	15.1
C-12	0.010	0.0044	420.4	508.9	739.9	643.8	13.0
C-13	0.100	0.0046	715.7	618.4	896.6	828.2	7.6
$P_0=1,000$ kPa							
C-15	0.003	0.0025	158.3	409.2	611.2	477.4	21.9
C-16	0.010	0.0046	541.0	662.9	947.9	837.1	11.7

Figure Captions

Fig. 2.1: Actual and idealized side-on blast pressure time histories: (a) Actual blast load time history, (b) Triangular load approximation, (c) Using tangent line in approximating blast load

Fig. 2.2: SDOF model: (a) Actual structural element, (b) Equivalent SDOF model, (c) Typical resistance-displacement curve

Fig. 2.3: Free body diagram of a simply supported beam subjected to blast load

Fig. 2.4: Schematic view of MDOF model based on lumped mass approach

Fig. 2.5: Strain rate effects: (a) *DIF* for concrete under tension, (b) *DIF* for concrete under compression, (c) Scaled stress-strain curve for reinforcing steel, (d) Scaled stress-strain curve for concrete

Fig. 2.6: Strain rate distribution at the midspan of a simply supported beam

Fig. 2.7: Flow chart of the overall numerical procedure

Fig. 2.8: Maximum response quantities for the simply supported beam versus number of nodes: (a) Displacement, (b) Shear, (c) Curvature

Fig. 2.9: Maximum response quantities for the clamped-clamped beam versus number of nodes: (a) Displacement, (b) Shear, (c) Curvature

Fig. 2.10: Comparison between different models and experimental data

Fig. 2.11: Variations of maximum response quantities with the number of nodes for a failed simply supported beam ($P_0=2,500$ kPa, $T_L=0.005$ s): (a) Curvature, (b) Shear

Fig. 2.12: Variations of maximum response quantities with the number of nodes for a failed clamped-clamped beam ($P_0=2,500$ kPa, $T_L=0.006$ s): (a) Curvature, (b) Shear

Fig. 2.13: Required number of nodes to reach failure criteria for different loading: (a) Simply supported beam, (b) Clamped-clamped beam

Fig. 2.14: General form of pressure-impulse diagram

Fig. 2.15: Pressure-impulse diagrams for simply supported beam by using 10 and 30 nodes: (a) Curvature ductility=2.0, (b) Curvature ductility=3.5, (c) Curvature ductility=5.0

Fig. 2.16: Pressure-impulse diagrams for clamped-clamped beam by using 15 and 45 nodes: (a) Curvature ductility=2.0, (b) Curvature ductility=3.5, (c) Curvature ductility=5.0

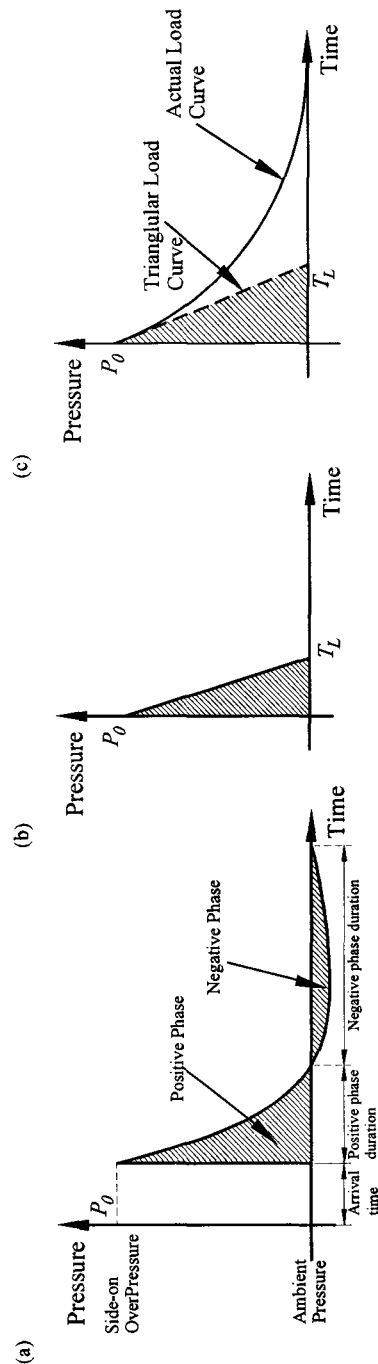


Fig. 2.1: Actual and idealized side-on blast pressure time histories: (a) Actual blast load time history, (b) Triangular load approximation, (c) Using tangent line in approximating blast load

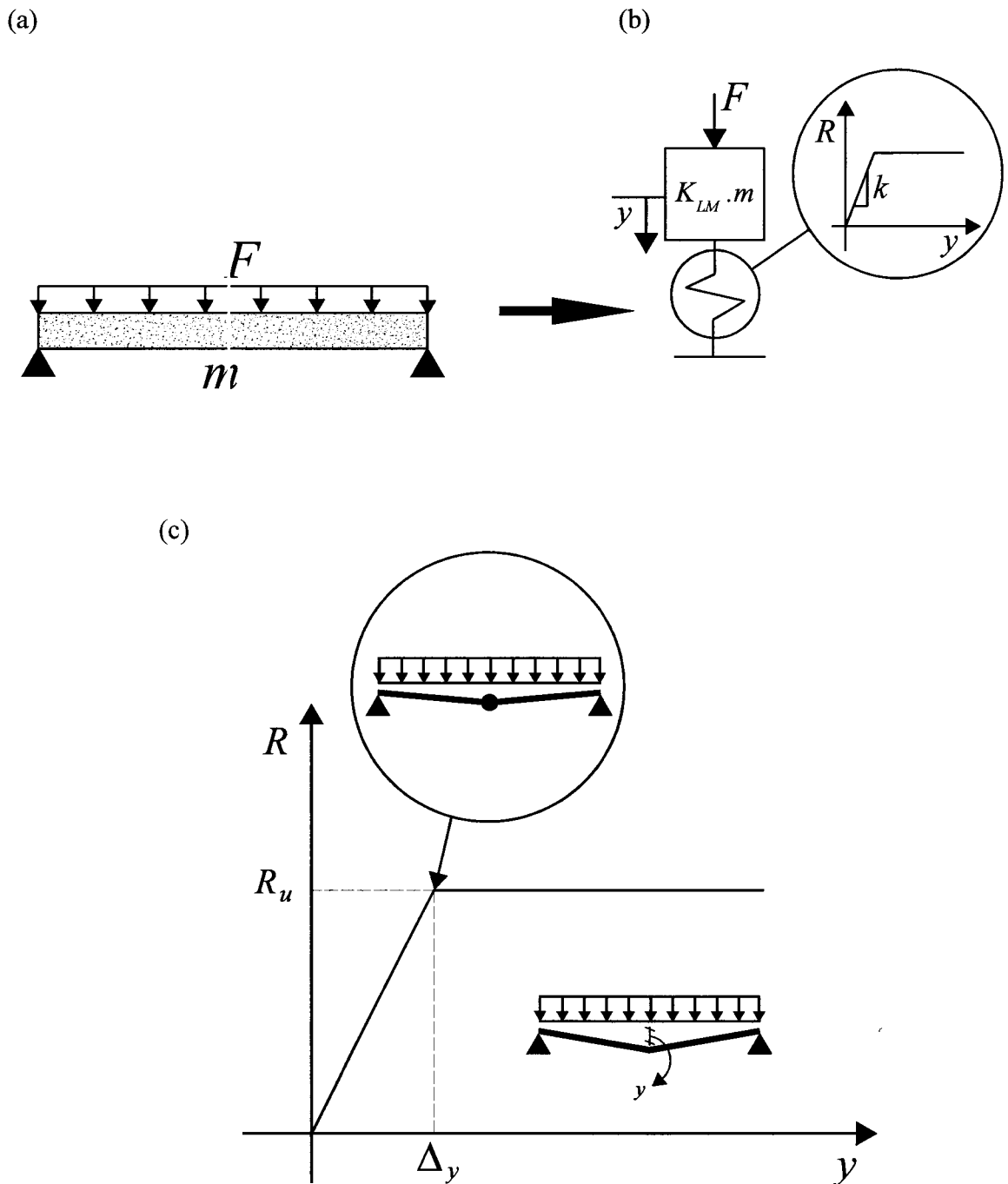


Fig. 2.2: SDOF model: (a) Actual structural element, (b) Equivalent SDOF model, (c) Typical resistance-displacement curve

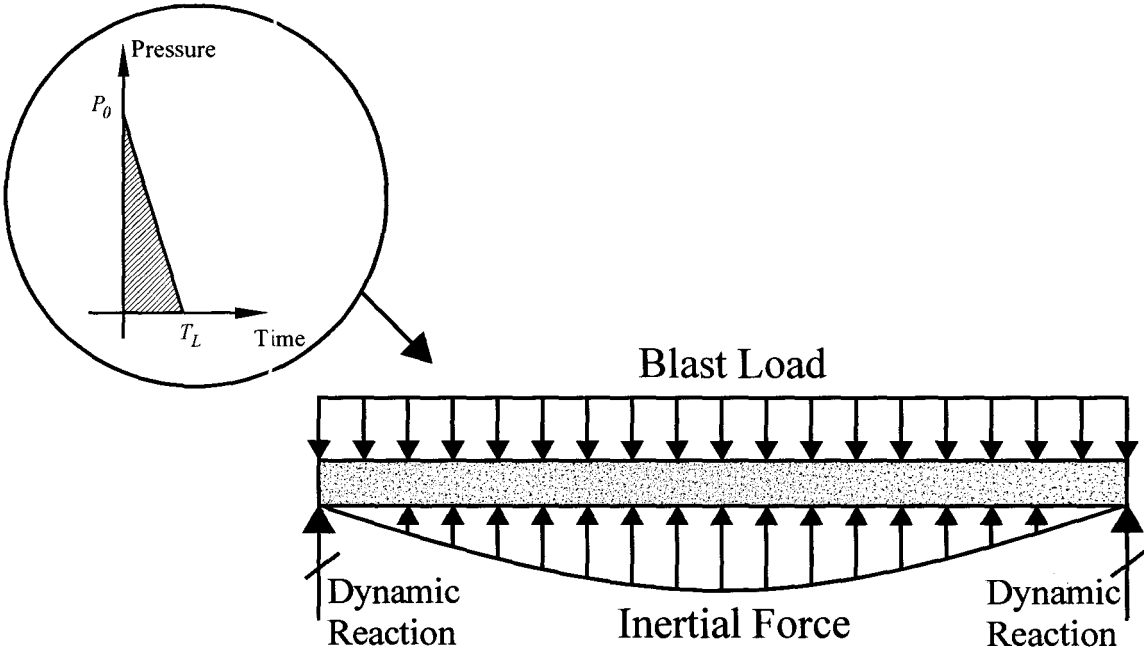


Fig. 2.3: Free body diagram of a simply supported beam subjected to blast load

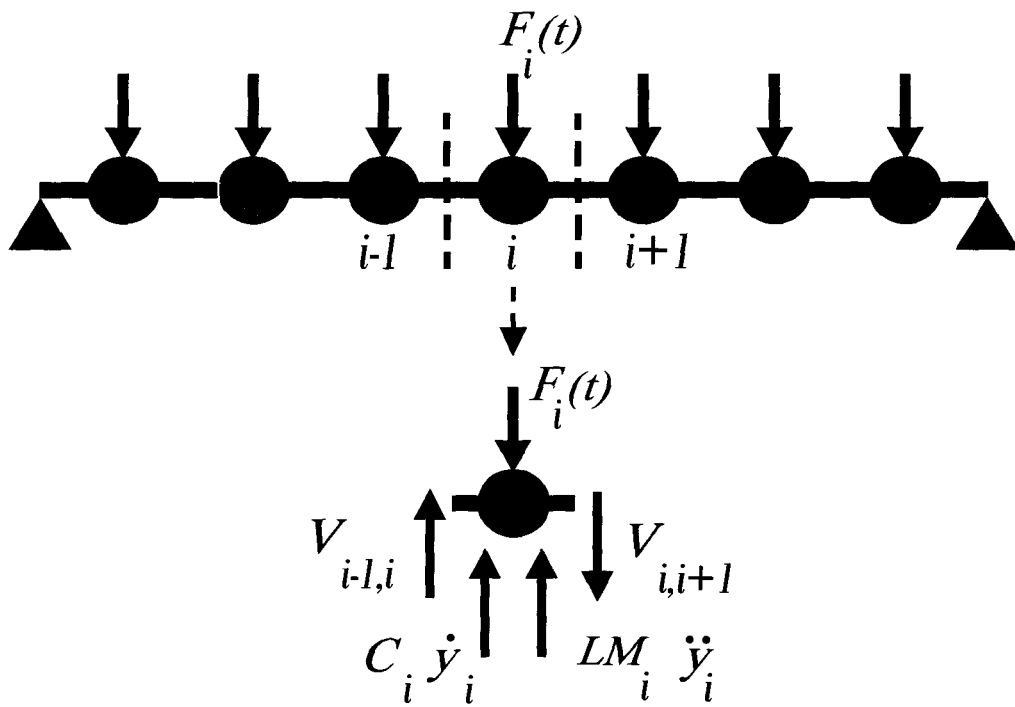
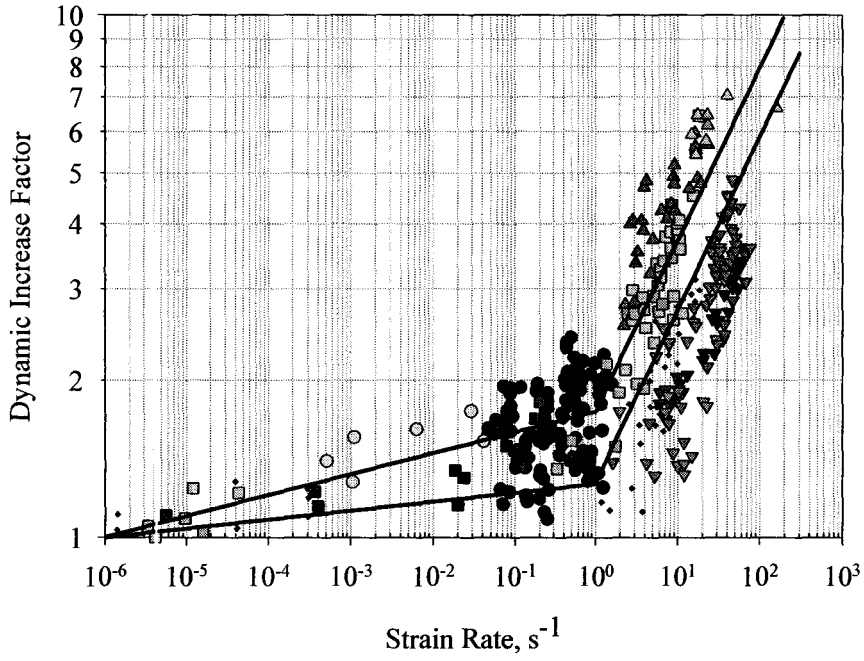
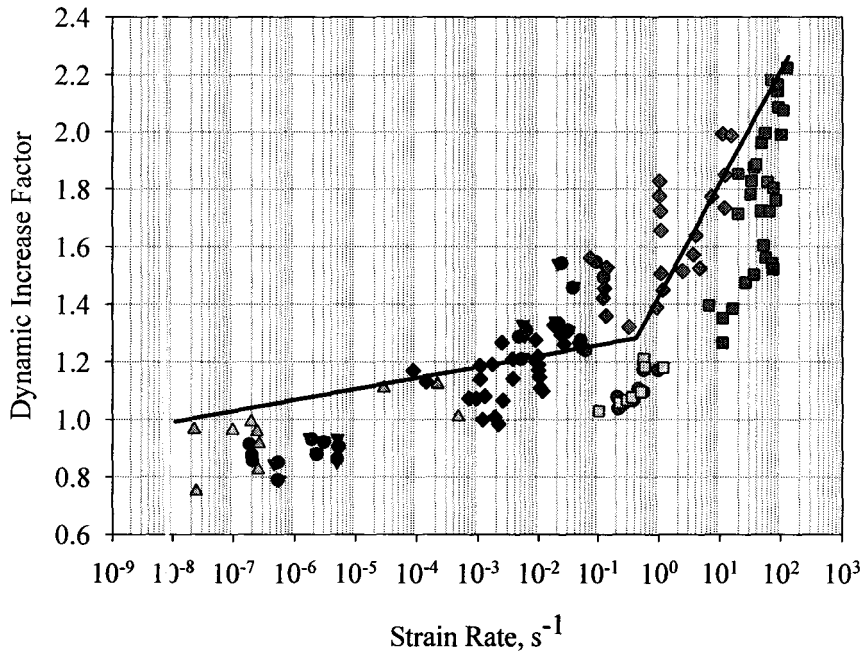


Fig. 2.4: Schematic view of MDOF model based on lumped mass approach

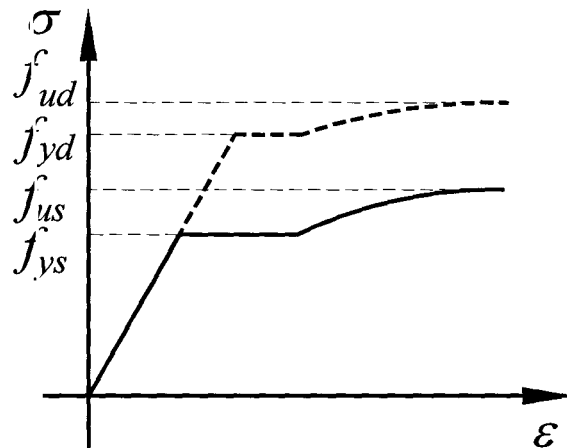
(a)



(b)



(c)



(d)

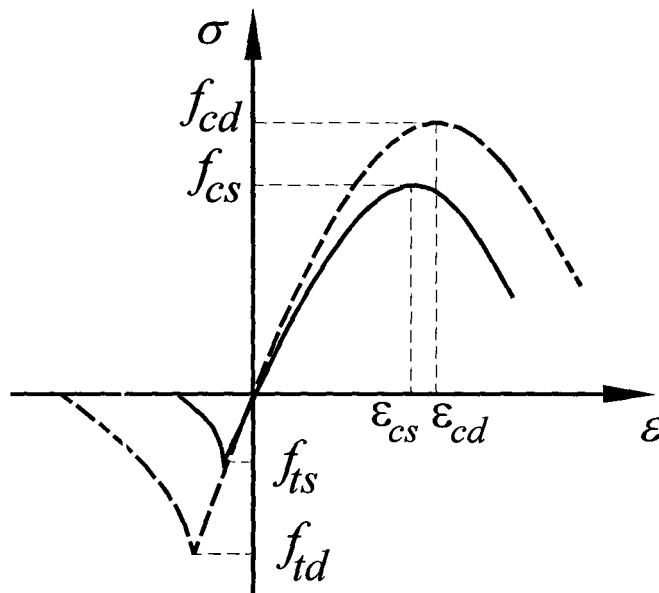


Fig. 2.5. Strain rate effects: (a) *DIF* for concrete under tension, (b) *DIF* for concrete under compression, (c) Scaled stress-strain curve for reinforcing steel, (d) Scaled stress-strain curve for concrete

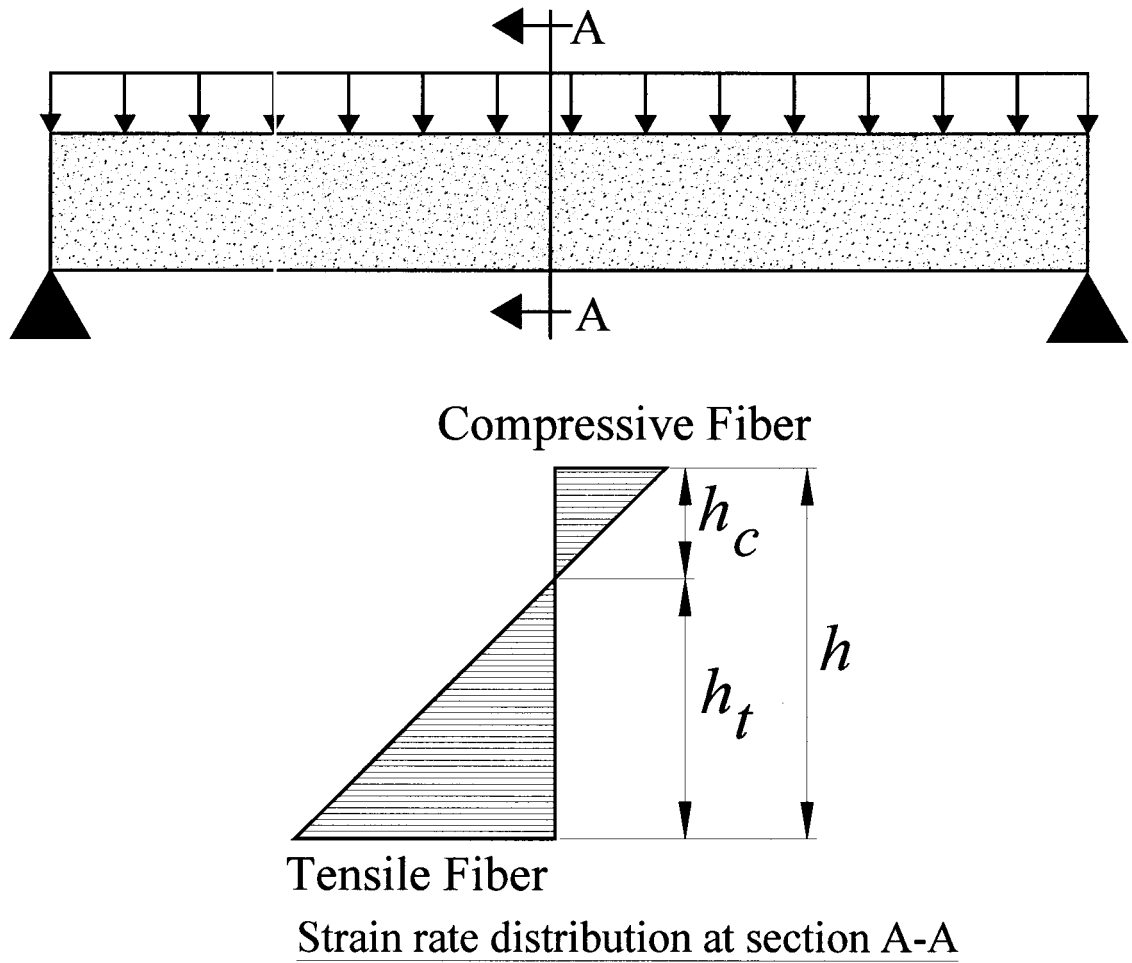


Fig. 2.6: Strain rate distribution at the midspan of a simply supported beam

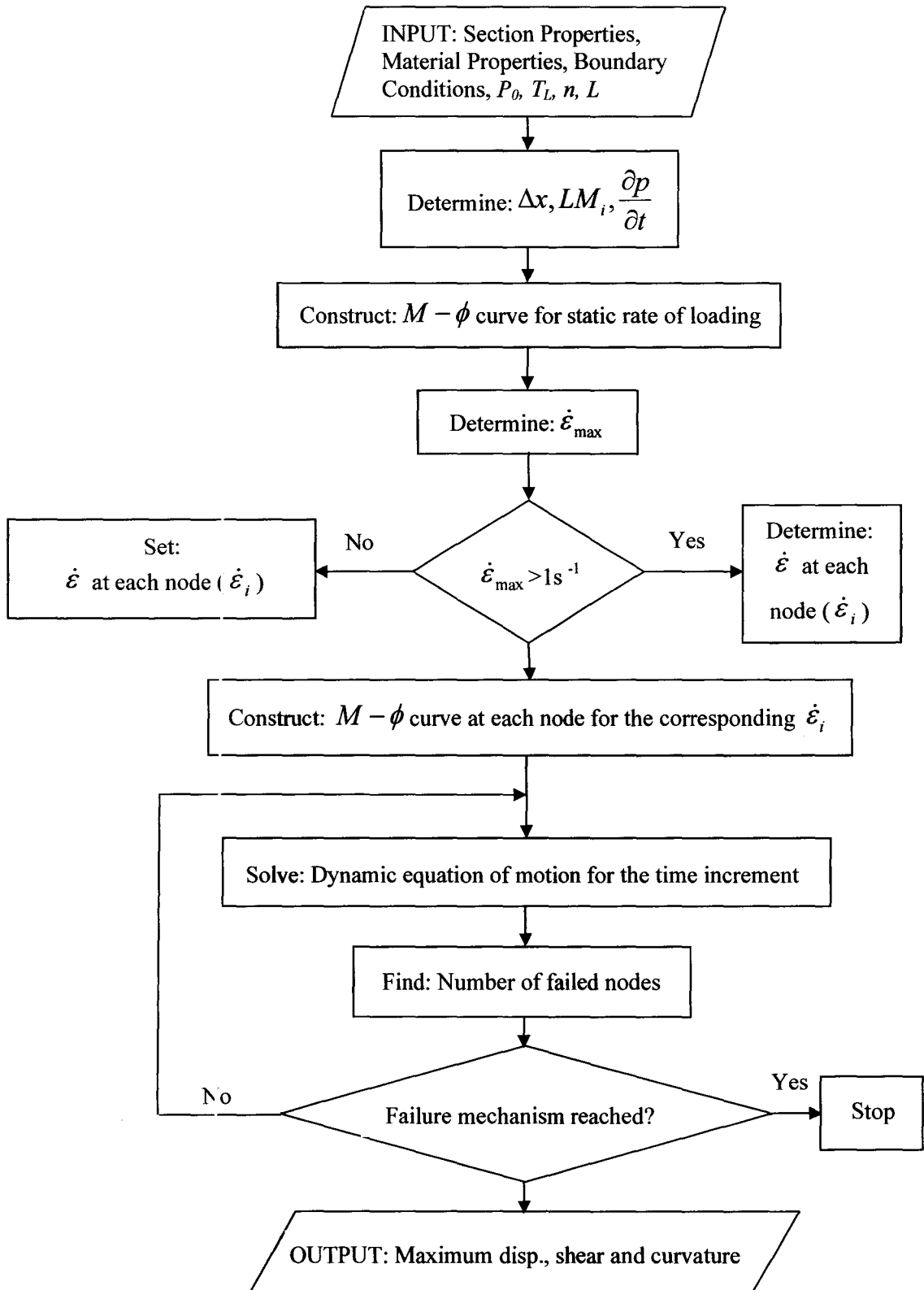


Fig. 2.7: Flow chart of the overall numerical procedure

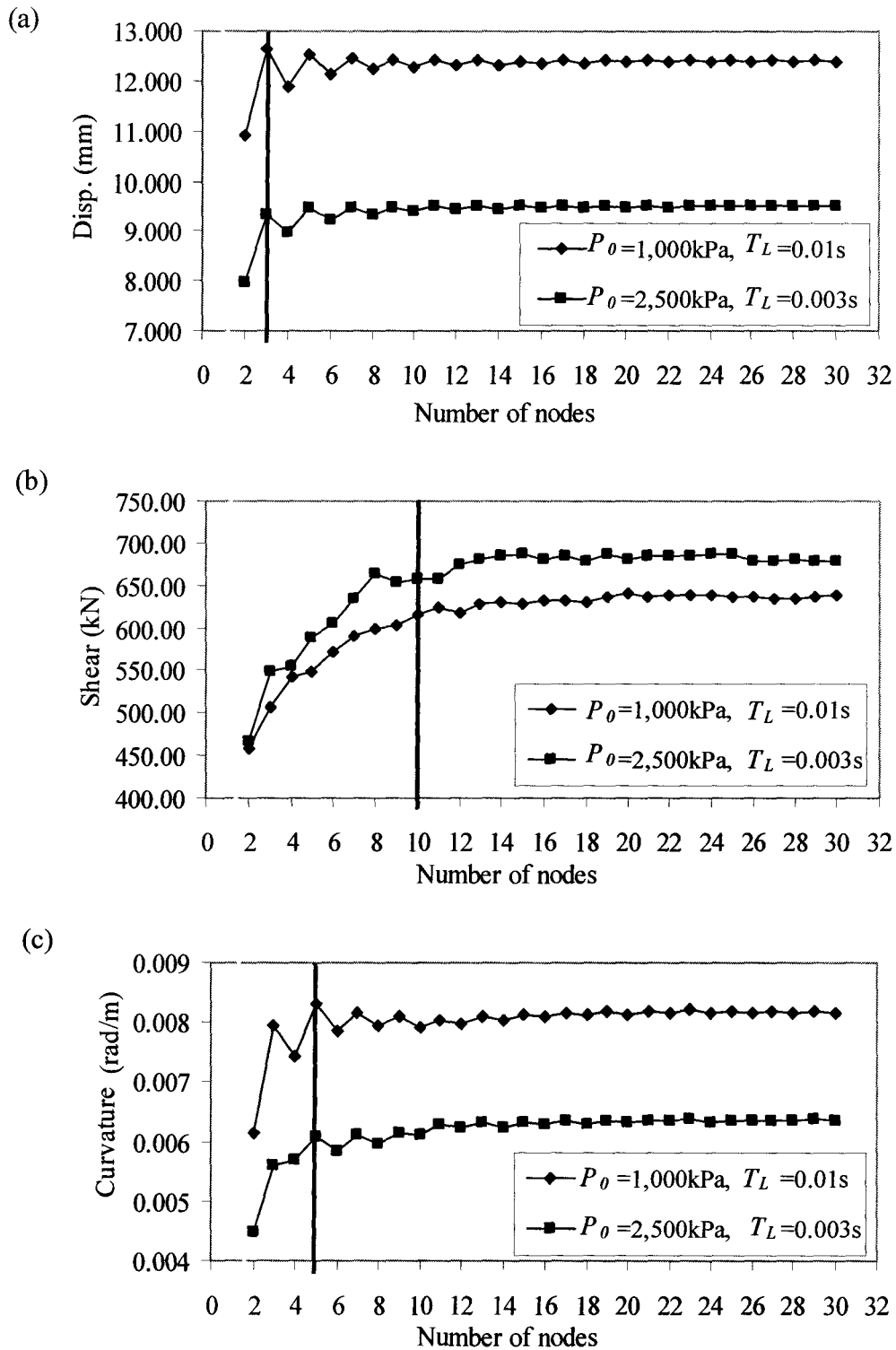
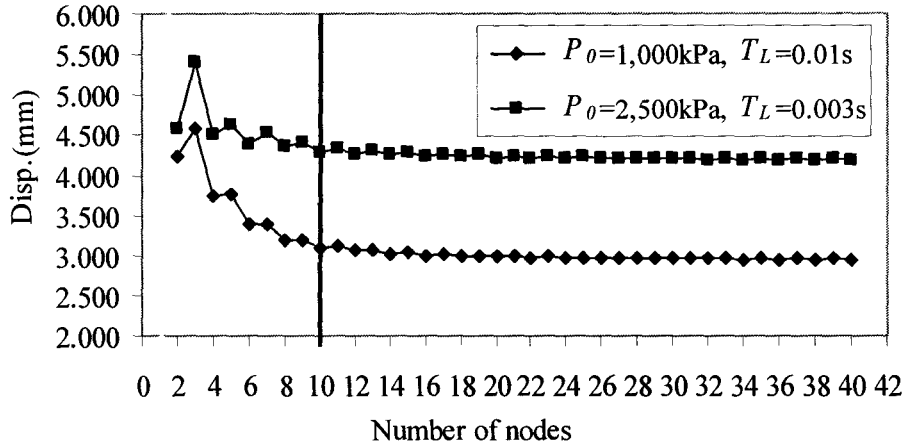
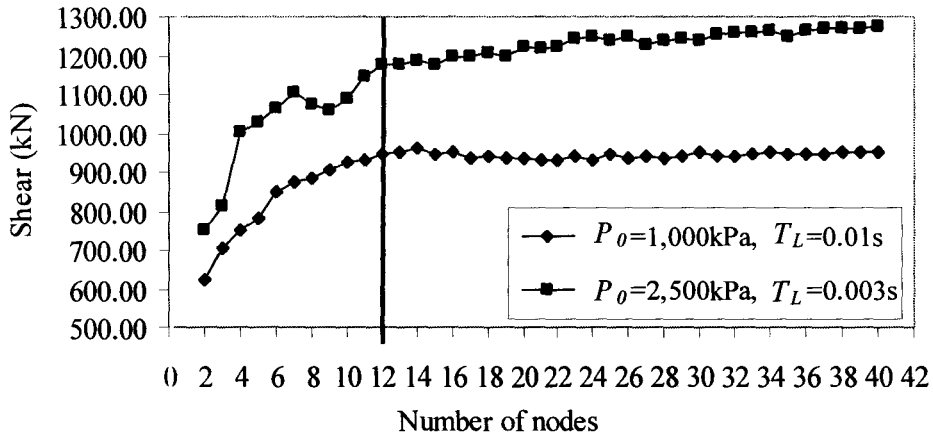


Fig. 2.8: Maximum response quantities for the simply supported beam versus number of nodes: (a) Displacement, (b) Shear, (c) Curvature

(a)



(b)



(c)

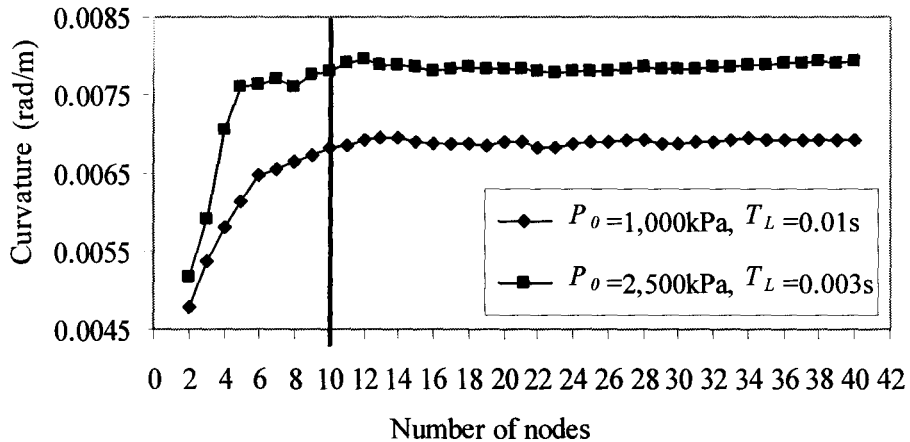


Fig. 2.9: Maximum response quantities for the clamped-clamped beam versus number of nodes: (a) Displacement, (b) Shear, (c) Curvature

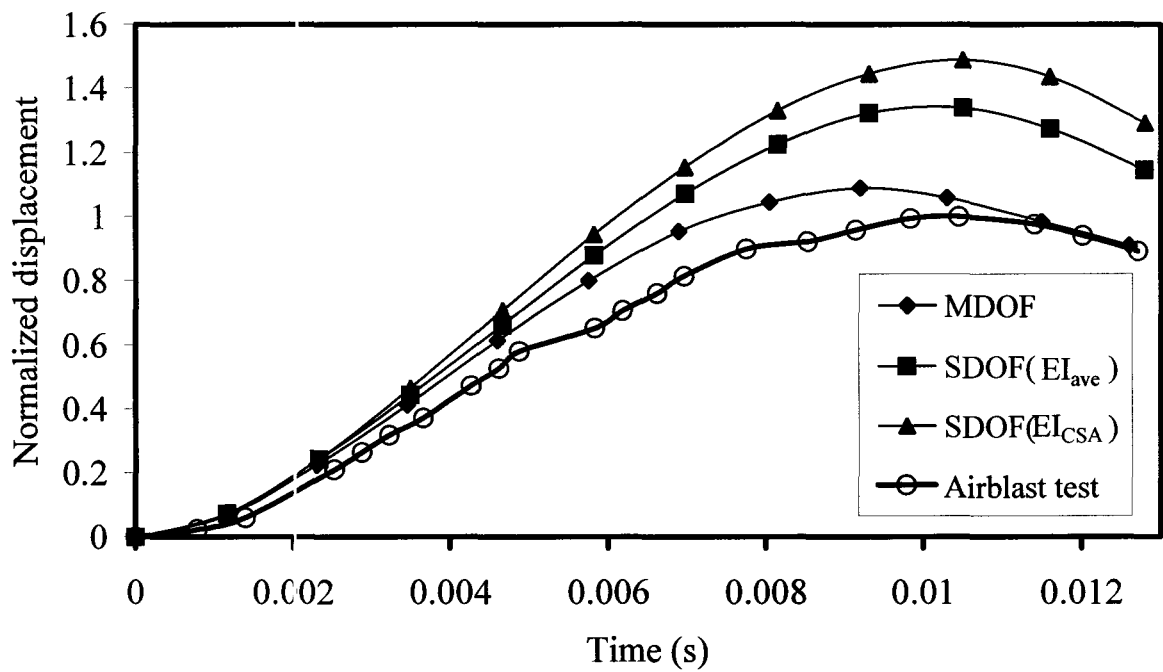
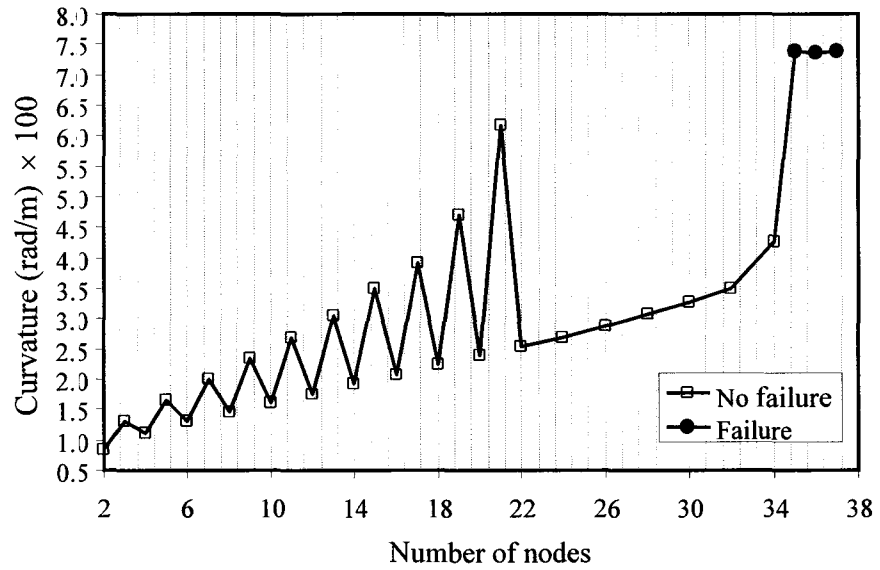


Fig. 2.10: Comparison between different models and experimental data

(a)



(b)

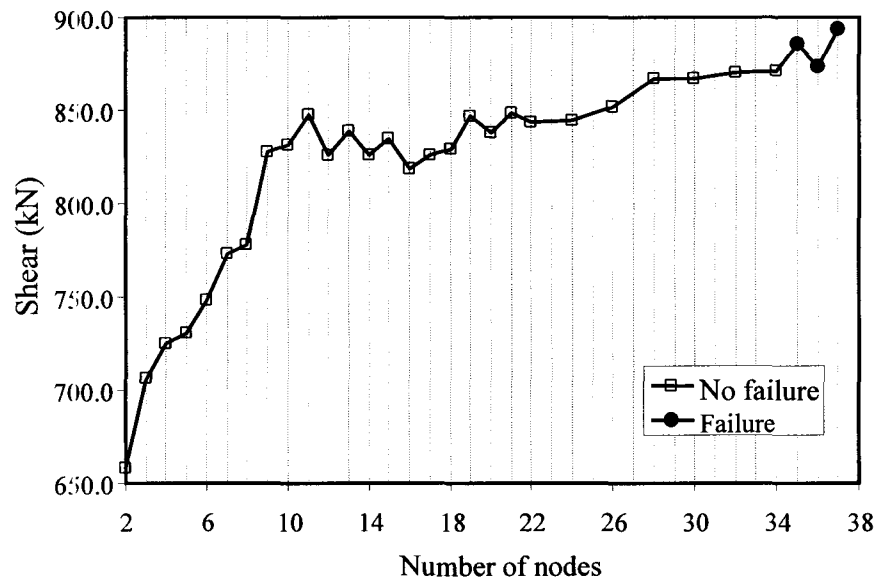
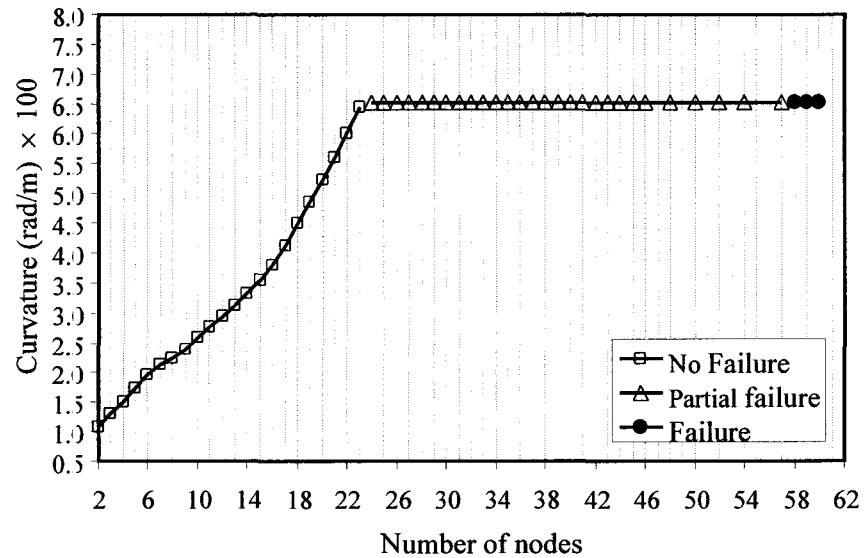


Fig. 2.11: Variations of maximum response quantities with the number of nodes for a failed simply supported beam ($P_0=2,500$ kPa, $T_L=0.005$ s): (a) Curvature, (b) Shear

(a)



(b)

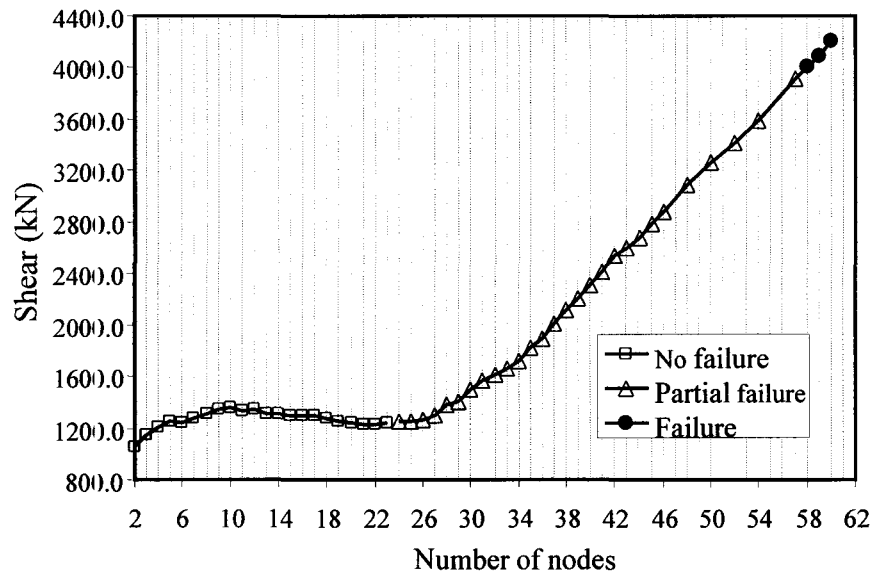
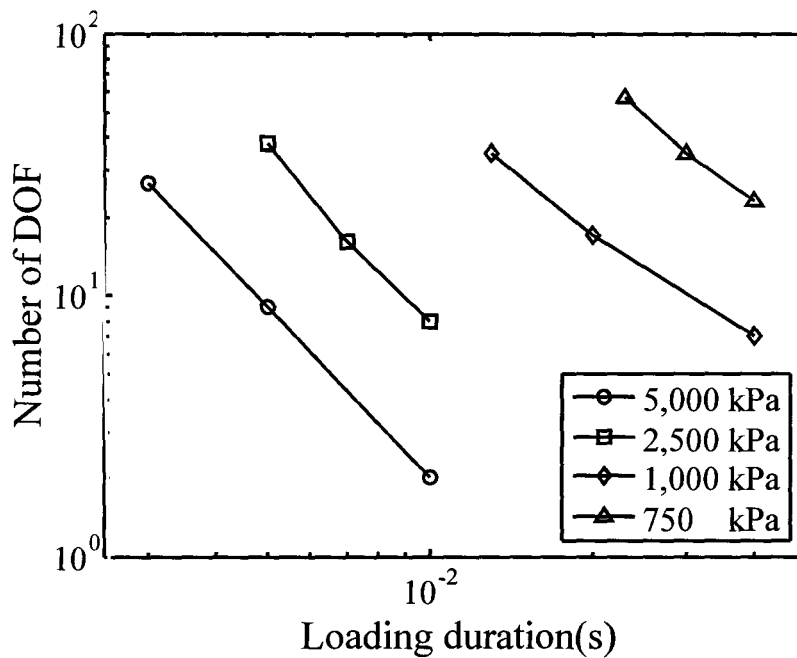


Fig. 2.12: Variations of maximum response quantities with the number of nodes for a failed clamped-clamped beam ($P_0=2,500$ kPa, $T_L=0.006$ s) : (a) Curvature, (b) Shear

(a)



(b)

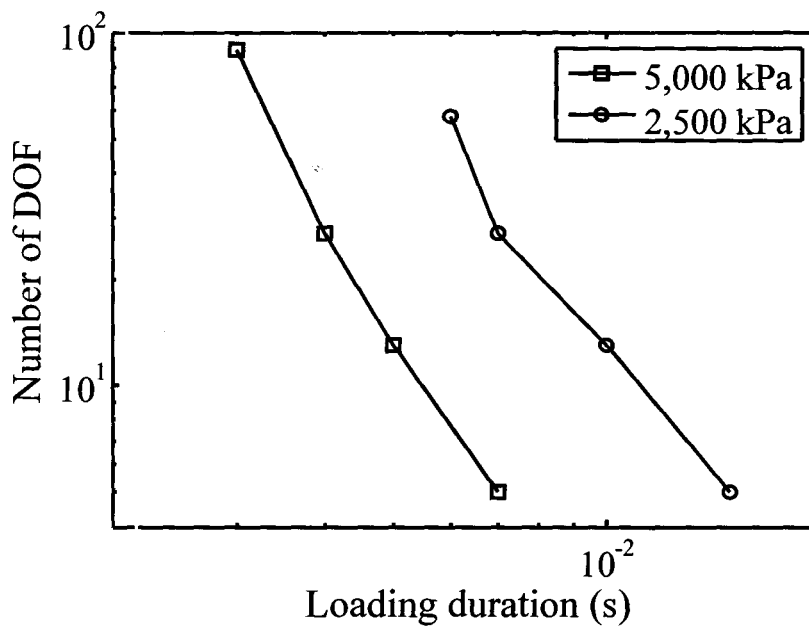


Fig. 2.13: Required number of nodes to reach failure criteria for different loading: (a)

Simply supported beam, (b) Clamped-clamped beam

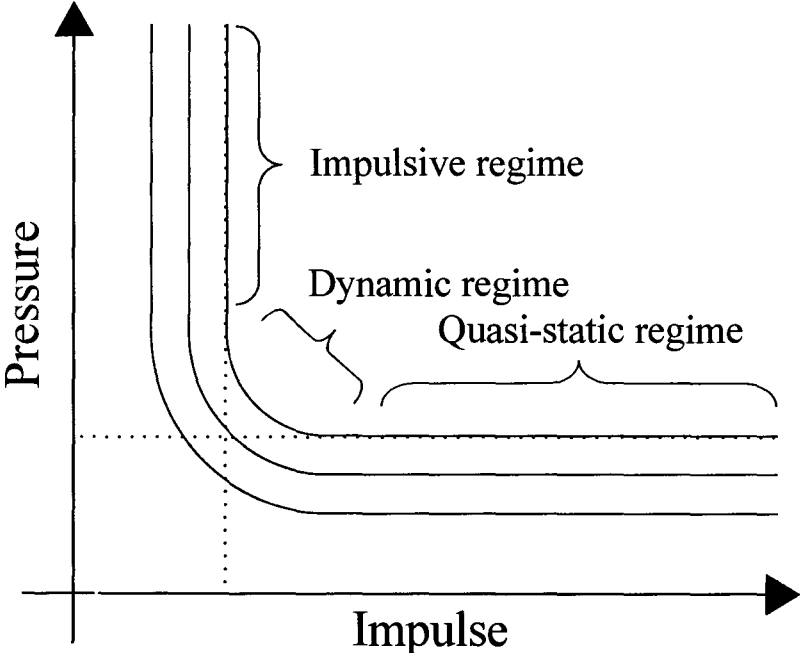
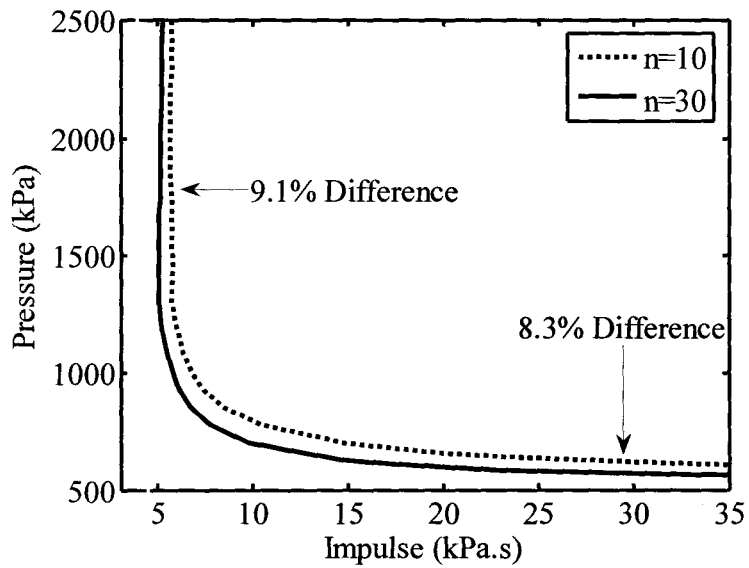
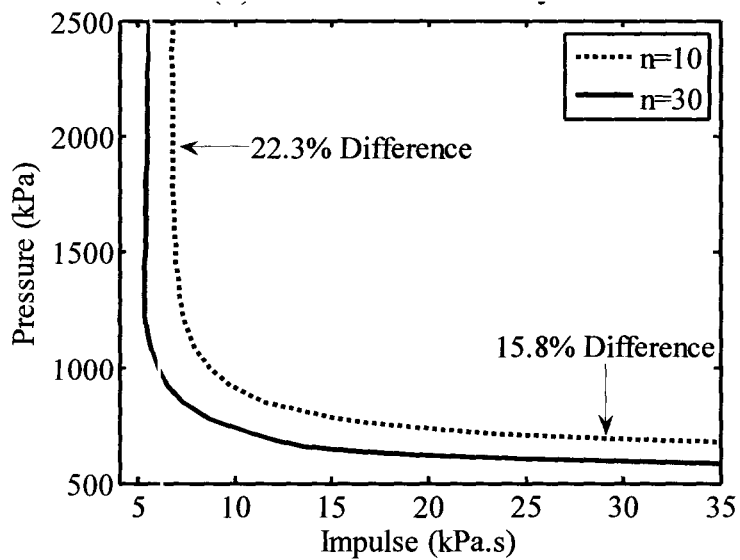


Fig. 2.14: General form of pressure-impulse diagram

(a)



(b)



(c)

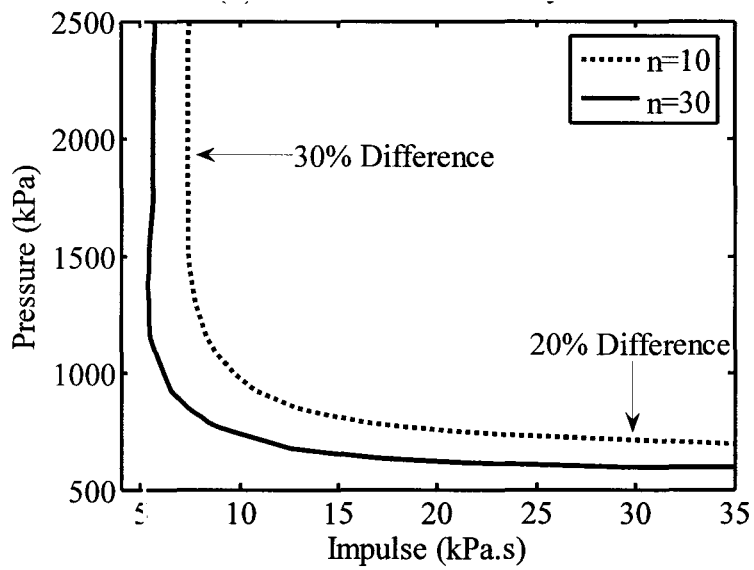
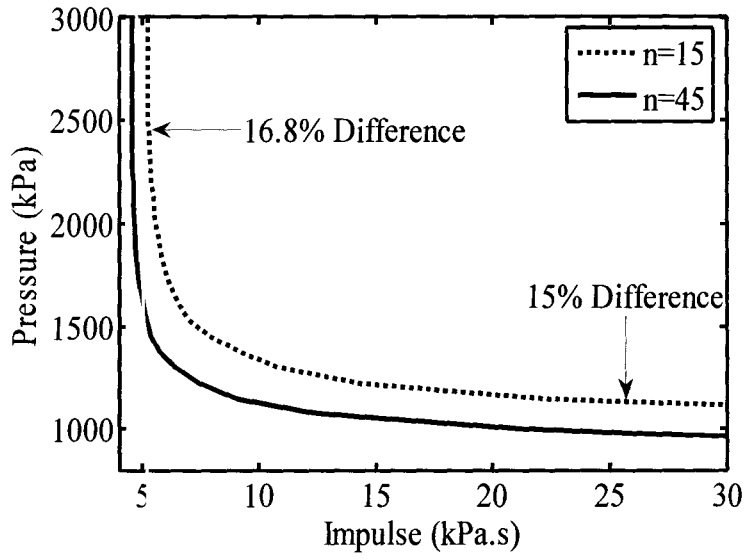
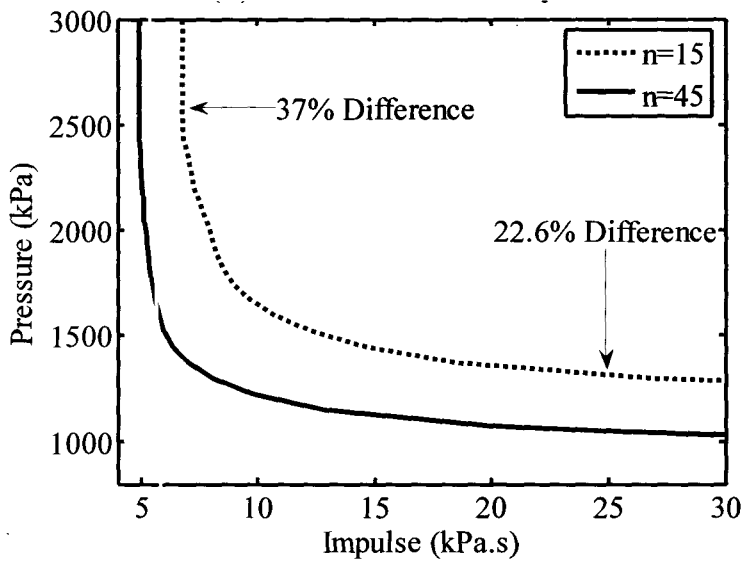


Fig. 2.15: Pressure-impulse diagrams for simply supported beam by using 10 and 30 nodes: (a) Curvature ductility=2.0, (b) Curvature ductility=3.5, (c) Curvature ductility=5.0

(a)



(b)



(c)

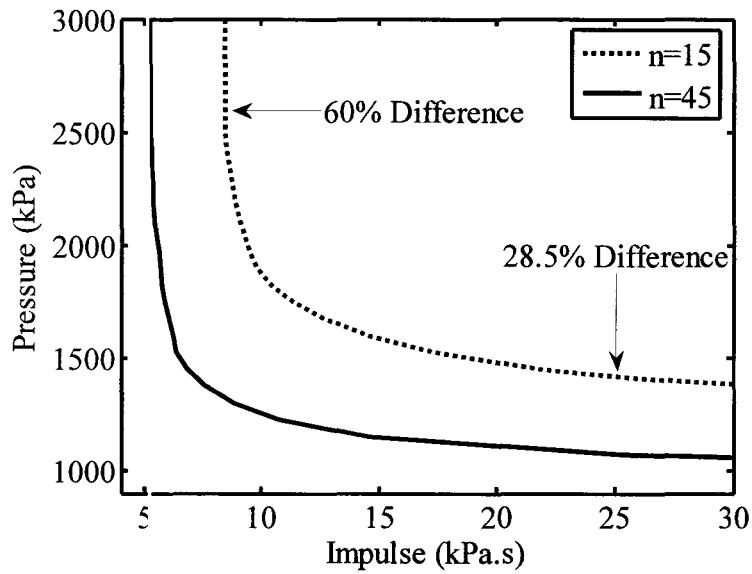


Fig. 2.16: Pressure-impulse diagrams for clamped-clamped beam by using 15 and 45 nodes: (a) Curvature ductility=2.0, (b) Curvature ductility=3.5, (c) Curvature ductility=5.0

Chapter 3: Response of Two-Way Reinforced Concrete Panels to Blast

Abstract: Analysis of reinforced concrete (RC) structures subjected blast loading is complicated due to the nonlinear behavior of concrete and reinforcement and the various failure modes to be considered. Therefore, simple analytical tools based on Single-Degree-of-Freedom (SDOF) idealization of structural elements were developed by many researchers to investigate the response of blast loaded RC beams, columns and panels. However, most of these approaches were limited to simple cases of one way structural element and did not consider many factors known to significantly alter the dynamic response. In this study, a SDOF model based on the guidelines of the US army Technical Manual TM 5-1300 is developed that takes into account the nonlinear behavior of RC panels. In addition, the model considers the material strength and deformation dependency on the strain rate as well as the post-failure membrane resistance. Using this model, a series of dynamic analyses were carried out using Pressure-Impulse ($P-I$) diagrams generated for two-way RC panels with different dimensions, aspect ratios, reinforcement ratios and support conditions. The $P-I$ diagram predictions were compared with the data obtained from a series of detailed explicit finite element (FE) analyses and the SDOF analysis consistently overestimated displacement for all types of loading. The general trend of results and the major characteristics of $P-I$ diagrams were also discussed for SDOF models of panels with different flexural rigidities and a modification for the TM5-1300 method for dynamic reaction calculation is proposed. Unlike the current TM5-1300 method which significantly under predicts the reactions, the proposed modification leads to a much better prediction for the impulsive range of response to blast load.

Keywords: Blast loads, Concrete structures, Dynamic response, Finite element method, Models, Nonlinear analysis, Panels, Structural safety.

3.0 Introduction

In recent years, there was a growing concern about the response of lifeline infrastructure, federal buildings and power plants to accidental and man-made explosions. During explosions, a chemical reaction takes place resulting in a sudden rise in temperature and pressure. Consequently, a shock wave is generated which strikes the structure with the pressure greater than ambient pressure. Generally, the exact blast loading information including the peak over pressure value and pressure time history may not also be available as a result of many uncertainties associated with such loading. However, as can be seen in Fig. 3.1(a), for a typical blast loading time history, the blast pressure (side-on over pressure) decays in an exponential form during a very short time (positive phase duration) and finally, falls below ambient pressure for a longer time (negative phase duration) with less pressure intensity (Baker et al. 1983). In practice, the negative phase (suction) can be neglected and the exponential decay loading can be approximated by a triangle which has the same peak pressure and different duration, T_L .

As can be seen in Fig. 3.1(b), the duration is determined based on the time to reach the maximum response. If the maximum structural response occurs after the pressure is decayed to ambient pressure, the equivalent duration is obtained by equating the area (the *impulse*) under the actual pressure-time curve in the positive phase with the area of the idealized triangle load. On the other hand, if the time to reach the maximum response is less than the positive phase duration, the equivalent duration is found by equating the slope of tangent line (at arrival time) on the actual loading curve with the slope of triangle load (Beshara 1994) as shown in Fig. 3.1(c).

Because of the short time history associated with blast loading and the nonlinear behavior of most structures under such extreme loads, nonlinear dynamic analysis is usually required to predict the structure response during blast loads. The different techniques used for nonlinear dynamic analysis usually fall under two categories: analytical (macro) models and finite element (FE) models. Macro models typically employ a single-degree-of-freedom (SDOF) or a multi-degree-of-freedom (MDOF) idealization of the structural element under consideration. The models use the first mode of vibration or the first few modes to predict the structure's response to blast loading. These models require a limited number of input data and are simple to use and easy to calibrate. On the other hand, nonlinear dynamic analysis using FE models is usually time consuming, requires a large number of input parameters and generally demands significant experience and knowledge to obtain reliable and realistic results. This is why most design codes are based on a simplified SDOF technique and even for case of complex structures, SDOF analysis is conducted for preliminary design or verifying FE results.

Due to the inherent nonlinear behavior of concrete and reinforcement, reinforced concrete (RC) structures, the various failure modes, and the effect of the rapid dynamic loading on the material response, detailed analysis is typically needed to gain understanding of many aspects of the blast loading-response interaction. However, such level of analysis is not suitable for initial assessment and screening or even preliminary design. In this regard, a number of research programs focused at identifying simple analytical tools to enable

design engineers and government officials to conduct rapid screening and evaluate the risk level associated with a certain explosion near key elements within a structure.

There are a number of investigations in which SDOF techniques have been employed to study the response of structural members under blast or impact loading [Biggs (1964); Krauthammer et al. (1986); Krauthammer et al. (1990); Louca and Harding (1997); Pan and Watson (1998); Schleyer and Hsu (2000); Boutros (2000); Low and Hao (2002)]. However, in the aforementioned research programs, the focus was to evaluate the response of simple cases of one-way elements or steel plates to blast-type of loading.

In this study, a SDOF model based on the guidelines of the US army Technical Manual TM 5-1300 is developed that takes into account the nonlinear behavior of RC structures and the material strength and deformation dependency on the strain rate as well as the post-failure membrane resistance of RC panels. An approximate method is also given in order to estimate the strain rate and its consequent effect on material strength. Since reinforced RC structures deflects in a nonlinear way, it is important to choose appropriate flexural rigidity for the SDOF analysis. Using this model, a series of dynamic analyses were carried out to generate Pressure-Impulse ($P-I$) diagrams for two-way RC panels with different support conditions, aspect and reinforcement ratios in the two orthogonal directions and results were compared with the ones obtained from FE analysis. Trend of the curves and their main characteristics are discussed. Comparison with FE results shows that cracked flexural rigidity work well for clamped panels while average of

cracked and gross rigidity give better results for simply supported panels. It should also be noted that one of the important parameters of structural design is the support reaction which can be reached to the high values at the beginning of loading. But unfortunately, TM5-1300 neglect applied force and also inertial forces in finding the reactions. Therefore, the approximate numerical procedure, which accounts for applied load and inertial forces, is implemented in TM5-1300 calculations for dynamic shear and results of this modified method are also compared with those of other technique. The following sections outline the model features and details followed by a discussion of the numerical results.

3.1 Model Development

3.1.1 SDOF Model

Available SDOF analysis techniques (Biggs, 1964; Baker et al., 1983; Krauthammer et al., 1986, 1990 and TM5-1300, 1990) consider the fundamental vibration response mode of individual structural members and utilize a nonlinear dynamic analysis procedure to evaluate the member response to a certain level of blast loading. In SDOF techniques, the dynamic response of a structural member (Fig. 3.2(a)) is approximated with the first mode shape and the dynamic equation of motion is evaluated for an equivalent SDOF system (Fig. 3.2(b)). Deflection obtained by solving this equivalent system represents the actual deflection of the structural member at a certain key location (e.g. panels' central point). To establish the equivalent SDOF, one needs to evaluate the mass factor, K_M , the resistance factor, K_R and the load factor, K_L , which relate the equivalent mass, the

equivalent resistance, and the equivalent load, respectively, in the SDOF system to the actual quantities in the structural element. In general, by equating the external work, kinetic energy and strain energy of the two systems, these factors can be easily found (Biggs 1964). These factors can be evaluated as follows:

Equating the external work done by the load on the panel to that on the equivalent SDOF system:

$$\left(\iint_A K_L p \, dA \right) \times \Delta_0 = \iint_A p \, \Delta(x, y) \, dA \quad \xrightarrow{\phi(x,y)=\frac{\Delta(x,y)}{\Delta_0}} \quad K_L = \frac{\iint_A p \, \phi(x, y) \, dA}{\iint_A p \, dA} \quad (3.1)$$

Equating the kinetic energy for the equivalent and actual system:

$$\frac{1}{2} \left(\iint_A K_M m \, dA \right) \times (\omega \Delta_0)^2 = \frac{1}{2} \iint_A m [\omega \Delta(x, y)]^2 \, dA$$

$$\xrightarrow{\phi(x,y)=\frac{\Delta(x,y)}{\Delta_0}} \quad K_M = \frac{\iint_A m \, \phi^2(x, y) \, dA}{\iint_A m \, dA} \quad (3.2)$$

Equating the potential energy for the equivalent and actual systems:

$$\frac{1}{2} \left(\iint_A K_R r \, dA \right) \times \Delta_0 = \frac{1}{2} \iint_A r \, \Delta(x, y) \, dA$$

$$\xrightarrow{\phi(x,y)=\frac{\Delta(x,y)}{\Delta_0}} \quad K_R = \frac{\iint_A r \, \phi(x, y) \, dA}{\iint_A r \, dA} = K_L \quad (3.3)$$

In the above equations, Δ_0 is the deflection at the panel's central point and $\Delta(x, y)$ is the deflection at any point on the panel with x and y coordinates; $\phi(x, y)$ is the shape function and ω is the natural frequency of vibration; A is the panel area and m, p, r are the mass, applied blast load and resistance force per unit area of the panel, respectively.

Considering the above equations, it is clear that, for a nonlinear system, a different shape function should be considered for each stage of displacement (e.g. elastic, elastic-plastic, or fully plastic conditions). Consequently, as the shape function changes, new transformation factors are computed for each deflection stage. Using these factors, the dynamic equation of motion for the SDOF model can be written as:

$$K_M ma + K_R r(\Delta_0) = K_L p(t) \quad (3.4)$$

Where a is the panel's central point acceleration, $r(\Delta_0)$ is the static resistance force per unit area as a function of the central point deflection, Δ_0 , and $p(t)$ is the blast load as a function of time. By dividing the previous equation by K_L and noting that the load factor, K_L , is equal to resistance factor, K_R (Mays and Smith 1995) as can be inferred from Eqs. 3.1 and 3.3, a *Load-Mass factor*, K_{LM} , is introduced:

$$K_{LM} ma + r(\Delta_0) = p(t) \quad (3.5)$$

The values of the load-mass factors in tabulated format and can be found in references such as Biggs (1964), TM5-1300 (1990) and Mays and Smith (1995).

It should be noted, as can be observed from Eqs. 3.4 and 3.5, that damping is usually not considered in impulsive loading problems such as blast and impact since the maximum response, which is generally of interest, usually occurs during the first vibration cycle when damping has minimum contribution to the dynamic response.

As can be noted from Eq. 3.5, a relationship between the resistance force and the corresponding central point deflection is needed for the solution. A typical resistance-deflection relationship for a two-way RC panel is shown in Fig. 3.2(c). Such resistance-deflection relationships can be found experimentally, using appropriate code equations, or using plastic analysis. As can be seen in Fig. 3.2(c), the slope of the curve changes when a new yield line initiates within the panel or at the supports.

Generally, if plastic analysis is used, the force which initiates a plastic hinge within the structural member is calculated, thus, the corresponding static displacement is found and the resistance-deflection relationship is established.

When dealing with RC members, an effective flexural rigidity, EI_{eff} , is needed to compute the deflection obtained for the corresponding to a certain applied load. Biggs (1964) suggested using the average of the cracked section rigidity, EI_{cr} , and the gross rigidity, EI_g , for deflection calculation, where as other international RC design codes

[ACI 318-05 (2005); CSA A23.3-04 (2005); EuroCode 2 (1992)] employ different expressions for EI_{eff} .

Figure 3.3 shows a free body diagram of a two-way panel subjected to uniform blast load. Both the inertial force and the applied blast load should be considered in order to obtain the correct dynamic reaction at the supports. It is generally assumed that the distribution of inertial force follows the same as shape function associated with the first mode. Considering the primary response mode, Biggs (1964) used the equilibrium conditions for the forces shown in Fig. 3.3 to derive the following equation for the dynamic reaction:

$$V_d(t) = \gamma_R \cdot R(t) + \gamma_F \cdot F(t) \quad (3.6)$$

In this equation, $V_d(t)$, $R(t)$ and $F(t)$ are the dynamic reaction, resistance force and applied load at a time t ; γ_R and γ_F are parameters that depend on the panel aspect ratio, the span direction of support (i.e. short edge support or long edge support) and the stage of displacement (e.g. elastic, elastic-plastic, or fully plastic).

3.1.2 SDOF Model in TM5-1300

The US army technical manual TM5-1300 (1990) was prepared to design structures to withstand accidental blast load. At the time the manual was originally produced (1990), it was considered a significant advancement in blast resistant design compared to previous publications in this area. The TM5-1300 was used directly or indirectly, in all NATO countries (Morison 2006) for protective design applications. The manual is currently

going through revision and updates. The work presented in this paper is expected to contribute in improving the dynamic reaction provisions of the new TM5-1300. The following sections present the current TM5-1300 recommendation as employed in this study.

3.1.2.1 Load-Mass Factors

The same procedure described earlier is used to find load-mass factors for different ranges of deflection. Table 3.1 gives the load mass factors for the two-way panels with 4 edge supports, actual values have been calculated for square 4 edges supported panels only and linear interpolation for aspect ratios between 1.0 and 2.0 is applied. Similar tables exist in the TM5-1300 for other kinds of support condition.

For fully plastic behavior, the code employs a yield line-based procedure to establish the load-mass factors. Figure 3.4 shows a segment of a two-way panel which is bounded by the support and the yield line pattern. The dynamic equation of motion based on the free body diagram shown in Fig. 3.4 is given by:

$$\sum M = I_m \ddot{\theta} \quad (3.7)$$

where:

$\sum M$ = summation of moments about the axis of rotation

I_m = mass moment of inertia of the segment about the axis of rotation

$\ddot{\theta}$ = angular acceleration

Equation 3.7 can be rewritten, after expansion, as follows:

$$F \times c - (\sum M_N + \sum M_P) = (I_m \times \frac{a}{L_1}) \quad (3.8-a)$$

or

$$F - (\sum M_N + \sum M_P) / c = (\frac{I_m}{c \times L_1} \times a) \quad (3.8-b)$$

Where, as shown in Fig. 3.4, c is the distance between the resultant applied load and axis of rotation. L_1 is the dimension of the segment perpendicular to the axis of rotation and a is the translational acceleration of the point located at the end of sector. $\sum M_N$ and $\sum M_P$ are the total negative and positive moment developed within the panel cross section, respectively.

Considering the term $(\sum M_N + \sum M_P) / c$ as a resistance force, R , the previous equation can be simplified to:

$$F - R = (\frac{I_m}{c \times L_1} \times a) \quad (3.9-a)$$

or

$$F - R = M_e \times a \quad (3.9-b)$$

Where M_e is the equivalent mass of the segment and therefore the load-mass factor for this segment can be given by:

$$K_{LM} = \frac{I_m}{c \times L_1} \times \frac{1}{M_{seg}} \quad (3.10)$$

Where M_{seg} is the total mass of the considered segment. Following the same procedure for the other segments of the two-way panel, the load-mass factor of the entire panel can be found as the summation of each segment's load-mass factor:

$$K_{LM} = \sum \frac{I_m}{c \times L_1} \times \frac{1}{M_{seg}} \quad (3.11-a)$$

and for a two-way panel with a uniform thickness, the Eq. 3.11-a can be simplified to:

$$K_{LM} = \sum \frac{I}{c \times L_1} \times \frac{1}{A_{seg}} \quad (3.11-b)$$

Where A_{seg} is the area of each individual segment.

From the above calculations, it is obvious that the location of the yield lines is required to evaluate the load-mass factors. Therefore, the TM5-1300 uses yield line analysis to find the configuration of yield lines based on the plastic moment capacity of reinforcement in the x and y direction. The TM5-1300 provides results in graphical format that gives the yield line locations of two-way panel with different moment capacity and support condition in orthogonal direction.

3.1.2.2 Resistance Force Function

The typical resistance function in TM5-1300 is shown in Fig. 3.5. As this figure shows, the total resistance function can be divided in two parts: flexural resistance and tensile membrane resistance. In the former part, the RC panel cross sectional flexural capacity is the controlling resistance whereas in the latter, the tensile steel reinforcement predominantly provides resistance. The following sections describe the method to construct flexural part and membrane part of the resistance.

Flexural Part: TM5-1300 employs theory of elastic plates to obtain multi-stage resistance function for two-way panels. In fact, a procedure to find the maximum possible load is carried out at each stage of deformation (i.e. elastic, elastic-plastic, etc.). During this process, it considers certain key points in a panel with a specific support configuration (Fig. 3.6). At these points the largest moments are expected and therefore, yield lines are also expected to initiate from these points. Generally, the magnitude of moment at these locations is given as a function of the panel aspect ratio as:

$$M = \beta \times r \times H^2 \quad (3.12)$$

Where β is the coefficient found based on the location of the point and also the panel aspect ratio; r is the resistance force, and H is the dimension of the panel in y -direction.

To find the maximum permissible load (resistance force) for a certain support configuration, the left hand side of the previous equation should be replaced with the

plastic moment capacity of different trial points and the equation should be solved for the minimum (governing) load. The deflection attained at a key point (e.g. central point for 4 edges supported, middle of the free edge for 3 edges supported and at the intersection of free edges in 2 edges supported panels) for this governing load can be obtained by:

$$\Delta_0 = \frac{(1-\nu)^2}{EI} \times \gamma \times r \times H^4 \quad (3.13)$$

Where EI is the flexural rigidity of the cross section per unit length; ν is the Poisson's ratio; γ is a coefficient found based on the panel's aspect ratio.

A sample of graphs for obtaining γ and β coefficients for a clamped panel is shown in Fig. 3.7. Similar graphs for panels with different support conditions can be found in the TM5-1300. It should be noted that in order to construct the resistance-deflection curve, the above procedure should continue to find load and deflection for the whole practical range of deflection. In fact, when one yield line is generated at one edge, a panel with new support configuration results. Therefore, the above procedure is repeated for the new panel in order to find the resistance and deflection increments up to the point where all possible yield line patterns are considered. It should also be taken into account that the rigidity of RC structure changes with increasing deformation. Therefore, different effective flexural rigidities, EI_{eff} , can be used in the previous equation in order to compute the deflection. The TM5-1300 recommends using a constant rigidity equal to the average of cracked rigidity, EI'_{cr} , and gross rigidity, EI_g , similar to Biggs' (1964) suggestion.

The TM5-1300 recognizes that the post ultimate resistance for two-way panels as the remaining resistance after failure in 1 edge or 2 edges. In other words, the moment considers the average deflection in which two-way spanning changes to one-way spanning and the remaining resistance is the corresponding ultimate resistance of the one-way panel. The failure criteria at this transition point is considered a partial flexural failure whereas, complete collapse is referred to the ultimate flexural failure.

The deflection at partial and ultimate failure can be found based on the available plastic rotation capacity as follow:

Considering the yield line configuration for the 4 edges supported element shown in Fig. 3.8, the central point deflection at partial failure, Δ_1 , can be found as:

$$\Delta_1 = (H \times \tan \theta_v) / 2 \quad (3.14)$$

Where θ_v is the rotation about the vertical support of the panel.

Considering partial failure at vertical support, the corresponding rotation about the horizontal support, α , can be given by:

$$\alpha = \tan^{-1} \left(\frac{H \times \tan \theta_v}{2x} \right) \quad (3.15)$$

Where x as is shown in Fig. 3.8.

As the element deflects more, the rotation about horizontal support increases and, at the ultimate failure, the rotation in excess of α can found as:

$$\lambda = \theta_H - \tan^{-1} \left(\frac{H \times \tan \theta_V}{2x} \right) \quad (3.16)$$

Where λ is the small extra rotation and θ_H is the rotation about the horizontal support.

Replacing θ_V and θ_H with the maximum rotational capacity, θ_{\max} , the ultimate deflection, Δ_u , can be expressed as:

$$\Delta_u = x \tan \theta_{\max} + (L/2 - x) \times \tan \left[\theta_{\max} - \tan^{-1} \left(\frac{H \times \tan \theta_{\max}}{2x} \right) \right] \quad (3.17)$$

In this way, partial and ultimate deflections are estimated based on the maximum plastic rotation.

Tensile Membrane Part: Under extreme dynamic loading such as blast, RC structural elements usually deform the plastic stage and larger displacements occur. Consequently, tension membrane action may develop depending on amount of the continuous reinforcement steel. The supports should restrain membrane movement and continuous reinforced bars should be adequately anchored and fixed into the panel supports to allow the development of the tension membrane resistance. The tensile membrane resistance for two way panels can be found as follow:

Considering the free body diagram of small element shown in Fig. 3.9, the equilibrium of forces can be written as:

$$r_T dx dy + T_x dy \frac{\partial z}{\partial x} - T_x dy \left(\frac{\partial z}{\partial x} + \frac{\partial^2 z}{\partial x^2} dx \right) + T_y dx \frac{\partial z}{\partial y} - T_y dx \left(\frac{\partial z}{\partial y} + \frac{\partial^2 z}{\partial y^2} dy \right) = 0 \quad (3.18-a)$$

or

$$\frac{T_x}{T_y} \times \frac{\partial^2 z}{\partial x^2} + \frac{\partial^2 z}{\partial y^2} = \frac{r_T}{T_y} \quad (3.18-b)$$

Where, r_T = the tensile membrane resistance (load per unit area due to tensile membrane action), z = deflection of the considered element, T_x = force in the continuous reinforcement in the horizontal direction, and T_y = force in the continuous reinforcement in the vertical direction.

And the solution to the previous equation can be given by:

$$r_T = \frac{\Delta_0 \pi^3 T_y / H^2}{4 \sum_{n=1,3,5} \left[\frac{1}{n^3} (-1)^{(n-1)/2} \left[1 - \frac{1}{\cosh \left[\frac{n\pi L}{2H} \left[\frac{T_y}{T_x} \right]^{1/2} \right]} \right] \right]} \quad (3.19)$$

Experimental results illustrates that the actual tensile membrane resistance is higher than the value obtained by Eq. 3.19 and that increase is attributed to the contribution of negative reinforcement in tensile membrane resistance (Park and Gamble (2000)). This

may also be the rationale behind the TM5-1300 provisions which give 50% greater membrane resistance than the amount obtained by Eq. 3.19. There may also be additional enhancement in resistance due to compression membrane action (arching) at deflections below the required deflection for initiating tension membrane (Park and Gamble (2000)), however, TM 5-1300 neglects this enhancement. This is, however, conservative and reasonable approach since in practice, support condition may not allow the panel to arch.

3.1.2.3 Support Reaction

The TM5-1300 acknowledges that support reactions are functions of applied loads and resistances, but it assumes that loading duration is very short and applied blast load goes to zero before the element reaches its maximum resistance and, as a result, it neglects the applied load in deriving the support reaction. Therefore, the code calculates the dynamic reaction panel by simply considering resistance force distributed between supports. In the case of two-way panel, it calculates the dynamic reactions during the plastic behavior stage and distributes resistance as a static load between supports. It also assumes the same distribution, for all other stages of element behavior (e.g. elastic, elastic-plastic, etc.).

3.1.3 Strain Rate Effects

Comparing the duration of typical blast load, which is in the order of milliseconds, with the duration of other dynamic loads such as earthquake, which is in the order of seconds, one can understand that a blast load is usually characterize with high rate of loading.

Therefore, the material characteristics in terms of the strength and deformation capacities under high strain rates are needed to be considered for the analysis of extreme dynamic loads with short durations such as blast (Bischoff and Perry 1991).

Generally, the ratio of the material dynamic strength to its static strength, referred to as the Dynamic Increase Factor (*DIF*), is given as a function of strain rate either graphically (TM5-1300 1990) or presented in the form of formulas. To obtain the *DIF* factors, Split-Hopkinson Pressure Bar (SHPB) test is usually employed and material properties are investigated at different strain rate (Bischoff and Perry 1991).

3.1.3.1 Concrete compressive strength

In order to assess the dynamic strength of concrete, different parameters such as concrete static compressive strength, aggregate, curing and moisture, age were discussed by Bischoff and Perry (1991). It was concluded that the concrete compressive strength was the predominant factor and concrete with lower compressive stress showed higher increase in strength. Several expressions for the enhancement of concrete compressive strength are given in literature. One of the widely acceptable formulations for the *DIF* for concrete compressive strength is proposed by Comité Euro-International du Béton (CEB) (1988) and is considered:

$$f_{cd} / f_{cs} = \left(\frac{\dot{\epsilon}}{\dot{\epsilon}_s} \right)^{1.026\alpha_s} \quad \text{for } \dot{\epsilon} \leq 30 \text{ s}^{-1} \quad (3.20\text{-a})$$

$$= \gamma_s \left(\frac{\dot{\epsilon}}{\dot{\epsilon}_s} \right)^{1/3} \quad \text{for } \dot{\epsilon} > 30 \text{ s}^{-1} \quad (3.20-b)$$

Where f_{cd} and f_{cs} are the dynamic and static compressive strength, $\dot{\epsilon}$ is the strain rate, $\dot{\epsilon}_s = 30 \times 10^{-6} \text{ s}^{-1}$ (static strain rate), $\gamma_s = 10^{(6.156\alpha_s - 2)}$, $\alpha_s = 1/(5+9(f_{cs}/f_{co}))$, $f_{co} = 10 \text{ MPa} = 1,450 \text{ psi}$.

3.1.3.2 Steel yield stress

Similar to concrete, expressions for steel *DIF* were proposed by Soroushian and Choi (1987); CEB (1988); Malvar (1998) with Malvar (1998) formulation used in an earlier investigation by the authors (Changiz Rezaei et al., 2007). Malvar's formulations were used in the present analyses because of the large number of test results at different strain rates that were used to verify his expressions:

$$DIF = \left(\frac{\dot{\epsilon}}{10^{-4}} \right)^{\alpha_{fy}} \quad (3.21-a)$$

where:

$$\alpha_{fy} = 0.074 - 0.040 \frac{f_y}{414} \quad (3.21-b)$$

In the above equation, $\dot{\epsilon}$ is the strain rate and f_y is the bar yield stress in MPa.

In this study, the concrete compressive stress and the steel yield stress is amplified by the mentioned *DIF* and moment capacity of the section is calculated based on the ACI 318-

05 (2005) design provisions. The other rationale behind selecting the expressions given in Eq. 3.20 and Eq. 3.21 is that the FE models discussed later in this study employ the same *DIF* for concrete and steel strength.

3.1.3.3 *DIF* estimation

As explained earlier, material strength should be scaled by the appropriate *DIF* in order to be used in the SDOF analysis. As a result, strain rate should be estimated by a procedure in order to compute the corresponding *DIF* for the analysis. Different techniques such as finding maximum curvature rate (Kulkarni and Shah 1998) or deriving the approximate strain rate equation (Krauthammer et al. 1994) exist. All of these methods are limited to one way structural elements and also give predictions for the order of strain rate, not the exact value since the correct modeling of strain rate dependency is so complicated and cannot be achieved using simple tools. Moreover, in the case of two-way panels with different distribution of curvature, finding the constant strain rate for the whole system becomes more difficult.

An approximate and simple technique was developed as follows: In this study, the maximum velocity of the central point before reaching the plastic stage of the deformation is found. Then, the strain rate is estimated based on the measured velocity and analysis is repeated with the modified material properties. This procedure continues until the same maximum velocity is obtained from the two successive iterations and convergence is reached. In this way, a basis is provided to calculate the strain rate and corresponding *DIF* for a two-way panels. To derive the approximate equation relating the

central point velocity and strain rate, the following relations can be used to modify strain rate for each iteration:

The deflected shape (see Fig. 3.10) is divided in two segments and using central difference technique, the curvature, Φ , at midspan section in x -direction can be expressed as:

$$\Phi \cong \frac{d^2y}{dx^2} \cong \frac{2 \times \Delta_0}{(L/2)^2} = \frac{8 \times \Delta_0}{L^2} \quad (3.22)$$

Then, the strains at the tensile and compressive fiber in the midspan of this section can be obtained as:

$$\varepsilon_c = \frac{8 \times h_c \times \Delta_0}{L^2} \quad (3.23-a)$$

$$\varepsilon_t = \frac{8 \times h_t \times \Delta_0}{L^2} \quad (3.23-b)$$

Where ε_c and ε_t are strains at the compressive fiber and the tensile fiber, respectively; h_c and h_t are the compression depth and the tension depth of the cross section, respectively.

Consequently, the strain rate at extreme fibers can be found by taking derivative with respect to time:

$$\dot{\epsilon}_c = \frac{8 \times h_c \times V_0}{L^2} \quad (3.24-a)$$

$$\dot{\epsilon}_t = \frac{8 \times h_t \times V_0}{L^2} \quad (3.24-b)$$

Where $\dot{\epsilon}_c$ and $\dot{\epsilon}_t$ are strain rates at the compressive fiber and the tensile fiber, respectively; V_0 is the panel's central point velocity.

And the average of the above strain rates can be taken for the strain rate in x -direction:

$$\dot{\epsilon}_x = 4 \times V_0 \times \left(\frac{h_t + h_c}{L^2} \right) \quad (3.25-a)$$

or

$$\dot{\epsilon}_x = 4 \times V_0 \times \left(\frac{h}{L^2} \right) \quad (3.25-b)$$

Where h is the thickness of the panel and $\dot{\epsilon}_x$ is the average strain rate in x -direction.

Following the same procedure for the y -direction, the average strain rate in y -direction, $\dot{\epsilon}_y$, can be found as:

$$\dot{\epsilon}_y = 4 \times V_0 \times \left(\frac{h}{H^2} \right) \quad (3.26)$$

And the strain rate, $\dot{\epsilon}$, can be assigned for the whole element by taking the average of the $\dot{\epsilon}_x$ and $\dot{\epsilon}_y$:

$$\dot{\epsilon} = 2 \times V_0 \times h \times \left(\frac{1}{L^2} + \frac{1}{H^2} \right) \quad (3.27)$$

As can be seen, the above equation relates the strain rate with the panel's central point velocity and in this way, strain rate can be modified for every new iteration.

3.2 Numerical Results and Discussion

3.2.1 Overall Procedure

Using the SDOF model developed with the features explained in the previous sections, 3 clamped panels and 3 simply supported panels were modeled. The details of these panels are listed in Table 3.2. These panels have different reinforcement and aspect ratios. The thickness of all panels was kept constant as 200 mm and their dimensions in x -direction were kept as 4.0 m. 30 MPa concrete compressive strength was used and the yield stress of the reinforcement was set to 400 MPa for the analysis. The maximum rotational capacity of the panels, which determined the end of the flexural resistance stage, was set to 2.0 degree. This value of the rotation is the minimum level of rotation considered and recommended for common panels by the TM5-1300. After this the clamped (but not the simple) panels were assumed to resist the load solely by the tensile membrane action.

As noted earlier, RC structures show nonlinear behavior under applied load and their flexural rigidity changes during the analysis. Therefore, an effective flexural rigidity, EI_{eff} , should be used in the SDOF models. Using the cracked flexural rigidity, EI_{cr} , and

the average of the cracked and the gross rigidities, two sets of $P-I$ diagrams were developed from the SDOF analysis as will be explained later. A number of points on these diagrams, which basically identifies sets of pressure and impulse pairs, were selected. FE models of these panels were generated and those selected pressure and impulse pairs were applied on these models. Then, the maximum deflection obtained from the FE analysis was compared with the ones predicted by the $P-I$ diagrams as will be described in the following sections.

As mentioned earlier, the TM5-1300 does not consider the effect of inertial force in calculating reaction forces. The inertial force was taken in to account by approximating it as a uniform load. The following sections also discuss and compare the dynamic reaction results found from the TM5-1300, the proposed modification, Biggs' formulation (Eq. 3.6) and the FE.

3.2.2 FE Models

The panels listed in Table 3.2 were modeled using the nonlinear dynamic analysis FE code LS-DYNA V.971 (2006). Schematic diagrams of the clamped and simply supported panels have been shown in Fig. 3.11.

The FE analysis employed non-linear material properties for both the steel and concrete and included large deformation. The software automatically accounted for strain rate effects.

LS-DYNA material model (MAT_CONCRETE_DAMAGE) was used for the concrete. This model has been developed to model concrete under impulsive loading and has been used successfully to predict the response of concrete under uniaxial, biaxial, and triaxial stresses in both tension and compression (Tavarez et. al. 2003). The formulation has also been used successfully to model the behavior of reinforced concrete walls subjected to blast loads (Malvar et al. 1997).

This concrete model is a plasticity-based formulation with three independent failure surfaces which change shape, depending on the confinement pressure. In LS-DYNA, this material model is used in conjunction with an equation of state (EOS_TABULATED_COMPACTION), which gives the current pressure as a function of current and previous volumetric strain. The inclusion of the strain rate effects in the concrete material model was based on the work by Malvar et al. (1998 and 1997).

The steel reinforcement was modeled explicitly as beam elements in full contact with the concrete solid elements at their coincident nodes. The steel material was modeled using a plastic kinematic material model (MAT_PLASTIC_KINEMATIC) in LS-DYNA. The strain rate effect was taken into account using the Cowper-Symonds model (Cowper and Symonds 1957) which scales the yield stress as follows:

$$\frac{f_{yd}}{f_{ys}} = 1 + \left(\frac{\dot{\epsilon}}{SRC} \right)^{1/SRP} \quad (3.28)$$

where f_{yd} and f_{ys} are the dynamic and static compressive strength of steel respectively and

$\dot{\epsilon}$ is the strain rate. The strain rate parameters SRP and SRC were adopted by considering the empirical formulation proposed by Malvar et al. (1998) and using regression analysis. The values used in this study were $SRC = 0.3213$ and $SRP = 4.8662$.

As can be seen in Fig. 3.11(a), supports were modeled with rigid plates for simply supported panel. As Fig. 3.11(b) depicts top rigid plate and bottom rigid plates were used to model the clamped condition. In order to benefit from tensile membrane action in clamped panels, steel element nodes were connected to lateral plates and these plates can move outward while their inward movement is prevented through contacting both the bottom and top plate. The `AUTOMATIC_SURFACE_TO_SURFACE CONTACT` algorithm in LS-DYNA was employed between the panel and the rigid plates shown in Figs. 3.11(a), 3.11(b) and also between the lateral plates and the other two plates shown in Fig. 3.11(b).

Figure 3.12 presents the typical FE meshes used in the analyses. Plates and the concrete panel were idealized by of $50 \text{ mm} \times 50 \text{ mm} \times 40 \text{ mm}$ solid elements and a 2-node beam element was used to model the reinforcing bars. In addition, fully integrated solid elements with nodal rotation were employed in the analysis and perfect bond was assumed between the bars and the concrete.

Blast load were applied as a uniform pressure with a triangle load history as shown before in Fig. 3.1(b). Total dynamic reaction was calculated by adding the total contact

forces between concrete and bottom plate. The displacement time-history of the node located at panel's central point on top surface of the panels is considered and the maximum displacement is found. In cases where there is a local failure at this node, the maximum deflection reached by the top reinforcements, located just below this node, will be reported.

3.2.3 SDOF Models with Different Flexural Rigidities

As pointed out earlier, an effective flexural rigidity, EI_{eff} , is needed to construct a resistance deflection curve. In this section, different SDOF models with three different flexural rigidities are considered. Two of them will be used in the analysis as it will be proven there is no need to consider the third one.

The three SDOF models with an assumed rigidity are listed as follow:

SDOF(EI_{ave}): The effective flexural rigidity of this model is based on the weighted average of cracked and gross rigidity in two orthogonal directions. This approach for rigidity calculation is recommended by the TM5-1300 and can be expressed as:

$$EI_{ave} = \frac{EI_g + EI_{cr}}{2} \quad (3.29-a)$$

Where:

$$EI_g = \frac{H \times EI_{g(x)} + L \times EI_{g(y)}}{H + L} \quad (3.29-b)$$

$$EI_{cr} = \frac{H \times EI_{cr(x)} + L \times EI_{cr(y)}}{H + L} \quad (3.29-c)$$

In the above equations:

$EI_{g(x)}, EI_{g(y)}$ = Gross flexural rigidities in x -direction and y -direction, respectively.

$EI_{cr(x)}, EI_{cr(y)}$ = Cracked flexural rigidities in x -direction and y -direction, respectively.

EI_g = Average gross flexural rigidity in orthogonal direction.

EI_{cr} = Average cracked flexural rigidity in orthogonal direction.

SDOF(EI_{cr}): The average cracked flexural rigidity in orthogonal direction is used for this SDOF system and is given by Eq. 3.29-c in the previous SDOF model.

SDOF($EI_{weighted}$):

For this SDOF mode, effective rigidity is considered based on the weighted average of cracked and gross rigidities over the panel surface. In this procedure, the RC panel is divided to regions with different rigidities as shown in Fig. 3.13. These regions are corner, edge (i.e. E(1), E(2), E(3) and E(4)) and central regions. The weighted contribution of each region's rigidity to the overall panel rigidity is considered by the ratio of its area over the total area of panel using the weighted mean approach as follow:

$$EI_{weighted} = \sum_{i=1}^4 \left[\left(\frac{A_{E(i)}}{A_{tot}} \right) \times EI_{E(i)} \right] + \frac{A_{mid}}{A_{tot}} \times EI_{mid} + \frac{A_{corners}}{A_{tot}} \times EI_{corners} \quad (3.30)$$

Where:

$$EI_{E(i)} = EI_g \quad \text{if } E(i) \text{ region is located near simple support;}$$

$$EI_{E(i)} = EI_{cr} \quad \text{if } E(i) \text{ region is located near fixed support;}$$

$$EI_{corners} = EI_g \quad \text{and}$$

$$EI_{mid} = \frac{n_s}{n_s + n_f} \times EI_{cr} + \frac{n_f}{n_s + n_f} \times EI_g \quad (3.31)$$

In these equations:

$A_{E(i)}$ = Area of the panel bounded by i^{th} region

A_{mid} = Area of the panel at midspan region

$A_{corners}$ = Total area of the corner regions

A_{tot} = Total area of the panel

$EI_{E(i)}$ = flexural rigidity at the i^{th} edge region ($i = 1,2,3,4$)

EI_{mid} = flexural rigidity at the central region

$EI_{corners}$ = flexural rigidity at the corner regions

EI_g = Average gross flexural rigidity of reinforcement in orthogonal direction.

EI_{cr} = Average cracked flexural rigidity of reinforcement in orthogonal direction.

n_s = number of simple supports

n_f = number of fixed supports

3.2.4 Pressure-impulse diagrams

The concepts of the pressure-impulse ($P-I$) diagrams was introduced in order to characterize the level of damage induced by the pulse loads (Baker et al. 1983). As depicted by Fig. 3.14, it consists of several contours corresponding to different levels of damage or deflection.

As illustrated in Fig. 3.14, each contour gives different combinations of pressure and impulse that will result in the same maximum deflection, maximum curvature, ductility level or level of damage in the member. Pressure and impulse combinations to the right and/or above each curve produce damage (deflection) greater than that represented by this curve while the ones to the left and/or below the curve would result in lower damage (deflection) level than indicated by the curve. Each curve in the $P-I$ diagram can be divided into three segments: impulsive loading realm, dynamic loading realm and quasi-static loading realm. It can also be observed that an impulse asymptote for the impulsive regime and pressure asymptote for the quasi-static regime can be identified for each curve. This means that maximum level of damage the load impulse is more dependent on the load's impulse for the impulsive regime and the peak pressure for the quasi-static regime. It should also be noted the level of damage is dependent on the combination of both pressure and impulse in the dynamic loading realm. In general, the $P-I$ diagram approach is considered a simplified tool to assess the performance of the structural members under specific level of blast load (Baker et al. 1983).

3.2.4.1 *P-I* diagrams for the simply supported panels

Using the SDOF model with a specific rigidity, *P-I* curves was constructed for different level of deflection and results are reported in Fig. 3.15, Fig. 3.16 and Fig. 3.17. In these figures, different level of deflections, $L/400$, $L/200$ and $L/100$, have been identified beside each curve as a fraction of panel length in horizontal direction. As depicted in these diagrams, three points have been selected and marked in each curve. These points are taken from different parts of a curve and, as can be seen, there is one selected point for each regime (i.e. impulsive, dynamic and quasi-static).

As described before, the points marked on the *P-I* diagrams represent combinations of pressure and impulse. These loads were applied on the FE model and the maximum displacement from the FE analysis was found. This displacement was then divided by the value predicted by the corresponding *P-I* diagram and the FEM/SDOF ratio was reported beside of each marked point. Typical FE results obtained for the deflection of simply supported panel are shown in Fig. 3.18.

Figures 3.15 and 3.16 show the *P-I* curves obtained by using EI_{ave} and EI_{cr} . Use of the former rigidity is also recommended by TM5-1300 (1990). Comparing the two figures, it can be seen both SDOF models overestimate the deflections (all ratios are lower than 1.00) but employing SDOF (EI_{ave}) overall provides a better estimation for the detailed FE model results compared to the results obtained from SDOF (EI_{cr}). As can be seen in Fig. 3.16, implementation of cracked rigidity, EI_{cr} , in the SDOF model will result in the

significant overestimation of the deflection. As shown by both figures, the ratios are higher in the impulsive regime compared to the other parts of the curves. This can be the results of contribution of higher modes in response for such regimes. In fact, it has been pointed that the contribution of higher modes can be more significant for impulsive loading (Subbaraj and Dokainish 1989; Ebeling et al. 1997). Therefore, FE models, which can take the accounts of higher modes, can give larger deflection in the impulsive region and consequently the ratios become higher in this region.

It can also be observed that use of EI_{cr} yields a wider space between $P-I$ curves, especially in the quasi-static regime, compared to the curves obtained by SDOF (EI_{ave}). As Fig. 3.15 depicts, SDOF (EI_{ave}) overestimate the results in quasi-static regime significantly as the deflection increase and the space between curves become much closer. This can be attributed to the dependency of the pressure asymptote, the part of the $P-I$ curves parallel to the horizontal (impulse) axes, to the ultimate resistance, r_u , and stiffness, k . For an elasto-plastic SDOF model, Smith and Hetherington (1994) obtain the pressure asymptote, P_c , by equating the external work and strain energy. Therefore, P_c can be expressed as:

$$P_c = r_u \cdot \left(1 - \frac{r_u}{2 \cdot k \cdot \Delta_m}\right) \quad (3.32)$$

where Δ_m is the maximum level of deflection.

Taking the derivative of previous equation with respect to level of displacement, Δ_m , the variation of the pressure asymptote with displacement can be obtained as:

$$\frac{\partial P_c}{\partial \Delta_m} = \frac{r_u^2}{2.k.\Delta_m^2} \quad (3.33)$$

The above equation shows that the change in pressure asymptote is directly proportion to the square of resistance and the reciprocal of the stiffness. This means that the variation in P_c becomes significantly larger by using higher resistance values or lower values of stiffness. In fact, the difference between two successive value of pressure asymptote will be greater (i.e. the space between $P-I$ curves become wider) for the structural system with higher resistance or lower stiffness.

Overall, the overestimations can be attributed to the resistance underestimation in SDOF model. In fact, TM5-1300 neglects the tensile capacity of the concrete, but at high rate of loading, this property of concrete increase much more than its compressive strength (Malvar and Ross 1998) and therefore, higher enhancement in strength can be expected. Furthermore, as described earlier, the resistance function is constructed by finding and adding the static load increments which can create plastic moment in certain points of a panel. However, greater load can be expected for creating a yield line which consists of a series of yielded points not a single yielded point and this means that resistance can be greater. In addition, noting that the thickness of the panel is significantly less than its

other dimensions, it can be concluded that the problem in hand is a plain stress problem with the concrete under a biaxial state of stress and hence, there is also additional enhancement for the concrete strength. Moreover, using smooth transition toward the plastic stage instead of employing constant value of stiffness will also bring about lower effective stiffness for the SDOF model and this will result in a wider space between $P-I$ curves.

It can also be noted that, similar to Eq. 3.32, an expression is given by Smith and Hetherington (1994) for the values of impulse asymptote (the part of $P-I$ curve parallel to the pressure axes), I_c , as:

$$I_c = r_u \cdot \left(\sqrt{m \cdot \left(\frac{2 \cdot \Delta_m}{r_u} - \frac{1}{k} \right)} \right) \quad (3.34)$$

and if the derivative of previous equation is calculated with respect to Δ_m , the variation can be found as:

$$\frac{\partial I_c}{\partial \Delta_m} = \sqrt{\frac{m \cdot r_u \cdot k}{2 \cdot k \cdot \Delta_m - r_u}} \quad (3.35)$$

It can be seen that the change in the value of impulse asymptote with variation of stiffness and resistance cannot be explained explicitly as in Eq. 3.33. However, it can be inferred that the variation of these parameters has less effect on the variation of I_c

compared to their effect on P_c since the square root of these parameters determines the change in I_c with displacement.

Fig. 3.17 also shows the results obtained by implementing the $EI_{weighted}$ in the SDOF model. It can be noted that the same trends, which were explained for the two previous figures, exists for the $P-I$ diagrams developed by this SDOF model. Comparing to the results of SDOF (EI_{ave}), the ratios becomes a little greater and the changes between the results presented in Fig. 3.15 and Fig. 3.17 are not significant. Therefore, considering the simplicity and ease of effective rigidity calculation, SDOF(EI_{ave}) is more advantageous than SDOF ($EI_{weighted}$).

3.2.4.2 $P-I$ diagrams for clamped panels

Using the developed SDOF model, $P-I$ diagrams were developed for the clamped panels. Cracked and average flexural rigidity were used and results are depicted in Fig. 3.19 and Fig. 3.20, respectively. As specified on these figures, these $P-I$ curves include different levels of displacement expressed as a ratio of long span length. $L/400$, $L/200$ and $L/100$ falls in the flexural part of resistance function while $L/12$ placed in the tensile membrane part. Next to the curve generated for the $L/12$ value, another curve for the same value of displacement was constructed using a modified resistance function. In fact, it was assumed that the maximum rotation of RC section is not limited to 2 degrees and that the flexural action continues until plastic part intersects with tensile membrane resistance

which results in the drop shown in Fig. 3.10 to disappear in the modified resistance function (Fig. 3.21).

Based on these assumption new $P-I$ curves was built for a deflection of $L/12$ and are shown in Figs. 3.19 and 3.20. Again, there was no need to consider SDOF($EI_{weighted}$) model (Eq. 3.30) for clamped panels since it will result in the same value as the simplified SDOF(EI_{ave}) .

Results for Flexural Part: Similar to the process described in the previous section, three pressure and impulse pairs were identified for each curve and the ratio of maximum displacement found from FE analysis over the one predicted by the $P-I$ diagram is reported next to each point. Sample of FE results are shown in Fig. 3.22.

Considering Figs. 3.19 and 3.20, it can be observed that similar to simply supported slabs, both SDOF($EI_{,ve}$) and SDOF(EI_{cr}) overestimate the maximum deflection but SDOF(EI_{ave}) gives much better predictions than SDOF(EI_{cr}). The same trend in results same as the ones explained for the simply supported can also be seen in these figures. On other hand, in contrast to the simply supported panels, use of EI_{ave} in SDOF model of the clamped panel correlates better with the result of FE analysis and the ratios shown in Fig. 3.19 are higher than the ones presented in Fig. 3.15. This can be attributed to the contribution of higher modes in FE model response. In fact, more modes can be excited in clamped panels as a result of higher vibration frequency and consequently, contribution of higher modes can be more significant when they are subjected to the blast

loads with high rate of loading (Subbaraj and Dokainish 1989; Ebeling et al. 1997). Therefore, larger deflection can be found by the FE models and the ratios become greater, especially in the impulsive regime.

Again, it can also be observed the curves become closer in the quasi-static regime which is more pronounced for the $P-I$ diagrams constructed by SDOF(EI_{ave}). Similar to the previous section, the observed overestimations can be attributed to reasons such as strength and stiffness parameters. Another factor may be the presence of tensile membrane resistance in the flexural part of the resistance function. As Fig. 3.5 shows, the tensile membrane resistance increases with increasing displacement and it also exists in the flexural part of resistance function. However, the TM5-1300 neglects this extra resistance during flexural-dominated stage.

It should also be noted that although the SDOF(EI_{cr}) model results in a $P-I$ diagrams with wider space between curves, the space does not change significantly compared to the simply supported panels and the curves become closer with increasing the deflection. In fact, this occurred since clamped conditions for the panels results in a very stiff model regardless of what kind of flexural rigidity is used in the analysis. Hence, the variation of flexural rigidity between EI_{ave} and EI_{cr} has lower effect on the space between $P-I$ diagrams.

Results for Tensile Membrane Part: As pointed before, SDOF model benefit from tensile membrane resistance when the maximum displacement reaches $L/12$. For this type of loading, the concrete is usually distorted due to high intensity of the load and therefore, the typical deflections reached for the reinforcement are shown in Fig. 3.23. Considering both Figs. 3.19 and 20, it can be seen that all the ratios are below 1.00 (i.e. SDOF model overestimate the FE results). It can also be observed that use of the modified resistance function will also shift the curves up in the quasi-static regime but the ratios still remain much lower than 1.00. As explained before, this may be attributed to the same reasons given in previous parts for the overestimation of FE results, especially in the quasi- static regime. Moreover, this trend occurs since the developed code based on TM5-1300 guidelines decouples the flexural resistance and tensile membrane resistance while the behavior can exist together. In fact, the maximum rotation capacity of the RC section cannot be accurately specified and therefore, panels can also have some flexural resistance although it enters tensile membrane part of the resistance function.

3.2.5 Support Reactions

The TM5-1300 neglects the dynamic behavior of the two-way panels and expresses the shear in terms of resistance force. A simplified approach is outlined here to implement the effect of inertial force in support dynamic reaction calculations and results are compared with available closed form solution for the reaction (Biggs 1964) reaction and the TM5-1300's predicted reaction.

3.2.5.1 Implementing the Effect of Applied Load in TM5-1300's Method

The distribution of inertial force over the entire panel can be given by the shape function considered for the dynamic analysis, as shown in Fig. 3.24 for a one way element. Therefore, as an approximation, the inertial force can be replaced by a uniform inertial load with the same total value. As a result, there would be a net uniform load due to the blast and inertial loads and consequently, the resultant of this uniform load is divided between supports to obtain the approximate dynamic shear. The same procedure can be applied to a two-way panel by considering a two-way shape function. The net load should be distributed between all supports using the procedure outlined in the following section:

As shown in Fig. 3.25, by considering the cross sections of a two-way panel in the two orthogonal directions, each section can be considered as a section in an one-way element and therefore, the multiplication of the shape function associated with these two one way elements can result in a shape function for the two way element made from these elements:

$$\phi(x, y) = \phi(x) \times \phi(y) \quad (3.36)$$

Where:

$\phi(x, y)$ = The shape function of the two way element

$\phi(x)$ = The shape function of one way element associated with the x-cross section

$\phi(y)$ = The shape function of one way element associated with the y-cross section

The TM5-1300 considers the resistance load as a uniform load and by evaluating the equilibrium equations for a panel at the plastic stage, it obtained coefficients to calculate the support reaction. The same expressions will be used to distribute the mentioned uniform net load.

3.2.5.2 Results for Different Methods

Some of the loads shown in the $P-I$ diagrams were considered and applied on SDOF(EI_{ave}) for clamped panels and simply supported panels. The Total dynamic reaction was calculated using TM5-1300 current method, the proposed modified TM5-1300 method and the closed form solution [Biggs (1964); Eq. 3.6] and the maximum value was compared with the result of FE analysis. Tables 3.3 and 3.4 give the maximum reaction found from FE analysis and the load specifications. The maximum values predicted by other methods were normalized by dividing them by the FE values and were also reported in these tables. The first column determines the location of the load on the $P-I$ diagrams. In this column, I, D and Q, denote *impulsive*, *dynamic* and *quasi-static* regime, respectively. The next two columns give the peak pressure and loading duration. The rest of columns show the FE dynamic reaction and the normalized values calculated from different methods.

The ratios in Table 3.3 show that the current TM5-1300 significantly underestimates the FE predictions in the impulsive regime while the other two methods result in the better estimation of the FE results. In the other regimes, no significant difference can be

observed between the three methods employed in SDOF analysis. Moreover, the underestimation of reactions (data with lower value than 1.00) in the dynamic regime and even more in the quasi-static regime can be attributed to the underestimation of resistance force. As illustrated by Eq. 3.6, combination of applied load and resistance force determines the dynamic reaction. Therefore, it is quite obvious that contribution of resistance force becomes more significant for loads with low values of pressure and, as explained before, resistance force is underestimated during SDOF analysis. This can also be the reason for underestimation of some of the loads shown in the impulsive regime which has high peak pressure and long duration of loading.

Similar data are given in Table 3.4 for the clamped panels. In the impulsive regime, reactions are highly underestimated by TM5-1300 whereas better prediction has been obtained by using the other two methods in the impulsive regime. It can also be observed that all ratios are lower than 1.00 in other regimes and, similar to simply supported panels, deficiencies in resistance force can lead to the underestimation of reaction.

Overall, it can be concluded that there is not significant difference between the results of the TM5-1300 method and the proposed modified technique for low pressure since the effect of resistance force is more predominant for this kind of loads. However, considering loads with high pressure also reveals that it is better and more conservative to use the proposed modification in TM5-1300 method in order to account for the considerable contribution of load in the reaction force.

3.3 Conclusions

Focusing on blast loaded two way panels, the major characteristics of SDOF model in TM5-1300 manual were highlighted and presented. A SDOF model was developed that takes into account strain rate effects in addition to the TM5-1300 SDOF model characteristics. A simplified procedure was established in order to estimate strain rate for two way elements. TM5-1300 method for obtaining support reaction was also modified and the effect of applied load was implemented in the analysis. Using different flexural rigidity in SDOF analysis, $P-I$ diagrams have been constructed for different level of deflection and $P-I$ curve predictions were compared with results of FE analysis. Moreover, maximum dynamic reaction obtained from different methods including FE analysis were considered and compared for the different blast load levels.

Using SDOF models with different rigidity, $P-I$ curves are generated for different level of deflection and results were compared with the ones obtained from FE analysis. It was shown that use of average of cracked and gross flexural rigidity, which is also recommended by TM5-1300, correlates better with FE results in the impulsive regime compared to the other realm of loading. It was shown that SDOF analysis results in conservative prediction of displacement for all type of loading and it also overestimates displacement significantly for the loads with low pressure amplitude and long duration of loading. The overestimation of results was attributed to the deficiencies which were present in resistance function. Expressions for the variation of pressure and impulse

asymptote with respect to level of deflection were derived and dependency of these asymptotes to stiffness and resistance was discussed.

A modification proposed for TM5-1300 dynamic reaction calculation which can take the effect of inertial force into account. It was pointed that support reactions calculated from TM5-1300 method significantly under predict the FE results but the proposed modification yield to significantly better prediction of FE results for impulsive loading regime. Therefore, it was concluded that it is better to consider the proposed modified method for impulsive loads and use of this modification in TM5-1300 calculation does not make significant change in results for other kind of loading.

All in all, it seems that the SDOF analysis recommended by TM5-1300 is conservative for displacement and unconservative for dynamic reaction. In this paper modification was given so that the reaction prediction was significantly improved in the impulsive regime but the shear prediction is still underestimated for other type of loading and this is mainly due to the resistance underestimation. Therefore, considering that the recent developments in computers have made the analysis easier than before, efforts can be made to modify the analysis recommended by TM5-1300 in order to find more realistic results and consequently, save the cost of construction.

Acknowledgements

This study forms a part of an ongoing research program in McMaster University Centre for Effective Design of Structures (*CEDS*) funded through the Ontario Research and Development Challenge Fund (*ORDCF*). This research falls under *CEDS Focus Area II: Earthquake Engineering and Extreme Dynamic Loading*. The financial support of the Centre is greatly appreciated.

Notation

The following symbols are used in this paper:

A = Area

a = central acceleration

c = the distance between the resultant applied load and axis of rotation

DIF = dynamic increase factor

EI = flexural rigidity

F = total applied load

f_{cd} = concrete dynamic compressive strength

f_{co} = parameter of CEB's equation for DIF of concrete

f_{cs} = concrete static compressive strength

f_y = reinforced bar yield stress

H = Dimension of panels in vertical direction

h = Panel thickness

h_c = compression depth

- h_t = tension depth
- I_c = impulse asymptote in the $P-I$ diagram
- I_m = mass moment of inertia about the axis of rotation
- k = stiffness of the SDOF model with an elasto-plastic resistance
- K_L = load factor
- K_R = resistance factor
- K_M = mass factor
- K_{LM} = load-mass factor
- L = dimension of panels in horizontal direction
- L_1 = length of the dimension perpendicular to the axis of rotation
- m = mass per unit area of panel
- M_e = equivalent mass of the element segment
- M_N = negative moment
- M_P = positive moment
- M_{seg} = total mass of the element segment
- n_s = number of simple supports
- n_f = number of clamped supports
- p = blast load per unit area
- P_0 = peak pressure
- P_c = pressure asymptote in the $P-I$ diagram
- $R(t)$ = total resistance force as a function of time

- r = resistance force per unit area
 r_T = the tensile membrane resistance per unit area
 SRC = the strain rate parameter in Cowper-Symonds model
 SRP = the strain rate parameter in Cowper-Symonds model
 T_L = loading duration
 T_x = tensile force in the continuous reinforcement in the short direction
 T_y = tensile force in the continuous reinforcement in the long direction
 V_0 = central velocity
 V_d = dynamic reaction
 x = x -coordinate
 y = y -coordinate
 z = z -coordinate
 α = support rotation
 α_{f_y} = parameter of reinforced bar yield stress in Malvar's equation
 α_s = parameter of CEB's equation for DIF of concrete
 β = a coefficient for the moment calculation in TM5-1300
 γ = a coefficient for the deflection calculation in TM5-1300
 γ_F = applied load coefficient Biggs' equation for dynamic reaction
 γ_R = resistance force coefficient in Biggs' equation for dynamic reaction
 γ_s = parameter of CEB's equation for DIF of concrete
 $\Delta(x, y)$ = deflection of a point in a two-way panel with x and y coordinates

- Δ_0 = deflection at a certain point of a two-way panel
- Δ_1 = the deflection at the partial flexural failure
- Δ_m = maximum central deflection of a two-way panel
- Δ_u = the deflection at the ultimate flexural failure
- ε_c = strain at the compressive fiber
- ε_t = strain at the tensile fiber
- $\dot{\varepsilon}$ = strain rate
- $\dot{\varepsilon}_c$ = strain rate at the compressive fiber
- $\dot{\varepsilon}_t$ = strain rate at the tensile fiber
- $\dot{\varepsilon}_s$ = concrete static strain rate
- $\dot{\varepsilon}_x$ = strain rate for x-direction
- $\dot{\varepsilon}_y$ = strain rate for y-direction
- $\phi(x)$ = the shape function of one way element associated with the x-cross section
- $\phi(y)$ = the shape function of one way element associated with the y-cross section
- $\phi(x, y)$ = the shape function of the two-way panel
- φ = curvature
- λ = the small extra rotation
- θ_H = horizontal rotation
- θ_{max} = the maximum rotation capacity
- θ_V = vertical rotation

$\ddot{\theta}$ = angular acceleration

ν = Poisson's ratio

ω = the natural frequency of vibration

Subscripts and Superscripts

ave = average

corners = corner regions

cr = cracked

$E(i)$ = i th region near the support ($i=1,2,3,4$)

g = gross

mid = midspan region

tot = total

u = ultimate

References

ACI Committee 318-05. 2005. Building code requirements for structural concrete (ACI 318-05) and commentary (318R-05). American Concrete Institute, Farmington Hills, Mich., USA.

Baker, W.E. et al. 1983. Explosion hazards and evaluation. Elsevier Scientific Publishing Company, Oxford, UK.

Beshara, F. B. A. 1994. Modeling of blast loading on aboveground structures - I. General phenomenology and external blast. *Computers and Structures*, 51(5): 597-606.

Biggs, J.M. 1964. Introduction to structural dynamics. McGraw-Hill Book Company, New York. .

Bischoff, P. H, and Perry, S. H. 1991. Compressive behavior of concrete at high strain rates. *Materials and Structures*. 24, 425–450.

Boutros, M. K. 2000. Elastic-plastic model of pinned beams subjected to impulsive loading. *J. Eng. Mech.*, 126(9):920-927.

Clough, R., and Penzien, J. 1993. Dynamics of structures. McGraw-Hill, Inc., New York.

Collins, M. P., and Mitchell, D. 1987. Prestressed concrete basics. Canadian Prestressed Concrete Institute, Ottawa.

Cowper, G. R. and Symonds, P. S. 1957. Strain hardening and strain-rate effects in the impact loading of cantilever beams. Brown University Division of Applied Mathematics, Report No. 28.

CEB, Comité Euro-International du Béton, 1988. Concrete structures under impact and impulsive loading. CEB Bulletin 187, Lausanne, Switzerland.

CSA A23.3-04. 2005. Design of concrete structures. Canadian Standards Association, Mississauga, Ontario, Canada.

Ebeling, R. M., Green, R. A., and French, S. E. 1997. Accuracy of response of single-degree-of-freedom systems to ground motion. Technical Report ITL-97-7, U.S. Army Engineer Waterways Experiment Station, Vicksburg, MS.

Eurocode 2, European Committee for Standardization (CEN), 1992. Design of concrete structures, part 1-6: General rules and rules for buildings. Brussels.

Krauthammer, T., Bazeos, N., Holmquist, T.J. 1986. Modified SDOF analysis of RC box-type structures. J. Struct. Eng. ,112(4) :726–744.

Krauthammer, T., Shahriar, S. and Shanaa, H. M. 1990. Response of reinforced concrete elements to severe impulsive loads. *J. Struct. Eng.*, 116(4): 1061-1079.

Krauthammer, T., Shanaa, H.M. and Assadi-Lamouki, A. 1994. Response of reinforced concrete structural elements to severe impulsive loads. *Computers and Structures*, 53(1): 119-130.

Kulkarni, S.M., and Shah, S.P. 1998. Response of reinforced concrete beams at high strain rates. *ACI J.*, 95(6): 705-715.

Livermore Software Technology Corporation, 2006. LS-DYNA keyword user's manual version 971.

Louca, L. A. and Harding, J. E. 1997. Non-linear analysis of imperfect plates under transient lateral pressure loading. *Computers and Structures*, 63(1): 27–37.

Low, H. Y., and Hao, H. 2002. Reliability analysis of direct shear and flexural failure modes of RC panels under explosive loading. *Engineering Structures*, 24: 189–198.

Malvar, L. J. 1998. Review of static and dynamic properties of steel reinforcing bars. *ACI J.*, 95(5): 609-616.

Malvar, L. J., and Ross C. A. 1998. Review of strain rate effects for concrete in tension. *ACI J.*, 95(6): 735-739

Malvar, L. J., Crawford, J. E., Weswwich, J. W. and Simons, D. 1997. A plasticity concrete material model for dyna3D. *Int. J. Impact Eng.*, 19:847–873.

Mays, G. C., and Smith, P. D. 1995. Blast effects on buildings: design of buildings to optimize resistance to blast loading. Thomas Telford, New York, NY.

Morison, C. M. 2006. Dynamic response of walls and panels by single-degree-of-freedom analysis – a critical review and revision. *International Journal of Impact Engineering*, 32, 1214-1247.

NZS 3101:1995, (1995). NZS 3101:1995. Part1: The design of concrete structures. Concrete Structures Standard, Wellington, Standards New Zealand.

Pan, Y., and Watson, A. 1998. Effect of panel stiffness on resistance of cladding panels to blast loading. *J. Eng. Mech.*, 124(4): 414–421.

Park, R., and Gamble, W. L. 2000. Reinforced concrete panels. John Wiley & Sons Inc., USA.

Schleyer, G. K., and Hsu, S. S. 2000. A modelling scheme for predicting the response of elastic plastic structures to pulse pressure loading. *Int. J. Impact Eng.*, 24, 759-777.

Smith, P. D., and Hetherington, J. G. 1994. Blast and ballistic loading of structures. Butterworth-Heinemann Ltd., London.

Soroushian, P. , and Choi, K. 1987. Steel mechanical properties at different strain rates. *J. Struct. Eng.*, 113(4): 863-872.

Subbaraj, K. and Dokainish, M.A. 1989. A survey of direct time-integration methods in computational structural dynamics-II. Implicit methods. *Computers and Structures*, 32(6): 1387-1401.

Tavarez, F. A., Bank, L. C., and Plesha, M. E. 2003. Analysis of fiber-reinforced polymer composite grid reinforced concrete beams. *ACI J.*, 100(2): 250-258.

TM5-1300, US Department of Army Technical Manual, 1990. Design of structures to resist the effects of accidental explosions. Washington, DC.

Table 3.1: Load mass factors for the four edges supported element in TM5-1300

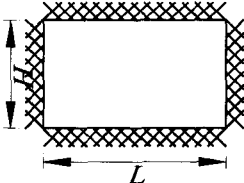
Support Conditions		Value of L/H	K_{LM} For Elastic and Elasto-Plastic Ranges(Support Conditions)				
			All Supports Fixed	One Support Simple, Other Supports Fixed	Two Supports Simple, Other Supports Fixed	Three Supports Simple, Other Supports Fixed	All Supports Simple
Four edges supported		$L/H=1$	0.61	0.61	0.62	0.63	0.63
		$1 \leq L/H \leq 2$	$0.61+0.16(\frac{L}{H}-1)$	$0.61+0.16(\frac{L}{H}-1)$	$0.62+0.16(\frac{L}{H}-1)$	$0.63+0.16(\frac{L}{H}-1)$	$0.63+0.16(\frac{L}{H}-1)$
		$L/H \geq 2$	0.77	0.77	0.78	0.79	0.79

Table. 3.2: The analytical specifications of panels

(a) Simply supported panels ⁽¹⁾

ID	$H(m)$	$L(m)$	Aspect Ratio	A_{s_x} (mm^2/m)	A_{s_y} (mm^2/m)	ρ_x (%)	ρ_y (%)
S-1	4.0	4.0	1.0	1,200	1,200	0.75	0.75
S-2	3.2	4.0	0.8	960	1,200	0.60	0.75
S-3	2.4	4.0	0.6	720	1,200	0.45	0.75

⁽¹⁾ Thickness=200 mm(b) Clamped panels ⁽¹⁾

ID	$H(m)$	$L(m)$	Aspect Ratio	A_{s_x} (mm^2/m)	A_{s_y} (mm^2/m)	ρ_x (%)	ρ_y (%)
C-1	4.0	4.0	1.0	960	960	0.60	0.60
C-2	3.2	4.0	0.8	768	960	0.48	0.60
C-3	2.4	4.0	0.6	576	960	0.36	0.60

⁽¹⁾ Thickness=200 mm

Tabel 3.3: Dynamic reaction of the simply supported panels
(a) S-1

Loading Realm	P_0 (kPa)	T_L (ms)	V_{FE} (kN)	$\frac{V_{TM\ 5-1300}}{V_{FE}}$	$\frac{V_{Biggs}}{V_{FE}}$	$\frac{V_{Modified\ TM\ 5-1300}}{V_{FE}}$
I	1,000	1.18	4,790	0.38	0.94	1.09
I	1,000	2.09	6,583	0.3	0.68	0.79
I	1,000	3.24	7,895	0.25	0.57	0.66
D	84	21.64	1,754	1.04	0.83	0.79
D	126	27.81	2,579	0.74	0.69	0.67
D	158	34.80	3,297	0.58	0.59	0.59
Q	57	877.20	1,480	1.21	1.05	1.02
Q	89	561.80	2,276	0.83	0.78	0.76
Q	108	463.00	2,709	0.71	0.69	0.68
Average				0.67	0.76	0.78
C.O.V				0.49	0.21	0.22

(b) S-2

Loading Realm	P_0 (kPa)	T_L (ms)	V_{FE} (kN)	$\frac{V_{TM\ 5-1300}}{V_{FE}}$	$\frac{V_{Biggs}}{V_{FE}}$	$\frac{V_{Modified\ TM\ 5-1300}}{V_{FE}}$
I	1,000	1.53	4,683	0.4	0.77	1.01
I	1,000	2.57	6,498	0.29	0.55	0.73
I	1,000	3.92	7,414	0.26	0.48	0.64
D	132	17.18	1,997	0.93	0.79	0.77
D	180	21.93	2,745	0.68	0.66	0.65
D	210	29.72	3,366	0.56	0.58	0.59
Q	90	555.60	1,882	0.98	0.87	0.85
Q	120	416.70	2,438	0.76	0.72	0.71
Q	138	362.30	2,729	0.68	0.67	0.67
Average				0.62	0.68	0.74
C.O.V				0.26	0.13	0.13

Table 3.3(continued)

(c) S-3

Loading Realm	P_0 (kF'a)	T_L (ms)	V_{FE} (kN)	$\frac{V_{TM\ 5-1300}}{V_{FE}}$	$\frac{V_{Biggs}}{V_{FE}}$	$\frac{V_{Modified\ TM\ 5-1300}}{V_{FE}}$
I	2,000	1.08	7,529	0.27	0.66	1.09
I	2,000	1.69	9,122	0.22	0.55	0.9
I	2,000	2.50	11,311	0.18	0.44	0.73
D	240	13.38	2,703	0.73	0.68	0.66
D	290	17.76	3,407	0.58	0.59	0.6
D	300	28.79	3,917	0.51	0.54	0.56
Q	156	320.50	2,461	0.79	0.74	0.72
Q	186	268.80	2,871	0.68	0.66	0.65
Q	206	242.70	3,123	0.63	0.63	0.63
Average				0.51	0.61	0.73
C.O.V				0.23	0.09	0.17

Table. 3.4: Dynamic reaction of the clamped panels

(0) C-1

Loading Realm	P_0 (kPa)	T_L (ms)	V_{FE} (kN)	$\frac{V_{TM\ 5-1300}}{V_{FE}}$	$\frac{V_{Biggs}}{V_{FE}}$	$\frac{V_{Modified\ TM\ 5-1300}}{V_{FE}}$
I	2,000	0.80	8,960	0.26	1.43	1.91
I	2,000	1.25	11,422	0.21	1.12	1.5
I	2,000	1.87	13,964	0.17	0.92	1.22
D	180	12.12	5,557	0.41	0.36	0.35
D	210	17.74	6,947	0.33	0.33	0.33
D	240	23.29	7,996	0.29	0.31	0.32
Q	105	666.70	5,025	0.45	0.42	0.41
Q	126	555.60	5,892	0.39	0.37	0.37
Q	138	507.20	6,353	0.36	0.36	0.35
Average				0.32	0.62	0.75
C.O.V				0.09	0.42	0.62

(b) C-2

Loading Realm	P_0 (kPa)	T_L (ms)	V_{FE} (kN)	$\frac{V_{TM\ 5-1300}}{V_{FE}}$	$\frac{V_{Biggs}}{V_{FE}}$	$\frac{V_{Modified\ TM\ 5-1300}}{V_{FE}}$
I	2,000	0.98	9,194	0.25	1.06	1.57
I	2,000	1.51	11,795	0.2	0.82	1.22
I	2,000	2.25	13,708	0.17	0.71	1.05
D	240	11.68	6,281	0.36	0.34	0.33
D	260	18.38	7,745	0.3	0.3	0.3
D	280	26.28	9,090	0.25	0.27	0.28
Q	144	486.10	5,674	0.4	0.38	0.37
Q	164	426.80	6,447	0.35	0.34	0.34
Q	175	400.00	6,888	0.33	0.33	0.33
Average				0.29	0.51	0.64
C.O.V				0.08	0.28	0.5

Table 3.4(continued)

(c) C-3

Loading Realm	P_0 (kPa)	T_L (ms)	V_{FE} (kN)	$\frac{V_{TM\ 5-1300}}{V_{FE}}$	$\frac{V_{Biggs}}{V_{FE}}$	$\frac{V_{Modified\ TM\ 5-1300}}{V_{FE}}$
I	3,500	0.77	11,540	0.23	1.05	1.76
I	3,500	1.15	13,896	0.19	0.87	1.46
I	3,500	1.67	16,537	0.16	0.73	1.23
D	370	11.63	6,551	0.39	0.39	0.39
D	420	15.16	8,015	0.32	0.34	0.35
D	480	18.20	9,372	0.28	0.31	0.34
Q	237	295.40	5,925	0.43	0.42	0.41
Q	260	269.20	6,477	0.4	0.39	0.39
Q	277	252.70	6,685	0.38	0.39	0.39
Average				0.31	0.54	0.75
C.O.V				0.1	0.27	0.57

Figure Captions

Fig. 3.1: Actual and idealized side-on blast pressure time histories: (a) Actual blast load time history, (b) Triangular load approximation, (c) Using tangent line in approximating blast load

Fig. 3.2: SDOF model: (a) Actual structural element, (b) Equivalent SDOF model, (c) Typical resistance-displacement curve for a two-way RC element

Fig. 3.3: Free body diagram of a two-way element subjected to blast load

Fig. 3.4: The segment of a two-way panel bounded by yield lines

Fig. 3.5: Resistance function of the SDOF model

Fig. 3.6: Four edges support element with different support conditions

Fig. 3.7: The coefficients for finding moment and deflection at the certain points of element

Fig. 3.8: Determining the deflection at the end of flexural action

Fig. 3.9: Determining the tensile membrane resistance

Fig. 3.10: Deflected shape of a two-way element from a view in x-direction cross section

Fig. 3.11: The specifications of FE model geometry: (a) Simply supported panel, (b) Clamped panel

Fig. 3.12: Typical mesh configuration for simply supported panels and clamped panels: (a) Panel S-1, (b) Panel C-1

Fig. 3.13: Dividing the area of a two-way element into different regions

Fig. 3.14: The general form of pressure-impulse diagram

Fig. 3.15: $P-I$ diagrams for the simply supported panels using SDOF(EI_{ave})

Fig. 3.16: $P-I$ diagrams for the simply supported panels using SDOF(EI_{cr})

Fig. 3.17: $P-I$ diagrams for the simply supported panels using SDOF($EI_{weighted}$)

Fig. 3.18: Deflection of panel S-1 ($P_0=1000$ kPa, $T_L=2.09$ ms): (a) Deflection contours at $t = 0.83$ ms, (b) Deflection contours at $t = 1.68$ ms, (c) Deflection contour at $t = 5.67$ ms, (d) Displacement-time history for the central point of the panel

Fig. 3.19: $P-I$ diagrams for the clamped panels using SDOF(EI_{ave})

Fig. 3.20: $P-I$ diagrams for the clamped panels using SDOF(EI_{cr})

Fig. 3.21: Modified resistance function for the SDOF model

Fig. 3.22: Deflection of panel C-1 ($P_0=2000$ kPa, $T_L=1.25$ ms): (a) Deflection contours at $t = 1.08$ ms, (b) Deflection contours at $t = 1.91$ ms, (c) Deflection contour at $t = 5.52$ ms, (d) Displacement-time history for the central point of the panel

Fig. 3.23: Deflection of reinforcement in panel C-1 ($P_0=2000$ kPa, $T_L=5.92$ ms): (a) Deflection contours at $t = 14.00$ ms, (b) Displacement-time history for a reinforcement node near the central point of the panel

Fig. 3.24: Implementing the effect of applied load in reaction for TM5-1300

Fig. 3.25: Shape function of x-direction and y-direction section of a two-way panel

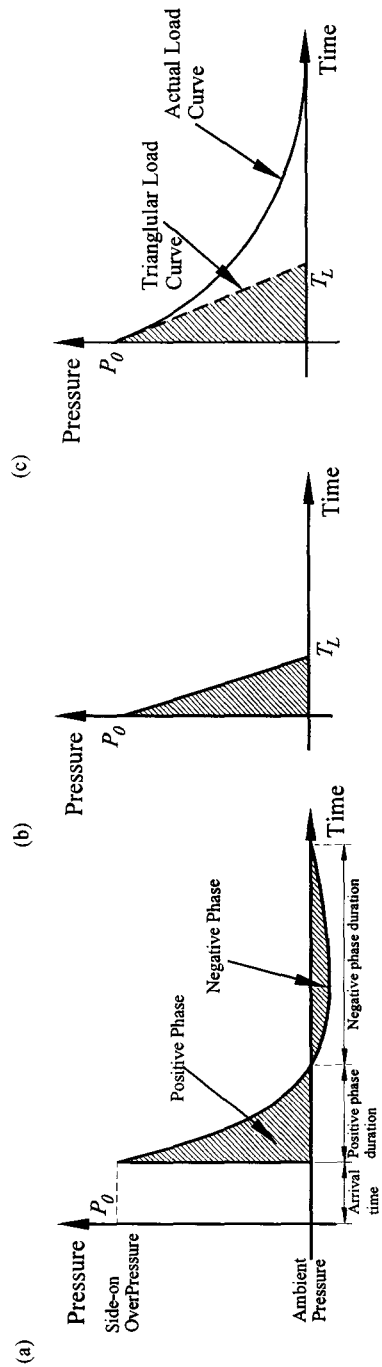


Fig. 3.1: Actual and idealized side-on blast pressure time histories: (a) Actual blast load time history, (b) Triangular load approximation, (c) Using tangent line in approximating blast load

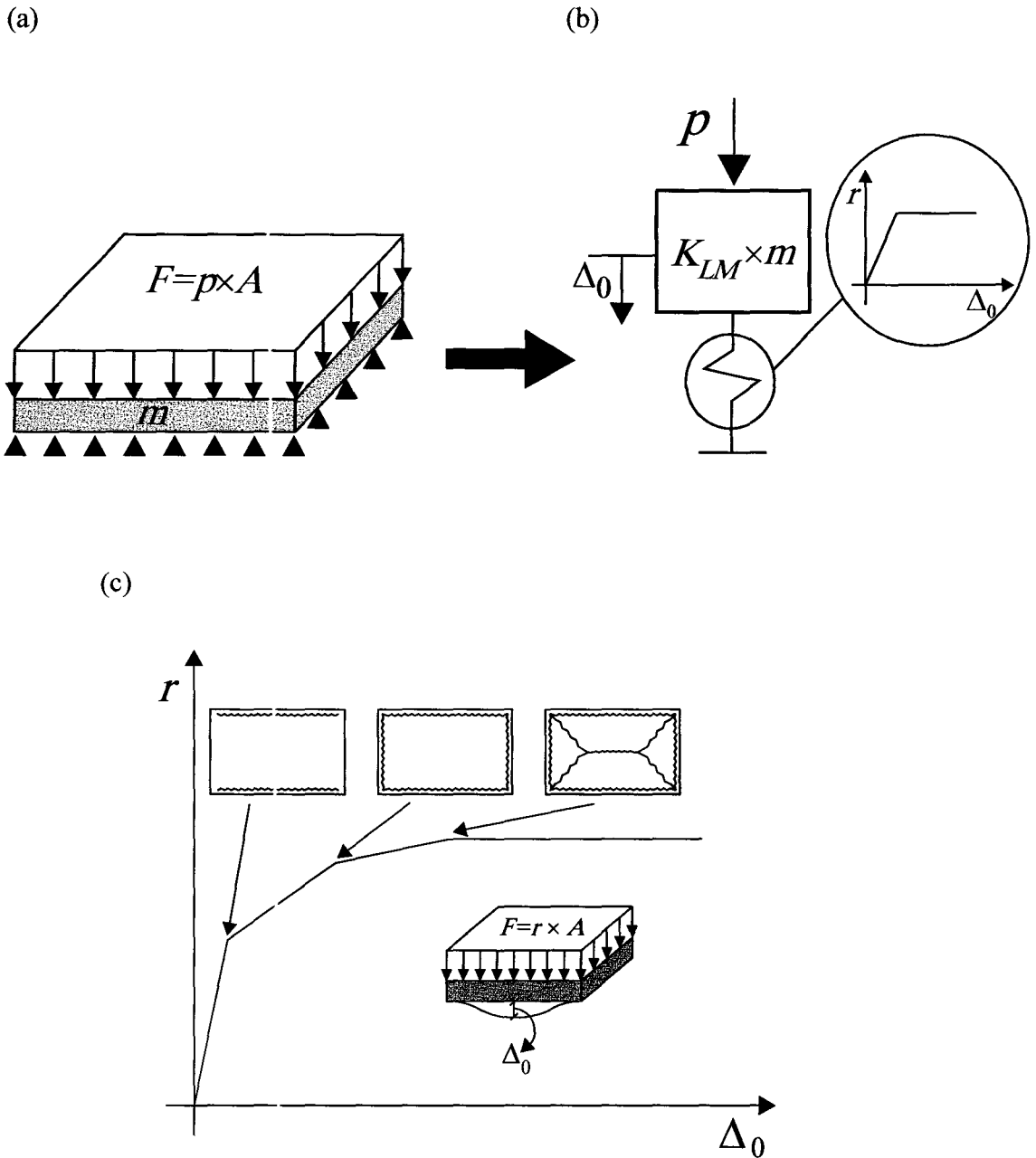


Fig. 3.2: SDOF model: (a) Actual structural element, (b) Equivalent SDOF model, (c) Typical resistance-displacement curve for a two-way RC element

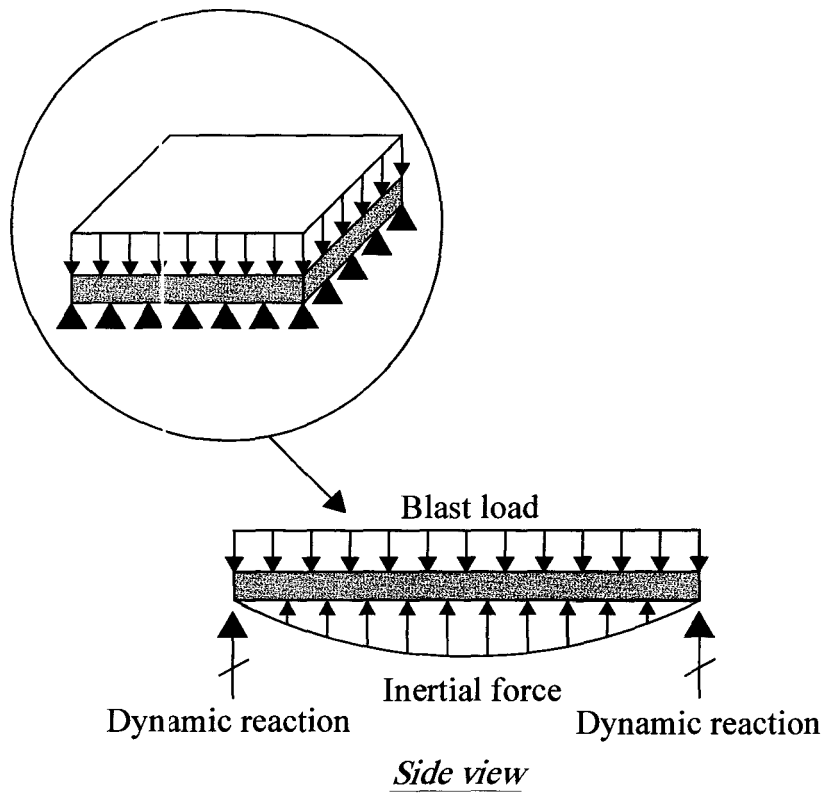


Fig. 3.3: Free body diagram of a two-way element subjected to blast load

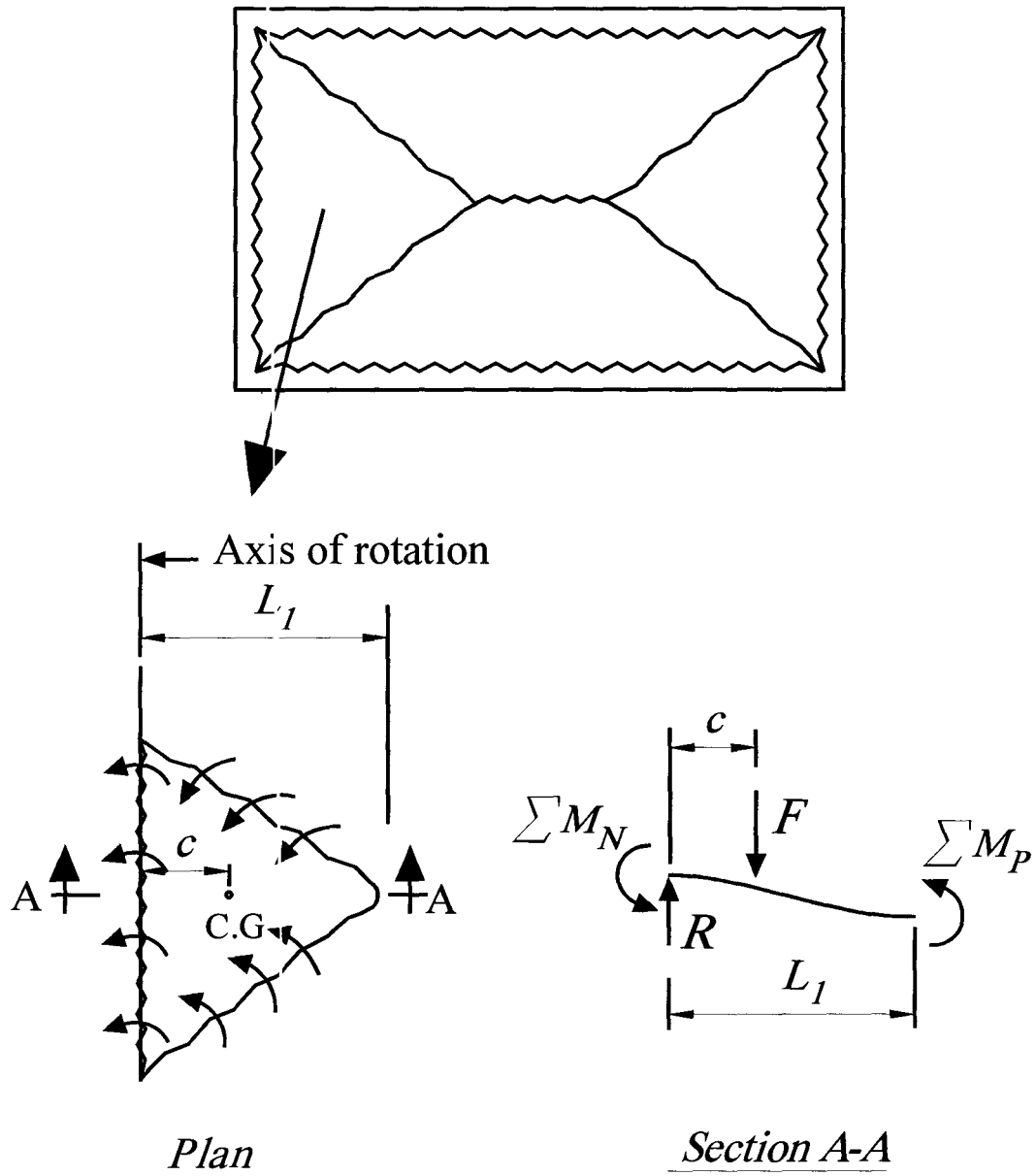


Fig. 3.4: The segment of a two-way panel bounded by yield lines

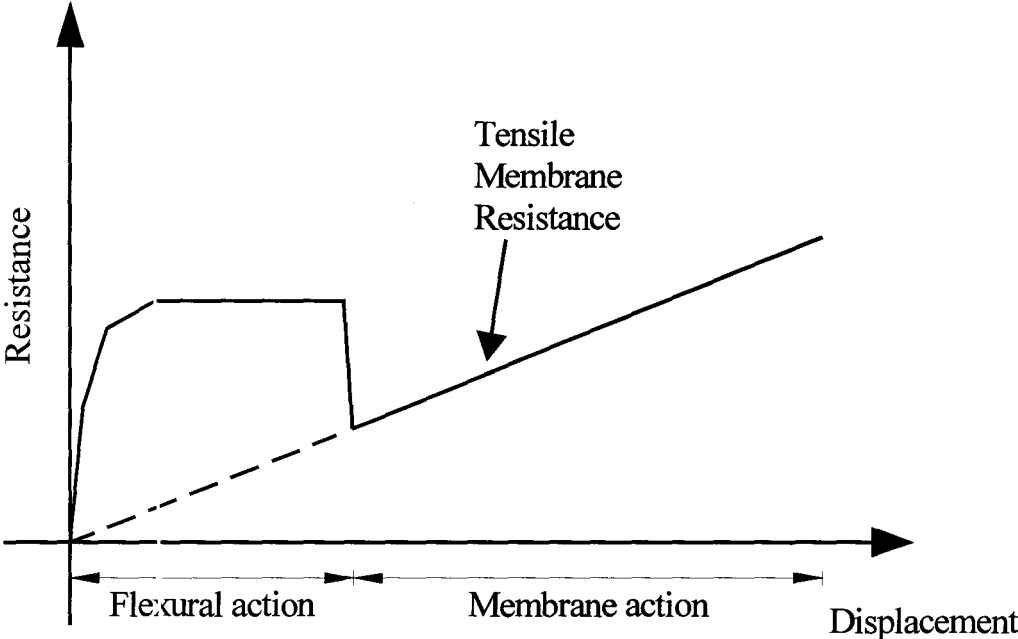


Fig. 3.5: Resistance function of the SDOF model

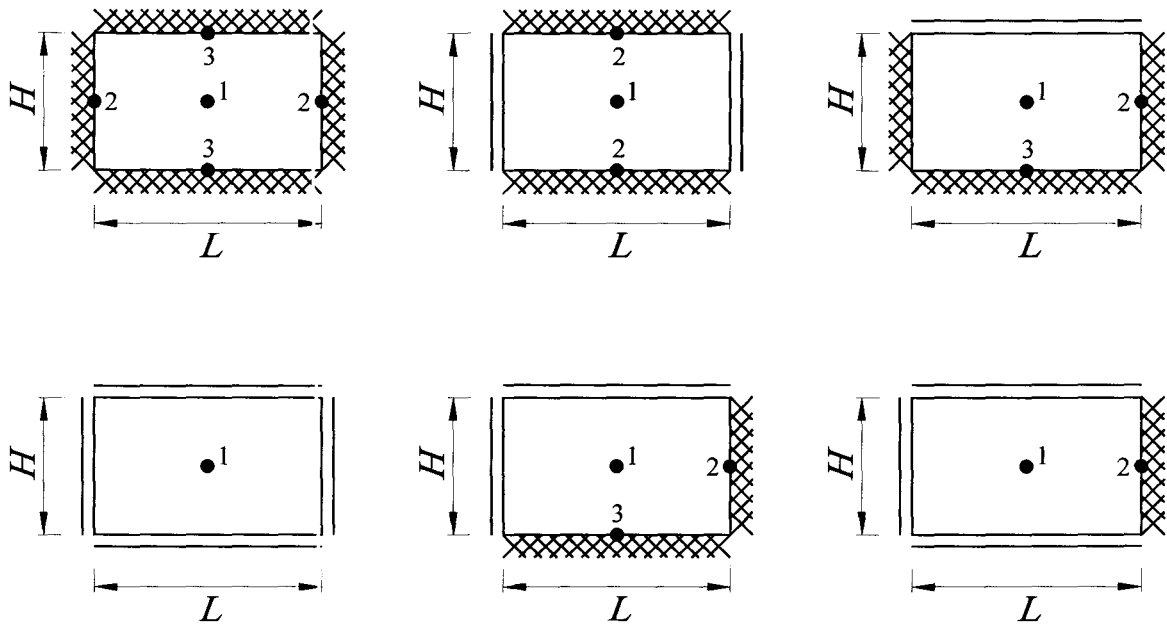


Fig. 3.6: Four edges support element with different support conditions

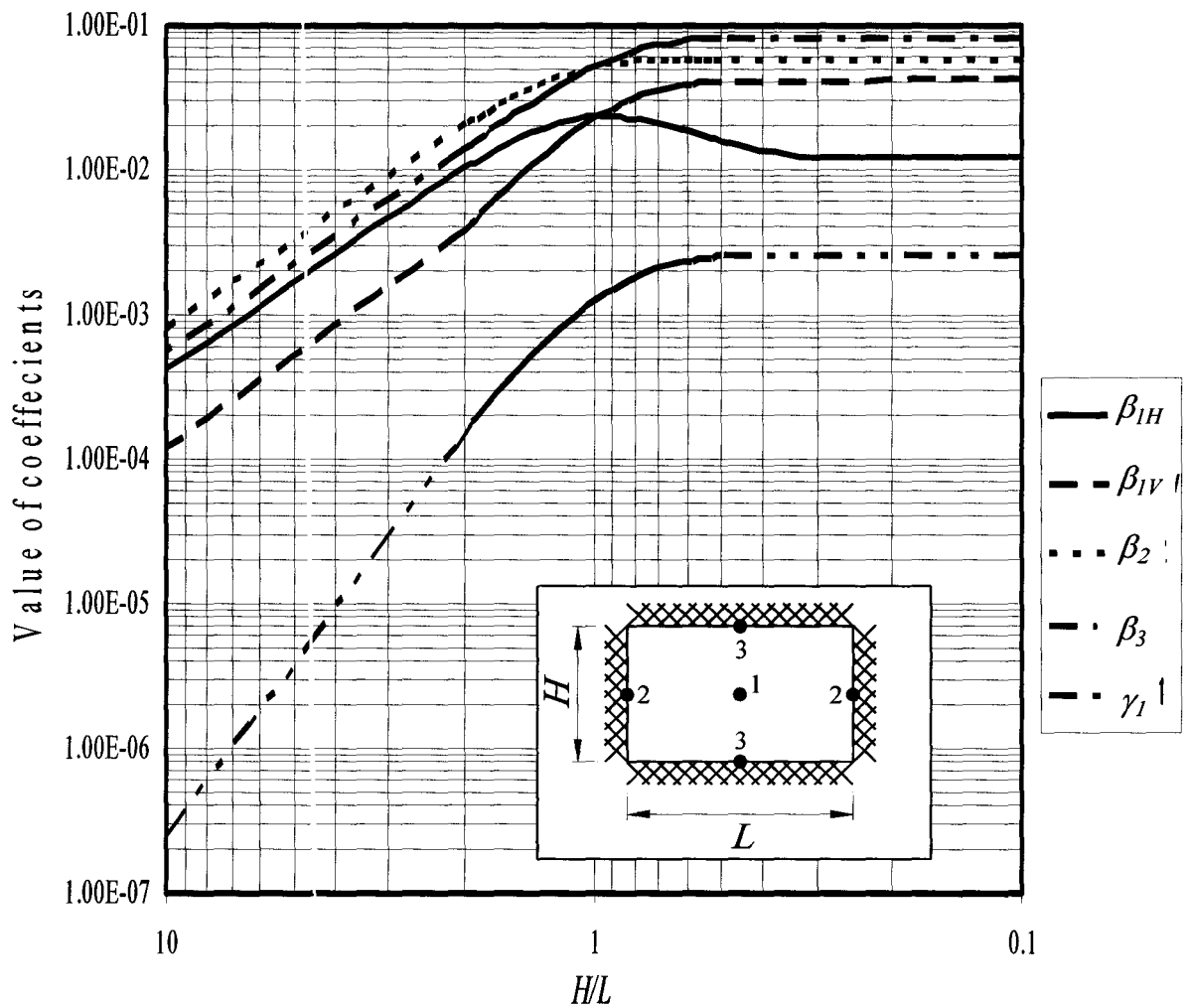


Fig. 3.7: The coefficients for finding moment and deflection at the certain points of a panel

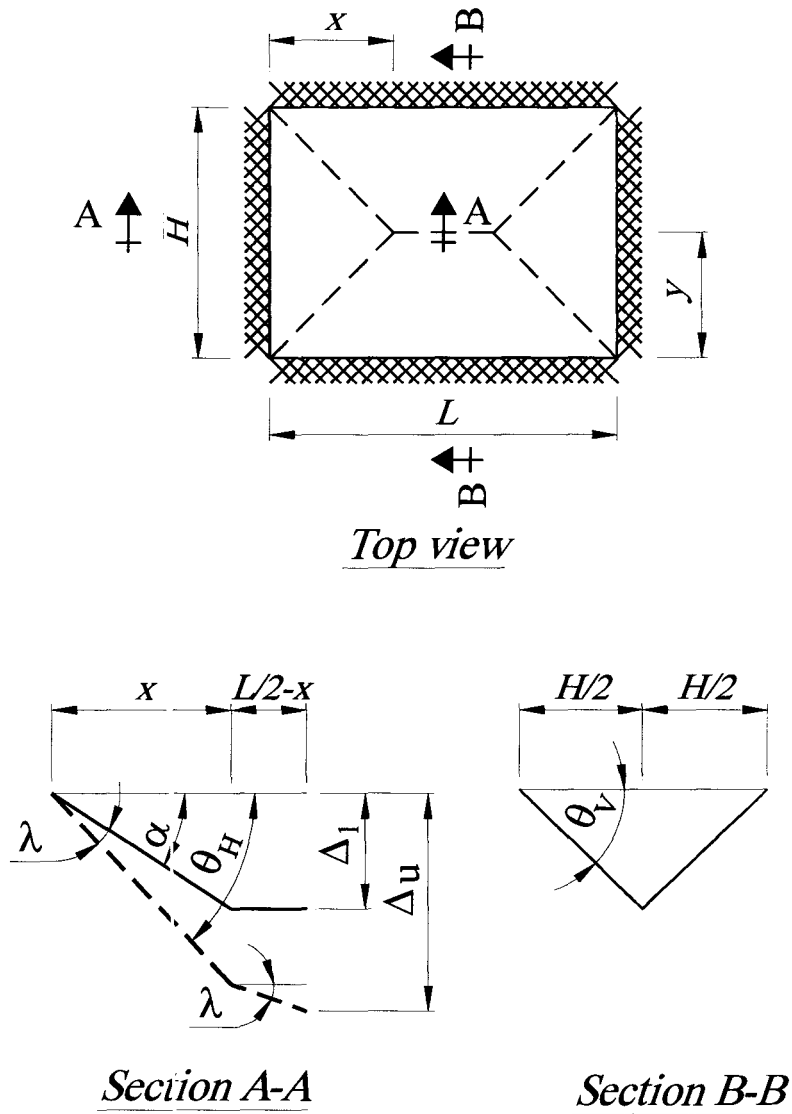
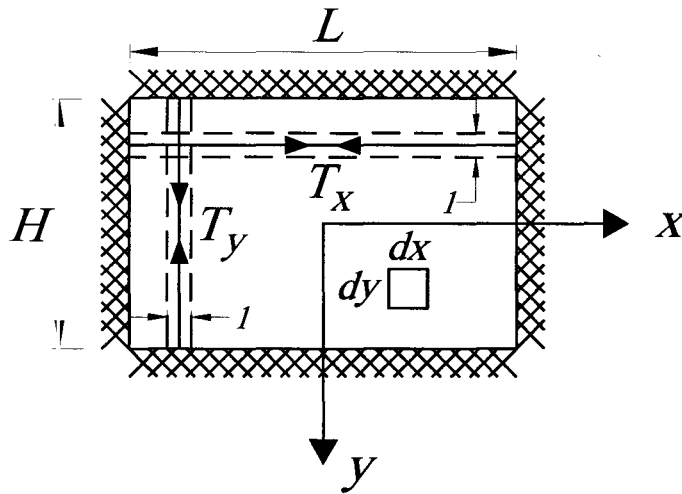
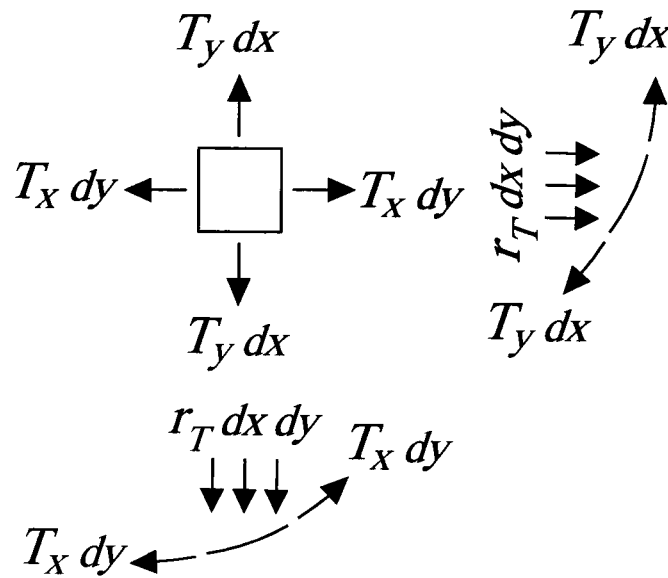


Fig. 3.8: Determining the deflection at the end of flexural action



(a) Tensile membrane



(b) Forces acting on an element

Fig 3.9: Determining the tensile membrane resistance

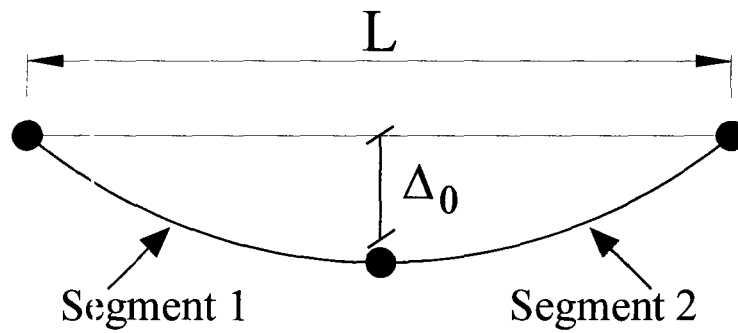
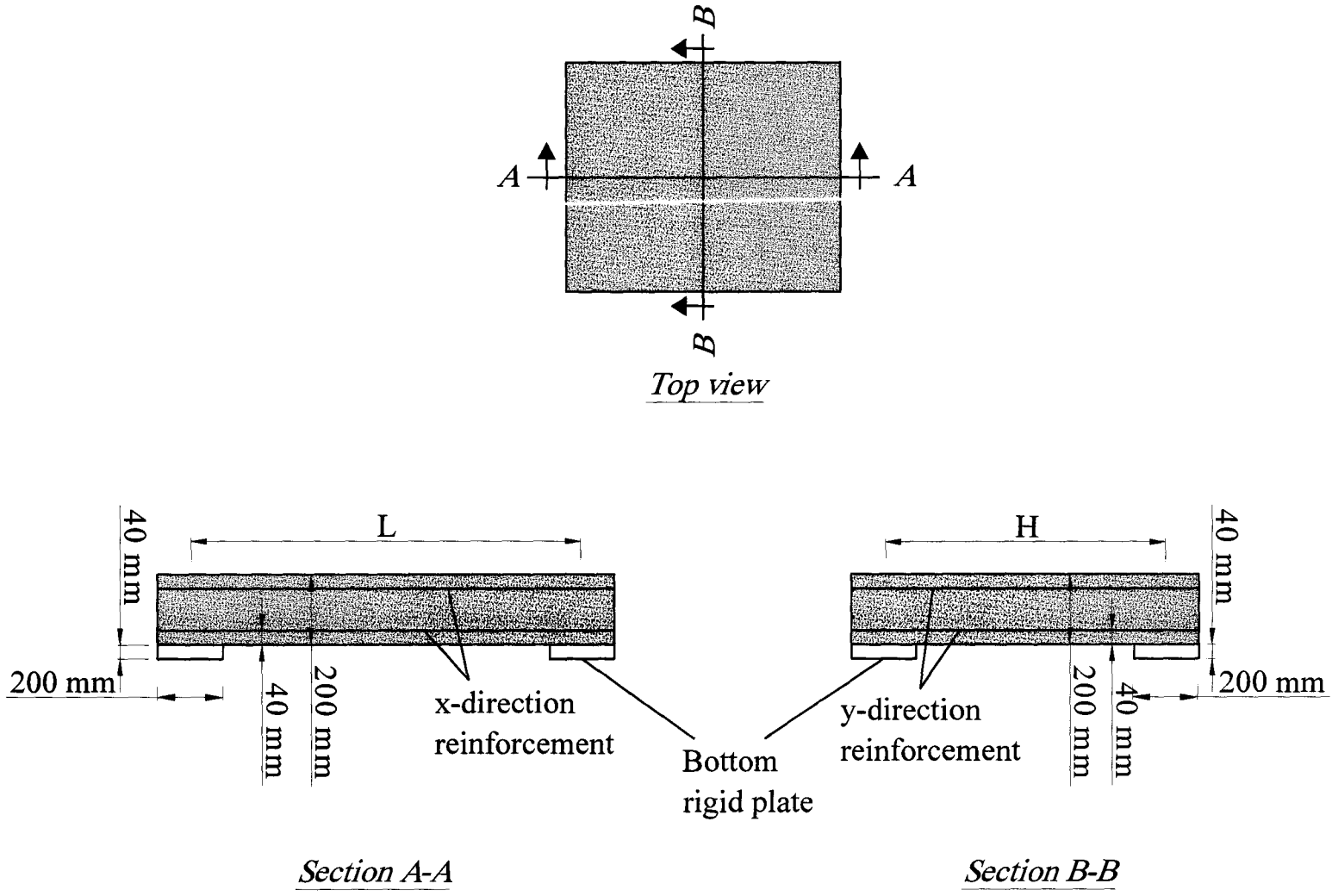


Fig. 3.10: Deflected shape of a two-way element from a view in x -direction cross section

(a)



(b)

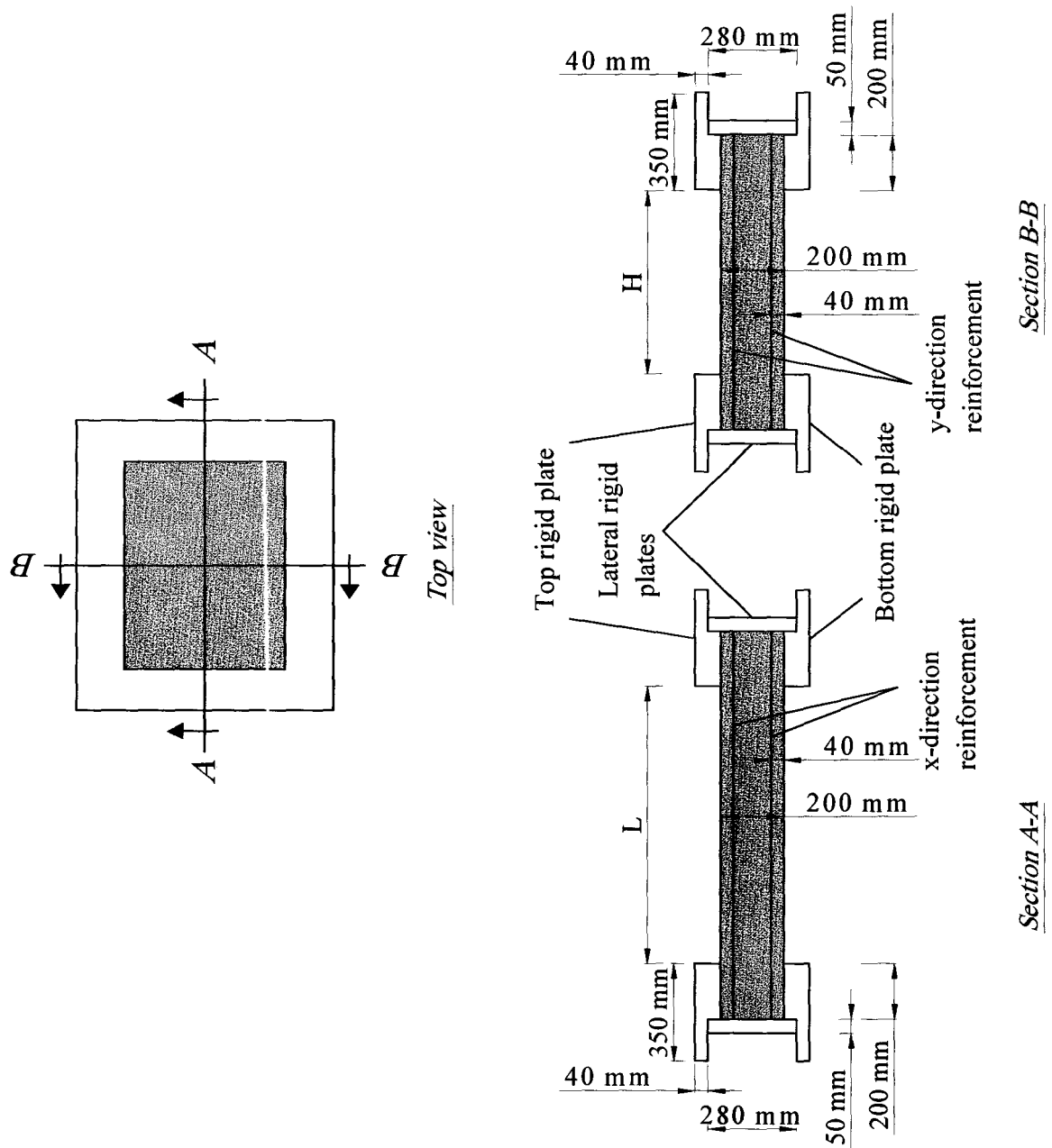
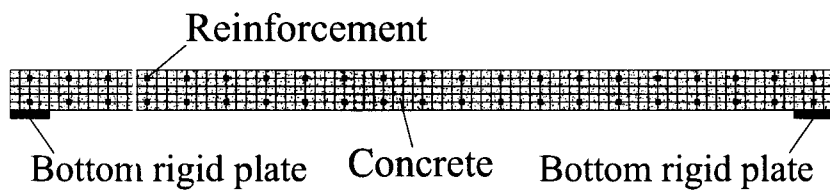
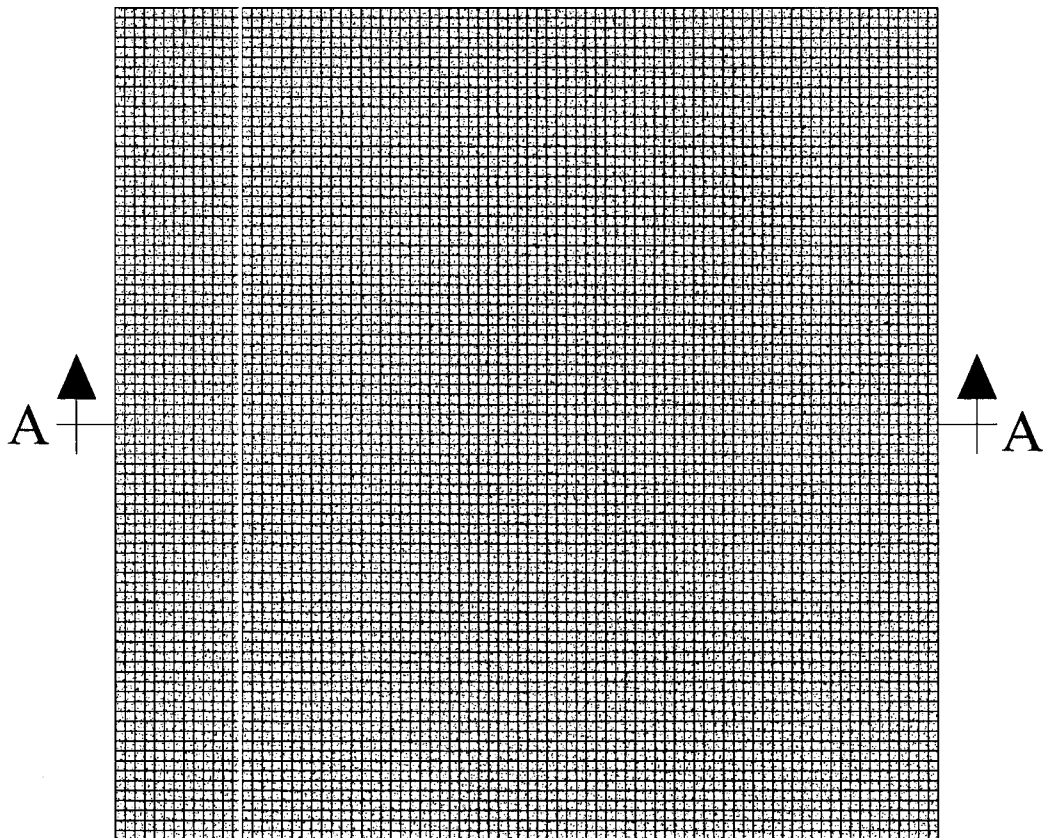


Fig. 3.11: FE models geometry: (a) Simply supported panel, (b) Clamped panel

(a)



Section A-A

(b)

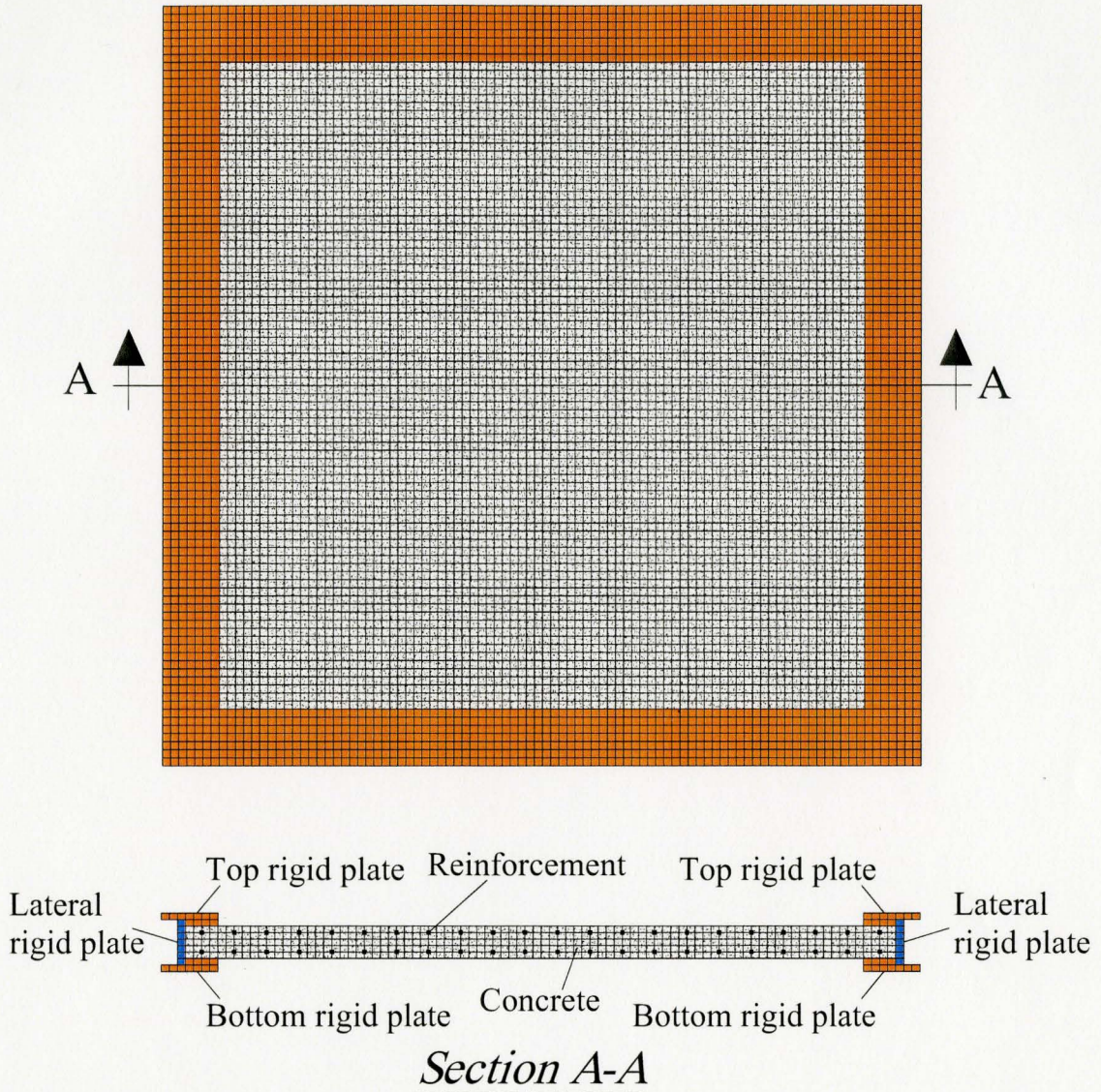


Fig. 3.12: Typical mesh configuration for simply supported panels and clamped panels:

(a) Panel S-1, (b) Panel C-1

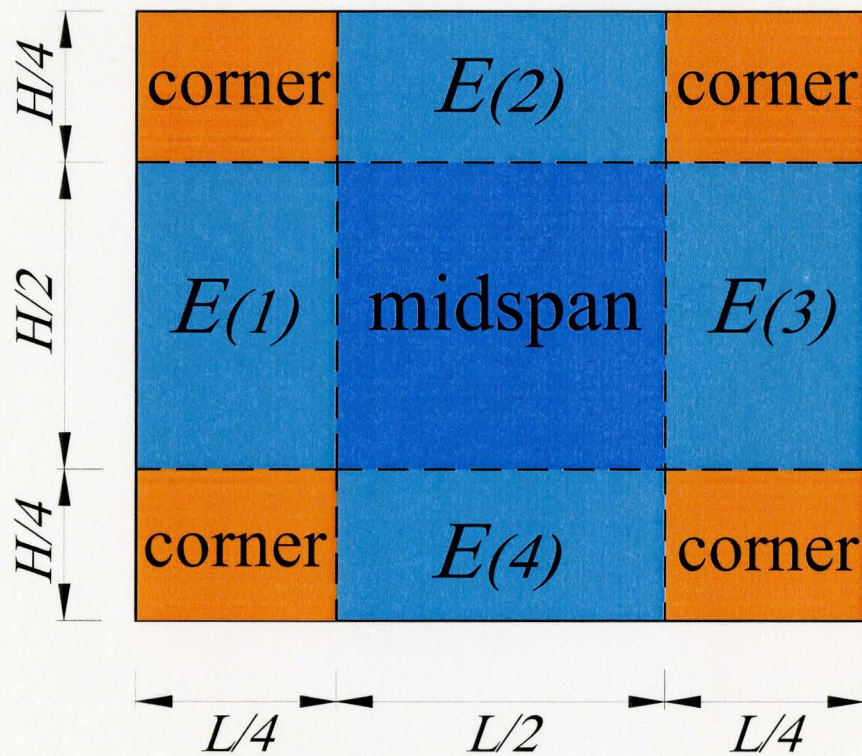


Fig. 3.13: Dividing the area of a two-way element in to different regions

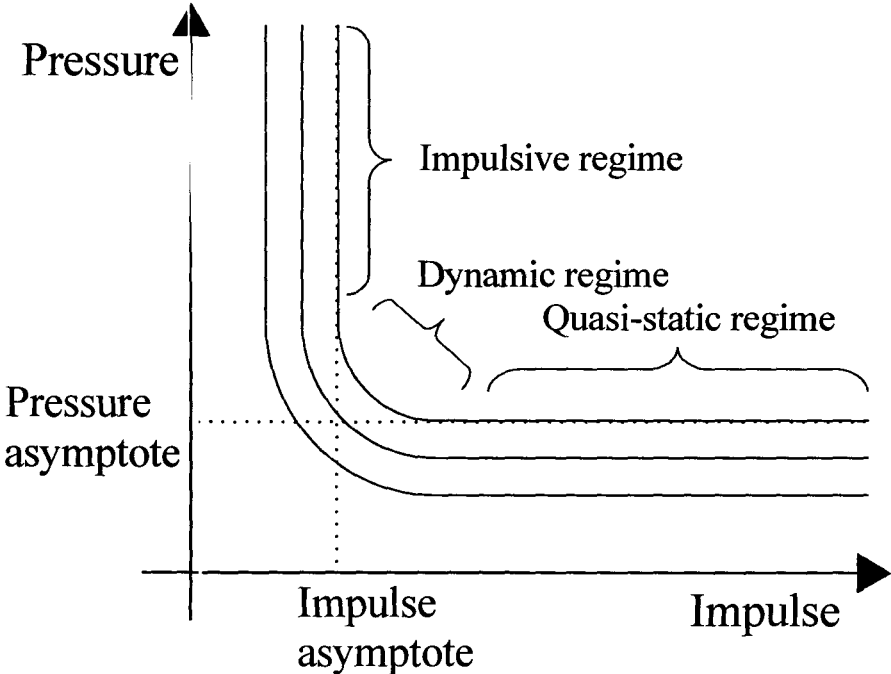
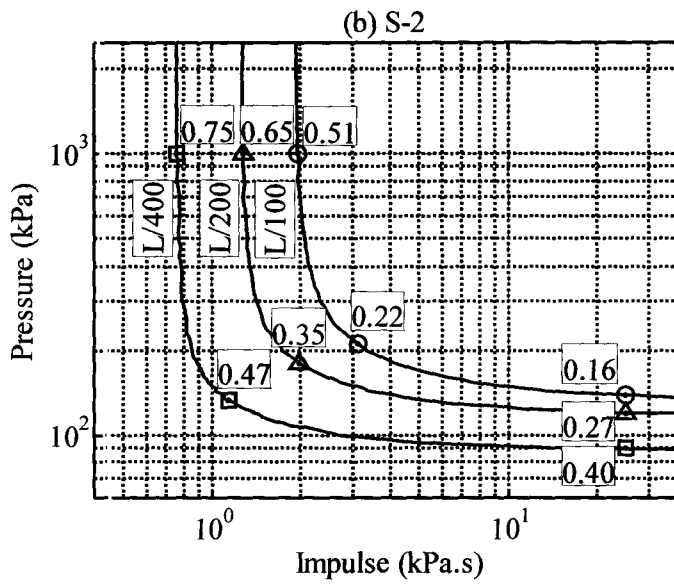
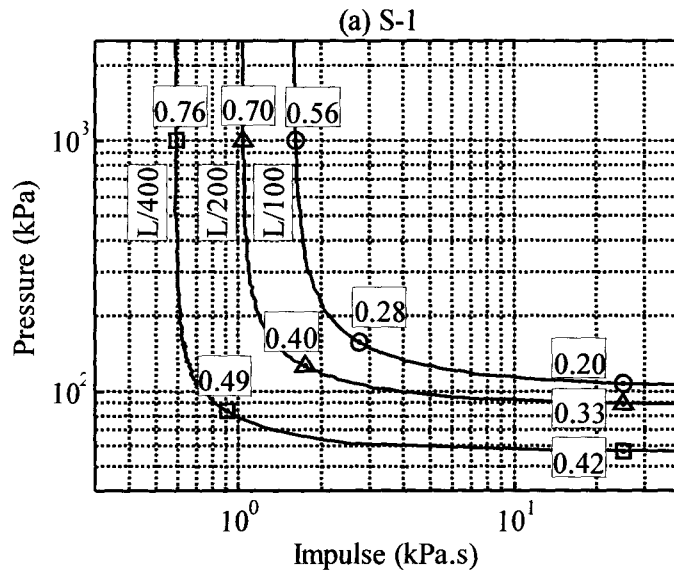


Fig. 3.14: The general form of pressure-impulse diagram



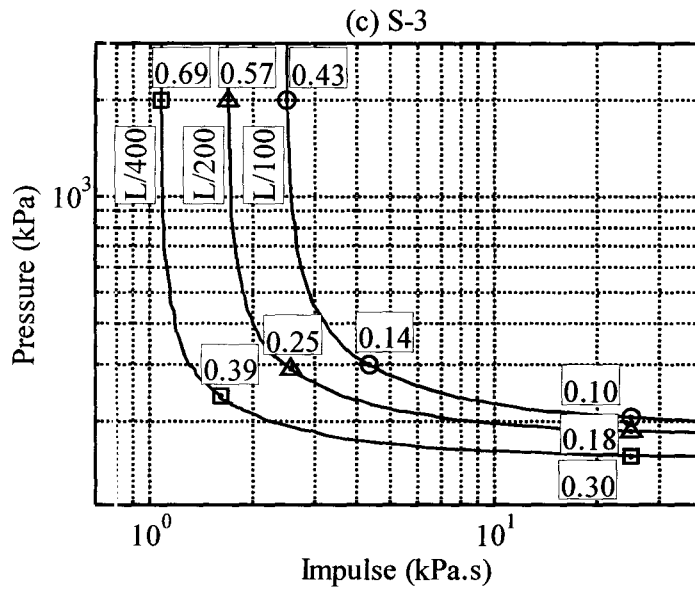
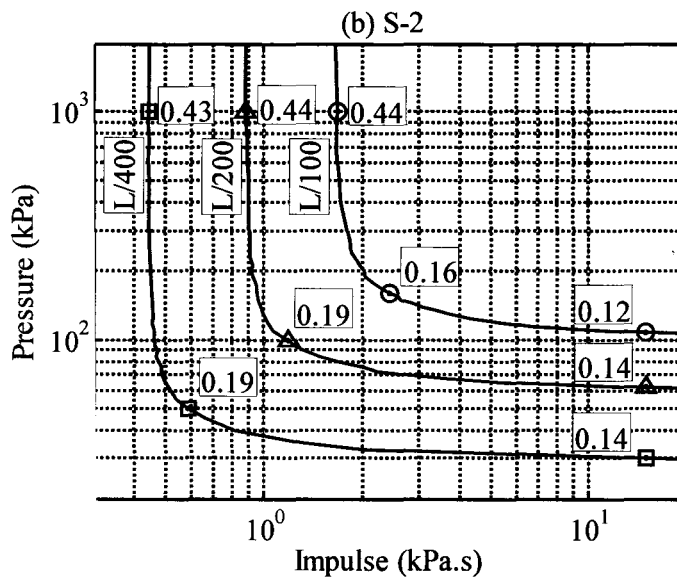
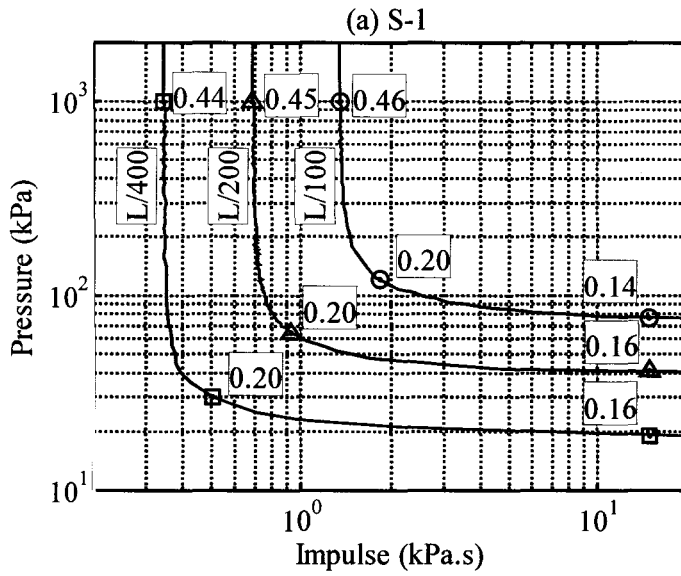


Fig. 3.15: *P-I* diagrams for the simply supported panels using SDOF(EI_{ave})



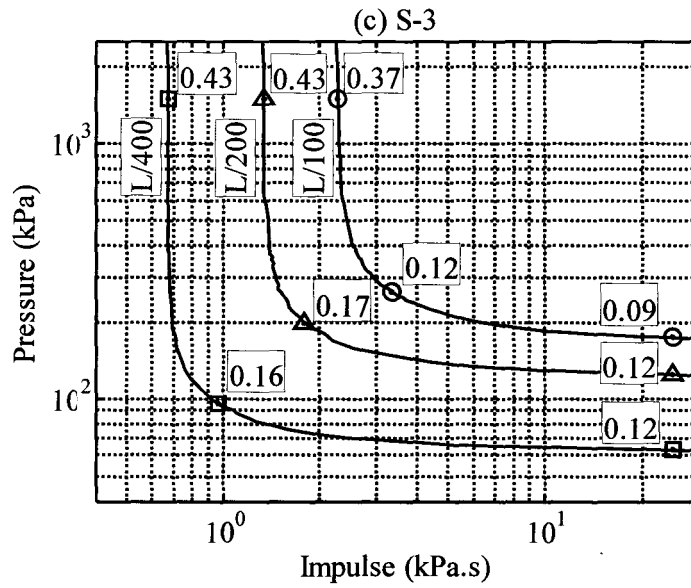
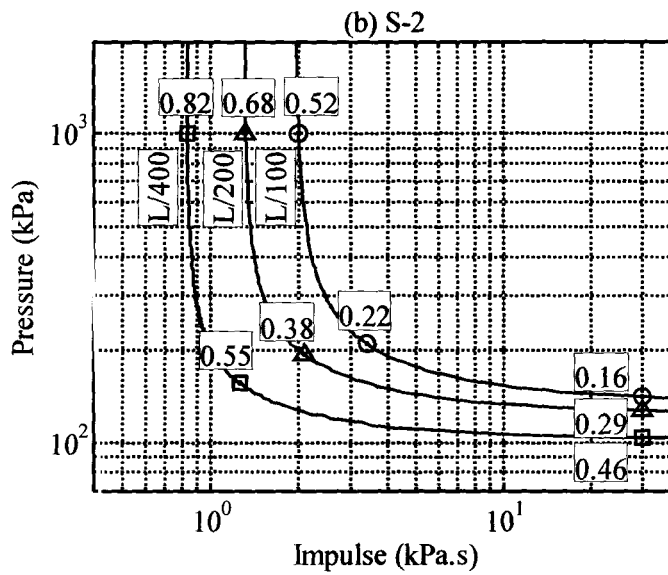
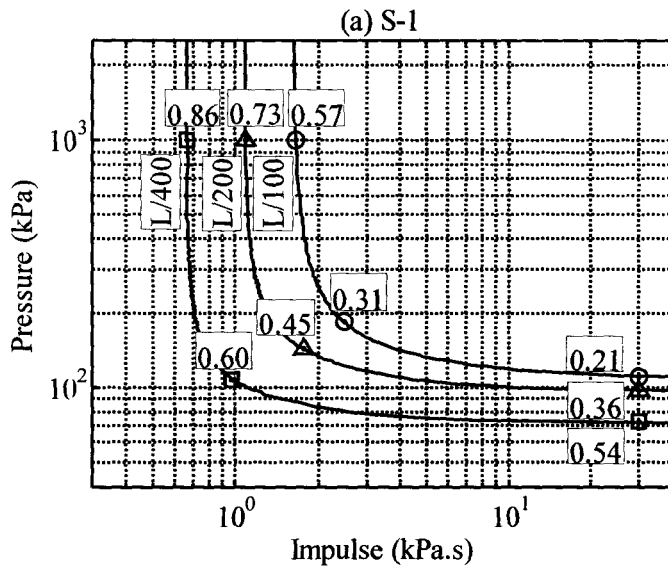


Fig. 3.16: $P-I$ diagrams for the simply supported panels using $SDOF(EI_{cr})$



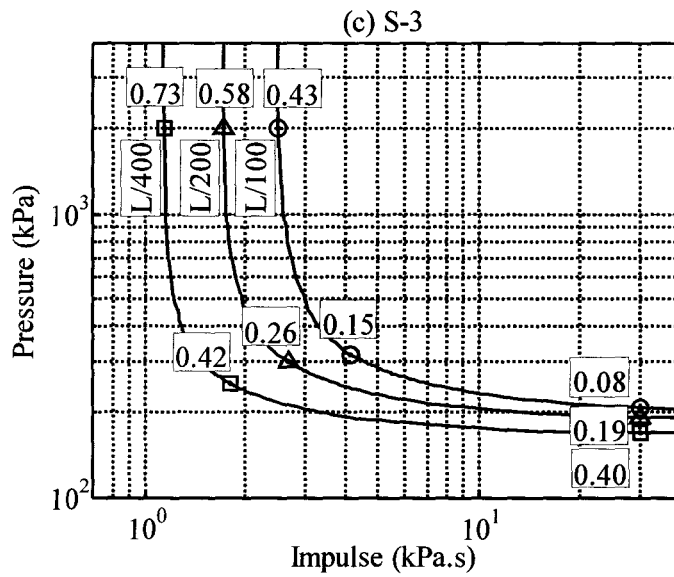
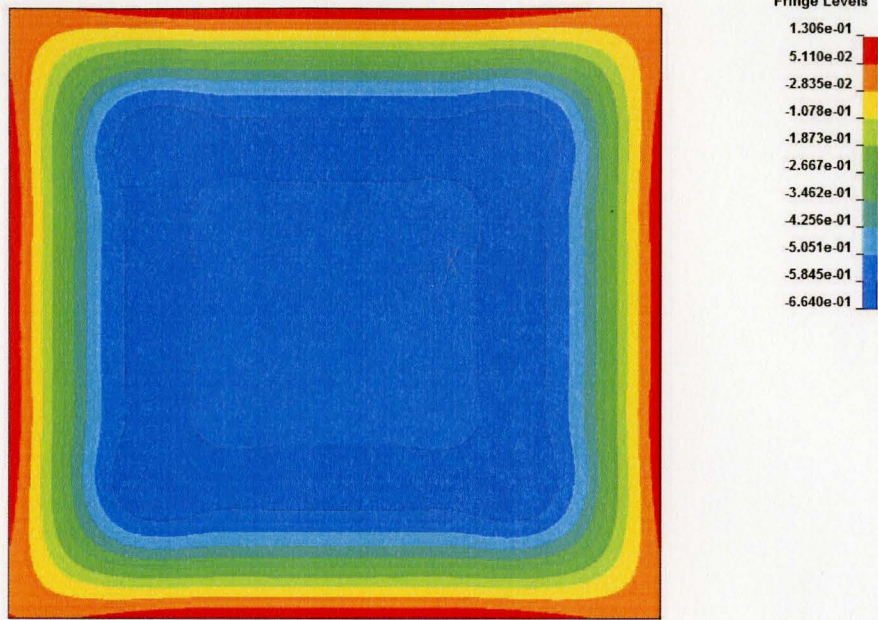
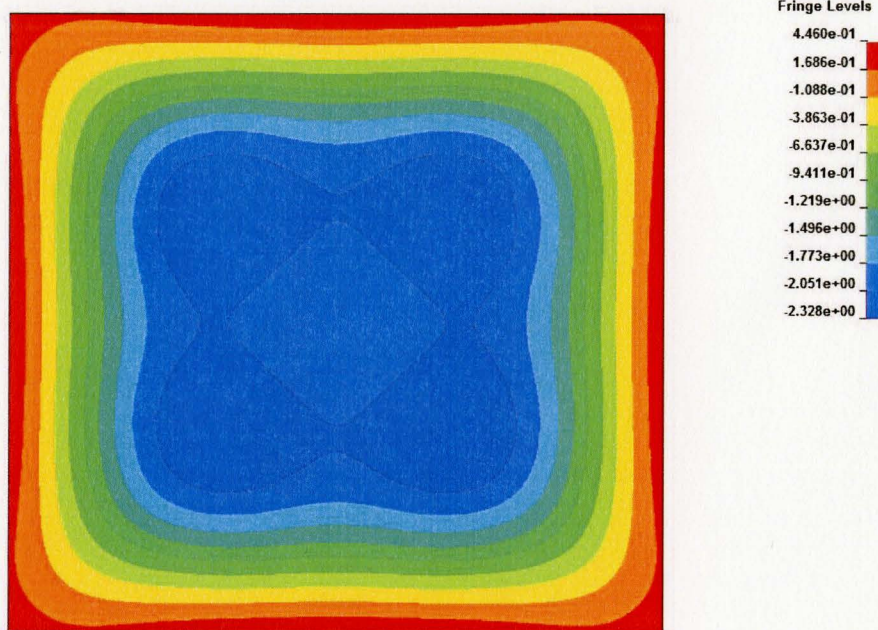


Fig. 3.17: $P-I$ diagrams for the simply supported panels using SDOF(EI_{weighted})

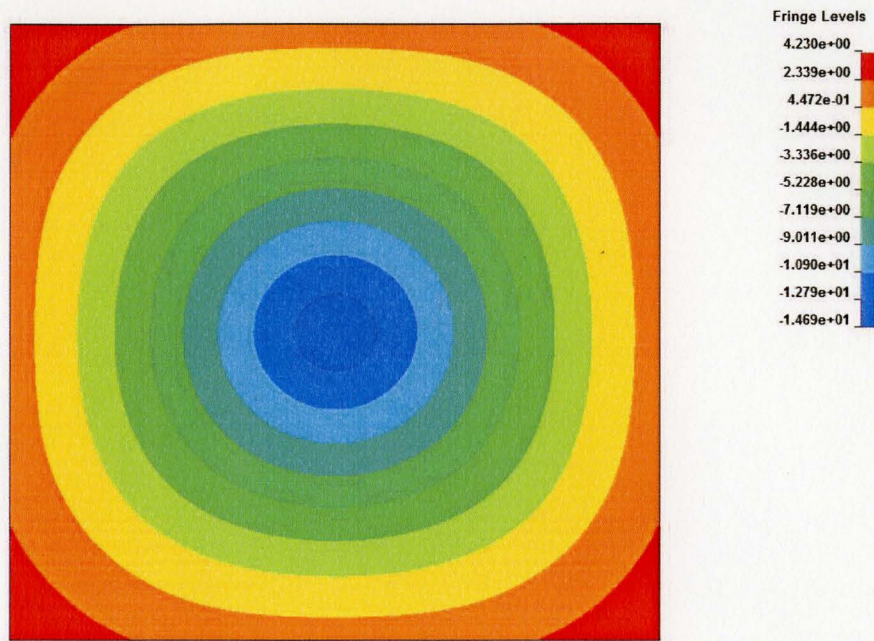
(a)



(b)



(c)



(d)

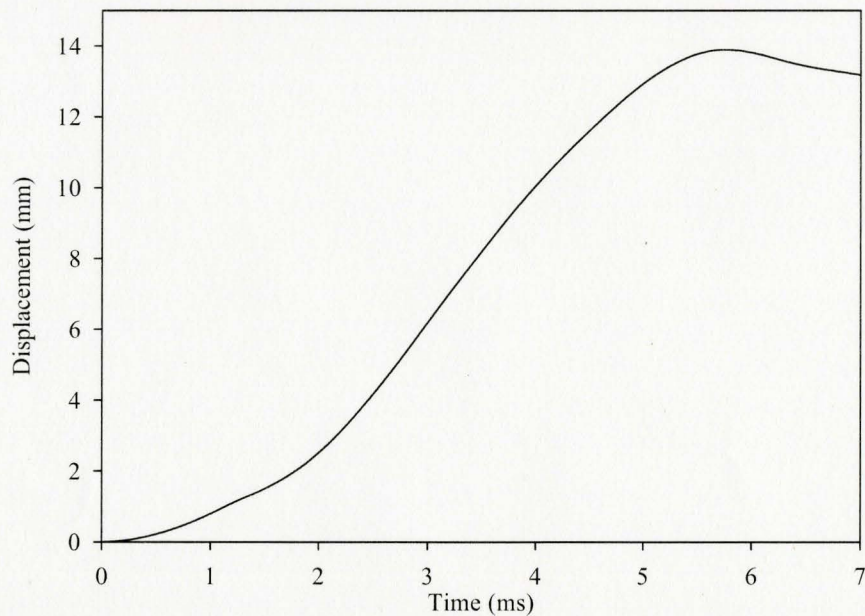
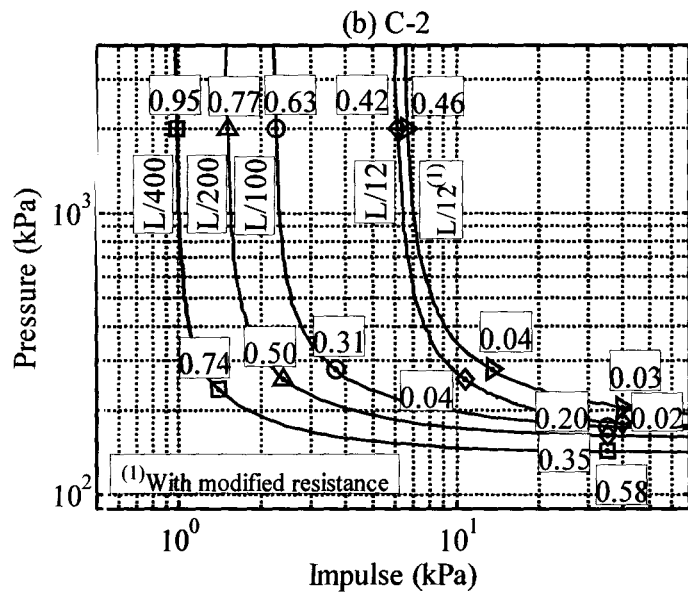
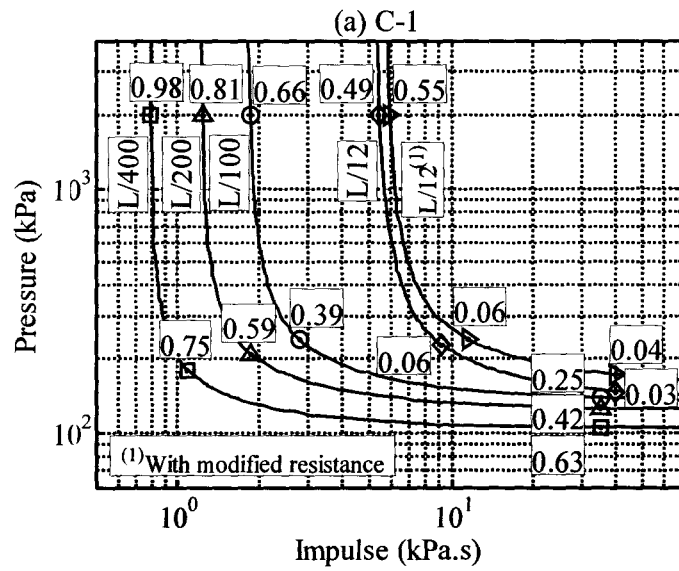


Fig. 3.18: Deflection of panel C-1 ($P_0=1000$ kPa, $T_L=2.09$ ms): (a) Deflection contours at $t = 0.83$ ms, (b) Deflection contours at $t = 1.68$ ms, (c) Deflection contour at $t = 5.67$ ms, (d) Displacement-time history for the central point of the panel



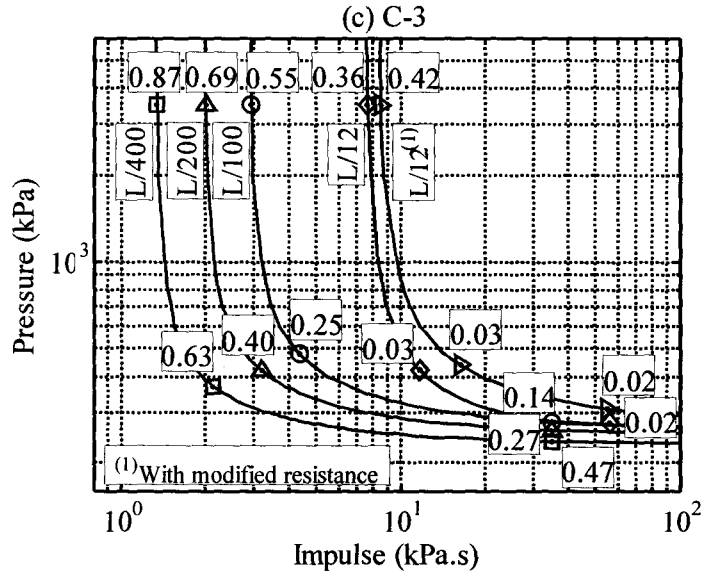
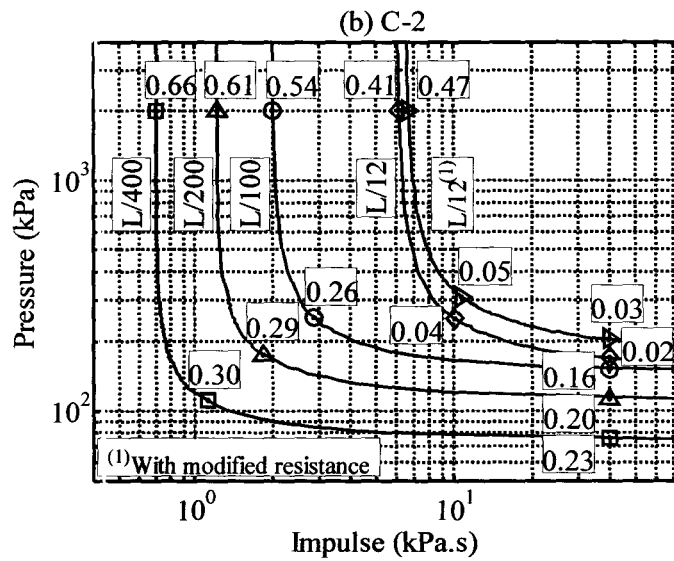
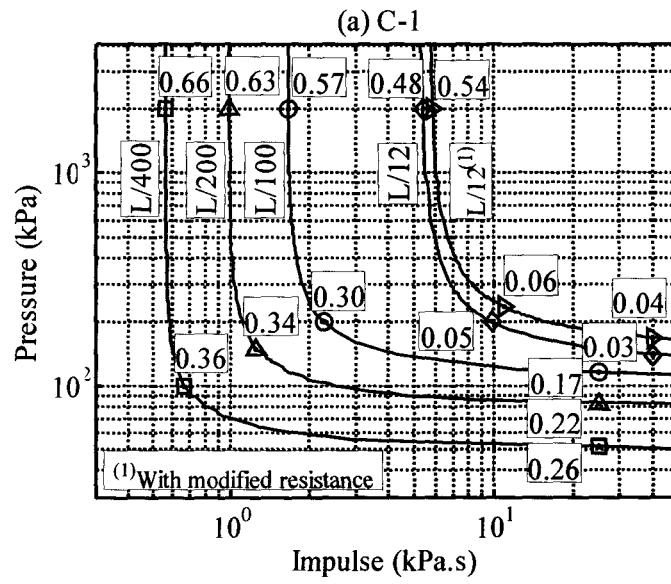


Fig. 3.19: $P-I$ diagrams for the clamped panels using SDOF(EI_{ave})



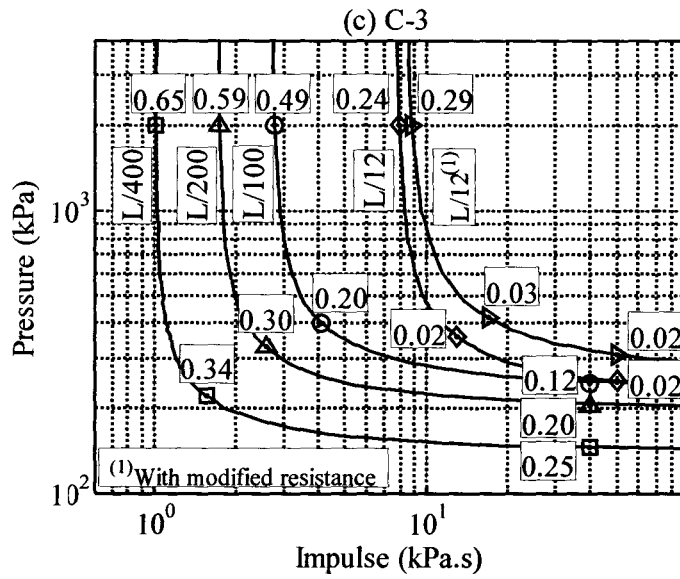


Fig. 3.20: *P-I* diagrams for the clamped panels using SDOF(EI_{cr})

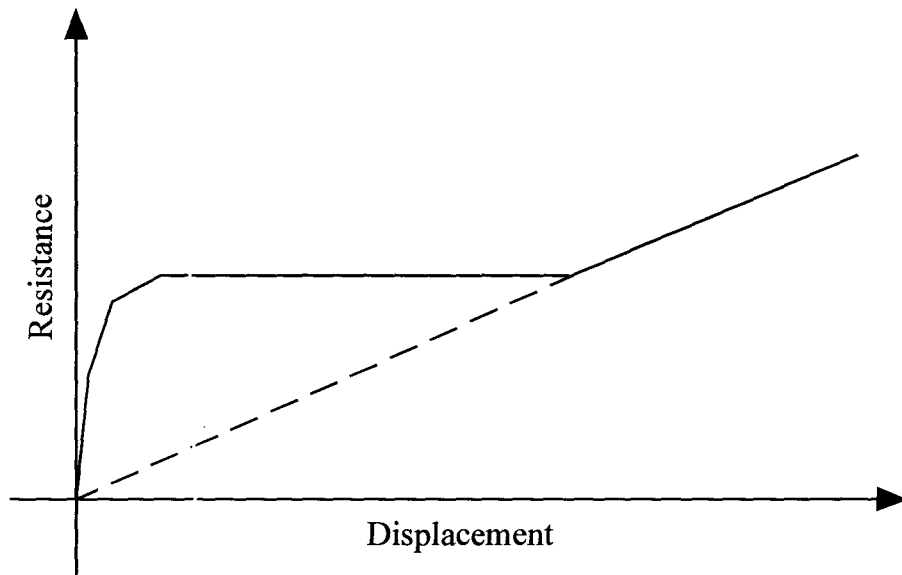
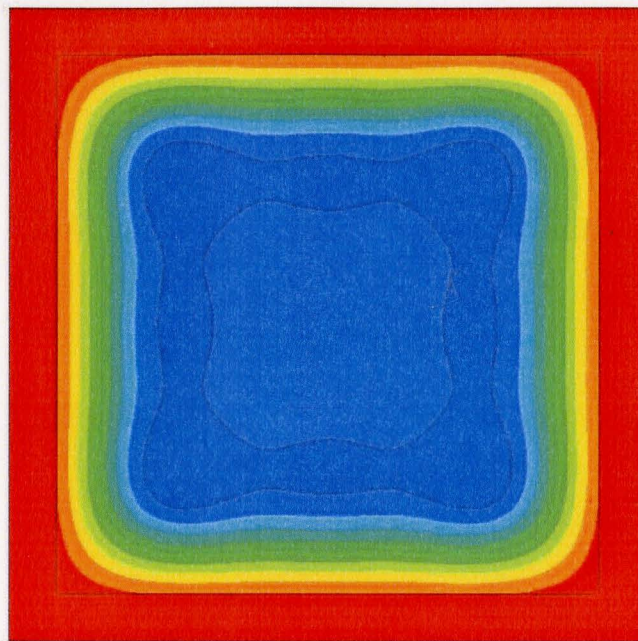
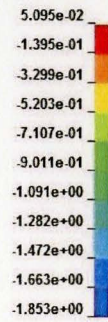


Fig. 3.21: Modified resistance function for the SDOF model

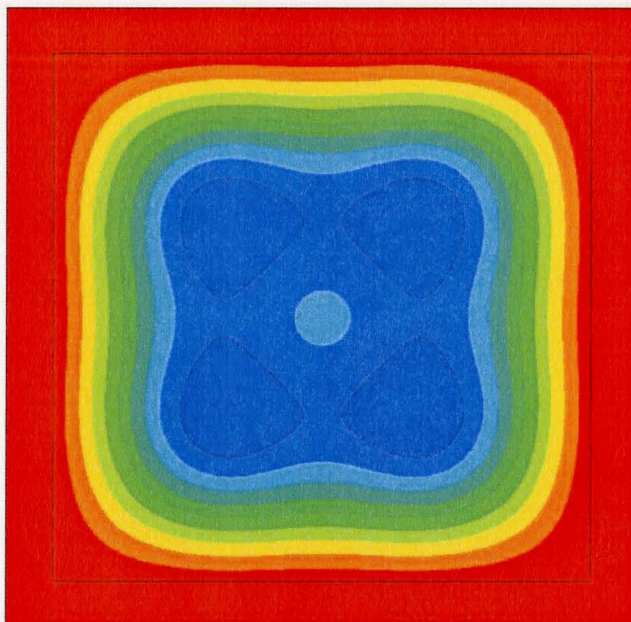
(a)



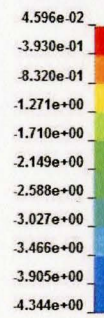
Fringe Levels



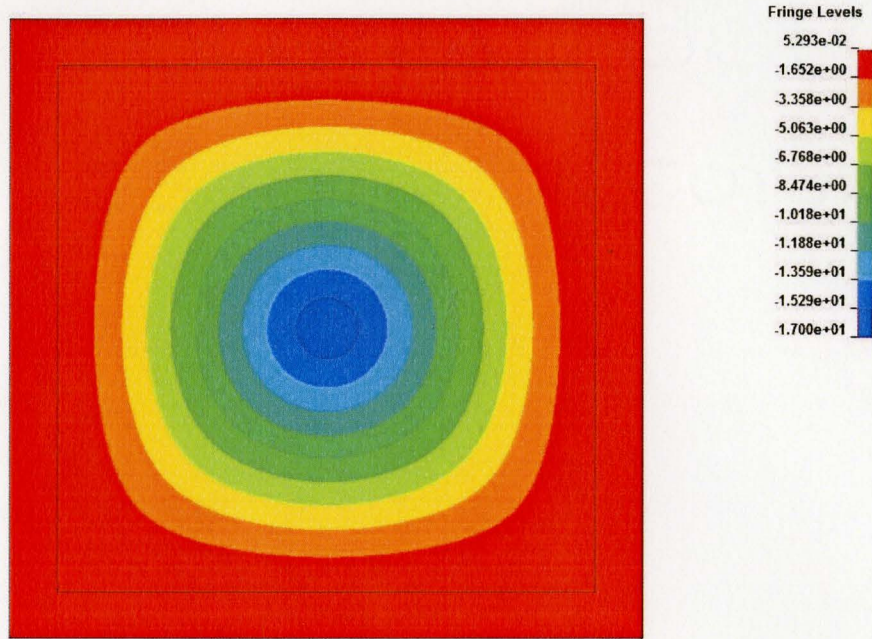
(b)



Fringe Levels



(c)



(d)

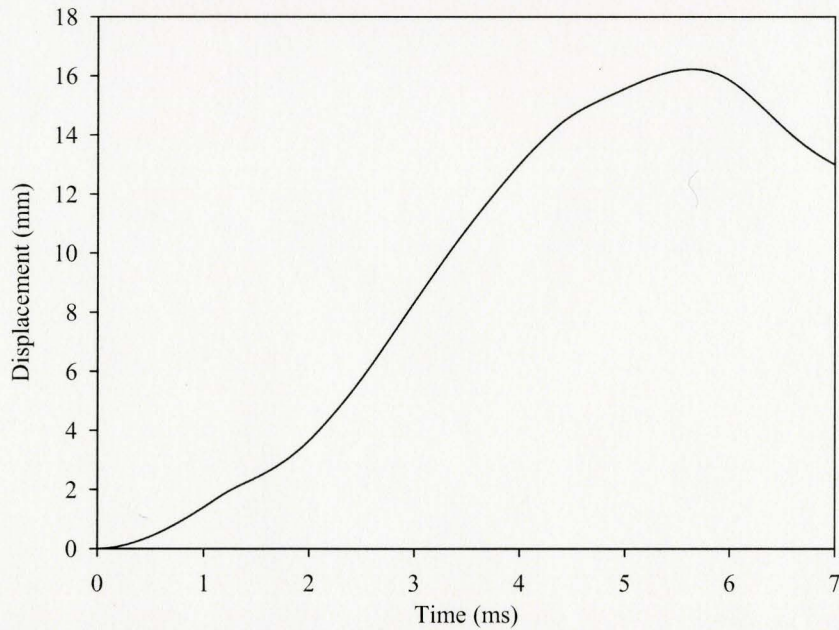
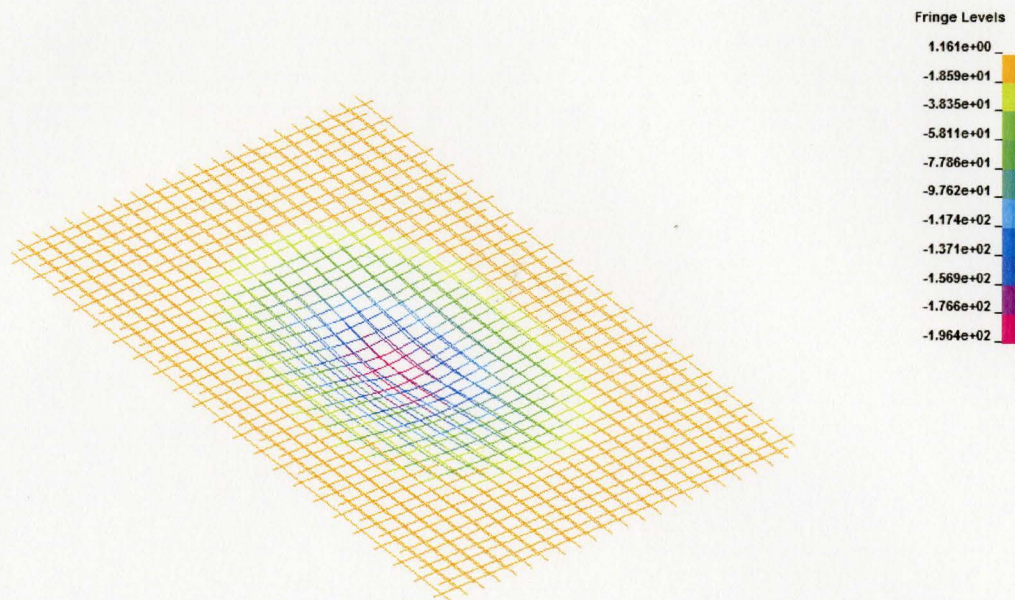


Fig. 3.22: Deflection of panel C-1 ($P_0=2000$ kPa, $T_L=1.25$ ms): (a) Deflection contours at $t = 1.08$ ms, (b) Deflection contours at $t = 1.91$ ms, (c) Deflection contour at $t = 5.52$ ms, (d) Displacement-time history for the central point of the panel

(a)



(b)

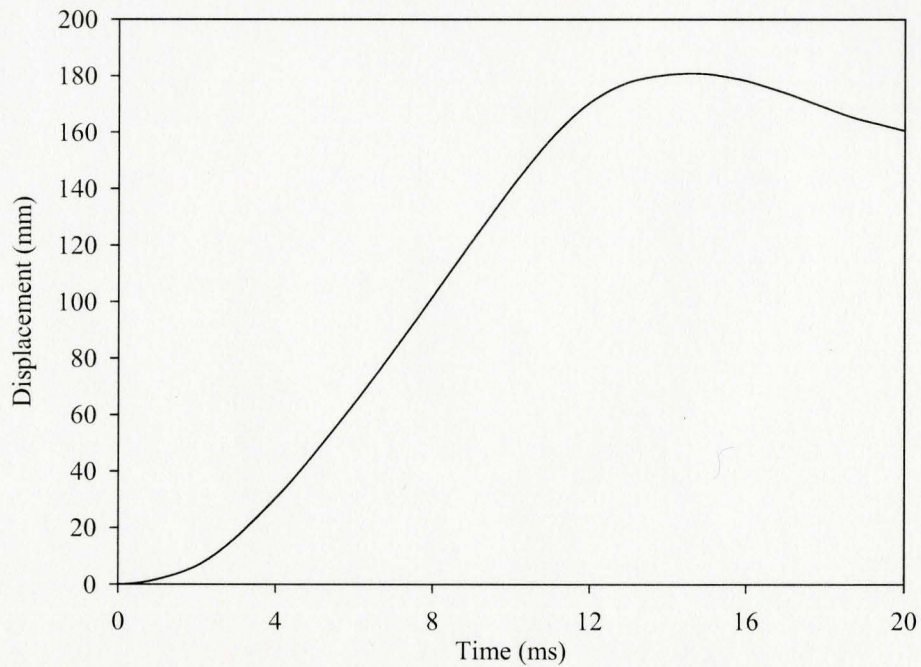
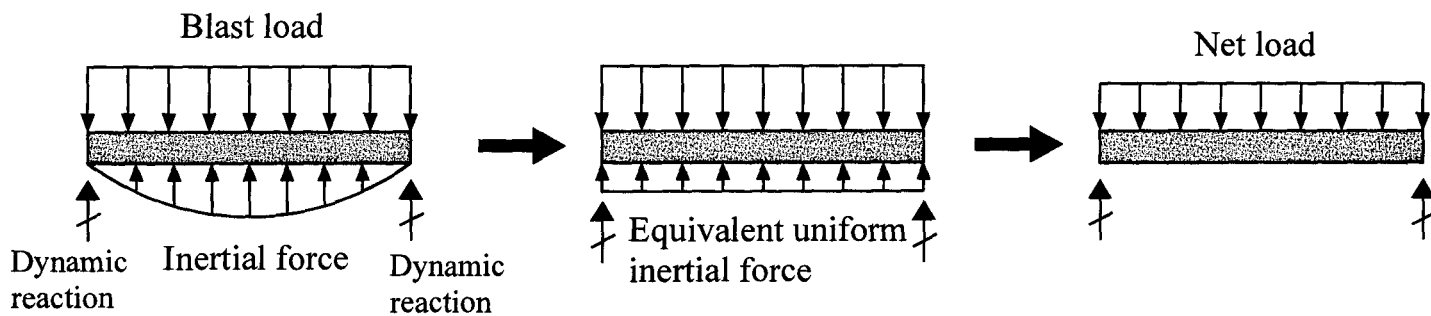


Fig. 3.23: Deflection of reinforcement in panel C-1 ($P_0=2000$ kPa , $T_L=5.92$ ms): (a) Deflection contours at $t = 14.00$ ms, (b) Displacement-time history for a reinforcement node near the central point of the panel

Fig. 3.24: Implementing the effect of applied load in reaction for TM5-1300



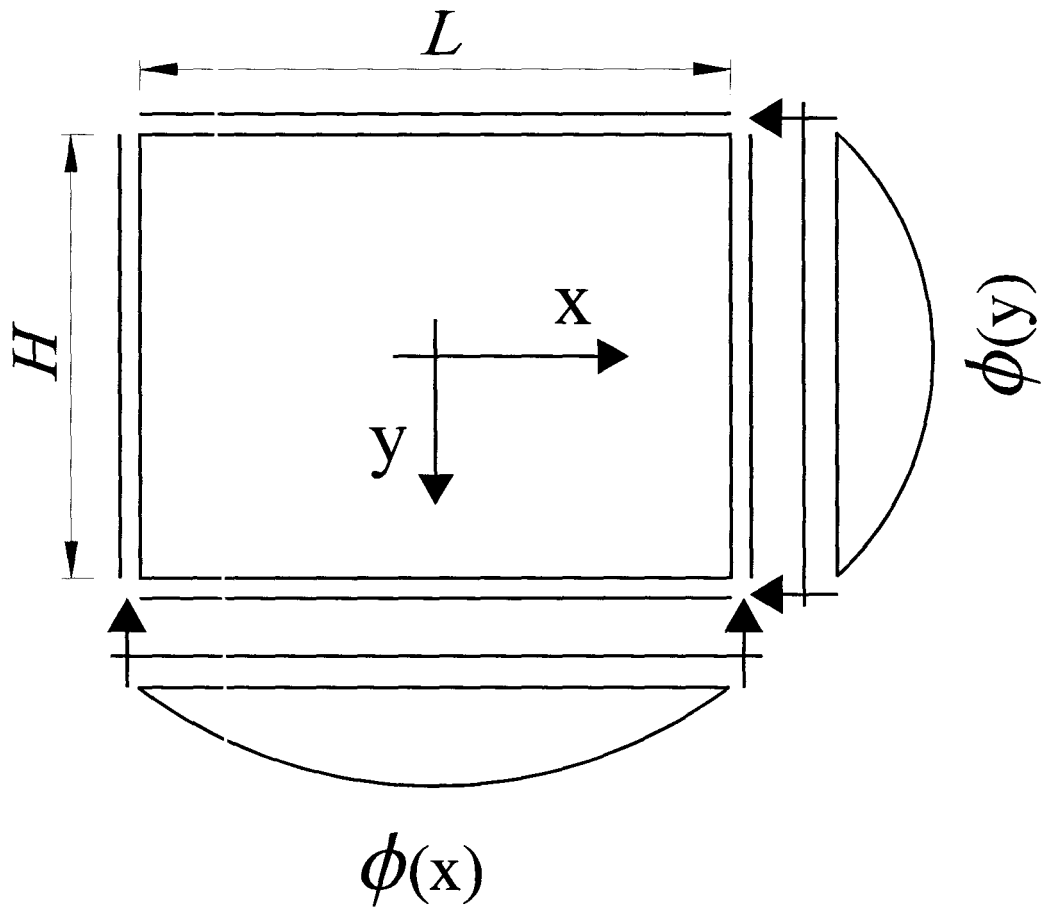


Fig. 3.25: Shape function of x -direction and y -direction section of a two-way panel

Chapter 4: Capacity Assessment of Reinforced Concrete Columns Subjected to Blast

Abstract: Due to their beneficial characteristics, Reinforced Concrete (RC) structures are used extensively for protective design against blast. However, the inherent nonlinearity associated with concrete structures makes the exact analysis of these types of structures very complicated. Therefore, simplified techniques are used to investigate the dynamic response of RC structural elements under blast. Many of the available studies were limited to study structural elements subjected to no axial loads such as beams. In this study, a multi-degrees-of-freedom (MDOF) model is developed to study the response of blast loaded RC columns which are the most critical elements to the overall stability of a structure and, when they fail, are the main cause for progressive collapse. The effect of axial load levels, strain rates and variation of flexural rigidity along the column heights has been implemented in the model. Effect of strain rate and axial load on column section properties has been investigated by constructing moment-curvature diagrams and bending moment-axial force interaction diagrams. Pressure-Impulse ($P-I$) diagrams were developed for two different types of steel detailing and parameters such as the effect of axial load on the $P-I$ diagrams, deflection at each level of damage, the effect of proper detailing on load carrying capacity and the column rotational capacity at fully damaged state were studied. Analysis results showed that section properties are enhanced with increasing strain rate. Increasing the level of axial load reduced the deflection capacity and the column rotation capacity. It was also found that good detailing at the supports can significantly enhance the load carrying capacity of column. The proposed model can also be used as a tool for damage screening purposes.

Keywords: Blast loads, Concrete columns, Damage assessment, Dynamic response, Models, Nonlinear analysis, Structural safety.

4.0 Introduction

In recent years, there has been a growing number of research activities focusing on protective design. For blast resistant design, reinforced concrete (RC) structures are usually used because of their ductile response and good fire and high inertial resistance.

In blast resistant design, structures should be proportioned and detailed to withstand local and global damage levels. When the local response of critical RC elements such as columns is considered, the design strategy should aim at preventing specific failure modes by proportioning the columns so that they can sustain a specific level of damage and inelastic deformation. On the other hand, when the global stability or the overall failures are evaluated, the design philosophy should aim at providing alternative load paths and increasing the structural redundancy in order to prevent progressive collapse.

Because of the nature of blast loading and the inherent nonlinearity of RC structures, nonlinear dynamic analysis must be carried out to evaluate the structural response. The different techniques used for nonlinear dynamic analysis usually fall under two categories, namely: analytical (macro) models and finite element (FE) models. Macro models typically employ either a single-degree-of-freedom (SDOF) or a multi-degree-of-freedom (MDOF) approach. These models employ the first mode of vibration or the first few modes to predict the structure's response to blast loading. Macro models require a limited number of input data and they are usually simple and easy to calibrate. On the other hand, nonlinear dynamic analysis using FE models requires large number of input

parameters and would usually demand a significant experience and knowledge to obtain reliable and realistic results. This is in addition to costs associated with building the model, solution time and the availability of computational facilities. Thus, most codes are based on SDOF approaches and even for complex structures, SDOF analysis is used for preliminary design or to check the FE results.

During an explosion, a chemical reaction takes place which results in a sudden rise in temperature and pressure. Consequently, the generated shock wave travels and strikes the structure with a pressure greater than ambient pressure referred to as “side-on over-pressure” or simply “over-pressure”. Figure 4.1(a) depicts the typical pressure time history during a blast event. As shown in the figure, the overpressure decays in an exponential form during a very short time (positive phase) and finally, drops below ambient pressure with a longer duration (negative phase) and a less pressure intensity (Baker et al. 1983). Generally, the exponential decay loading is approximated by a triangle pulse and the negative phase (suction) is neglected in the analysis. In this approximation, the triangle load has the same peak pressure as the actual blast load but different load duration, T_L . As can be seen in Fig. 4.1(b), the duration is determined based on the time to reach the maximum response. If the structural element reaches its maximum displacement after the pressure drops to ambient pressure, the equivalent duration is calculated through equating the area under the actual blast pressure time history curve in the positive phase (this area is the *impulse* of the blast load) with the triangle pulse area. On the other hand, if the element reaches the maximum response

within a time less than the positive phase duration, the equivalent duration is obtained by equating the slope of tangent line (at arrival time) of the actual loading curve with the slope of triangle load (Beshara 1994) as shown in Fig. 4.1(c).

Many researchers have employed SDOF or MDOF techniques and investigated the response of structural elements under blast or impact loading [Biggs (1964); Krauthammer et al. (1986); Krauthammer et al. (1990); Louca and Harding (1997); Pan and Watson (1998); Schleyer and Hsu (2000); Boutros (2000); Low and Hao (2002)]. However, most of these studies employed simplified models to study the dynamic response of one-way elements with no axial loads. On the other hand, critical structural elements such as columns are typically subjected to axial loads. In addition, columns located in the building perimeter are the most susceptible elements for damage during a blast event. Failure of these critical elements may lead to a partial or complete progressive collapse of the structure.

In this study, a MDOF model based on lumped mass approach is employed to study the response of RC columns under blast. The additional moment caused to presence of axial load were considered explicitly in the analysis. The strain rate effects were also incorporated in the analysis in order to consider the effect of the high rate of loading on the column response. The effect of strain rate was studied on section properties. Assuming different details at the column ends, Pressure-Impulse ($P-I$) diagrams were constructed. The effect of axial load level on the blast load carrying capacity of the column, the deflection and the column rotational capacity at different levels and the effect

of good detailing at supports were investigated. The following sections outline the details of the MDOF model. This will be followed by numerical results and concluding remarks of this study.

4.1 Model development

4.1.1 MDOF Model for a RC Column

In nonlinear analysis of RC elements subjected to dynamic loading the material stiffness should be adjusted for each loading increment with increasing displacement. The column must also be discretized to account for the variation of stiffness along the column height.

In this regard, MDOF models based on the lumped mass approach are usually employed in order to minimize the difficulties associated with nonlinear dynamic analysis of continuous systems. In these techniques, the structural element is replaced by a series of discrete connected nodes and the material properties are concentrated at these nodes. Using a finite difference method, the dynamic analysis of RC column subjected to blast can be performed as follows:

Figure 4.2 shows a column divided into $(n+1)$ segments. The lumped mass and load at the i^{th} node are, respectively: $LM_i = \rho_m (\Delta x)$ and $F_i = p(\Delta x)$, in which ρ_m and p are mass and load per unit length of the column, respectively and Δx is the segment length. The dynamic equilibrium equation for the i^{th} node can be written as:

$$LM_i \ddot{y}_i + V_{i-1,i} - V_{i,i+1} + C_i \dot{y}_i = F_i(t) \quad (4.1)$$

Where:

$y_i, \dot{y}_i, \ddot{y}_i$ = i^{th} node displacement, velocity and acceleration, respectively.

LM_i = Lumped mass at the i^{th} node

C_i = Damping for the i^{th} node

$F_i(t)$ = Lumped blast load at the i^{th} node

$V_{i-1,i}, V_{i,i+1}$ = Shear force values between the $(i-1)^{th}$ and the i^{th} node, and shear between the i^{th} and the $(i+1)^{th}$ node, respectively.

Considering the additional moment caused by axial force, F_a , and using the following equations:

$$V_{i-1,i} = \frac{M_i - M_{i-1} + F_a(y_{i-1} - y_i)}{\Delta x} \quad (4.2)$$

$$V_{i,i+1} = \frac{M_{i+1} - M_i + F_a(y_i - y_{i+1})}{\Delta x} \quad (4.3)$$

Where:

M_{i-1}, M_i, M_{i+1} = Moment at the $(i-1)^{th}$, the i^{th} and the $(i+1)^{th}$ node, respectively.

Δx = Segment length

Employing Eqs. 4.2 and 4.3, Eq. 4.1 can be written as:

$$LM_i \ddot{y}_i - \frac{M_{i-1} - 2M_i + M_{i+1} - F_a(y_{i-1} - 2y_i + y_{i+1})}{\Delta x} + C_i \dot{y}_i = F_i(t) \quad (4.4)$$

The Curvature (ϕ) can be obtained at each node using the following approximation:

$$\phi \cong -\frac{d^2 y}{dx^2} \cong \frac{-1}{\Delta x^2} (y_{i+1} - 2y_i + y_{i-1}) \quad (4.5)$$

Thus, the corresponding moment at each node can be found from the moment-curvature diagram evaluated for the column cross section whereas the above equation is solved numerically for each time increment.

Using the above technique, the nonlinear behavior of RC column is considered and the post damage state can be predicted using the MDOF approach. It should also be noted that damping is usually not considered for the impulsive loading problems such as blast and impact since the maximum response, which is generally of interest, usually occurs during the first vibration cycle when damping has minimum contribution to the dynamic response.

4.1.2 Material Stress-Strain Relationship

4.1.2.1 Concrete

Numerous stress strain relationships for concrete and reinforcing steel can be found in the literature. For concrete under compression, different expressions were proposed (Popovics 1973; Scott et al. 1982; Dilger et al. 1984; Soroushian et al. 1986; Mander et al. 1988). Typically, these relationships are expressed in terms of the compressive strength, the strain at this compressive strength and the concrete modulus of elasticity. In this study, the relationship proposed by Saatcioglu and Razvi (1992) for confined concrete is adopted:

$$\sigma_c = f'_{cc} \left[2\left(\frac{\varepsilon}{\varepsilon_c}\right) - \left(\frac{\varepsilon}{\varepsilon_c}\right)^2 \right]^{1/(1+2K)} \leq f'_{cc} \quad \text{for } \varepsilon \leq \varepsilon_c \quad (4.6-a)$$

$$\sigma_c = \frac{0.15f'_{cc}}{\varepsilon_c - \varepsilon_{85}} (\varepsilon - \varepsilon_c) + f'_{cc} \quad \text{for } \varepsilon_c < \varepsilon \quad (4.6-b)$$

Where:

ε, σ_c = Strain and corresponding compressive stress

f'_{cc}, ε_c = Maximum compressive stress for confined concrete and corresponding strain

K = Curve parameter for confined concrete

ε_{85} = Strain corresponding to $0.85f'_{cc}$ on the descending branch of stress-strain curve

In the above equation, $f'_{cc}, \varepsilon_c, \varepsilon_{85}$ and K are determined based on the cross section of the column, configuration of ties and concrete properties. Saatcioglu and Razvi (1992) also give a constant residual stress equal to $0.2f'_{cc}$ for strains greater than ε_{20} (strain corresponding to $0.2f'_{cc}$), and this residual strength has been neglected in this study.

For tension stiffening, different formulations have been proposed by Vecchio and Collins (1982); Collins and Mitchell (1987); Tamai et al. (1987), Bentz (2005). Each of these formulations may be appropriate for a specific section and concrete mixture properties since tension stiffening is dependent on the bond characteristics which vary from case to case. In this study, Vecchio and Collins' (1982) relationship, given by:

$$\sigma_t = \frac{f_t}{1 + \sqrt{200\varepsilon}} \quad (4.7)$$

was used, in which, ε , σ_t are strain and corresponding tensile stress, and f_t is the tensile strength taken as 10% of the compressive strength.

4.1.2.2 Steel

A number of formulations are available in the literature for the reinforcing steel stress-strain relationship and all of these formulations consist of three parts: elastic, yield plateau and strain hardening part. In this study, Hoehler and Stanton (2006) model was used. According to their formulation, the strain-stress relationship for steel is given by:

$$\sigma = E \times \varepsilon \quad \text{for } \varepsilon \leq \varepsilon_y \quad (4.8-a)$$

$$\sigma = \sigma_y + (\varepsilon - \varepsilon_y) \times E_y \quad \text{for } \varepsilon_y \leq \varepsilon \leq \varepsilon_{sh} \quad (4.8-b)$$

$$\sigma = \sigma_u - (\sigma_u - \sigma_{sh}) \times \left(\frac{\varepsilon_u - \varepsilon}{\varepsilon_u - \varepsilon_{sh}} \right)^{C_1} \quad \text{for } \varepsilon_{sh} \leq \varepsilon \leq \varepsilon_u \quad (4.8-c)$$

Where:

ε, σ = Strain and corresponding stress in the reinforcing steel

σ_y, ε_y = Stress and strain at steel yield

$\sigma_{sh}, \varepsilon_{sh}$ = Stress and strain at the onset of strain hardening

σ_u, ε_u = Ultimate (peak) stress and strain

E = Elastic modulus

E_y = Slope of yield plateau

C_1 = Parameter that defines the curvature of the strain hardening curve.

4.1.3 Strain Rate Effects

There is a very high strain rate associated with blast as a result of the short time history of blast loads (in the range of milliseconds) compared to the duration of other dynamic loads such as earthquake (in the range of seconds). Hence, the material characteristics under such extreme dynamic loading may differ from those obtained under static loading condition. In fact, it has been shown by a number of experimental and numerical studies that concrete and steel exhibit significant strength increase under high strain rate of loading (Bischoff and Perry 1991). Hence, material properties should be modified and enhanced in the analysis of rapid dynamic loads such as blast and impact.

The ratio of the material's dynamic strength to its static strength is defined as the Dynamic Increase Factor (*DIF*) and is used to scale material properties under dynamic loading condition. This factor is usually expressed as a function of strain rate either graphically (TM5-1300, 1990) or presented in the form of formulas.

4.1.3.1 Concrete

For concrete under compression, it was shown that the increase in compressive strength is more significant than the enhancement of other concrete properties under compression such as ultimate strain and the elastic modulus. For strength enhancement, expressions

were proposed by Comité Euro-International du Béton (CEB) (1988); Tedesco et al. (1997); Malvar and Ross (1998). All these expressions differentiate between low to intermediate strain rates and intermediate to high strain rate, and give separate relationships for these ranges (Fig. 4.3(a)). It was also shown that the concrete tensile strength exhibited higher increase than its compressive strength (Fig. 4.3(b)). There were no consensus among different researchers on the effect of strain rate on the strain at the peak compressive stress and different results have been reported (Bischoff and Perry 1991).

Tedesco et al. (1997) used their experimental results from a number of Split-Hopkinson Pressure Bar (SHPB) tests for concrete with different strength and moisture, and implemented some regression equations in their concrete model. Malvar and Crawford (1998) considered a large number of test results and modified CEB (1988) formula for concrete under tension while as stated by Malvar and Crawford (1998), the CEB (1988) formula for concrete compressive stress enhancement is widely acceptable among the researchers. Therefore, in this study, CEB's (1988) relations for concrete under compression and Malvar's (1988) formula for concrete under tension are adopted. The equation proposed by Soroushian et al. (1986) is also considered for scaling the strain corresponding at the peak compressive stress. These relationships are expressed as follow:

CEB's (1988) formula for concrete under compression:

$$f_{cd} / f_{cs} = \left(\frac{\dot{\varepsilon}}{\dot{\varepsilon}_s} \right)^{1.026\alpha_s} \quad \text{for } \dot{\varepsilon} \leq 30 \text{ s}^{-1} \quad (4.9-a)$$

$$= \gamma_s \left(\frac{\dot{\varepsilon}}{\dot{\varepsilon}_s} \right)^{1/3} \quad \text{for } \dot{\varepsilon} > 30 \text{ s}^{-1} \quad (4.9-b)$$

Where f_{cd} and f_{cs} are the dynamic and static compressive strength, $\dot{\varepsilon}$ is the strain rate, $\dot{\varepsilon}_s = 30 \times 10^{-6} \text{ s}^{-1}$ (static strain rate), $\gamma_s = 10^{(6.156\alpha_s - 2)}$, $\alpha_s = 1/(5+9(f_{cs}/f_{co}))$, $f_{co} = 10 \text{ MPa} = 1450 \text{ psi}$.

Soroushian's (1986) expression for scaling strain at peak compressive stress:

$$\varepsilon_{cd} / \varepsilon_{cs} = 1.08 + 0.112 \log \dot{\varepsilon} + 0.0193 (\log \dot{\varepsilon})^2 \quad (4.9-c)$$

Where ε_{cd} is the strain corresponding to the concrete dynamic compressive strength and ε_{cs} is its static values, $\dot{\varepsilon}$ is the strain rate in s^{-1} .

Malvar's equation for concrete under tension:

$$f_{td} / f_{ts} = \left(\frac{\dot{\varepsilon}}{\dot{\varepsilon}_s} \right)^\delta \quad \text{for } \dot{\varepsilon} \leq 1 \text{ s}^{-1} \quad (4.10-a)$$

$$= \beta \left(\frac{\dot{\varepsilon}}{\dot{\varepsilon}_s} \right)^{1/3} \quad \text{for } \dot{\varepsilon} > 1 \text{ s}^{-1} \quad (4.10-b)$$

Where f_{td} and f_{ts} are the dynamic and static tensile strength, $\dot{\epsilon}$ is the strain rate, $\dot{\epsilon}_s = 30 \times 10^{-6} \text{ s}^{-1}$ (static strain rate), $\beta = 10^{(6\delta-2)}$, $\delta = 1/(1+8 f_{cs}/f_{co})$, $f_{co} = 10 \text{ MPa}$.

4.1.3.2 Steel

Similar to concrete, expressions are proposed for the enhancement of steel properties at high strain rate. For reinforcing steel, relationships given by Soroushian and Choi (1987); CEB (1988); Malvar (1998) were proposed. It has been observed that yield and ultimate stress increased with increasing strain rate whereas the steel modulus of elasticity is not affected by the rate of loading. For the MDOF model developed in this study, Malvar's (1998) formulations are used because of the large number of test results at different strain rates that were used to verify their expressions:

$$DIF = \left(\frac{\dot{\epsilon}}{10^{-4}} \right)^\alpha \quad (4.11-a)$$

Where:

$$\alpha = 0.074 - 0.040 \frac{f_y}{414} \quad \text{For the } DIF \text{ of yield stress} \quad (4.11-b)$$

$$\alpha = 0.019 - 0.009 \frac{f_u}{414} \quad \text{For the } DIF \text{ of ultimate stress} \quad (4.11-c)$$

$\dot{\epsilon}$ is the strain rate, f_y and f_u are the bar yield stress and ultimate stress in MPa.

As can be seen in Fig. 4.3(b) and Fig. 4.3(c), the stress-strain curves is scaled corresponding to a certain strain rate level. The maximum concrete compressive stress

with its corresponding strain, maximum concrete tensile stress and steel yield and ultimate stress will be amplified by the corresponding *DIF*.

4.1.4 Strain Rate Estimation

In order to modify the material properties by the appropriate *DIF*, a procedure should be established to predict the strain rate for a specific blast loading conditions. Different technique such as finding maximum curvature rate (Kulkarni and Shah 1998) or deriving the approximate strain rate equation (Krauthammer et al. 1994) can be used. All of these techniques gave an estimation of the order of strain rate, not the exact value since the correct modeling of strain rate dependency is very complicated and cannot be achieved using simple analysis. Nevertheless, the method described by Krauthammer et al (1994) provided a simple and accurate methodology for estimating strain rates and therefore was used in this study. In this technique, the relationship between the strain and applied uniform load in an element cross section must be evaluated. Considering the fixed column shown in Fig. 4.4, the strains at the tensile and compressive fiber at midspan of this column can be given by:

$$\varepsilon_c = \left(\frac{pL^2}{24}\right)\left(\frac{h_c}{EI_{eff}}\right) \quad (4.12-a)$$

$$\varepsilon_t = \left(\frac{pL^2}{24}\right)\left(\frac{h_t}{EI_{eff}}\right) \quad (4.12-b)$$

Where ε_c and ε_t are strains at the compressive fiber and the tensile fiber, respectively. p is the uniform blast load. h_c and h_t are the compression depth and the tension depth of the cross section, respectively. EI_{eff} is an effective flexural rigidity and L is the column height.

Consequently, the strain rate at extreme fibers can be obtained by evaluating the derivative with respect to time:

$$\frac{\partial \varepsilon_c}{\partial t} = \frac{\partial p}{\partial t} \left(\frac{L^2}{24} \right) \left(\frac{h_c}{EI_{eff}} \right) \quad (4.13-a)$$

$$\frac{\partial \varepsilon_t}{\partial t} = \frac{\partial p}{\partial t} \left(\frac{L^2}{24} \right) \left(\frac{h_t}{EI_{eff}} \right) \quad (4.13-b)$$

And the strain rate, $\dot{\varepsilon}$, for the whole cross section can be considered by taking the average of strain rates obtained from Eqs. 4.13-a and 4.13-b:

$$\dot{\varepsilon} = \frac{\partial p}{\partial t} \left(\frac{L^2}{48} \right) \left(\frac{h_c + h_t}{EI_{eff}} \right) \quad (4.14)$$

or

$$\dot{\varepsilon} = \frac{\partial p}{\partial t} \left(\frac{L^2}{48} \right) \left(\frac{h}{EI_{eff}} \right) \quad (4.15)$$

Where h is the cross section height.

In order to estimate an effective flexural rigidity (EI_{eff}) for the element cross section, the moment-curvature diagram is constructed. Then, the moment and curvature at the yield point (M_y, ϕ_y) are found on the moment curvature diagram and EI_{eff} is obtained by

calculating the value of M_y/ϕ_y . Hence, for a triangular load idealization, the previous equation can be simplified to:

$$\dot{\varepsilon} = \frac{p_0}{T_L} \left(\frac{L^2 h}{48} \right) \left(\frac{\phi_y}{M_y} \right) \quad (4.16)$$

Where p_0 and T_L are the peak uniform load per unit length and the loading duration, respectively.

Similarly, strain rates can be estimated for RC columns with different loading and support conditions. Following the above approximation, the strain rate for each section along the column height can also be calculated. Thus, in this way, the proposed model is capable of considering the distribution of strain rate along the height of the column.

4.2 Numerical Results and Discussion

4.2.1 Overall Procedure

The developed MDOF model was used to study the column shown in Fig. 4.5 with height that varied between 3.0 m and 6.0 m and the shown cross section. The concrete compressive stress was set to 30 MPa and reinforcement yield stress was assumed to be 400 MPa. Using these material properties, the change in cross section behaviors such as moment-curvature diagrams and moment-interaction diagrams was studied for different levels of axial loads and strain rates. In addition, four levels of axial loads, as a fraction of the column axial load capacity, F_{a-max} , found under static rate of loading ($1E-7 \text{ s}^{-1}$), were

considered. These levels were $0.2 F_{a-max}$, $0.35 F_{a-max}$, $0.5 F_{a-max}$ and $0.7 F_{a-max}$. The column MDOF model was used with 40 degrees of freedom based on the previous study by the authors (Changiz Rezaei et al. 2008) that dealt with degrees of freedom optimization for RC structures under blast loads. For the MDOF analysis, the strain rate was also calculated for each node based on the method explained earlier and material properties were modified accordingly. Considering the point that concrete tensile strength and compressive strength shows higher sensitivity to strain rates greater than $1s^{-1}$ and $30s^{-1}$, respectively, the separate strain rates and moment-curvature relationships were evaluated for each node in cases where the load produced strain rates greater than $1s^{-1}$. The numerical procedure has been summarized in the flow chart shown in Fig. 4.6. Moreover, two column support capacities were defined and *P-I* diagrams, which represent combination of pressure and impulse producing the same level of deflection, were developed for these two support conditions. The effect of axial loads as well as good detailing on blast load carrying capacity and the column rational capacity were investigated. The following sections present the findings of these studies.

4.2.2 Section Properties

4.2.2.1 Moment-Curvature Diagrams

Using the stress-strain relationships described earlier, the moment-curvature diagram for a given column cross section can be constructed. For a specified curvature, the strain distribution is adjusted so that the summation of the internal compressive and tensile forces is equal to the applied axial load. After obtaining the strain distribution, the

moment is calculated by evaluating the sum of the internal force moments about the geometrical centroid of the column cross section. Following this procedure, moment curvature diagrams were generated for different level of axial loads (i.e. no axial load, $0.2 F_{a-max}$, $0.35 F_{a-max}$, $0.5 F_{a-max}$ and $0.7 F_{a-max}$) as shown in Fig. 4.7. In this figure, variation of moment-curvature diagrams are shown at different levels of strain rate, which are $1E-7 s^{-1}$ (static rate of loading), $1 s^{-1}$, $10 s^{-1}$, $100 s^{-1}$ and $500 s^{-1}$ for the different levels of axial load. The results obtained by amplifying the material properties with 25% ($1.25 \times St$), which is the current practice (Rodriquez-Nik 2006), are also shown in the figure.

Ultimate curvatures in Fig. 4.7 are limited to a maximum concrete strain corresponding to 85% of the concrete compressive strength (ϵ_{85}) at the descending portion of the stress-strain relationship. Comparing the ultimate curvatures at different strain rates and the same at no axial load, it can be observed that axial loads significantly reduce the ultimate curvature of the column cross section. In fact, axial loads increase the depth of compression zone in the section and, as a result, the ultimate curvature is reduced as shown in Figs. 4.8(a) and 4.8(b). It can also be observed that enhancement of material properties at higher strain rate also results in increase in the ultimate curvature values. Fig. 4.8(c) depicts the amount of reduction in ultimate curvature for the moment-curvatures shown in Fig. 4.7. Fig. 4.8(c) also shows that, in average, there is a 40% reduction in curvature values for low levels of axial load ($0.2 F_{a-max}$) and the average reduction can be as high as 70% for high value of axial load ($0.7 F_{a-max}$). Because ultimate curvatures may increase with increasing strain rates, the reduction in ultimate

curvatures due to presence of axial load is more pronounced for low strain rates. Considering the significant reduction in the value of ultimate curvature, it can be concluded that the possibility of column failure under blast increases by considering axial load in the analysis.

The cracking moment can be identified on the moment-curvature diagrams can be identified at the onset of reduction in the slope of the curves. It can be observed that this section property also increase with increasing strain rate due to the significant increase in tensile capacity of concrete at high strain rates.

Considering Fig. 4.7, it can also be observed that the moment-curvature diagrams obtained by using 25% enhancement to the material properties can reach the values corresponding to the strain rate of 1 s^{-1} . Therefore, it is quite obvious that simply amplifying the static material properties by the factor of 1.25 cannot capture material enhancement at the very high strain rates such as 100 s^{-1} and 500 s^{-1} corresponding to blast. Consequently, employing the 25% factor would result in underestimation of material resistance at such strain rates.

4.2.2.2 Axial Force-Moment Interaction Diagrams

Generally, interaction diagrams are used to find the load carrying capacity of a column cross section for a combination of axial force and bending moment. Fig. 4.9(a) shows the interaction diagrams for the column cross section at different levels of strain rate. At

higher strain rates the material properties are enhanced resulting in higher load carrying capacity. As can be seen, the larger the value of strain rate, the more the interaction diagrams move outward and the column cross section resistance, in terms of both axial load and bending moment, increases. Similar to the previous section, it can also be seen that using scale factor of 1.25 for material enhancement cannot capture the interaction diagrams at high strain rates and that results in underestimation of the axial force and bending moment capacity at high strain rates.

The values of the maximum axial force, F_{a-max} , the balanced axial force, F_{a-b} , balanced bending moment, M_b and pure bending moment capacity, M_0 , at different strain rates were normalized by their corresponding value at the static rate of loading ($1E-7 s^{-1}$) and results are shown in Fig. 4.9(b). As this figure shows a significant increase is obtained at high strain rates and, as can be expected, the rate of amplification for F_{a-max} , F_{a-b} and M_b increase at strain rate greater than $30 s^{-1}$ since these quantities are dependent on concrete compressive strength which is amplified at higher rate for strain rate greater than $30 s^{-1}$ as can be seen in Fig. 4.3(b).

4.2.3 Damage Assessment

The concept of the Pressure-Impulse ($P-I$) diagrams is widely used to find the maximum deflection or damage reached for a certain combination of pressure and impulse (time integral pressure). Two connection behavior will be defined at column ends and using the MDOF model, the corresponding $P-I$ diagrams is developed for each connection type.

The first connection (referred to as type *N*) resembles a poorly detailed (non ductile connection). The second connection (referred to as type *D*) is a ductile connection that maintains its moment capacity till the full moment capacity is developed at the column midspan. Consequently, parameters such as axial load level, deflection at each damage level, RC section capacity and detailing effects will be studied.

4.2.3.1 *P-I* Diagrams

P-I diagrams represent combinations of pressure and impulse pairs producing the same maximum level of damage or deflection within the structural element (Baker et al. 1983). A typical *P-I* diagram has been depicted in Fig. 4.10. As this figure shows, *P-I* diagrams consist of several contours, each corresponds to a certain level of deflection (damage) and the further a contour is from the origin, the higher the deflection (damage) is.

As can be seen in Fig. 4.10, each *P-I* diagram can be divided to three parts: impulsive loading realm, dynamic loading realm, quasi-static loading realm and a pressure and a impulse asymptote shown in the figure can be identified for each curve. In this classification, the maximum deflection may depend only on the applied impulse (impulsive), impulse and pressure (dynamic), or pressure (quasi-static). The pairs of pressure impulse falling below or to the left of each curve produce a maximum deflection lower than the value specified by the curve while the points above or to the right of the curve indicates a greater deflection.

4.2.3.2 Effect of Axial Load on the $P-I$ Diagrams

Using the MDOF model subjected to triangular blast load, the $P-I$ diagrams were generalized for the two connection types, N and D .

Damaged state of type N is defined as a state in which the supports are starting to fail in flexure and the curvature has reached its ultimate value at these regions. Column damage for type D is defined as yielding at supports that is followed by column midspan yielding which will lead to a mechanism. In other words, to progress from the partially damaged state (type N) to the fully damaged one (type D), it is assumed that there is good detailing at supports and the plastic moment can be sustained at these regions until the midspan fails in flexure.

Considering the above definitions, $P-I$ diagrams were generated for different levels of axial load (i.e. no axial load, $0.2 F_{a-max}$, $0.35 F_{a-max}$, $0.5 F_{a-max}$ and $0.7 F_{a-max}$) for the connection type of N and D . These diagrams are shown for the two column heights (i.e. 3.0 m and 6.0 m) in Fig. 4.11 and Fig. 4.12, respectively. In these figures, the deflections at these damage states have also been reported as a fraction of column length beside each levels of axial load.

Considering Figs. 4.11 and 4.12 and comparing the $P-I$ curves with the case with no axial load, it can be observed that the difference becomes more pronounced in the impulsive regime as the axial load becomes high and it reaches the maximum negative shift of

about 40%. As the load moves towards quasi-static regime, the variation of $P-I$ curves with respect to the case with no axial load becomes less significant and, in average, it can reach the maximum of about 20%.

Comparing the deflection of the column with N and D connection type, for both column heights, it can be seen that the inclusion of the axial load will result in a significant reduction in deflection value for both types. Fig. 4.13 shows the reduction in deflection as percentage of its value for the column with no axial load. As can be seen, for type N connection the reduction in average varied from 27%, at low axial loads (i.e. $0.2 F_{a-max}$), up to 46% at high levels of axial load (i.e. $0.7 F_{a-max}$). For type D connection, the reduction in average varied from 38% to 62% for the low and high levels of axial load.

4.2.3.3 Effect of Good Detailing on Load Carrying Capacity

Comparing the $P-I$ diagrams generated for type D and type N connections, it can be noticed that providing good detailing at supports can significantly enhance the column capacity in terms of increase in deflection, pressure asymptote and impulse asymptote. In average, for all levels of axial load, the good connection detailing (type D) can increase the deflection up to about 3.8 times greater for the 3.0 m high column and up to 3.4 times for the 6.0 m column. In addition, the pressure asymptote is amplified by a factor of 1.5 for the both column. The impulse asymptote is also enhanced by a factor of about 2.6 for 3.0 m column and 2.2 for the 6.0 m column.

4.2.3.4 Rotational Capacity at the Fully Damaged State

The RC section rotation at the fully damaged state (type *D* connection) is approximately obtained by dividing the deflection by half of the column height. This angle of rotation were calculated and reported in Fig. 4.14 for different levels of axial load. As can be seen, with increasing the axial load from zero to $0.7 F_{a-max}$, the rotational capacity decreased from 0.82° to 0.29° for the 3.0 m column and decreased from 1.53° to 0.64° for the 6.0 m column.

It can be noted that the angle of rotation is not constant and it can be much lower than the typical values assumed (e.g. 2° suggested by the TM5-1300, 1990). In addition, the angle of rotation is the function of axial load and it decreases with increasing the level of axial load. Furthermore, the angles are also dependant on the stiffness of the column. As noted earlier, the 6.0 m column had the higher rotation compared to the 3.0 m column which is significantly stiffer than the 6.0 m column.

4.2.3.5 Damage Screening

Considering the *P-I* curves shown in Fig. 4.11 and Fig. 4.12, the *P-I bands* shown in Fig. 4.15 can be generated for rapid damage screening of RC columns. Depending on the level of axial load, which may change during blast as a result of partial progressive or collapse of certain columns, the *P-I bands* can be used as a quick analysis tool for column with different connection details. If the pairs of pressure and impulse falls out of these regions, the state of damage can be identified easily while if pressure and impulse pairs falls

inside these shaded regions dynamic analysis is required to perform in order to assess on the damage state. This kinds of information and graphs can be helpful for the emergency response team for rapid assessment of the column damage after blast and by considering the distribution of columns and their damage extents, they can facilitate the estimation of the overall damage of the building in order to decide whether it is safe to approach the damaged building or not.

4.3 Conclusions

Using the moment curvature diagrams, nonlinear dynamic analysis of RC columns under blast load was investigated through a simplified MDOF model. The strain rate effects on the material properties and the level of axial load effects were implemented in the MDOF model.

Moment-curvature diagrams were presented for the column cross section considered in this study. Results showed that the ultimate curvature is reduced significantly with increasing axial load. Axial force-bending moment interaction diagrams were generated for different levels of strain rates and it was shown that the interaction diagrams were amplified significantly as the strain rate increases. In addition, it was observed that simply amplifying material properties by a factor of 1.25 (which is the current practice) cannot capture material enhancement at the very high strain rates such as 100 s^{-1} and 500 s^{-1} .

Two different connection details at supports were used for the RC columns considered in this study. Considering the *P-I* diagram as an important tool for assessing structural damage under blast load and using the MDOF model, *P-I* curves were developed for different levels of axial load at the two connection details. The difference between *P-I* curves drawn for different levels of axial load and the curves constructed for the column with no axial load became more significant for high values of axial load particularly in the impulsive regime. The maximum difference of 40% was observed by increasing the axial load level to 70% of column axial load capacity.

Deflections for the columns with both connection details decreased significantly by increasing the level of axial load. By evaluating the column rotation at the fully damaged state, it was found out that the angle of rotation is not constant and it can be much lower than the values recommended by current design codes. In addition to the cross section properties, both the levels of axial load and the column stiffness were found to affect the column rotation at the fully damage states. It was also shown that the higher the level of axial load and stiffness were, the lower the column rotation at the fully damaged state was.

Comparing the *P-I* curves for the two different connection types, it indicated that the column blast load carrying capacity can be enhanced significantly by providing good detailing at supports. Ultimate deflection can also be amplified by a factor about 3.6 and

both the pressure and impulse asymptotes can be amplified by factors of 1.5 and about 2.4, respectively, for ductile connections compared to non-ductile connections.

Acknowledgements

This study forms a part of an ongoing research program in McMaster University Centre for Effective Design of Structures (*CEDS*) funded through the Ontario Research and Development Challenge Fund (*ORDCF*). This research falls under *CEDS Focus Area II: Earthquake Engineering and Extreme Dynamic Loading*. The financial support of the Centre is greatly appreciated.

Notation

The following symbols are used in this paper:

C_i = damping coefficient for i^{th} node

C_1 = parameter that defines the curvature of the strain hardening curve in reinforcing steel

DIF = dynamic increase factor

E = elastic modulus of reinforcing steel

EI_{eff} = effective flexural rigidity

F = total applied load

F_{a-b} = axial force capacity at the balanced point

F_{a-max} = maximum axial load carrying capacity

- F_i = lumped load at i^{th} node
- f'_c = concrete maximum compressive stress
- f'_{cc} = Maximum compressive stress for confined concrete
- f_{cd} = concrete dynamic compressive strength
- f_{co} = parameter of Malvar's equation for concrete
- f_{cs} = concrete static compressive strength
- f'_t = concrete maximum tensile stress
- f_{td} = concrete dynamic tensile strength
- f_{ts} = concrete static tensile strength
- f = reinforced bar stress
- h = column section height
- h_c = compression depth
- h_t = tension depth
- K = curve parameter for confined concrete model
- L = column length
- LM_i = lumped mass at i^{th} node
- M_o = pure bending moment capacity
- M_b = balanced bending moment
- M_{i-1} = moment at $(i-1)^{th}$
- M_i = moment at i^{th} node

M_{i+1} = moment at $(i+1)^{th}$ node

M_y = yield moment

n = number of nodes

p = blast load per unit length

P_0 = peak pressure

p_0 = peak blast load per unit length

q = curve fitting parameter in concrete model

$R(t)$ = resistance force as a function of time

T_L = loading duration

$V_{i-1,i}$ = shear between $(i-1)^{th}$ and i^{th} node

$V_{i,i+1}$ = shear between i^{th} and $(i+1)^{th}$ node

y_i = i^{th} node displacement

\dot{y}_i = i^{th} node velocity

\ddot{y}_i = i^{th} node acceleration

α = parameter of Malvar's equation for reinforcing steel *DIF*

β = parameter of Malvar's equation for concrete *DIF*

δ = parameter of Malvar's equation for concrete *DIF*

Δx = segment length

ε = strain

ε_c = concrete strain at maximum confined compressive stress

ϵ_{cd} = concrete dynamic strain at peak compressive stress

ϵ_{cs} = concrete static strain at peak compressive stress

ϵ_{sh} = strain at the onset of strain hardening in reinforcing steel

ϵ_t = tensile strain

ϵ_y = strain at steel yield point

ϵ_u = ultimate (peak) strain in reinforcing steel

ϵ_{85} = Strain corresponding to $0.85f'_{cc}$ on the descending branch of stress-strain curve

$\dot{\epsilon}$ = strain rate

$\dot{\epsilon}_s$ = concrete static strain rate

ϕ = curvature

ϕ_y = yield curvature

$\phi(x)$ = assumed mode shape

σ = stress in the reinforcing steel

σ_c = compressive stress in concrete

σ_{sh} = stress at the onset of strain hardening in reinforcing steel

σ_t = tensile stress in concrete

σ_u = ultimate (peak) stress in reinforcing steel

σ_y = stress at steel yield point

ρ_m = mass per unit length

References

Baker, W.E. et al. 1983. Explosion hazards and evaluation. Elsevier Scientific Publishing Company, Oxford, UK.

Bentz, E. C. 2000. Sectional analysis of reinforced concrete members. PhD Thesis, Department of Civil Engineering, University of Toronto.

Bentz, E. C. 2005. Explaining the riddle of tension stiffening models for shear panel experiments. J. Struct. Eng., 131(9): 1422-1425.

Beshara, F. B. A. 1994. Modeling of blast loading on aboveground structures - I. General phenomenology and external blast. Computers and Structures, 51(5): 597-606.

Biggs, J.M. 1964. Introduction to structural dynamics. McGraw-Hill Book Company, New York.

Bischoff, P. H, and Perry, S. H. 1991. Compressive behavior of concrete at high strain rates. Materials and Structures. 24, 425–450.

Boutros, M. K. 2000. Elastic-plastic model of pinned beams subjected to impulsive loading. J. Eng. Mech., 126(9):920-927.

Changiz Rezaei, S. H., El-Dakhakhni, W. W., Mekky, W. F. and Razaqpur, A. G. 2008. Response sensitivity of blast loaded reinforced concrete structures to the number of degrees of freedom. Submitted to Canadian Journal of Civil Engineering.

Collins, M. P., and Mitchell, D. 1987. Prestressed concrete basics. Canadian Prestressed Concrete Institute, Ottawa.

CEB, Comité Euro-International du Béton, 1988. Concrete structures under impact and impulsive loading. CEB Bulletin 187, Lausanne, Switzerland.

Dilger, W. H, Koch, R., and Kowalczyk R. 1984. Ductility of plain and confined concrete under different strain rates. ACI J., 81(1):73-81.

Hoehler, M. S., and Stanton, J. F. 2006. Simple phenomenological model for reinforcing steel under arbitrary load."J. Struct. Engrg., 132(7): 1061-1069.

Krauthammer, T., Assadi-Lamouki, A., and Shanaa, H. M. 1993. Analysis of impulsively loaded RC structural elements, part 1-theory. Computers and Structures, 48(5):851-860.

Krauthammer, T., Bazeos, N., Holmquist, T.J. 1986. Modified SDOF analysis of RC box-type structures. J. Struct. Eng. ,112(4) :726-744.

Krauthammer, T., Shahriar, S. and Shanaa, H. M. 1990. Response of reinforced concrete elements to severe impulsive loads. *J. Struct. Eng.*, 116(4): 1061-1079.

Krauthammer, T., Shanaa, H.M. and Assadi-Lamouki, A. 1994. Response of reinforced concrete structural elements to severe impulsive loads. *Computers and Structures*, 53(1): 119-130.

Kulkarni, S.M., and Shah, S.P. 1998. Response of reinforced concrete beams at high strain rates. *ACI J.*, 95(6): 705-715.

Louca, L. A. and Harding, J. E. 1997. Non-linear analysis of imperfect plates under transient lateral pressure loading. *Computers and Structures*, 63(1): 27–37.

Low, H. Y., and Hao, H. 2002. Reliability analysis of direct shear and flexural failure modes of RC slabs under explosive loading. *Engineering Structures*, 24, 189–198.

Malvar, L. J. 1998. Review of static and dynamic properties of steel reinforcing bars. *ACI J.*, 95(5): 609-616.

Malvar, L. J., and Crawford, J. E. 1998. Dynamic increase factors for concrete. Twenty-Eighth DDESB Seminar, Orlando, FL.

Malvar, L. J., and Ross C. A. 1998. Review of strain rate effects for concrete in tension. *ACI J.*, 95(6): 735-739

Mander, J. B., Priestley, M. J. N., and Park, R. 1988. Theoretical stress-strain model for confined concrete. *J. Struct. Eng.*, 114(8): 1804-1826.

Pan, Y., and Watson, A. 1998. Effect of panel stiffness on resistance of cladding panels to blast loading. *J. Eng. Mech.*, 124(4): 414-421.

Priestly, M. J. N., Seible, F., and Calvi, G. M. 1996. *Seismic design and retrofit of bridges*. Wiley, New York.

Popovics, S. 1973. A numerical approach to the complete stress-strain curve of concrete. *Cement and Concrete Research*, 3(5): 583-599.

Rodriguez-Nik, T. 2006. Experimental simulations of explosive loading on structural components: reinforced concrete columns with advanced composite jackets. PhD Thesis, Department of Structural Engineering, University of California, San Diego.

Saatcioglu, M., and Razvi, S. R. 1992. Strength and ductility of confined concrete. *J. Struct. Eng.*, 118(6): 1590-1607.

Schleyer, G. K., and Hsu, S. S. 2000. A modelling scheme for predicting the response of elastic plastic structures to pulse pressure loading. *Int. J. Impact Eng.*, 24, 759-777.

Scott, B. D., Park, R., and Priestley, M. J. N. 1982. Stress-strain behavior of concrete confined by overlapping hoops at low and high strain rates. *ACI J.*, 79(1): 13-27.

Soroushian, P. , and Choi, K. 1987. Steel mechanical properties at different strain rates. *J. Struct. Eng.*, 113(4) 863-872.

Soroushian, P., Choi, K., and Alhamad, A. 1986. Dynamic constitutive behavior of concrete. *ACI J.*, 83(2): 251-258.

Tamai, S., Shima, H., Izumo, J., and Okamura, H. 1987. Average stress-strain relationship in post yield range of steel bar in concrete. *Concrete Library of JSCE*, No. 11, 117–129.

Tedesco, J. W., Ross, C. A., Powell, J. C., and Hughes, M. L. 1997. A strain rate dependent concrete material model for ADINA. *Computers and Structures*, 64(5), 1053-1067.

TM5-1300, US Department of Army Technical Manual, 1990. Design of structures to resist the effects of accidental explosions. Washington, DC.

Vecchio, F. J., and Collins, M. P. 1982. Response of reinforced concrete to in-plane shear and normal stresses. Publ. No. 82-03, Dept. of Civil Engineering, Univ. of Toronto.

Figure Captions

Fig. 4.1: Actual and idealized side-on blast pressure time histories: (a) Actual blast load time history, (b) Triangular load approximation, (c) Using tangent line in approximating blast load

Fig. 4.2: Schematic view of MDOF model based on lumped mass approach for a column

Fig. 4.3: Strain rate effects: (a) *DIF* for concrete under tension, (b) *DIF* for concrete under compression, (c) Scaled stress-strain curve for reinforcing steel, (d) Scaled stress-strain curve for concrete

Fig. 4.4: Strain rate distribution at the midspan of a simply supported column

Fig. 4.5: Cross section of the RC column considered in this study

Fig. 4.6: Flow chart of the MDOF analysis procedure

Fig. 4.7: Moment curvature for different level of axial load:(a) zero axial load, (b) $0.2F_{a-max}$, (c) $0.35F_{a-max}$, (c) $0.5F_{a-max}$, (d) $0.7F_{a-max}$

Fig. 4.8: Variation in ultimate curvature: (a) Strain distribution without axial load, (b) Strain distribution with axial load, (c) Reduction in ultimate curvature with increasing axial load compared to the case with no axial load

Fig. 4.9: Variation of section properties with strain rate: (a) Axial force-bending moment interaction diagrams, (b) Variation of pure bending moment, balanced moment, balanced axial force, and maximum axial force

Fig. 4.10: General form of the pressure-impulse diagrams

Fig. 4.11: *P-I* diagrams for different levels of axial load (3.0 m column): (a) Type *N* connection, (b) Type *D* connection

Fig. 4.12: $P-I$ diagrams for different levels of axial load (6.0 m column): (a) Type N connection, (b) Type D connection

Fig. 4.13: Reduction in deflections compared to the case with no axial load: (a) 3.0 m column, (b) 6.0 m column

Fig. 4.14: Column section rotation at the fully damaged state

Fig. 4.15: $P-I$ diagrams for damage screening: (a) 3.0 m column, (b) 6.0 m column

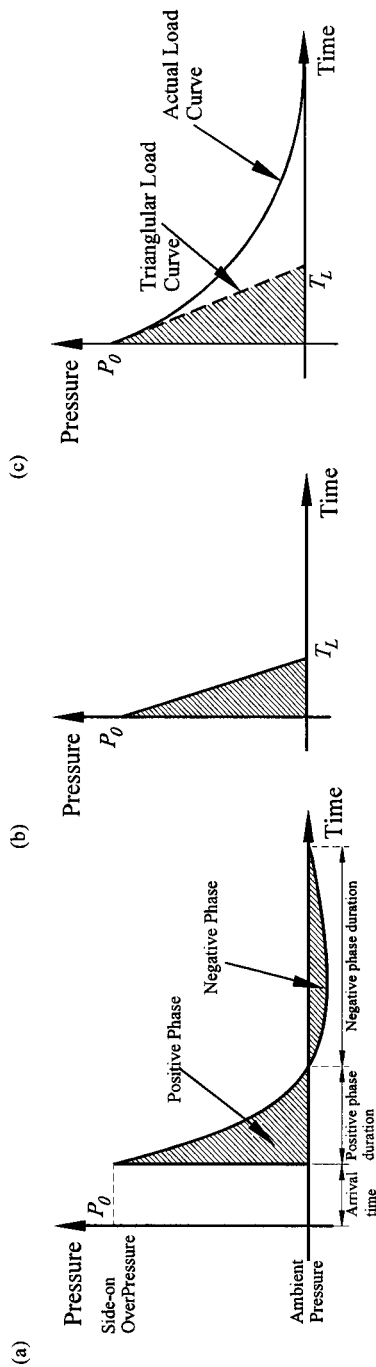


Fig. 4.1: Actual and idealized side-on blast pressure time histories: (a) Actual blast load time history, (b) Triangular load approximation, (c) Using tangent line in approximating blast load

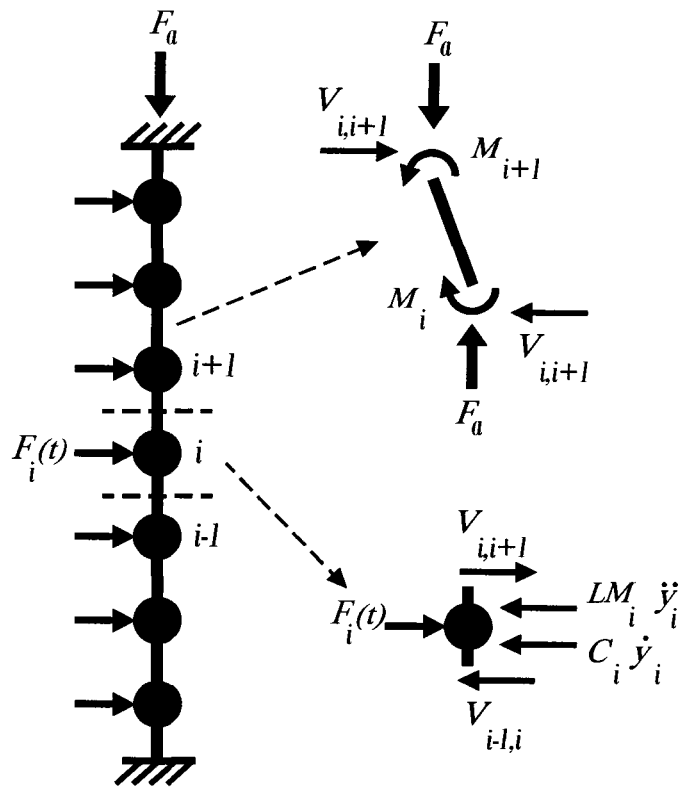
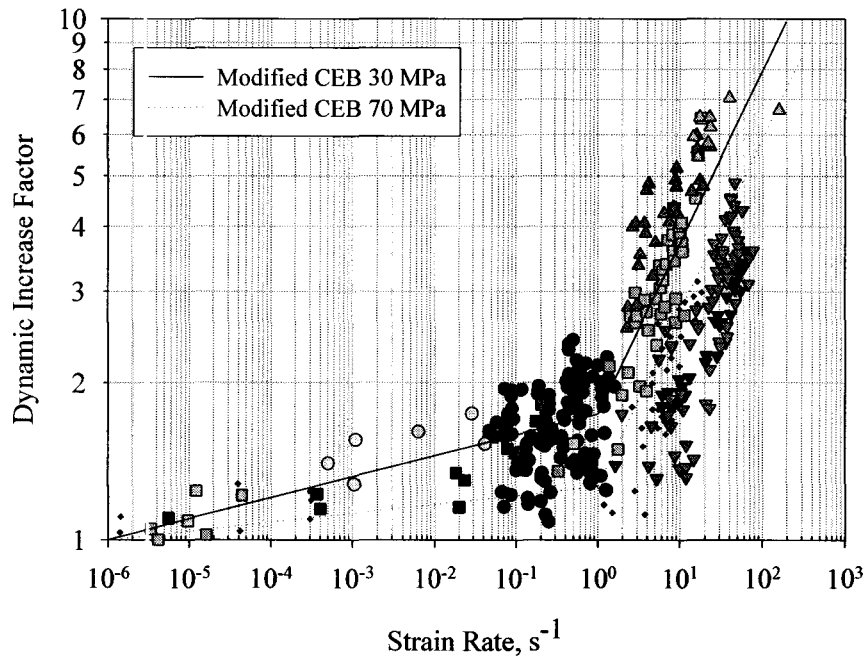
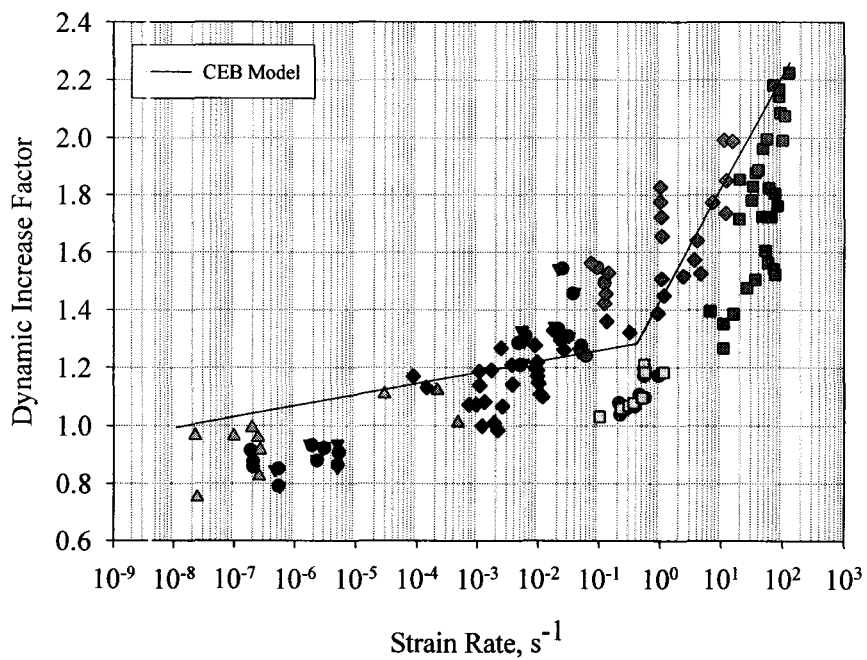


Fig. 4.2: Schematic view of MDOF model based on lumped mass approach for a column

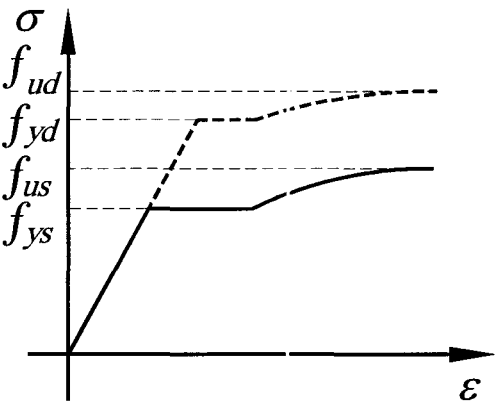
(a)



(b)



(c)



(d)

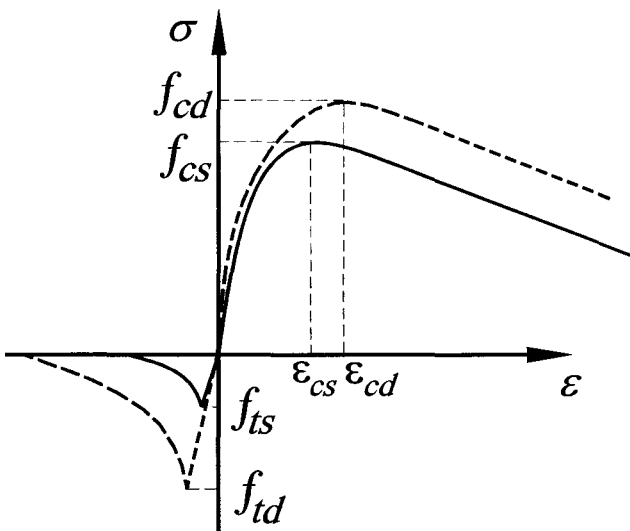


Fig. 4.3: Strain rate effects: (a) *DIF* for concrete under tension, (b) *DIF* for concrete under compression, (c) Scaled stress-strain curve for reinforcing steel, (d) Scaled stress-strain curve for concrete

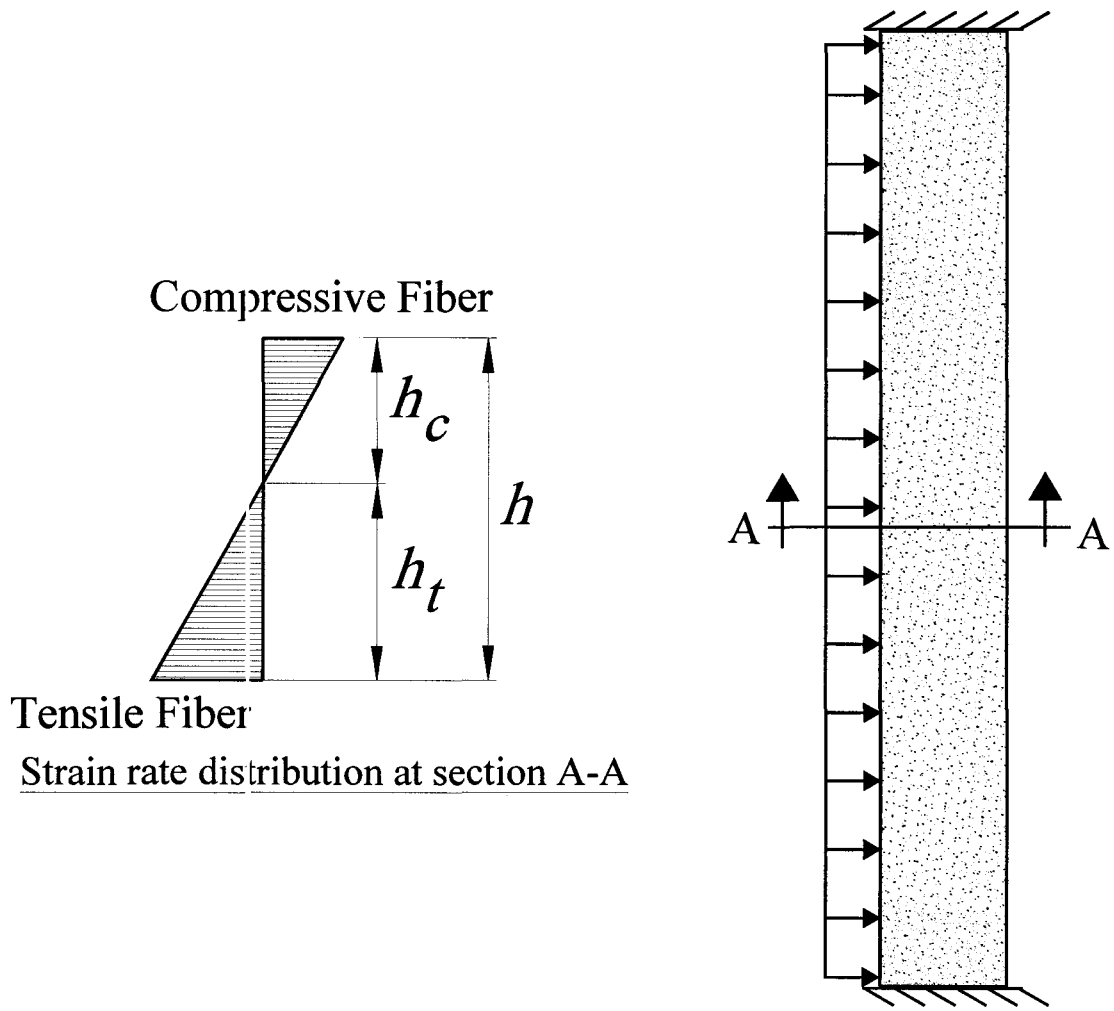


Fig. 4.4: Strain rate distribution at the midspan of a simply supported column

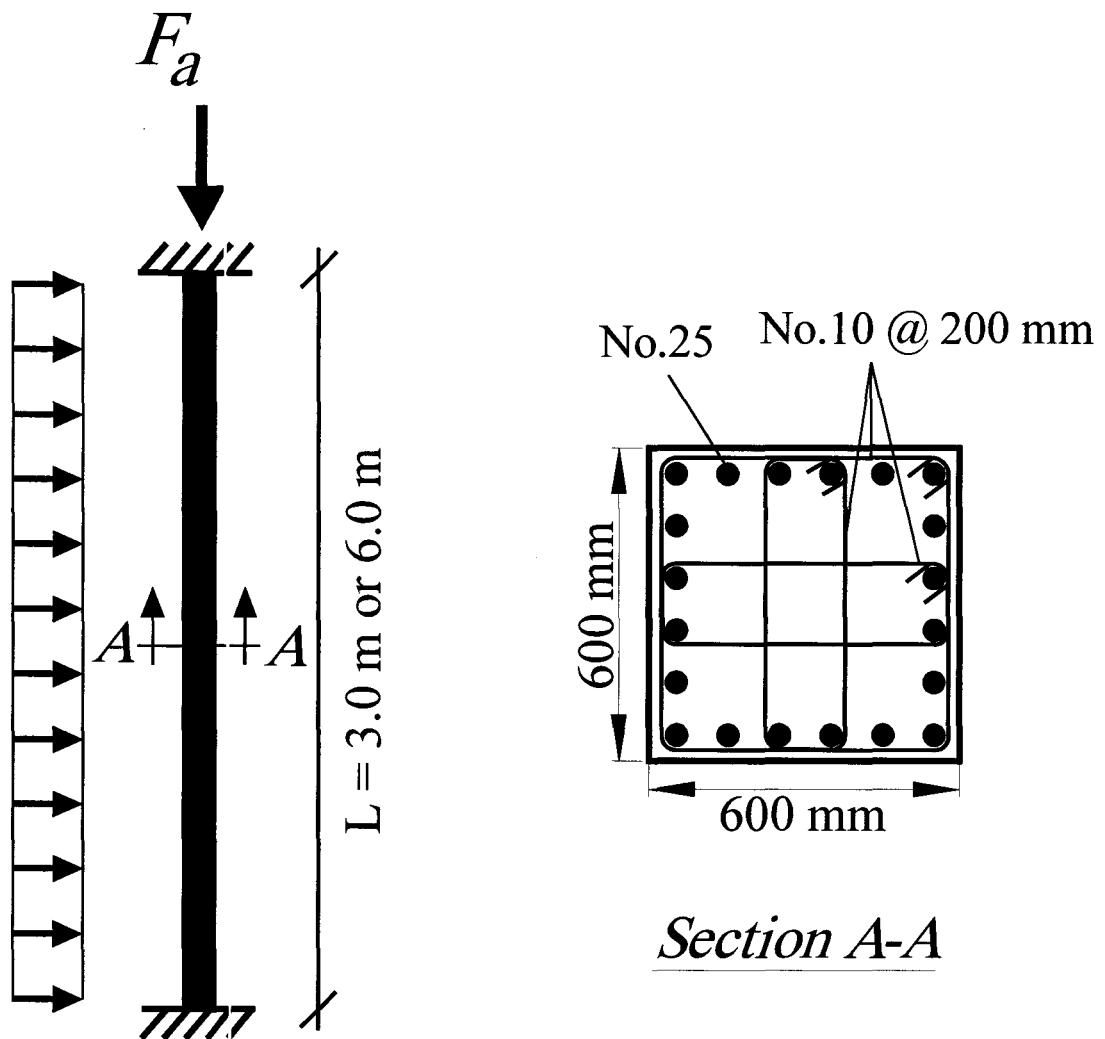


Fig. 4.5: Cross section of the RC column considered in this study

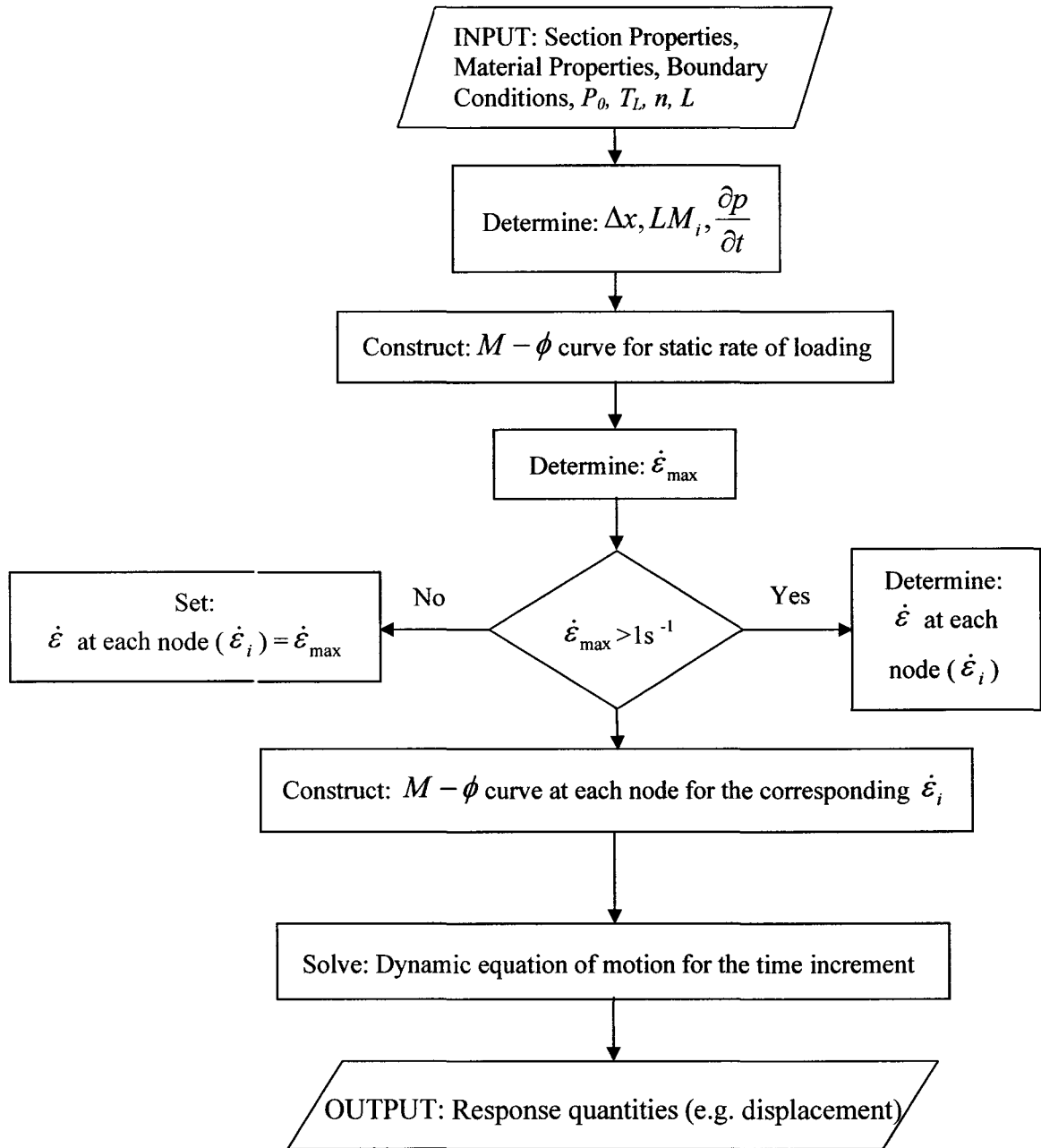
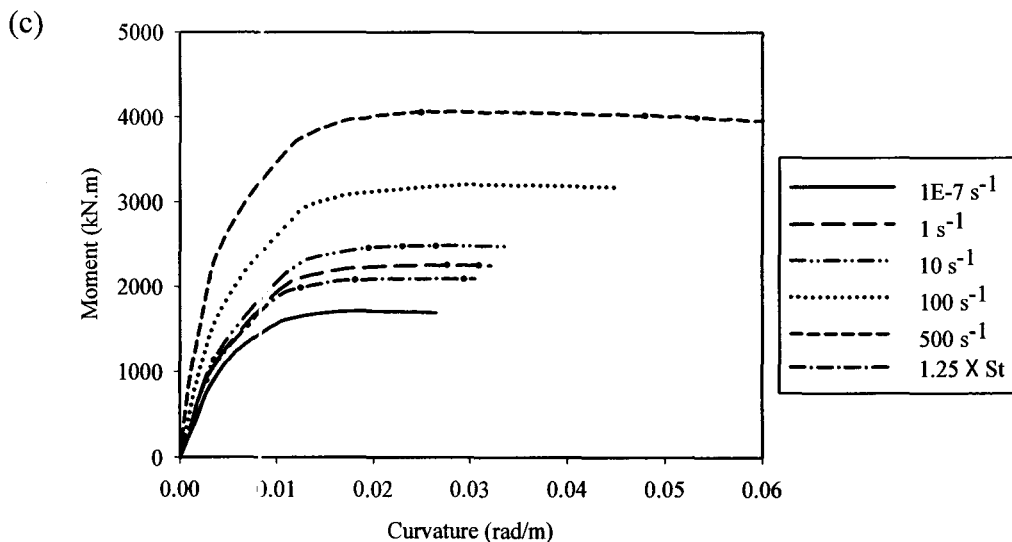
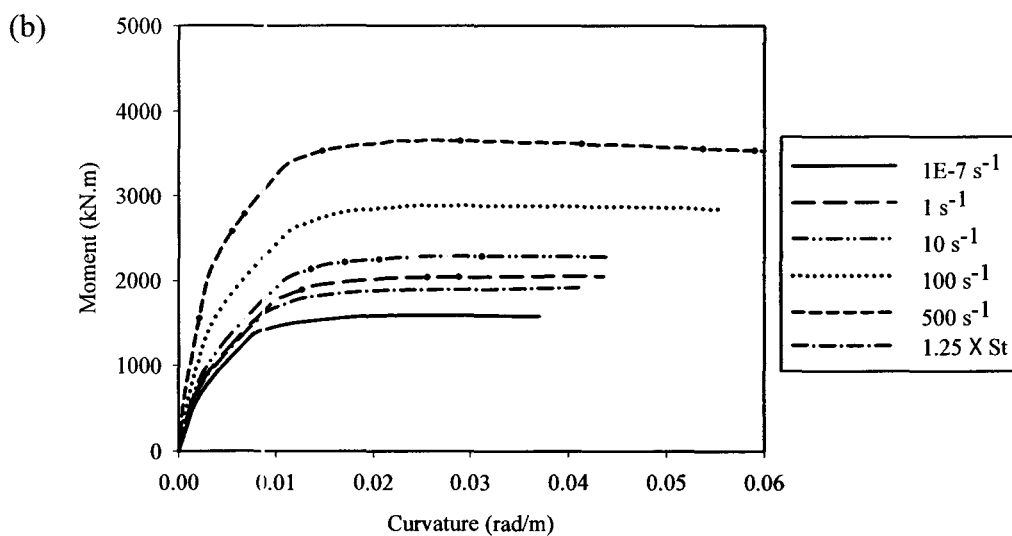
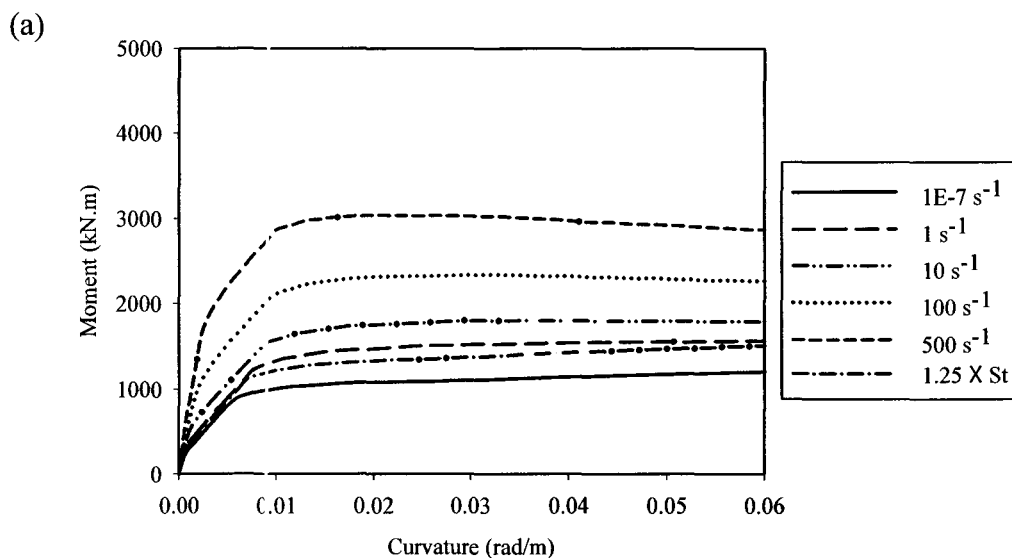
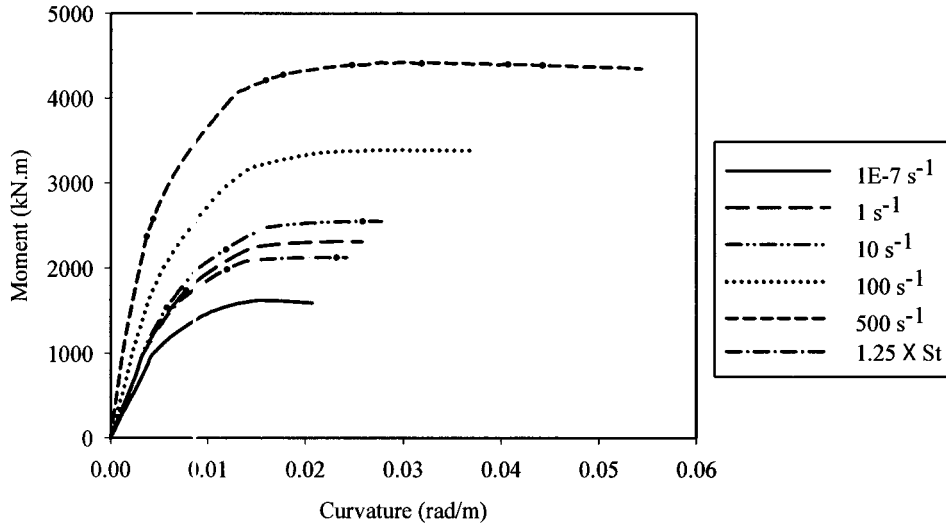


Fig. 4.6: Flow chart of the MDOF analysis procedure



(d)



(e)

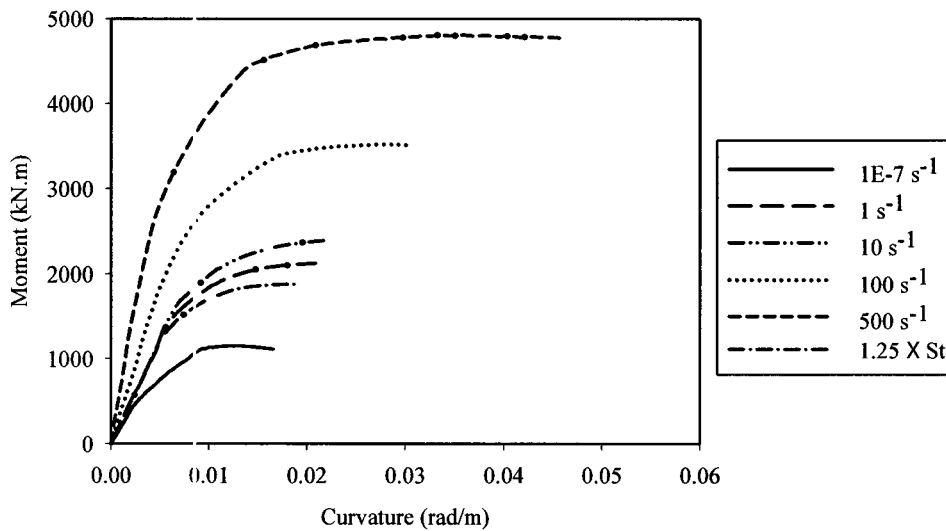
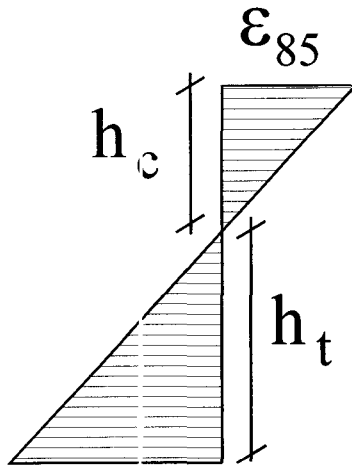
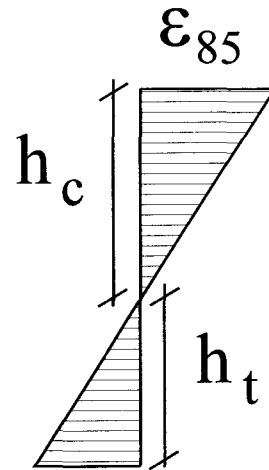


Fig. 4.7: Moment curvature for different level of axial load: (a) zero axial load, (b) $0.2F_{a-max}$, (c) $0.35F_{t-max}$, (d) $0.5F_{a-max}$, (e) $0.7F_{a-max}$

(a)



(b)



(c)

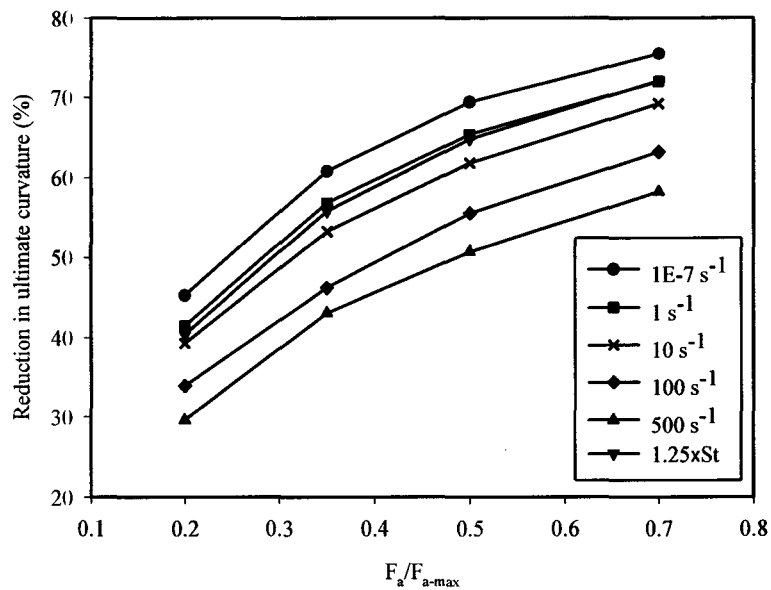


Fig. 4.8: Variation in ultimate curvature: (a) Strain distribution without axial load, (b) Strain distribution with axial load, (c) Reduction in ultimate curvature with increasing axial load compared to the case with no axial load

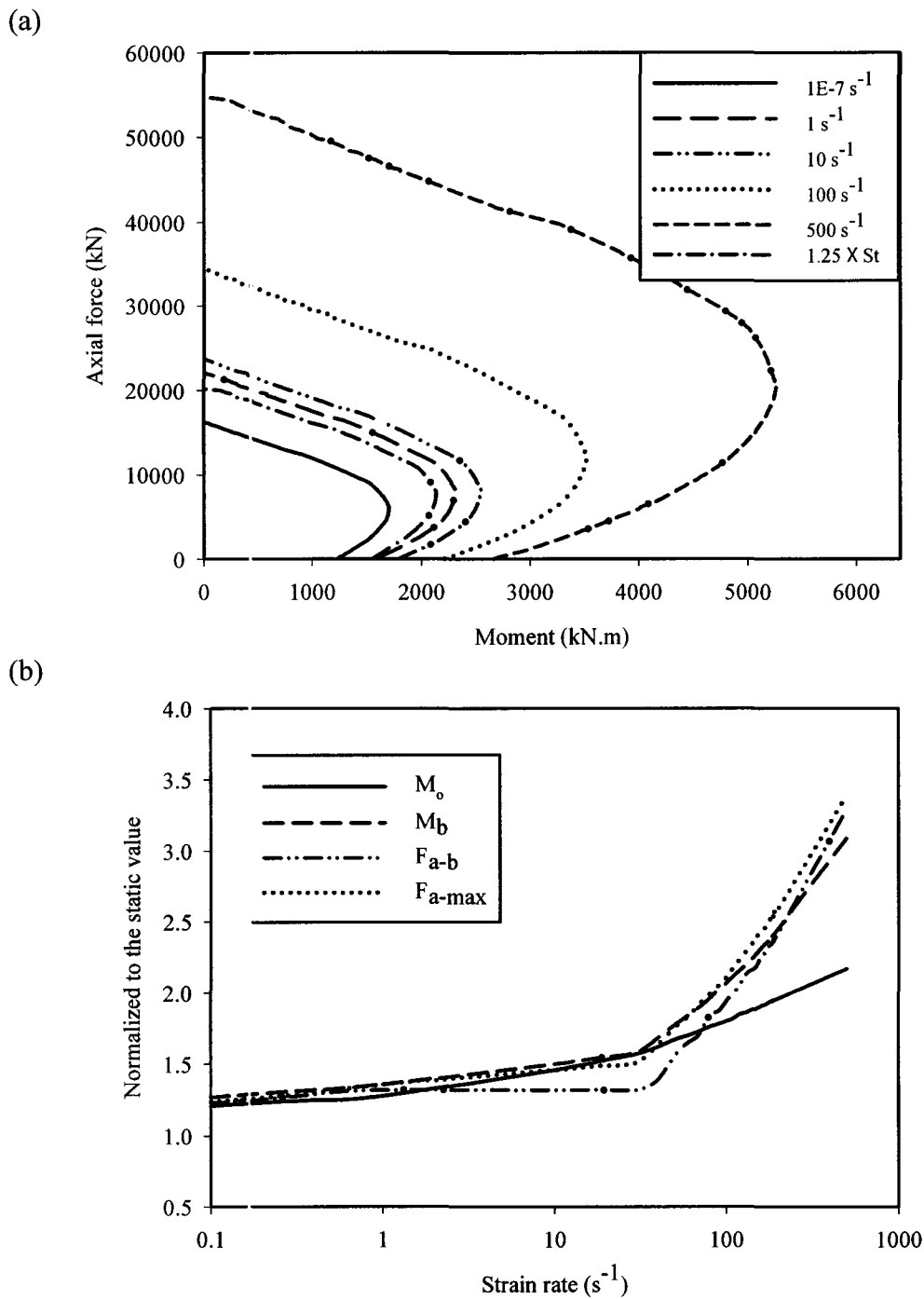


Fig. 4.9: Variation of section properties with strain rate: (a) Axial force-bending moment interaction diagrams, (b) Variation of pure bending moment, balanced moment, balanced axial force, and maximum axial force

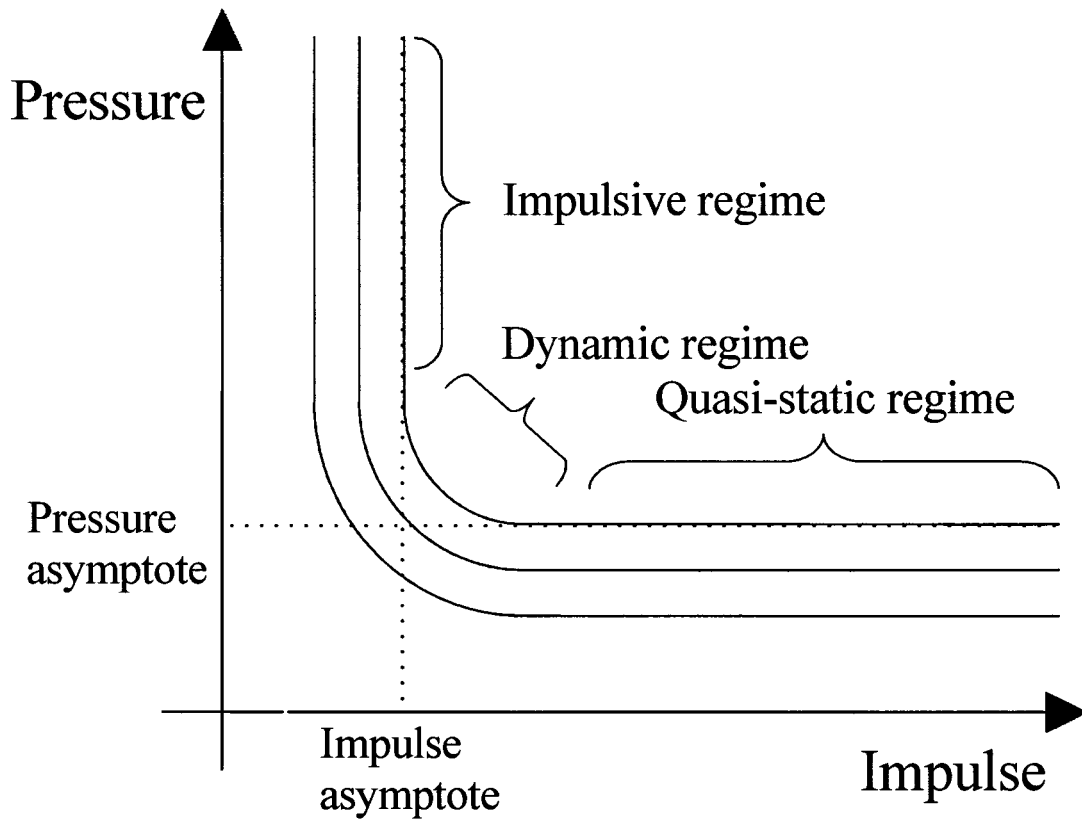
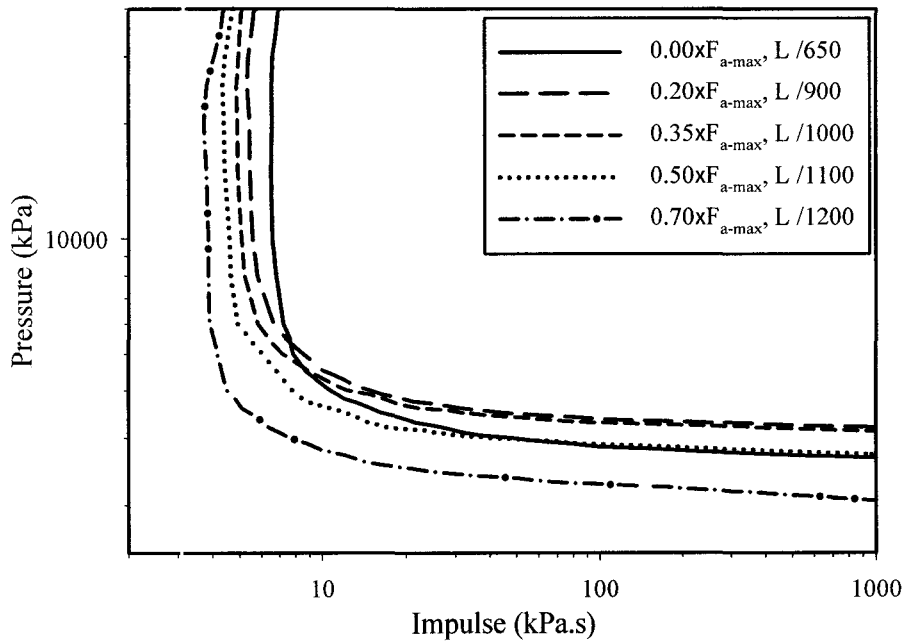


Fig. 4.10: General form of the pressure-impulse diagrams

(a)



(b)

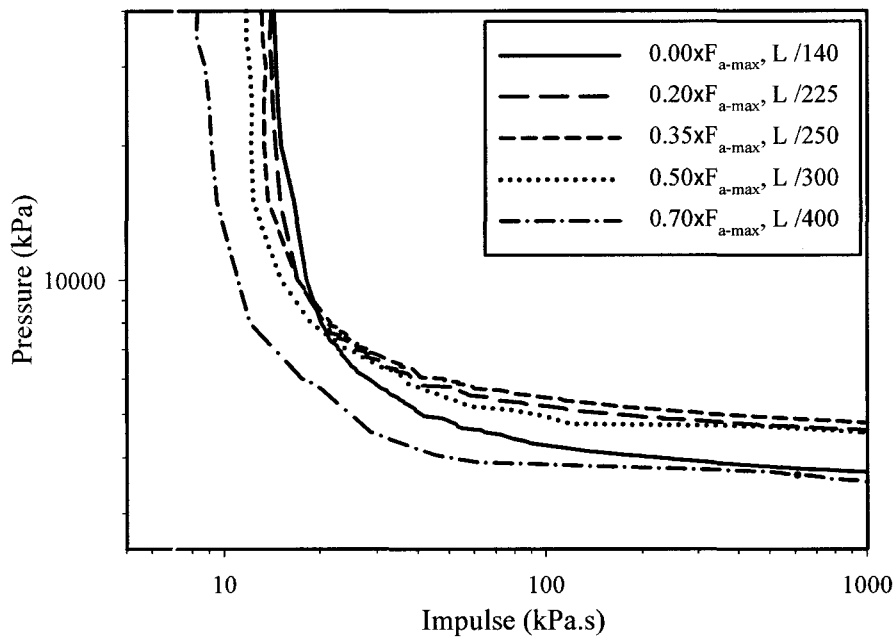
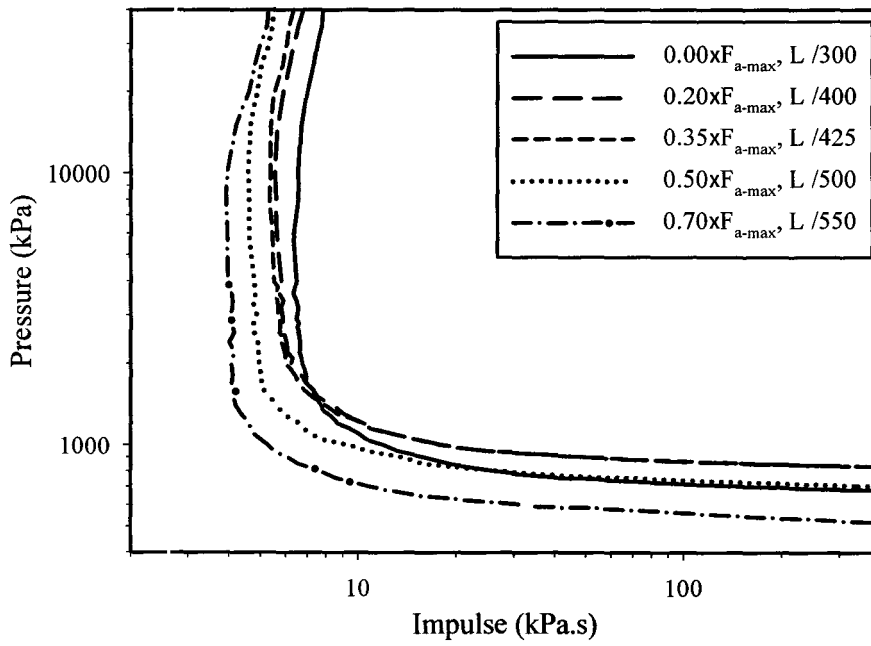


Fig. 4.11: P-I diagrams for different levels of axial load (3.0 m column): (a) Type N connection, (b) Type D connection

(a)



(b)

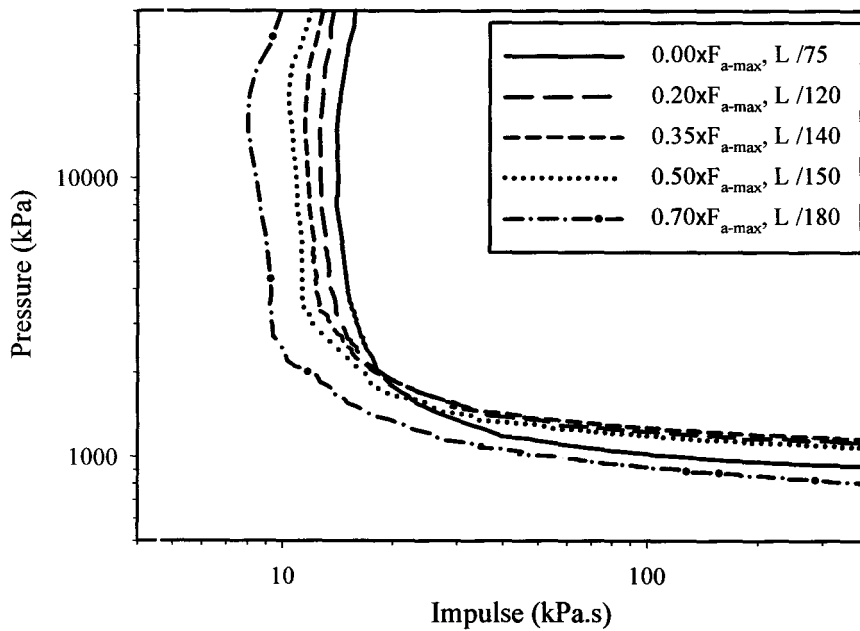
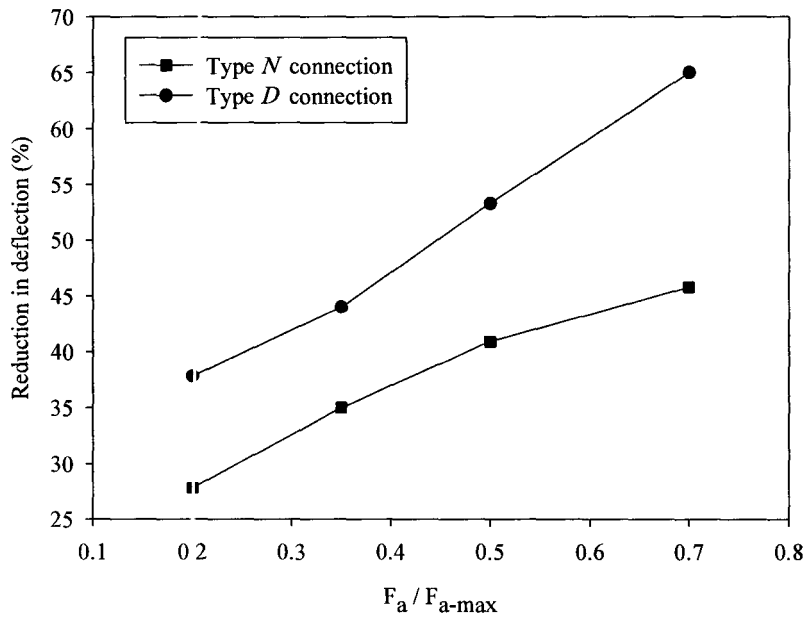


Fig. 4.12: *P-I* diagrams for different levels of axial load (6.0 m column): (a) Type *N* connection, (b) Type *D* connection

(a)



(b)

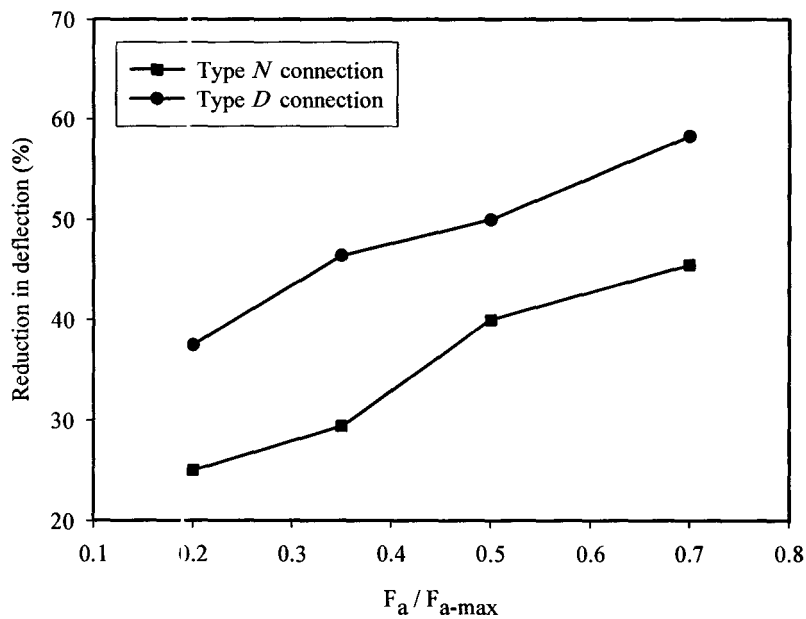


Fig. 4.13: Reduction in deflections compared to the case with no axial load: (a) 3.0 m column, (b) 6.0 m column

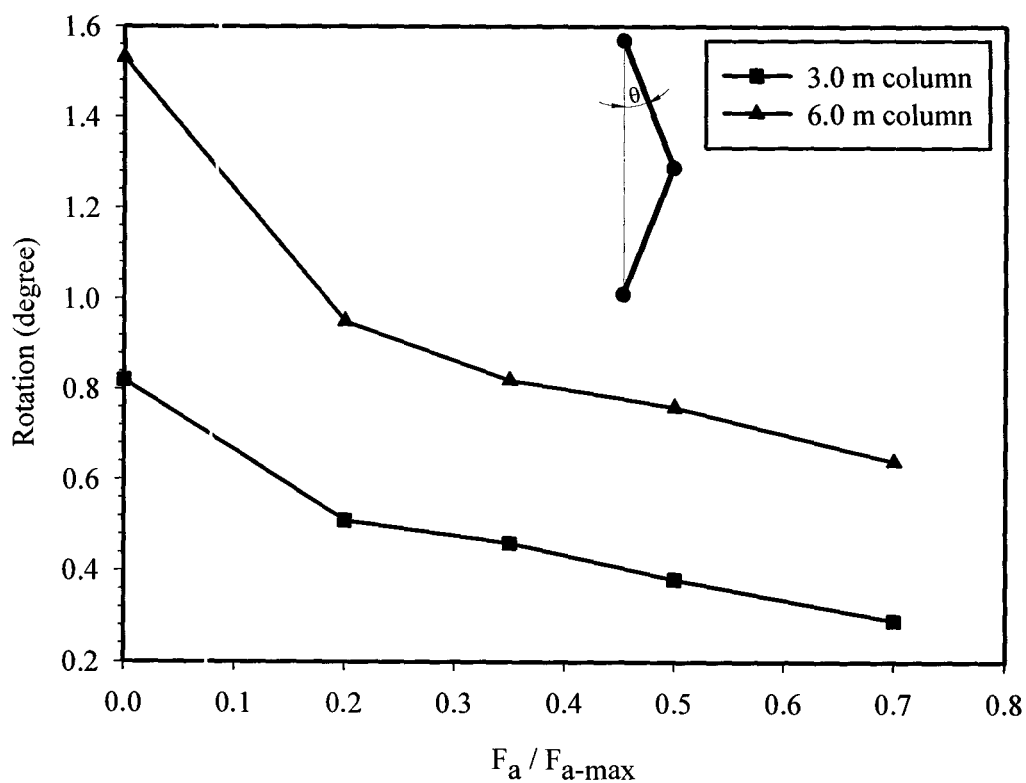


Fig. 4.14: Column section rotation at the fully damaged state

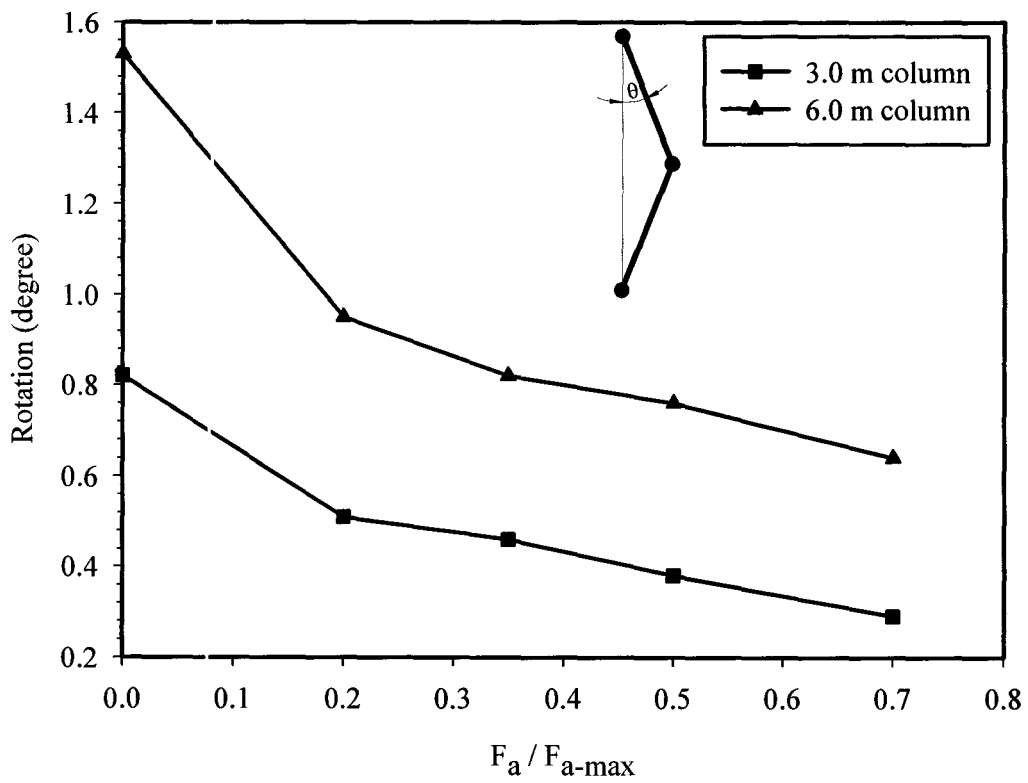
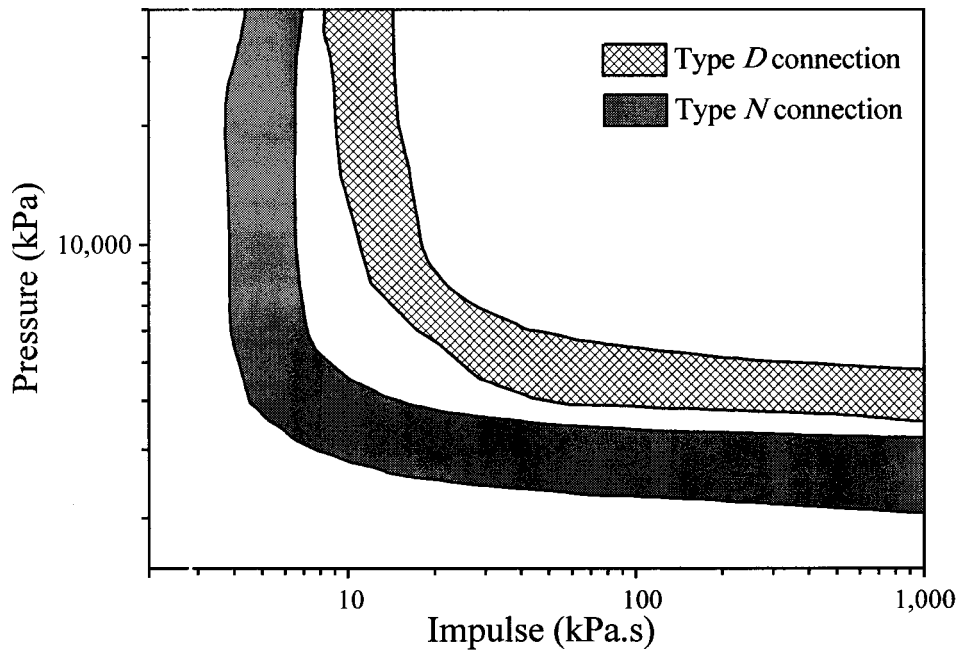


Fig. 4.14: Column section rotation at the fully damaged state

(a)



(b)

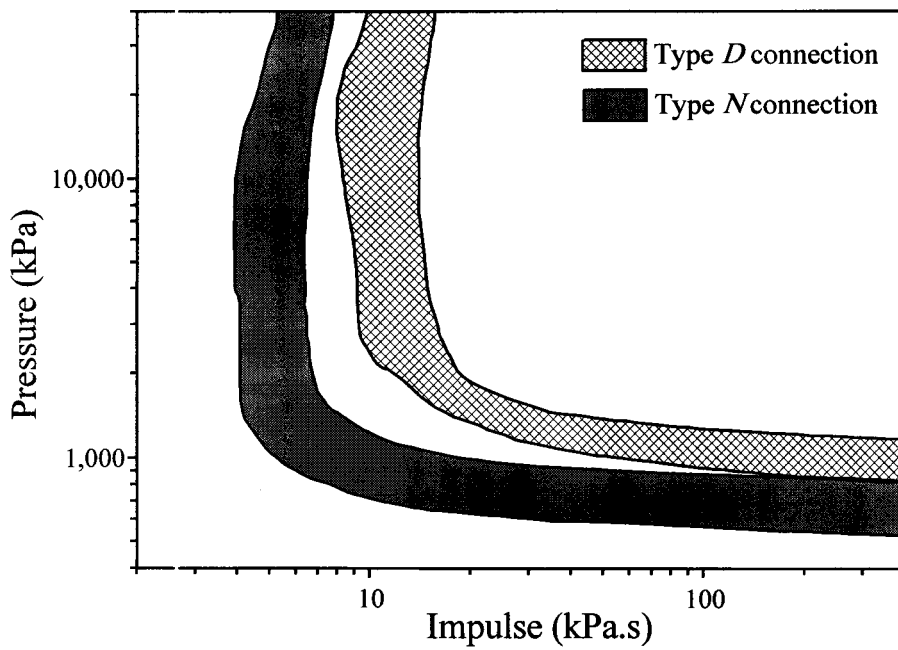


Fig. 4.15: *P-I* diagrams for damage screening: (a) 3.0 m column, (b) 6.0 m column